17737

NATIONAL LIBRARY
OTTAWA

CANADA

BIBLIOTHÈQUE NATIONALE
OTTAWA

NAME OF AUTHOR Stephen R. Winzer

TITLE OF THESIS Metamorphism and chemical equilibrium in some rocks from the central Kootenay Arc

UNIVERSITY Alberta

DEGREE FOR WHICH THESIS WAS PRESENTED Ph. D.

YEAR THIS DEGREE GRANTED 1973

Permission is hereby granted to THE NATIONAL LIBRARY OF CANADA to microfilm this thesis and to lend or sell copies of the film.

The author reserves other publication rights, and neither the thesis nor extensive extracts from it may be printed or otherwise reproduced without the author's written permission.

(Signed) Stephen R. Winzer

PERMANENT ADDRESS:

Code 644 Goddard
Space Flight Center
Greenbelt, Maryland
USA

DATED Sept. 24, 1973 19

NL-91 (10-68)

1 of

L A K E
1
2
T3-10
1
1
11
20
205-110W

2 of.

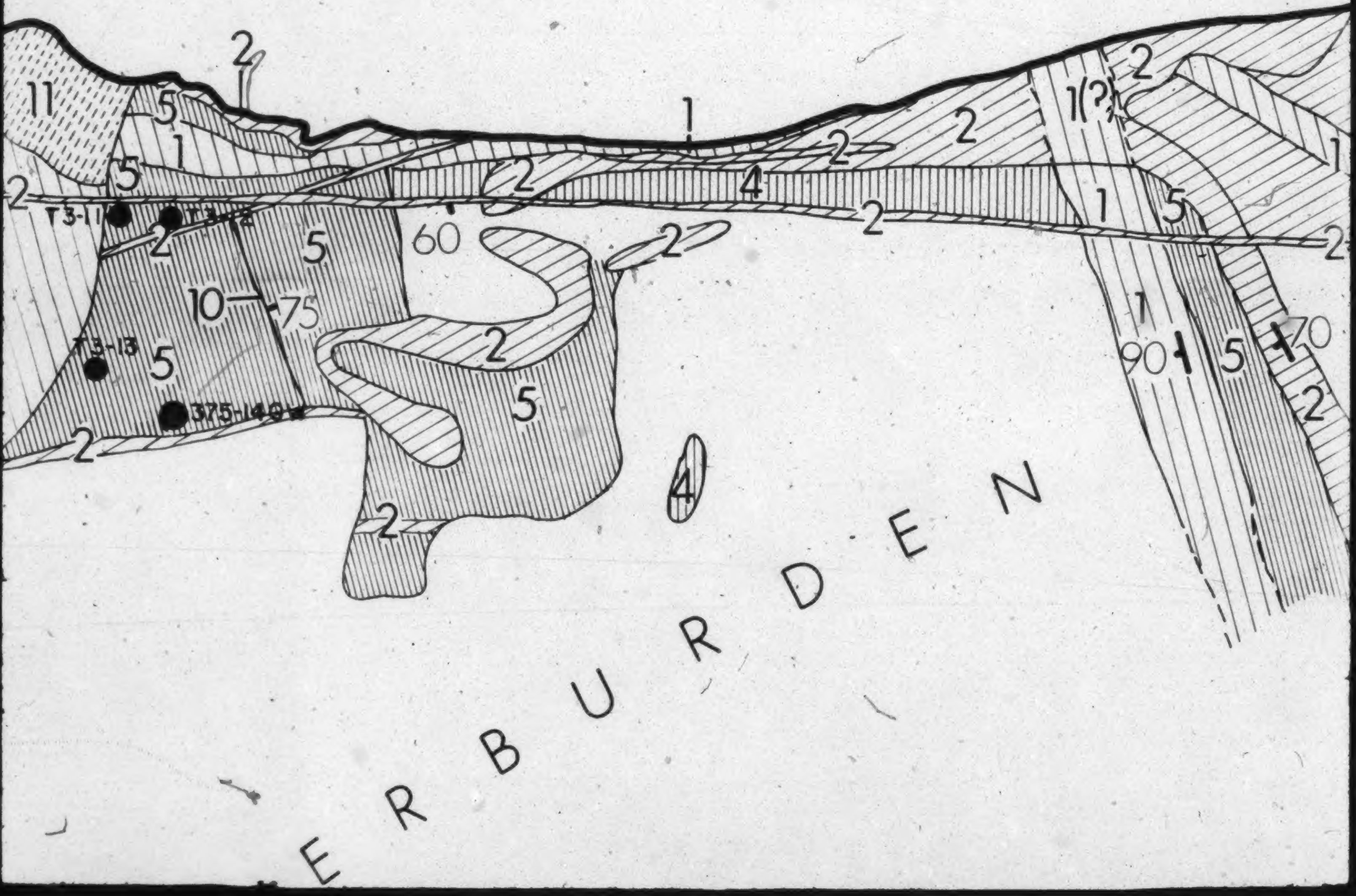
11
2
5
1
5
2
T3-11
T3-12
2
5
10
75
60
2
4
2
2
1
2
2
1(?)
2
1
1
5
2
1
90
5
70
2
T3-13
5
375-140
2
5
2
4
2
ERBURDEN

3 of

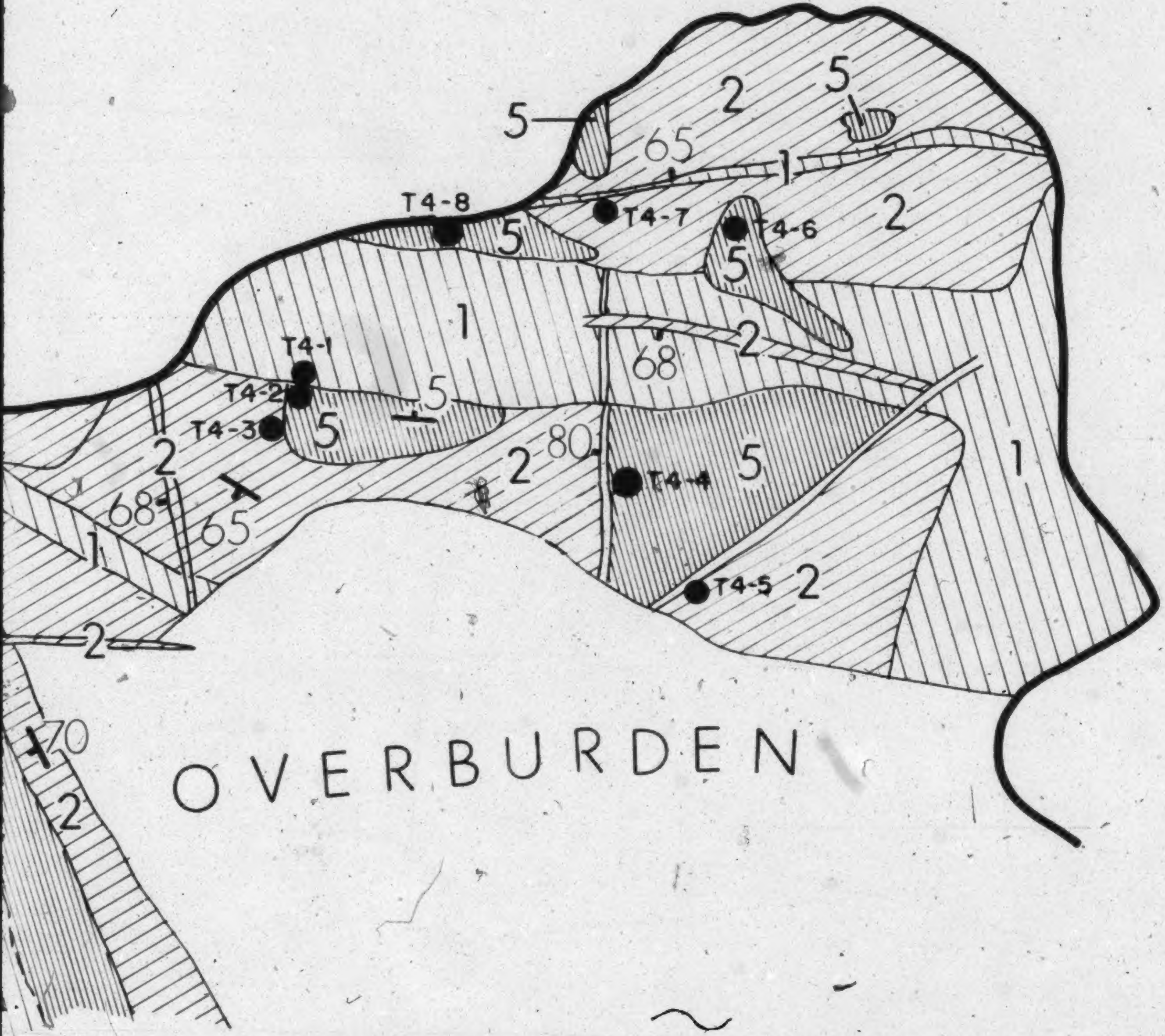
5
2
5
65
1
T4-8
T4-7
T4-6
2
5
5
1
2
68
T4-1
T4-2
T4-3
5
5
2
80
2
T4-4
5
1
68
65
1
2
T4-5
2
2
70
2
OVERBURDEN

PLUTONIC ROCKS

1 Aplite

4 of

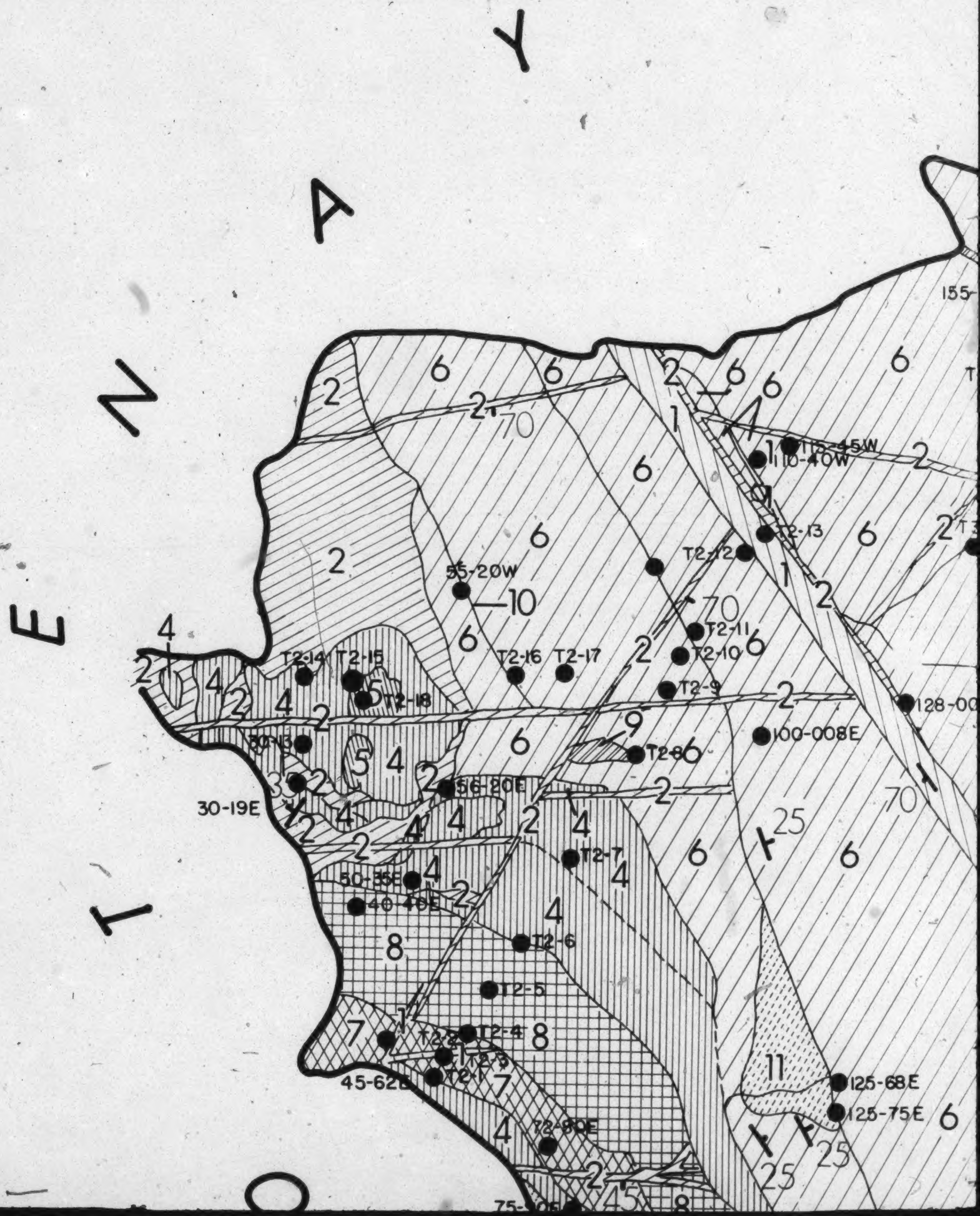
T E N A Y
155-
115-45W
110-40W
T2-13
T2-12
55-20W
10
70
T2-11
T2-10
T2-9
T2-14
T2-15
T2-18
T2-16
T2-17
128-00
100-008E
9
T2-8
30-13
56-20E
30-19E
T2-7
50-35E
40-40E
T2-6
T2-5
T2-4
T2-2
T2-3
T2-1
45-62E
72-80E
125-68E
125-75E
11
25
45
75-

5 of

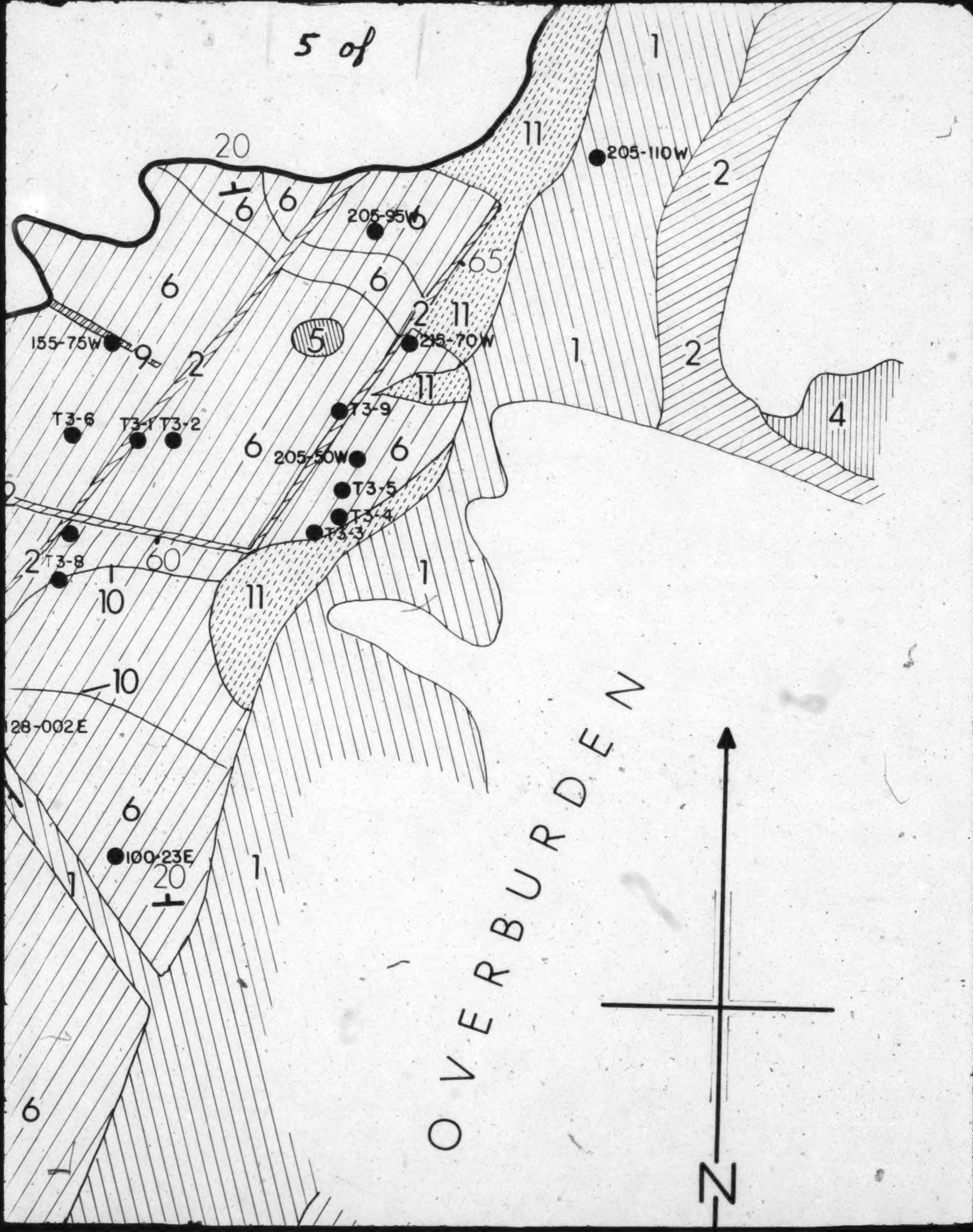

1
11
20
205-110W
2
6
6
205-95W
6
65
6
2
11
155-75W
9
2
5
215-70W
1
2
11
4
T3-9
T3-6
T3-1
T3-2
6
205-50W
6
T3-5
T3-4
T3-3
2
T3-8
1
60
10
11
1
10
128-002E
OVERBURDEN
6
100-23E
20
1
1
6
N

6 of

O V E R B U

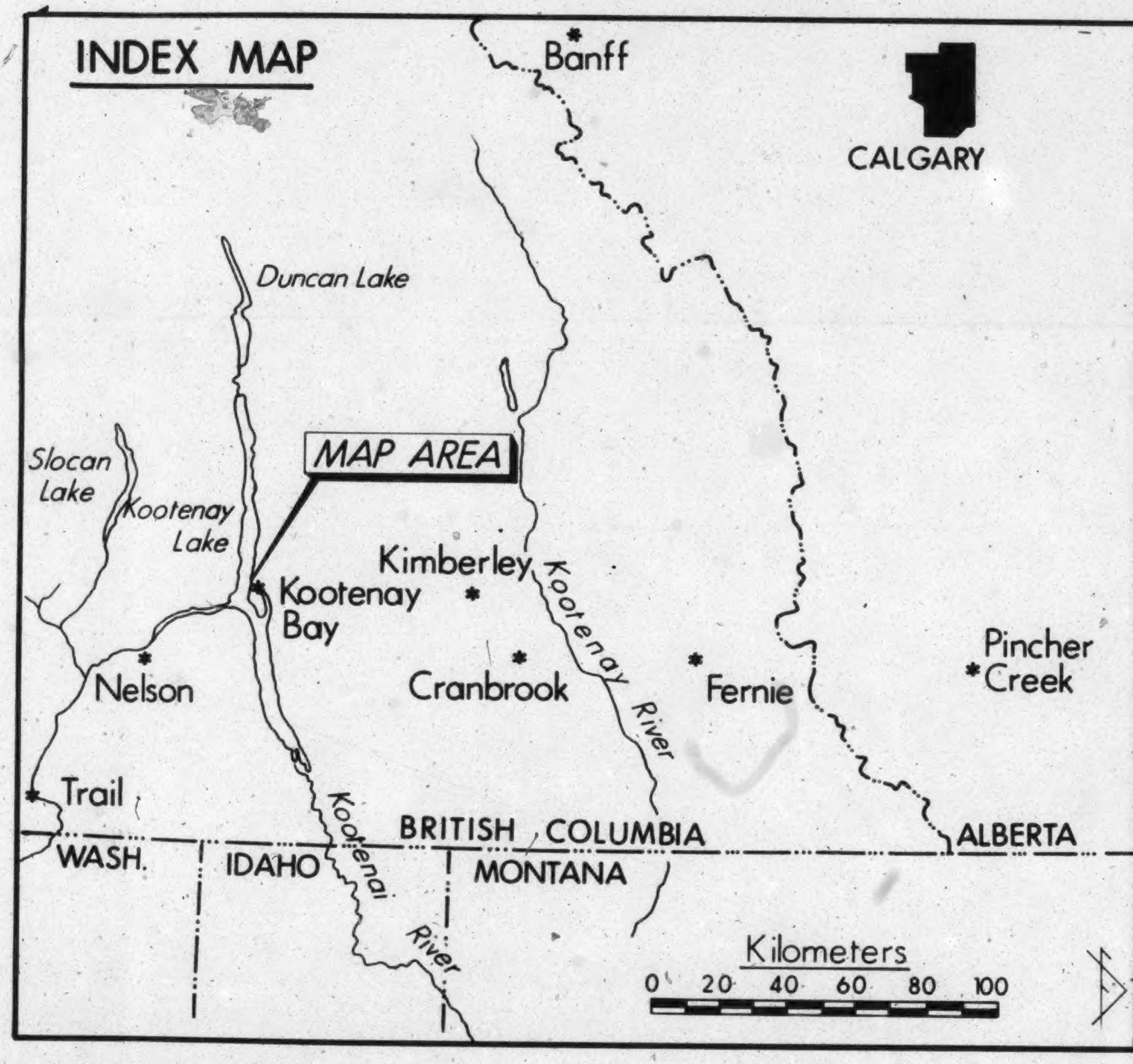
INDEX MAP
Banff
CALGARY
Duncan Lake
MAP AREA
Slocan Lake
Kootenay Lake
Kimberley
Kootenay Bay
Kootenay River
Nelson
Cranbrook
Fernie
Pincher Creek
Trail
Kootenai River
BRITISH COLUMBIA
ALBERTA
WASH.
IDAHO
MONTANA
Kilometers
0 20 40 60 80 100

7 of

PLUTONIC ROCKS

1	Aplite
2	Pegmatite
▩	Granite

LARDEAU FORMATION

METAMORPHIC ROCKS

4	Amphibolite
5	Biotite Amphibolite ± Epidote
6	Marble (incl. Tr.- Di.- Phl.- Musc. & Talc)
7	Biotite - Tremolite - Diopside Gneiss
8	Biotite - Tremolite - Diopside - K - Feldspar Gneiss
9	Actinolite "Pegmatite "
10	Diopside veins

RECENT

11	Sand and Detritus

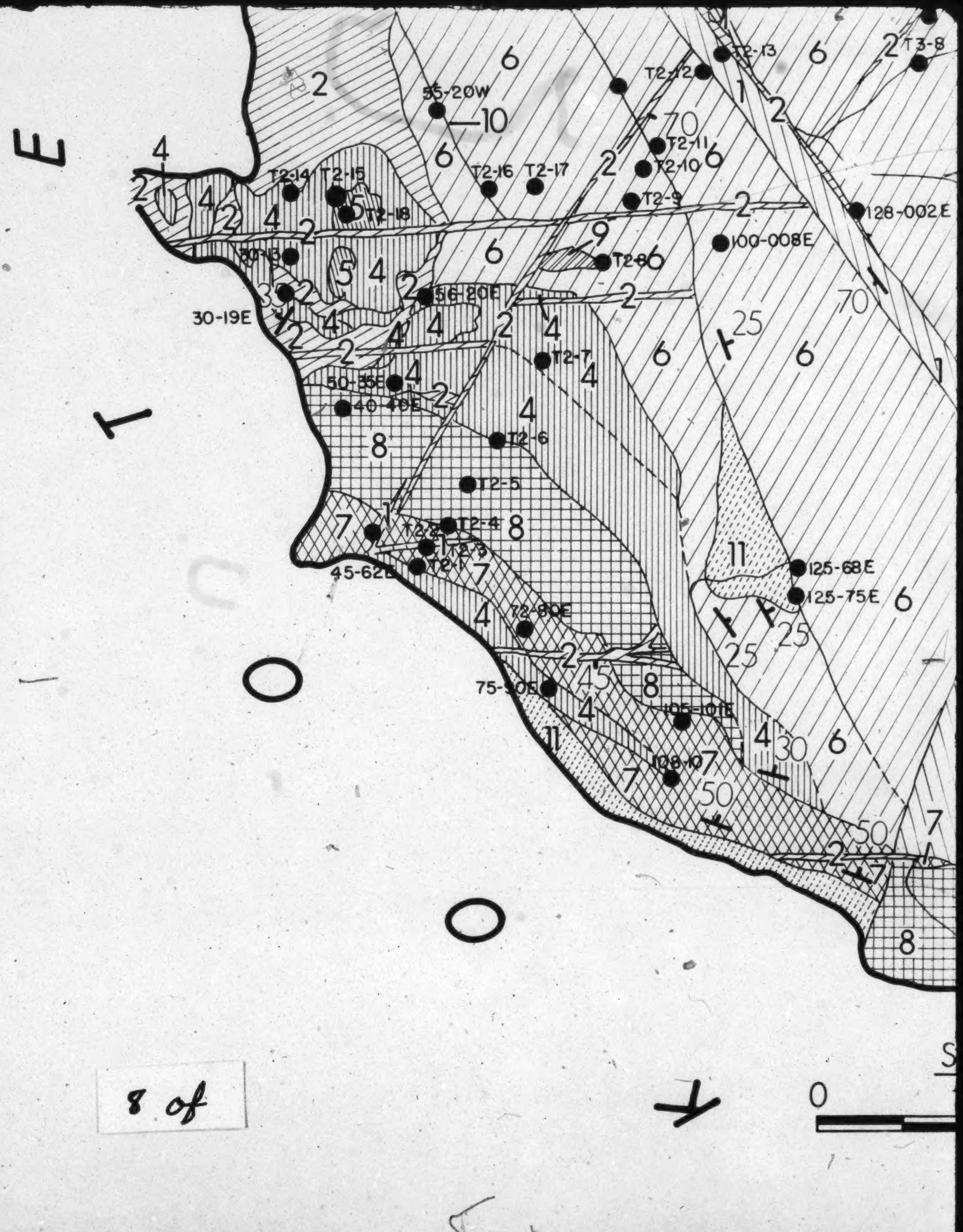
E
T
U
O
O
K
2
55-20W
10
6
T2-12
T2-13
T3-8
1
70
T2-11
T2-10
T2-14
T2-15
T2-16
T2-17
T2-18
T2-9
128-002E
100-008E
30-13
9
T2-8
56-20E
30-19E
25
T2-7
50-35E
40-40E
T2-6
T2-5
T2-4
T2-2
T2-3
T2-1
45-62E
125-68E
125-75E
72-80E
75-90E
45
105-101E
108-107
30
50
S
0
1
3
4
5
7
8
11

8 of

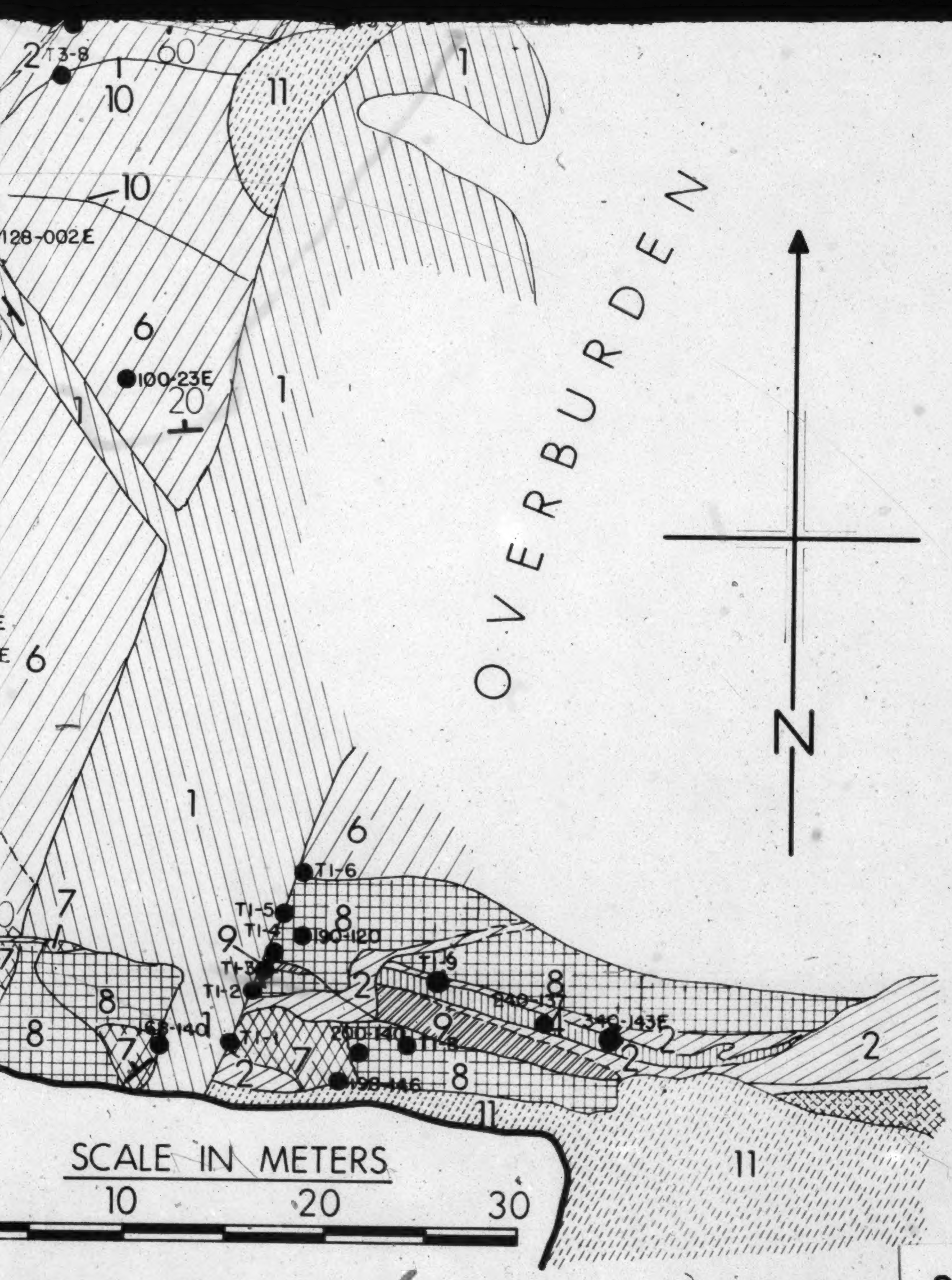
2
T3-8
60
1
10
11
1
10
128-002E
6
100-23E
20
1
OVERBURDEN
N
E
E 6
1
6
T1-6
7
T1-5
8
9
T1-4
190-120
T1-3
T1-2
T1-9
2
8
240-137
9
340-143E
7
8
8
7
168-140
T1-1
2
7
200-140
T1-8
2
2
2
198-146
8
11
11
SCALE IN METERS
10
20
30

9 of

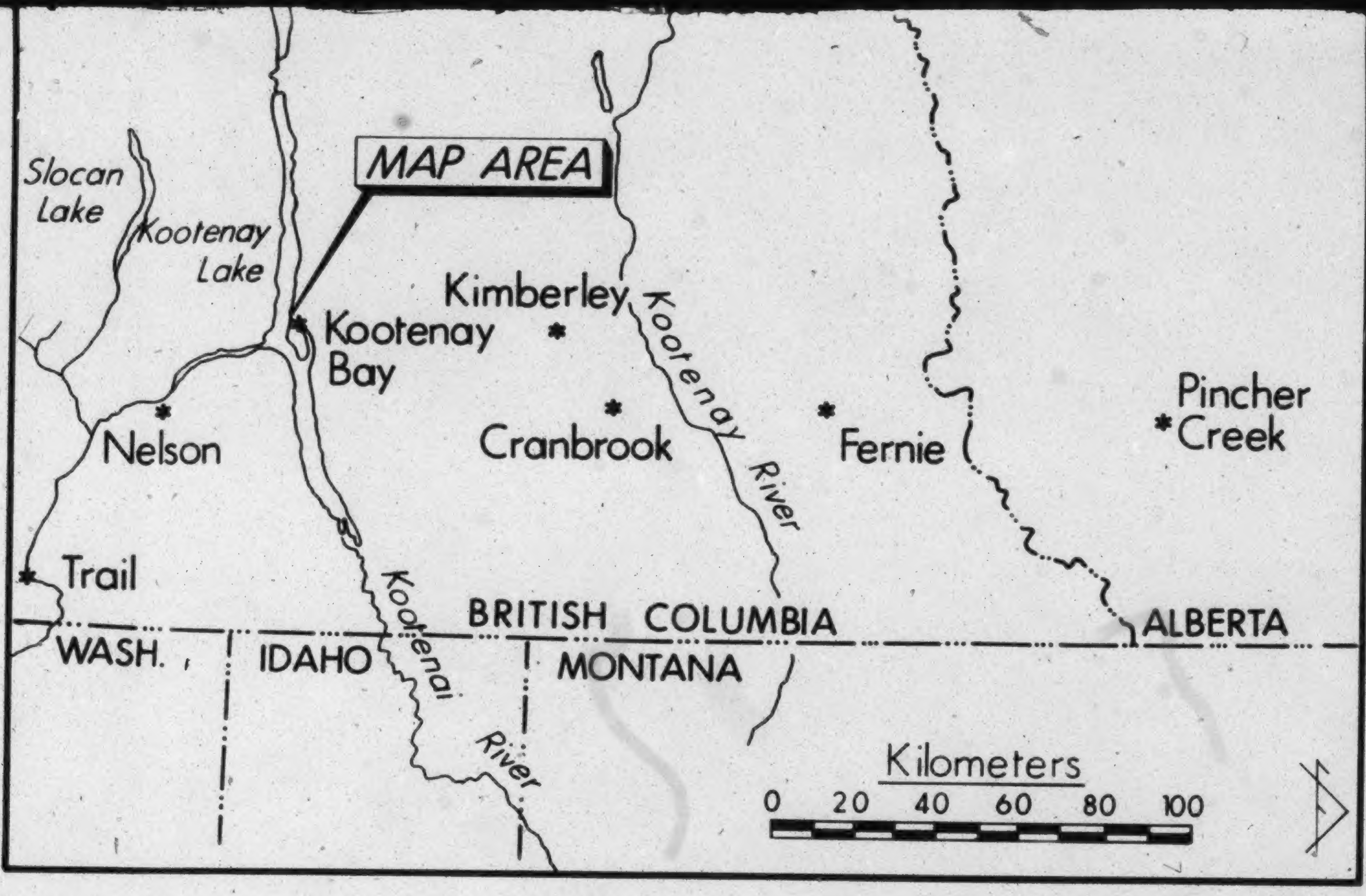
MAP AREA
Slocan Lake
Kootenay Lake
Kimberley
Kootenay Bay
Nelson
Cranbrook
Kootenay River
Fernie
Pincher Creek
Trail
Kootenai River
BRITISH COLUMBIA
ALBERTA
WASH.
IDAHO
MONTANA
Kilometers
0 20 40 60 80 100

METAMORPHIC

KOOTENAY BAY, BRITISH

FIGURE 3

10 of

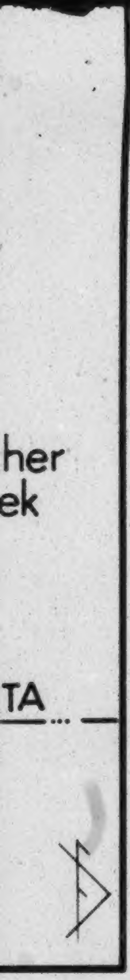

LARDEAU FORMATIO

▨ 5	Biotite Amphibolite ± Epidote
▨ 6	Marble (incl. Tr.- Di.- Phl.- Musc. & Talc)
▨ 7	Biotite - Tremolite - Diopside Gneiss
▦ 8	Biotite - Tremolite - Diopside - K - Feldspar Gneiss
▨ 9	Actinolite "Pegmatite"
☐ 10	Diopside veins

RECENT

▨ 11	Sand and Detritus

● Sample location

⤫ Dip and strike of bedding

C MAP

TISH COLUMBIA

11 of 11

1 of

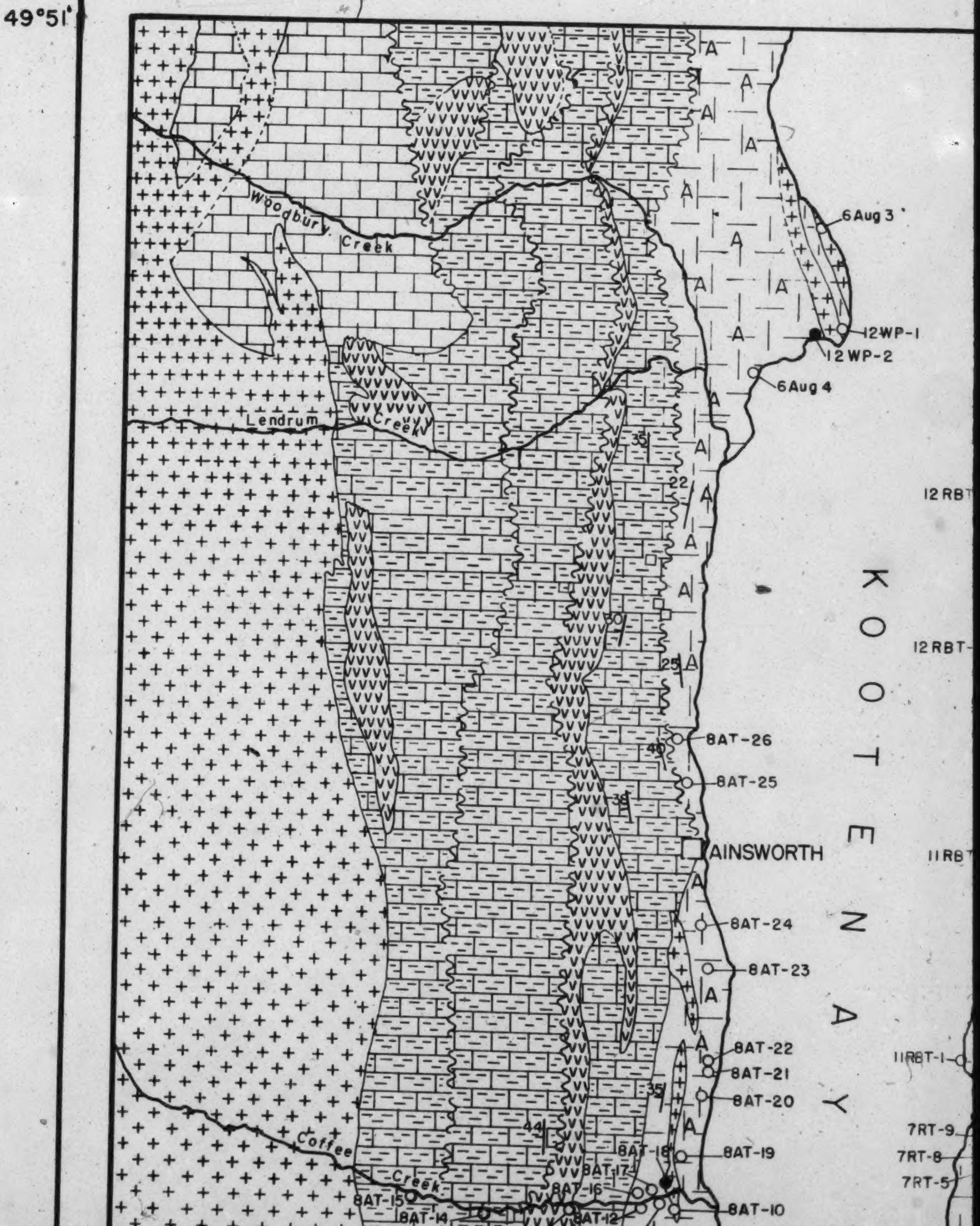
49°51'
Woodbury Creek
Lendrum Creek
Coffee Creek
KOOTENAY
AINSWORTH
6 Aug 3
12 WP-1
12 WP-2
6 Aug 4
12 RBT
12 RBT-
11 RB
11 RBT-1
7RT-9
7RT-8
7RT-5
8AT-26
8AT-25
8AT-24
8AT-23
8AT-22
8AT-21
8AT-20
8AT-19
8AT-18
8AT-17
8AT-16
8AT-15
8AT-14
8AT-12
8AT-10
35
22
30
25
40
38
35
44
A

2 of.

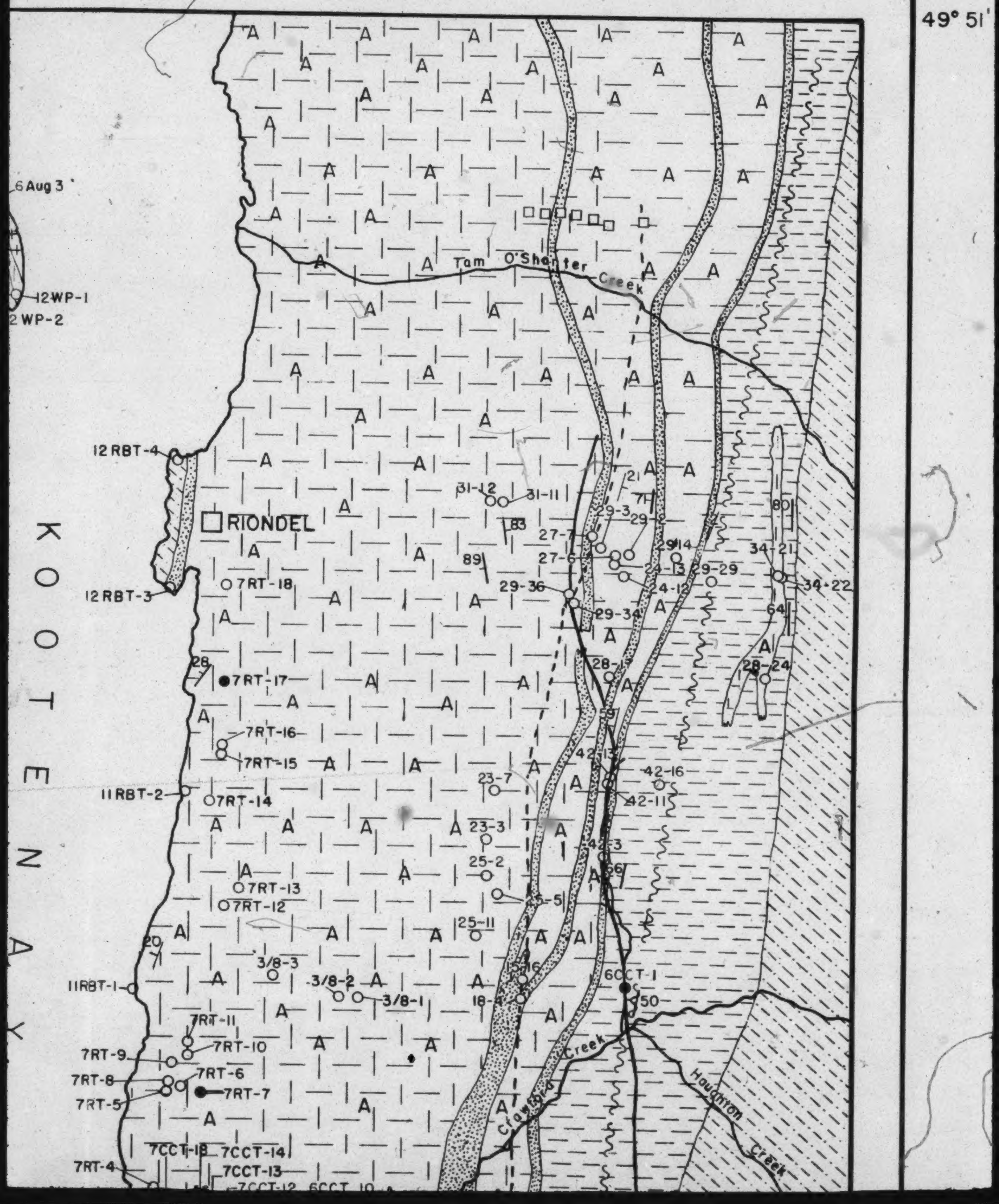
49° 51'
KOOTENAY
RIONDEL
Tam O'Shanter Creek
Crawford Creek
Houghton Creek
6 Aug 3
12WP-1
2WP-2
12RBT-4
12RBT-3
11RBT-2
11RBT-1
7RT-18
7RT-17
7RT-16
7RT-15
7RT-14
7RT-13
7RT-12
7RT-11
7RT-10
7RT-9
7RT-8
7RT-7
7RT-6
7RT-5
7RT-4
7CCT-18
7CCT-14
7CCT-13
7CCT-12
6CCT-10
6CCT-1
31-12
31-11
29-3
29-2
27-7
27-6
29-14
24-13
24-12
29-29
29-36
29-34
34-21
34-22
28-17
28-24
42-13
42-16
42-11
42-3
23-7
23-3
25-2
25-5
25-11
3/8-3
3/8-2
3/8-1
5-16
18-4
A
83
89
21
71
80
64
59
66
50
28
20

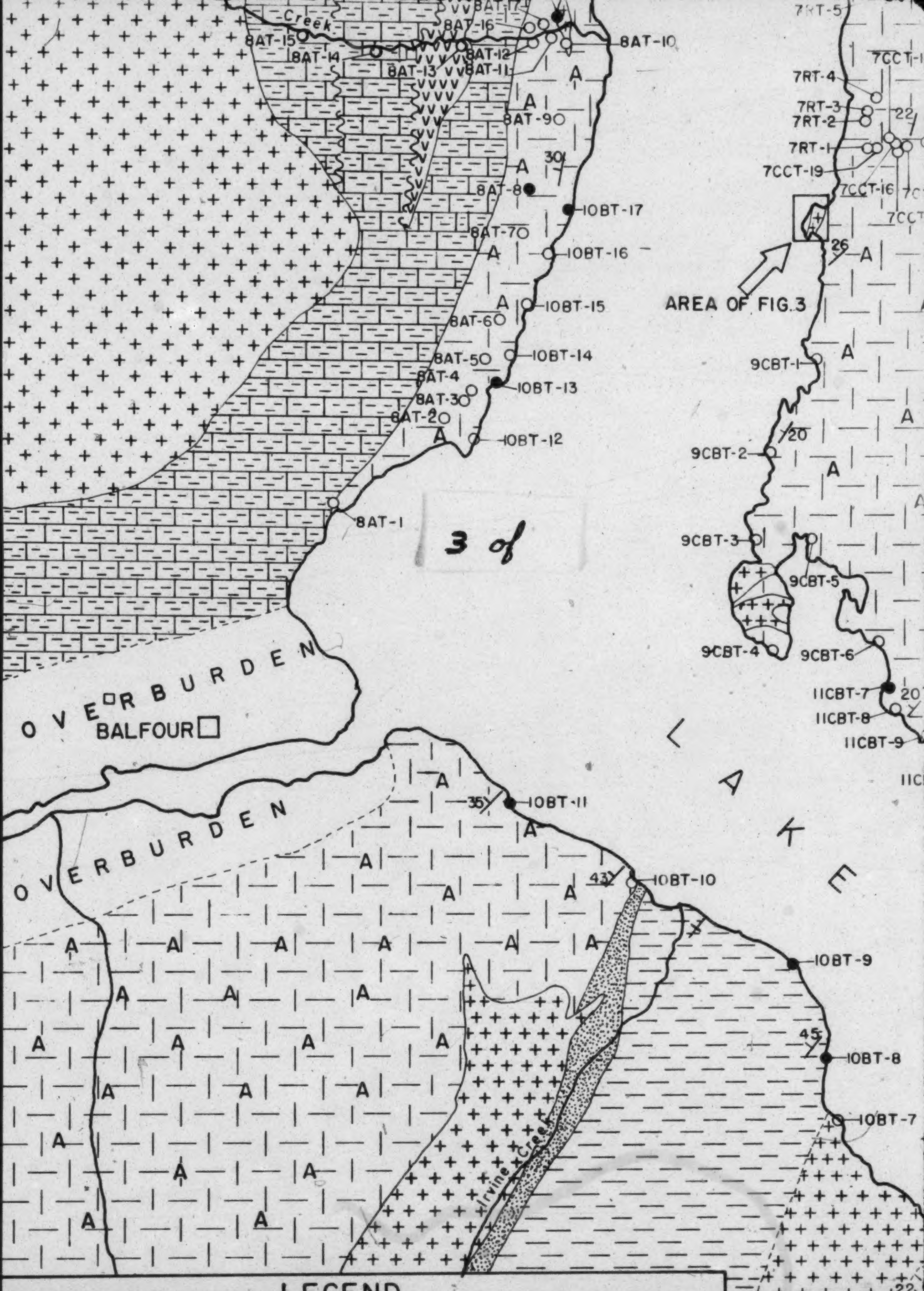
Creek
8AT-17
8AT-16
8AT-15
8AT-14
8AT-13
8AT-12
8AT-11
8AT-10
8AT-9
30
8AT-8
10BT-17
8AT-7
10BT-16
10BT-15
8AT-6
8AT-5
10BT-14
8AT-4
8AT-3
10BT-13
8AT-2
10BT-12
8AT-1
OVERBURDEN
BALFOUR
OVERBURDEN
35
10BT-11
43
10BT-10
10BT-9
45
10BT-8
10BT-7
Irvine Creek
A
7RT-5
7CCT-1
7RT-4
7RT-3
7RT-2
22
7RT-1
7CCT-19
7CCT-16
7CCT
26
AREA OF FIG. 3
9CBT-1
20
9CBT-2
9CBT-3
9CBT-5
9CBT-4
9CBT-6
11CBT-7
20
11CBT-8
11CBT-9
LAKE
22

3 of

LEGEND

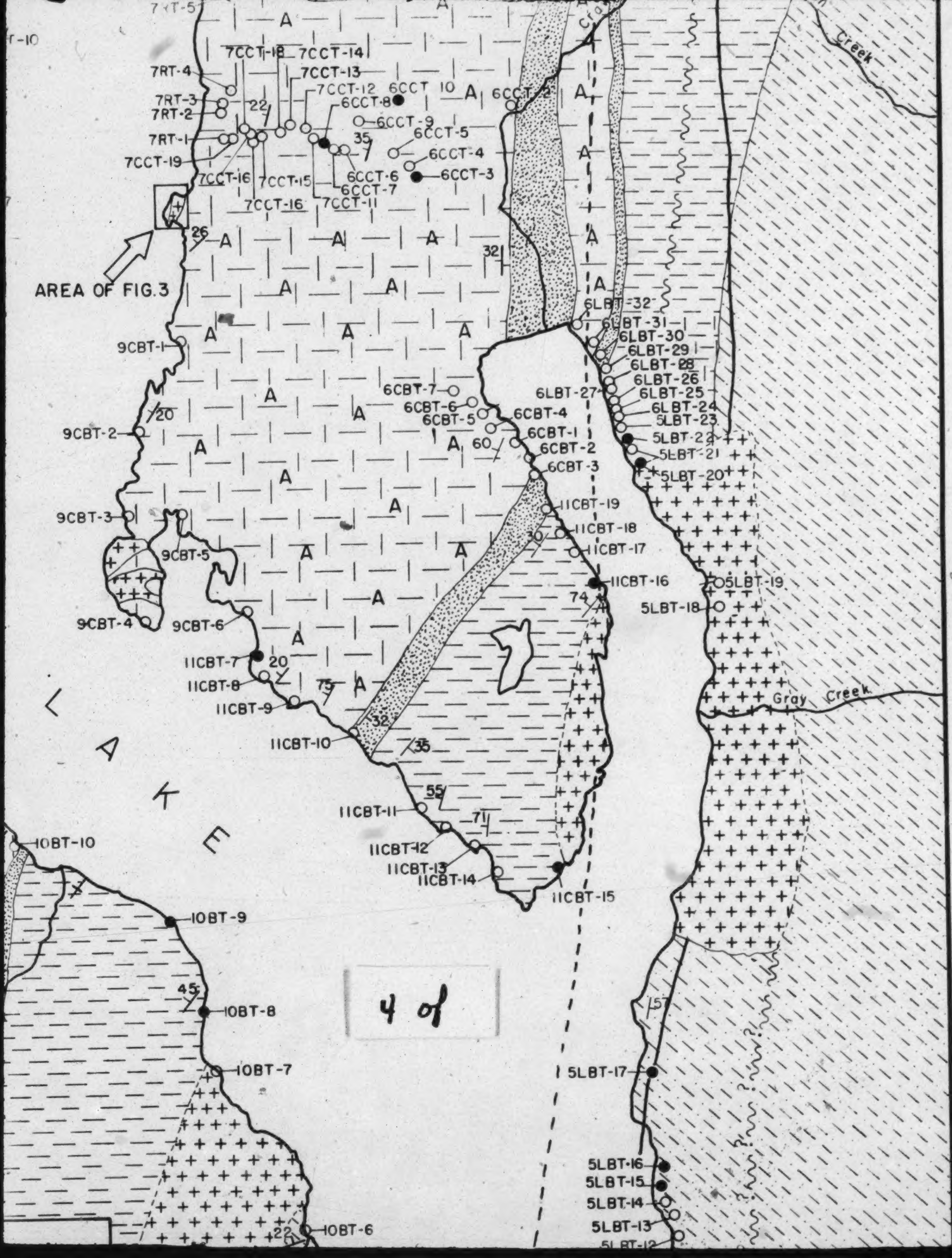

7RT-5
T-10
7CCT-18
7CCT-14
7CCT-13
7CCT-12
6CCT 10
6CCT-8
6CCT-9
6CCT-5
6CCT-4
6CCT-3
6CCT-2
6CCT-6
6CCT-7
7CCT-11
7CCT-15
7CCT-16
7CCT-19
7RT-4
7RT-3
7RT-2
7RT-1
22
35
26
32
AREA OF FIG.3
A
Creek
9CBT-1
9CBT-2
9CBT-3
9CBT-4
9CBT-5
9CBT-6
20
6CBT-7
6CBT-6
6CBT-5
6CBT-4
6CBT-1
6CBT-2
6CBT-3
60
6LBT-32
6LBT-31
6LBT-30
6LBT-29
6LBT-28
6LBT-27
6LBT-26
6LBT-25
6LBT-24
5LBT-23
5LBT-22
5LBT-21
5LBT-20
11CBT-19
11CBT-18
11CBT-17
11CBT-16
30
74
5LBT-19
5LBT-18
11CBT-7
11CBT-8
11CBT-9
11CBT-10
75
32
35
55
71
11CBT-11
11CBT-12
11CBT-13
11CBT-14
11CBT-15
Gray Creek
L A K E
10BT-10
10BT-9
45
10BT-8
10BT-7
10BT-6
22
57
5LBT-17
5LBT-16
5LBT-15
5LBT-14
5LBT-13
5LBT-12

4 of

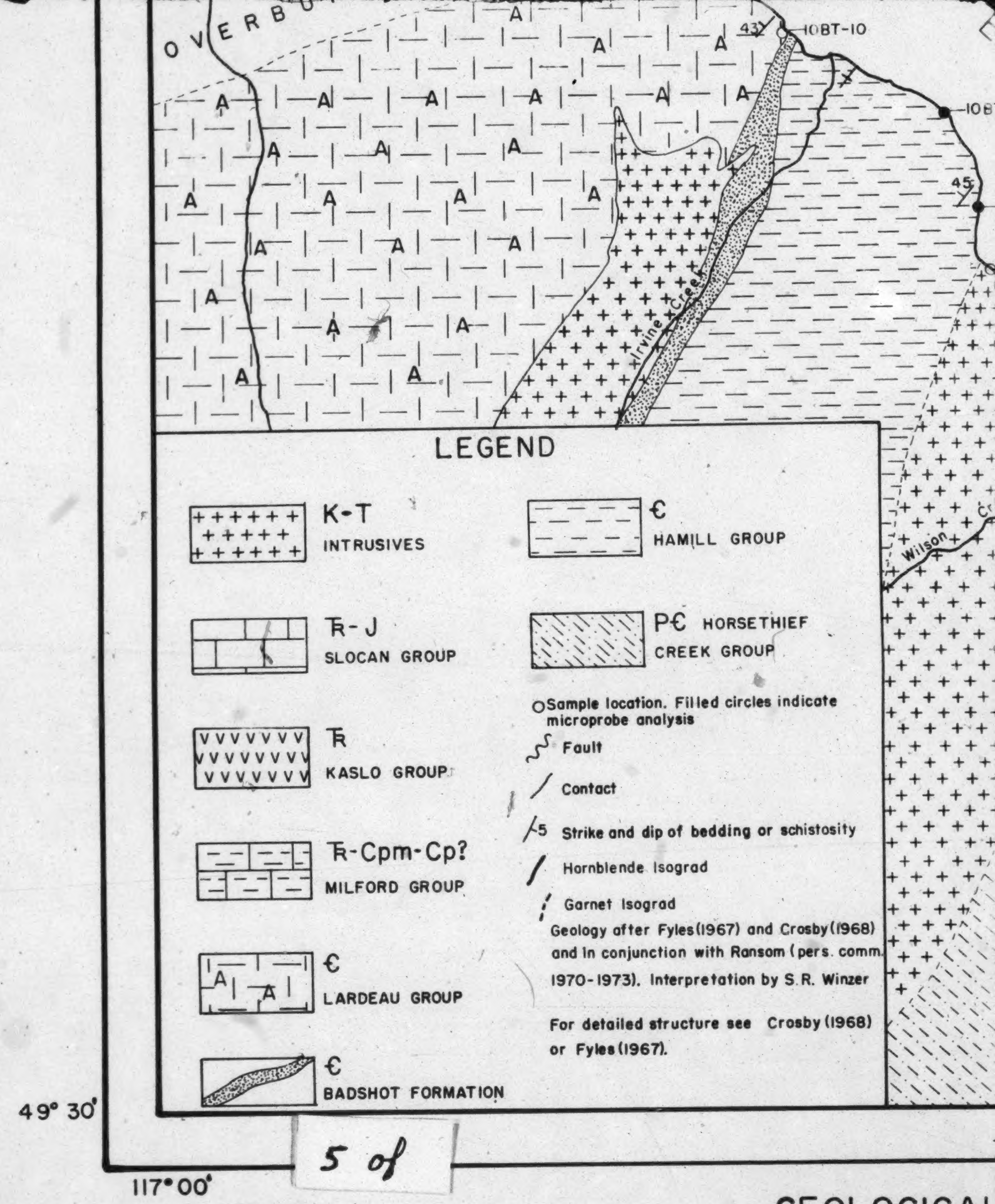
OVERBU
10BT-10
10B
43
45
Irvine Creek
Wilson
LEGEND
K-T INTRUSIVES
TR-J SLOCAN GROUP
TR KASLO GROUP
TR-Cpm-Cp? MILFORD GROUP
€ LARDEAU GROUP
€ BADSHOT FORMATION
€ HAMILL GROUP
P€ HORSETHIEF CREEK GROUP
○ Sample location. Filled circles indicate microprobe analysis
Fault
Contact
5 Strike and dip of bedding or schistosity
Hornblende Isograd
Garnet Isograd
Geology after Fyles (1967) and Crosby (1968) and in conjunction with Ransom (pers. comm. 1970-1973). Interpretation by S.R. Winzer
For detailed structure see Crosby (1968) or Fyles (1967).
49° 30'
117° 00'

5 of

GEOLOGICAL
of th
CENTRAL KOO

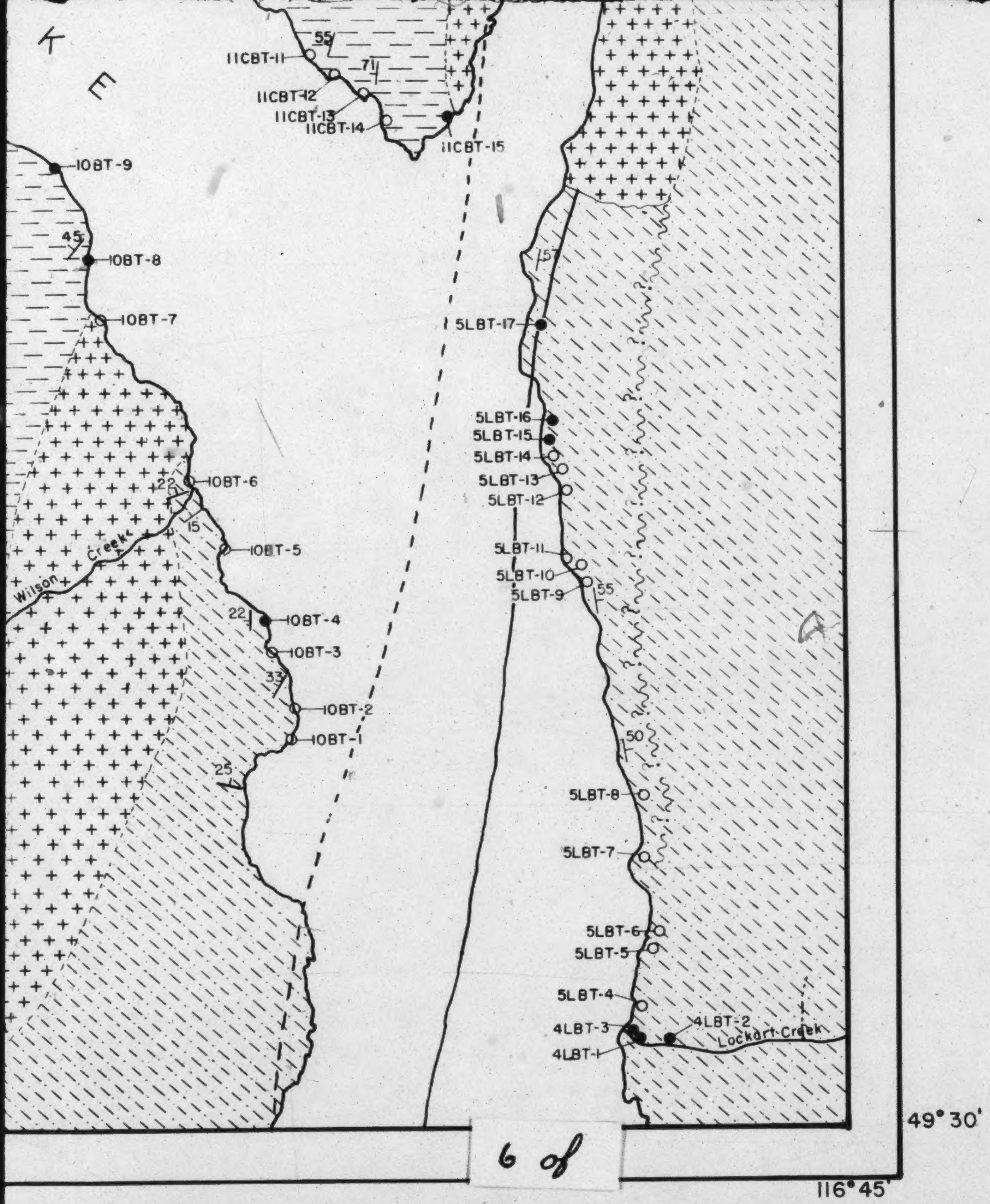
K
E
55
71
11CBT-11
11CBT-12
11CBT-13
11CBT-14
11CBT-15
10BT-9
45
10BT-8
10BT-7
22
10BT-6
15
Wilson Creek
10BT-5
22
10BT-4
10BT-3
33
10BT-2
10BT-1
25
57
5LBT-17
5LBT-16
5LBT-15
5LBT-14
5LBT-13
5LBT-12
5LBT-11
5LBT-10
5LBT-9
55
50
5LBT-8
5LBT-7
5LBT-6
5LBT-5
5LBT-4
4LBT-3
4LBT-2
4LBT-1
Lockart Creek
49° 30'
116° 45'
T.N.

6 of

GICAL MAP

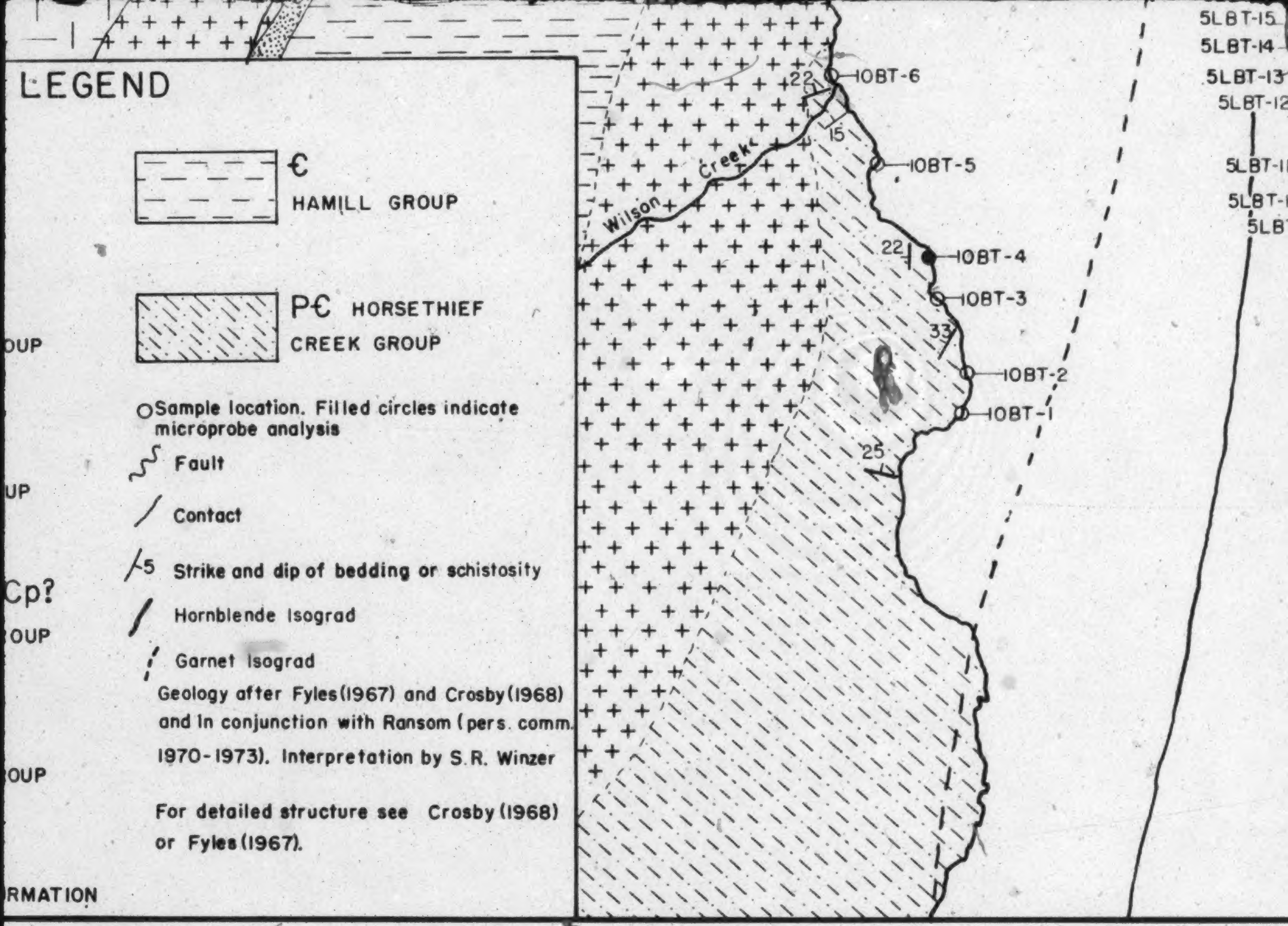
LEGEND
€
HAMILL GROUP
P€ HORSETHIEF CREEK GROUP
○ Sample location. Filled circles indicate microprobe analysis
Fault
Contact
5 Strike and dip of bedding or schistosity
Hornblende Isograd
Garnet Isograd
Geology after Fyles (1967) and Crosby (1968) and in conjunction with Ransom (pers. comm. 1970-1973). Interpretation by S.R. Winzer
For detailed structure see Crosby (1968) or Fyles (1967).
OUP
UP
Cp?
OUP
OUP
RMATION
Wilson Creek
22
15
22
33
25
10BT-6
10BT-5
10BT-4
10BT-3
10BT-2
10BT-1
5LBT-15
5LBT-14
5LBT-13
5LBT-12
5LBT-11
5LBT-1
5LBT

GEOLOGICAL MAP
# of the
CENTRAL KOOTENAY ARC
BRITISH COLUMBIA

SCALE 1:50,000

1000 0 1000 2000 3000 4000

METERS

T.N.

21° 43' M.N.

FIGURE 2

7 of 7

THE UNIVERSITY OF ALBERTA

METAMORPHISM AND CHEMICAL EQUILIBRIUM IN SOME ROCKS FROM THE CENTRAL KOOTENAY ARC

by

© STEPHEN R. WINZER

A THESIS

SUBMITTED TO THE FACULTY OF GRADUATE STUDIES AND RESEARCH

IN PARTIAL FULFILMENT OF THE REQUIREMENTS FOR THE DEGREE

OF DOCTOR OF PHILOSOPHY

Department of Geology

EDMONTON, ALBERTA

FALL, 1973

THE UNIVERSITY OF ALBERTA

FACULTY OF GRADUATE STUDIES AND RESEARCH

The undersigned certify that they have read, and recommend to the Faculty of Graduate Studies and Research for acceptance, a thesis entitled 'Metamorphism and Chemical Equilibrium in Some Rocks from the Central Kootenay Arc' submitted by Stephen Randolph Winzer in partial fulfillment of the requirements for the degree of Doctor of Philosophy.

R St J Lambert
....
Supervisor

H. Baadsgaard
....
Supervisor

G.L. Cumming
....

....

Bernard W. Evans
....
External Examiner

Date 24 Sept 1973

ABSTRACT

Earlier hypotheses concerning the type and degree of metamorphism in a portion of the central Kootenay Arc are revised in the light of new data. Electron microprobe analyses of micas, amphiboles, clinopyroxenes, carbonates, feldspars, scapolite, epidote, garnet, staurolite and sphene from metamorphic rocks are presented. Chemical analyses were obtained on all rocks from which mineral analyses were taken, allowing discussion of controls on mineral composition by bulk rock composition. Mineral analyses from lower to higher grade allow systematic changes in mineral composition with grade to be evaluated, and reactions resulting in widespread assemblages to be discussed. The following reactions can be shown to occur in rocks from the central Kootenay Arc:

1) 2Phengite + high Mg/Fe chl + 5qtz → bi + lower Mg/Fe chl + less phengitic mu + XH_2O

2) Phengitic mu + 1.33chl + cc + 2.65qtz + 2ilm or mt → bi + gnt + 0.16 calcic plag + CO_2 + XH_2O.

3) 2Fe-ep + 0.16Al-act + 1.20 low An plag + 0.71 ilm → Al-ep + hb + higher An plag + 0.70 sph + 0.20 Ab + 1.50 qtz

4) Fe-ep + 0.75 chl + 0.60 low An plag + 2cc → Al-ep + hb + 2.50 qtz + $2CO_2$ + XH_2O

5) Tr + 3cc + 2qtz → 5di + $3CO_2$ + H_2O

6) 5Dol + 8qtz + H_2O → Tr + 3cc + $7CO_2$

Reaction 2 defines the garnet isograd and takes place at about 430°C. Reactions 3 and 4 define the hornblende isograd and take place at slightly lower temperatures. Reactions 1 and 2 may take place simultaneously in areas smaller than a thin section, as may reactions 5 and

6. Reaction 5 takes place at temperatures equivalent to those of the hornblende isograd in rocks of suitable composition. Temperatures did not exceed 530°C in the highest grade rocks.

K and Na can be shown to be mobile during formation of metamorphic mineral assemblages from carbonate-rich rocks, calc-silicates and amphibolites. The reactions take place under varying conditions of f_{O_2}, P_{CO_2} and P_{H_2O}. P_{CO_2} behaves as an inert or initial value component in carbonate-rich rocks.

Detailed work on a small area at the highest grade indicates that chemical equilibrium was not attained. Eleven biotite-amphibole pairs were analyzed for trace elements Ga, Li, Cr, Cu, Co, Ni, Mn, Rb, Sr and Ba as well as major elements. An additional 12 pairs were analyzed for major elements including Mn. Rb/Sr and K-Ar isotopic analyses were also carried out. Fe and Ti are not equilibrated between hornblende-biotite pairs, while Mg closely approaches equilibrium. Cu, Co, Ni, Zn, Ga, Li, Rb and Ba are not equilibrated, based on partition studies. Mn, Cr and Sr appear to closely approach equilibrium in most of the eleven pairs. Disequilibrium results from incompleted reactions in systems open to K, Na and possibly Si and Al.

Ten K-Ar ages were obtained from biotites on which trace element analyses were performed. They yield a mean age of 52 ± 3 my and spread in age from 47 to 57 my. The eleven biotite-hornblende pairs were analyzed for Rb and Sr isotopes. An age of 48 ± 3 my was obtained from one pair thought to represent complete recrystallization of the minerals. This age is in good agreement with the K-Ar ages. Rb/Sr "isochrons" for the eleven pairs analyzed indicate incomplete homogenization of isotopes resulting from overprinting and lack of equilibration. The age pattern indicates overprinting of an earlier Jurassic (?) metamorphism by a later event occurring between 50 and 70 my ago.

The Kootenay Arc has a long metamorphic history, beginning with Precambrian and Paleozoic sedimentation in a continental margin shelf-slope-rise sequence. The first metamorphic event occurred during the Jurassic (?), but its character is uncertain. Further metamorphism occurred between 50 and 70 my ago, and is characterized in the central portion of the Kootenay Arc by a high pressure intermediate temperature facies series lying between Barrovian and Glaucophane schist. Although the development of the Kootenay Arc can be related to the movement of the North American plate from Triassic to present time, evidence does not support placement of a subduction zone in the region occupied by the Kootenay Arc.

ACKNOWLEDGMENTS

I would like to thank my major advisors, Dr. H. Baadsgaard and Dr. R. St. J. Lambert for their assistance on this project and for their encouragement and discussion of the ideas developed during the period it was undertaken. I am grateful to Dr. R. A. Burwash for suggesting the study area and for providing a suite of samples. Dr. D. G. W. Smith kindly provided the microprobe facilities, which are supported by N.R.C. Grant No. 554648. Dr. T. O. Frisch provided some standards and helpful discussion during the period when electron microprobe analyses were carried out, for which I am grateful.

I would like to acknowledge the help of D. Tomlinson, who introduced me to the microprobe and especially that of R. Bliss, who spent weekends and evenings in assistance above and beyond the call of duty. I would like to thank A. Stelmach for analyses on rock standards used in this work and S. Van Kessel for the Ni determinations. XRF raw data on whole rocks were done by Dr. J. G. Holland, Durham University, for which thanks are given. I would like to thank P. Ransom of Cominco, Ltd. for many helpful discussions and for making available his maps and specimens.

This work was carried out while tenuring an N.R.C. Predoctoral Scholarship and a University of Alberta Dissertation Fellowship. Further assistance was provided by a University of Alberta Teaching Assistantship.

I would like to thank especially my wife, Kathleen, for her support during the course of this work and for the typing and proofreading of this thesis.

I am indebted to all of the persons mentioned above. All errors and interpretations within this thesis are my own.

TABLE OF CONTENTS

PAGE

ABSTRACT iv
vi

ACKNOWLEDGMENTS vii

LIST OF TABLES xii

LIST OF FIGURES xiv

CHAPTER I 1

- Statement of the Problem 1
- Geologic Setting 2
- Lithologies 5
  - Precambrian Horsethief Creek Group 5
  - Cambrian Hamill Group 5
  - Cambrian Badshot Formation 7
  - Lardeau Group 8
  - Milford Group 9
  - Kaslo Group 10
  - Slocan Group 10
  - Intrusive Rocks 11
- Structure 12

CHAPTER II WHOLE ROCK CHEMISTRY AND METAMORPHIC MINERALOGY . . . 15

- Introductory Statement 15
- Sampling Procedure 16
- Whole Rock Chemistry 18
- Metamorphic Mineralogy 33
  - Muscovite 33
  - Biotite 43
    - General Chemistry 45
    - Y-Site Cations 54
    - Z-Site Cations 58
    - X-Site Cations 58
    - Anions 62
    - Biotite Composition in Relation to Bulk Chemistry. . . 62
    - Summary 68
  - Chlorite 68
  - Amphiboles 70
  - Pyroxene 87
  - Epidote 94
  - Feldspar 99
    - Potassium Feldspar 105
    - Plagioclase 105
  - Scapolite 109
  - Carbonates 116
  - Sphene, Staurolite and Garnet 122

PAGE

CHAPTER III METAMORPHIC PETROLOGY 133

Muscovite 136
Biotite 145
Chlorite 151
Amphiboles 152
Pyroxene 156
Epidote 158
Plagioclase 160
Carbonate 163
Garnet 166
Phase Relations and Metamorphic Reactions 168
Status of CO_2 183
Status of Oxygen 185
Pressure-Temperature Conditions of Metamorphism in the Central Kootenay Arc 186

CHAPTER IV 189

Chemical and Isotopic Equilibrium 189
Application of the Phase Rule 191
Partition Studies 193
Partitioning of Major and Minor Elements 200
    Iron 200
    Magnesium 202
    Manganese 204
    Titanium 206
    Aluminum 207
Trace Elements 209
    Gallium 209
    Lithium 209
    Nickel 212
    Chromium 212
    Cobalt 214
    Zinc 214
    Copper 217
    Barium 217
    Rubidium 220
    Strontium 222
Bearing of Trace Element Partitioning on Chemical Equilibrium 225
Isotope Geology 232
    K-Ar 232
    Rb-Sr 236

CHAPTER V GENERAL CONCLUSIONS REGARDING THE DEVELOPMENT OF THE KOOTENAY ARC 243

REFERENCES CITED 250

PAGE

APPENDIX 1 264

Electron Probe Microanalysis 264
Whole Rock Analyses 272

APPENDIX 2 TRACE ELEMENT AND ISOTOPIC ANALYSIS 279

K-Rb Procedure 279
Sr Procedure 280
Ba Procedure 280
Argon Procedure 281
Errors 281
Co, Cu, Zn, Cr, Mn, Li, Ga, Ni Separations and Determination 281
K_2O in Biotite, a note 284

APPENDIX 3 ASSEMBLAGES FROM REGIONAL METAMORPHIC ROCKS EXCLUSIVE OF THOSE LISTED IN TABLE 3 287

APPENDIX 4 ZONED AMPHIBOLES FROM THE CENTRAL KOOTENAY ARC, BRITISH COLUMBIA . . 298

LIST OF TABLES

		Page
Table 1.	XRF whole-rock semi-quantitative analyses-Kootenay Point, B.C.	19
Table 2.	Chemical analyses of regional metamorphic rocks.	22
Table 3.	Modal analyses of regional metamorphic rocks based on 1200 counts/section.	25
Table 4.	Modal analyses of metamorphic rocks from Kootenay Point based on 1200 counts/section.	27
Table 5.	Electron microprobe analyses of muscovites from regional metamorphic rocks.	36
Table 6.	Electron microprobe analyses of biotites from regional metamorphic rocks.	46
Table 7.	Electron microprobe analyses of biotites from Kootenay Point.	48
Table 8.	Electron microprobe analyses of chlorites from regional metamorphic rocks.	69
Table 9.	Electron microprobe analyses of amphiboles from Kootenay Point.	73
Table 10.	Electron microprobe analyses of amphiboles from regional metamorphic rocks.	76
Table 11.	Electron microprobe analyses of pyroxene from regional metamorphic rocks.	90
Table 12.	Electron microprobe analyses of pyroxene from Kootenay Point.	91
Table 13.	Electron microprobe analyses of epidotes.	96
Table 14.	Partial electron microprobe analyses of feldspar, Kootenay Point, B.C.	100
Table 15.	Electron microprobe analyses of feldspar from regional metamorphic rocks.	101
Table 16.	Electron microprobe analyses of scapolite from Kootenay Point.	111

Table 17.	Electron microprobe analyses of carbonates from Kootenay Point, B.C.	119
Table 18.	Electron microprobe analyses of calcite - regional metamorphic rocks.	120
Table 19.	Electron microprobe analyses of sphene and staurolite.	123
Table 20.	Electron microprobe analyses of garnet.	126
Table 21.	Trace element concentration (PPM) in mineral pairs from Kootenay Point.	196
Table 22.	Rb-Sr isotopic data.	197
Table 23.	K-Ar isotopic data for micas from Kootenay Point.	199
Table A-1.	Standards used in microprobe analyses.	267
Table A-2.	Repeat analyses of EPS 21-1, using EPS 21-2 as a standard.	268
Table A-3.	Standards used in electron microprobe analyses of regional metamorphic minerals.	269
Table A-4.	Standards used in electron microprobe analyses of minerals from Kootenay Point.	270
Table A-5.	General analytical error ranges in the microprobe mineral analyses.	273
Table A-6.	XRF analyses and wet chemical analyses of four selected rocks from Kootenay Point.	275
Table A-7.	Rock composition by modal analysis, after the method of Friedman (1960).	278
Table A2-1.	Analytical results for standards G-1 and W-1.	285
Table A2-2.	Comparison of K_2O in biotite analyzed by isotope dilution and by electron microprobe.	286

LIST OF FIGURES

		Page
Figure 1.	Index map.	3
Figure 2.	Geological map of the central Kootenay Arc, British Columbia (in pocket).	
Figure 3.	Geological map of Kootenay Point (in pocket).	
Figure 4.	ACF plot for rocks from Kootenay Point.	30
Figure 5.	ACF and AFK plots for regional metamorphic rocks.	32
Figure 6.	Portion of the AFM diagram for muscovites from regional metamorphic rocks.	38
Figure 7.	AKF plot for muscovites from regional metamorphic rocks.	40
Figure 8.	Plot of Na_2O rock against Na_2O muscovite.	41
Figure 9.	Plot of FeO muscovite against FeO rock.	42
Figure 10.	AFM plot for biotites from regional metamorphic rocks.	52
Figure 11.	AFM plot for biotites from Kootenay Point.	53
Figure 12.	Y-site occupancy (Σoct) against Mg (calculated on the basis of 22 (O)) for all biotites.	55
Figure 13.	a. Al^{IV}(%) against Fe (%), all biotites. b. Al^{IV}(%) against Mg (%), all biotites. c. Al^{IV}(%) against Fe/Fe + Mg, all biotites.	56
Figure 14.	a. Al^{VI}(%) against Al^{IV}(%), all biotites. b. Al^{VI}(%) against Ti (%), all biotites c. Al^{IV}(%) against Ti (%), all biotites	57
Figure 15.	Mg/Al plotted against Si (%), for all biotites analyzed.	59
Figure 16.	Al^{VI} plotted against Si calculated on the basis of 22 oxygens, all biotites analyzed.	60
Figure 17.	K_2O (%) plotted against SiO_2 (%), for all biotites analyzed.	61
Figure 18.	F + Cl (%) against SiO_2 (%), for all biotites analyzed.	63

Figure 19. a. Mg/Fe biotite against Mg/Fe rock for biotites from Kootenay Point. 64
b. Mg/Fe biotite against Mg/Fe rock for biotites from regional metamorphic rocks.

Figure 20. a. Mg/Al biotite against Mg/Al rock for biotites from Kootenay Point 65
b. Mg/Al biotite against Mg/Al rock for biotites from regional metamorphic rocks.

Figure 21. a. TiO_2 biotite against TiO_2 rock for biotites from Kootenay Point. 67
b. TiO_2 biotite against TiO_2 rock for biotites from regional metamorphic rocks.

Figure 22. AFM diagram for chlorites from regional metamorphic rocks. 71

Figure 23. A-site occupancy against tetrahedral Al for all amphiboles analyzed. 79

Figure 24. Classification of analyzed amphiboles. 81

Figure 25. Octahedral Al plotted against tetrahedral Al for all amphiboles analyzed. 83

Figure 26. a. Fe/Fe + Mg rock against Fe/Fe + Mg amphibole for amphiboles from Kootenay Point. 85
b. Fe/Fe + Mg rock against Fe/Fe + Mg amphibole for amphiboles from regional metamorphic rocks.

Figure 27. a. FeO (%) amphibole against FeO (%) rock for amphiboles from Kootenay Point. 86
b. MgO % amphibole against MgO % rock for amphiboles from regional metamorphic rocks.

Figure 28. a. TiO_2 amphibole against TiO_2 rock for amphiboles from Kootenay Point. 88
b. TiO_2 amphibole against TiO_2 rock for amphiboles from regional metamorphic rocks.

Figure 29. The pyroxene quadrilateral, after Deer et al. (1966). 93

Figure 30. Fe/Fe + Mg pyroxene plotted against Fe/Fe + Mg rock for all pyroxenes analyzed. 95

Figure 31. Ab-An-Or triangular plot for feldspars from Kootenay Point. 106

Figure 32. Ab-An-Or triangular plot for feldspars from regional metamorphic rocks. 107

Figure 33. 113
- a. Si atoms plotted against Ca atoms for all scapolites analyzed.
- b. Si atoms plotted against Na + K atoms for all scapolites.
- c. Cl atoms plotted against Ca atoms for all scapolites.
- d. C + S atoms plotted against Ca atoms for all scapolites.

Figure 34. Zoning trends for 7RT-17, a Type I garnet. 130

Figure 35. 131
- a. Zoning trends for 12WP-2a, a Type II garnet.
- b. Zoning trends for a smaller Type II garnet from 12WP-2a.

Figure 36. Zoning trends for 11CBT-16, a Type III garnet. 132

Figure 37. Mg (structural) plotted against Na (structural) for muscovites from regional metamorphic rocks. 138

Figure 38. Si (structural) in muscovites from regional metamorphic rocks plotted against comparison ranges from Cipriani *et al*. (1971). 139

Figure 39. Si (structural) against Na (structural) for muscovites from regional metamorphic rocks. 140

Figure 40. Plot of FeO (%) against Al_2O_3 (%) for muscovites from regional metamorphic rocks (after Butler, 1967) 142

Figure 41. 148
- a. FeO % against grade index, biotites from regional metamorphic rocks
- b. MgO % against grade index, biotites from regional metamorphic rocks.
- c. Mg/Fe ratio plotted against grade index, biotites from regional metamorphic rocks.
- d. TiO_2 (%) against grade index, biotites from regional metamorphic rocks.

Figure 42. Fe/Fe + Mg (rock) plotted against grade index, regional metamorphic rocks. 149

Figure 43. Al total (structural) plotted against Fe/Fe + Mg for amphiboles from regional metamorphic rocks. 154

Figure 44. Fe/Fe + Mg pyroxene plotted against grade index for pyroxenes from regional metamorphic rocks. 157

Figure 45. Plot of plagioclase composition (An content) against grade index for all plagioclases from regional metamorphic rocks and rocks from the Point. 161

Figure 46. Unique polybaric curve for magnesian calcite coexisting with dolomite, after Goldsmith and Newton (1969) 165

Figure 47. Phase relations for calcareous and noncalcareous pelites from chlorite (?) through garnet zones. 170

Figure 48. Phase relations for rocks containing kyanite and staurolite from Woodbury Point. 171

Figure 49.
- a. Partition diagram for Fe. 201
- b. Al^{IV} amphibole/Al^{IV} biotite plotted against $K_D\text{Fe}^{\text{Amph-Bi}}$.

Figure 50. Partition diagram for Mg. 203

Figure 51.
- a. Partition diagram for Mn from microprobe analyses. 205
- b. PPM Mn plotted against PPM Mn amphibole from bulk samples.
- c. Partition diagram for Mn from bulk samples.

Figure 52.
- a. Partition diagram for Ti. 208
- b. Al^{IV} amphibole/Al^{IV} bi plotted against $K_D\text{Ti}^{\text{Amph-Bi}}$.

Figure 53.
- a. Partition diagram for Ga. 210
- b. PPM Ga biotite plotted against PPM Ga amphibole.

Figure 54. PPM Li biotite plotted against PPM Li amphibole 211

Figure 55. a. PPM Ni (both amphiboles and biotites) plotted against PPM Mg x 10^3 for amphiboles and biotites. 213
b. Partition diagram for Ni.

Figure 56. a. PPM Cr biotite against PPM Cr amphibole. 215
b. Partition diagram for Cr.

Figure 57. PPM Co biotite against PPM Co amphibole. 216

Figure 58. PPM Zn biotite plotted against PPM Zn amphibole. 218

Figure 59. a. PPM Cu biotite plotted against PPM Cu amphibole. 219
b. Partition diagram for Cu.

Figure 60. Partition diagram for Ba. 221

Figure 61. a. Partition diagram for Rb. 223
b. PPM Rb biotite plotted against PPM Rb amphibole.

Figure 62. a. PPM Sr biotite plotted against PPM Sr amphibole. 224
b. Partition diagram for Sr.

Figure 63. K_2O (circles) and Na_2O (triangles) in weight percent plotted against SiO_2 for rocks from Kootenay Point. 228

Figure 64. a. Histogram plot of K-Ar ages from igneous rocks from the Kootenay Arc. 233
b. Histogram plot of K-Ar ages for metamorphic minerals from the Kootenay Arc.

Figure 65. Rb-Sr "isochron" plot for mineral pairs from Kootenay Point. 238

Figure A2-1. Extraction procedure for trace elements from biotites and amphiboles. 283

CHAPTER I

STATEMENT OF THE PROBLEM

Two major problems are discussed in this thesis. The problems are interrelated, but for purposes of clarity they will be dealt with separately. The first problem concerns the conditions of metamorphism in the central Kootenay Arc of British Columbia and stems from the original aim of this project to investigate the nature of chemical equilibrium in rocks of medium metamorphic grade.

For the last 75 years it has been known that metamorphic rocks of medium and perhaps higher grade crop out in a rather narrow band on the east and west sides of the central portion of Kootenay Lake. Crosby (1968) discusses these rocks and has placed Barrovian isograds on his geological map. Fyles (1967) has done similar work in the area of Ainsworth on the west side of the lake. Regional reconnaissance by this author in 1970 revealed several inconsistencies in the previous work. An expanded regional study was undertaken to better define the type and degree of metamorphism in the area, particularly with respect to reaction isograds and stably coexisting assemblages. Several lithologies are present in the region studied. The lithologic variation complicates clarification of the metamorphic relationships, but intensive chemical study of the Kootenay rocks has provided a somewhat clearer interpretation.

The question of chemical equilibrium in rocks from the medium grade portion of the central Kootenay Arc comprises the second part of this thesis. Discussions of metamorphic petrogenesis have long been dominated by an essentially static approach to the question of metamorphic reactions and phase assemblages. For the most part, regional metamorphic terrains have been viewed as closed systems in which chemical equilibrium has been attained or closely approached in all phases present. This interpretation has allowed the use of the phase rule of Gibbs to construct essentially static diagrams of stably coexisting minerals in a rock system. More recent work, especially with the electron microprobe, has turned up several inconsistencies within the older model. Garnets and amphiboles, as well as feldspars and epidote, have been shown to be zoned. Some studies of trace elements show that contiguous coexisting minerals are out of equilibrium with each other for some elements but not for others. Other work has indicated that there are domains of equilibrium, and that these may be very small. Isotopic studies indicate that models involving incomplete equilibration may be proposed for some metamorphic terrains.

The second half of this thesis discusses and tries to quantify the degree of equilibrium or disequilibrium in a small, chemically diverse section of the Arc. To this end major, minor and trace element mineral chemistry, Rb/Sr and K/Ar isotope data, whole rock chemistry and more classical methods in petrography and petrology have been applied to carefully selected rocks from this section.

GEOLOGIC SETTING

The Kootenay Arc is a narrow band of highly deformed Precambrian, Paleozoic and Mesozoic rocks stretching from Revelstoke, British Columbia, southeast, south and southwest to Washington state (Fig. 1). The Arc may extend for more than 100 km into the state of Washington, but

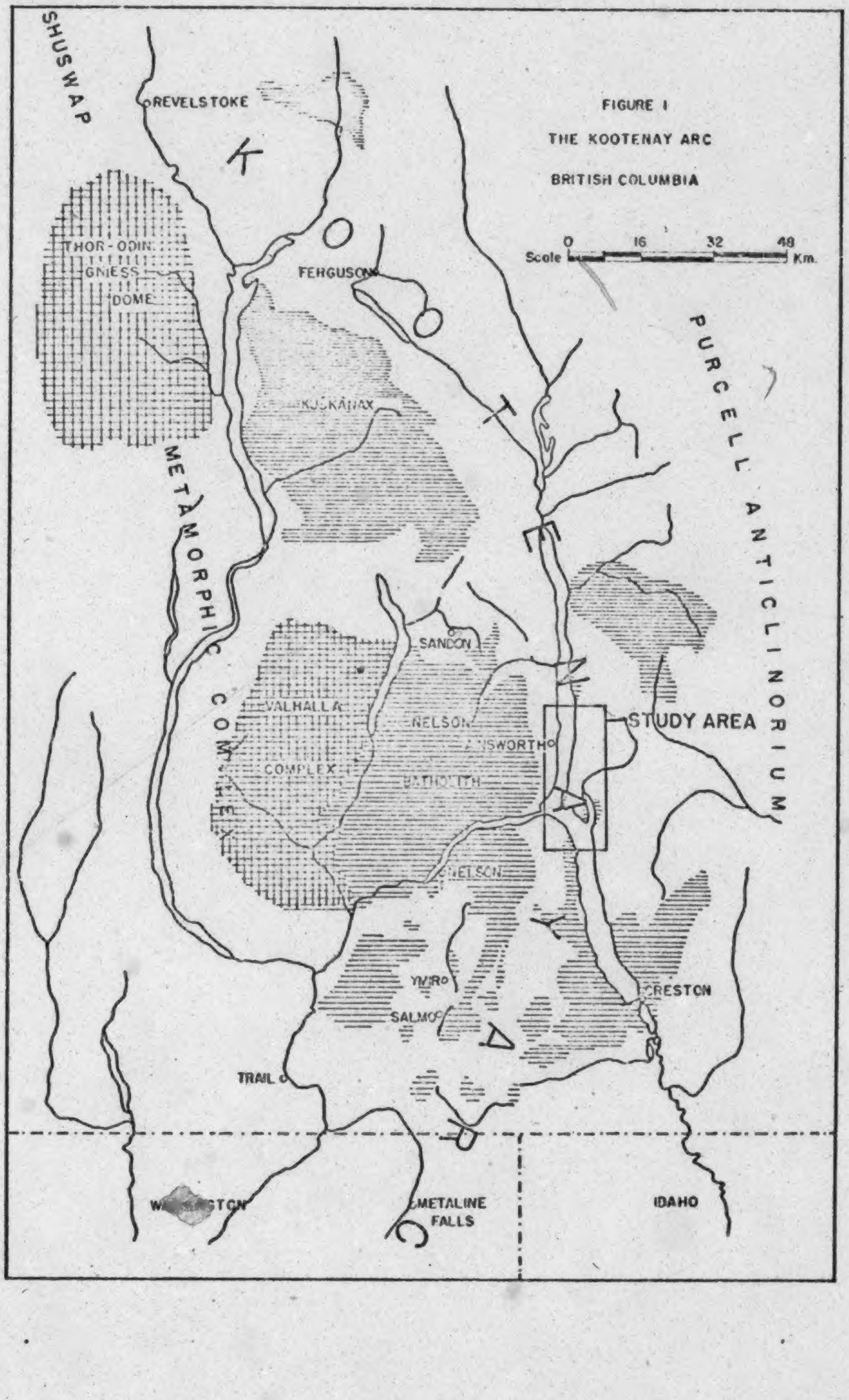

FIGURE I
THE KOOTENAY ARC
BRITISH COLUMBIA

SHUSWAP METAMORPHIC COMPLEX
REVELSTOKE
KOOTENAY ARC
THOR-ODIN GNIESS DOME
FERGUSON
KUSKANAX
SANDON
VALHALLA COMPLEX
NELSON BATHOLITH
AINSWORTH
STUDY AREA
NELSON
YMIR
SALMO
CRESTON
TRAIL
WASHINGTON
METALINE FALLS
IDAHO
PURCELL ANTICLINORIUM
Scale 0 16 32 48 Km.

correlations beyond Metaline Falls are uncertain. Rocks within the Kootenay Arc have experienced varying degrees of regional and contact metamorphism. The highest grades are from the central portion of the Kootenay Arc where kyanite and sillimanite have been reported (Fyles, 1967; Crosby, 1968).

The region has a fairly long history of exploration, stimulated by the occurrence throughout the Arc of both small and large deposits of ore. First reports of mapping in the Kootenay Arc were from Schofield in 1920, but geological exploration predates this report by a number of years. The first detailed maps are attributed to Walker (1928), Cairnes (1928) and Walker and Bancroft (1929), while later workers include Rice (1941), Park and Cannon (1943), Little (1960), Fyles and Eastwood (1962), Fyles (1964, 1967) and Crosby (1968).

This study concerns the central portion of the Kootenay Arc west of the Nelson batholith (Fig. 1). The central part of the Kootenay Arc has been mapped by Rice (1941), by Crosby (1968), and in part by Fyles (1967). Mapping by Cominco geologist Paul Ransom continued until 1971, while this author collected in the area during the 1970-71-72 field seasons. No attempt at exhaustive mapping has been made by this author. The map presented in Fig. 2 is the result of a synthesis of the present work and that of Fyles (1967) and Ransom (pers. comm. 1972, 1973).

Correlations both within and outside the map area are complicated by the intense deformation and moderate metamorphism of the rocks. Although metamorphism has not always destroyed original bedding, it has destroyed such features as grading and cross-bedding, and extensive deformation has often created structures which simulate bedding. Lithologies of several formations are similar, making transitions difficult or impossible to map. One marker horizon exists (the lower-middle Cambrian Badshot Formation), and most lithologic mapping was done by using this formation as a reference. The map presented should be considered with these problems in mind.

LITHOLOGIES

Precambrian Horsethief Creek Group

The Horsethief Creek Group marks the top of the Windermere Group as mapped by Walker (1928). It conformably overlies the Toby Conglomerate and conformably underlies the Hamill Group. In the type area, the Horsethief Creek Group consists of gray-green to purplish slate with several beds of lenticular conglomerate and quartzite and numerous thin interbeds of blue-gray, crystalline, mostly non-magnesian limestone (Walker, 1928). In the map area the formation is composed of rusty-red, greenish or black phyllites and bluish-gray carbonates with occasional blocky bands of reddish quartzite. The phyllites contain muscovite, chlorite and small amounts of biotite and carbonate, while the more greenish phyllites contain actinolite and chlorite. Carbonates contain calcite, dolomite, quartz and muscovite. Rocks of the Horsethief Creek Group are exposed from Lockhart Beach north to the contact with the Crawford Bay Stock, and along the extreme northeastern edge of the map area. Transition between the Horsethief Creek Group and the lower member of the Hamill Group is obscured by metamorphism and folding.

Cambrian Hamill Group

The Hamill Group was placed in the Precambrian Windermere Group by Walker (1928), Walker and Bancroft (1929), and Rice (1941). This assignment was made because of the absence of fossils in the area and still remains uncertain today, as good fossil localities do not exist for the Hamill Group throughout much of the Kootenay Arc. Little (1960) marks the Cambrian-Precambrian boundary at the lowest formation bearing Lower Cambrian fossils, which in the Nelson area is the lower limestone of the Laib Group (Reeves member). Park and Cannon (1943) report fossils (Olenellus) from the Quartzite Range Formation, which has been correlated with the Hamill Group (below the Reeves member) and a lower Cambrian age may be assigned to the Hamill Group on the basis of these correlations.

In the map area the Hamill Group is separated into two divisions by Crosby (1968), and two formations are defined by Fyles (1964) from the Duncan Lake area. The lower member (Marsh-Adams Formation) is a micaceous, locally garnetiferous quartzite and gray mica schist with thin lenses of buff weathering limestone (Fyles and Eastwood, 1962; Fyles, 1964). Wheeler (1963) describes intercalated greenstones within the Hamill Group in the Rogers Pass area. These greenstones are described as amygdaloidal and pillowed, occurring with breccia. They rapidly thin and die out to the south. No such intercalations are reported by Fyles and Eastwood (1962) or by Fyles (1964), and no greenstone members have been observed within the formation by the author. Crosby (1968) considers that amphibolites representative of the greenstones do occur within the Hamill Group on the east shore of the lake, but the author considers these units to be infolded Lardeau Group.

In the map area, Hamill Group rocks are represented by massive gray or grayish-white dolomitic limestones containing calcite, dolomite, tremolite, diopside and phlogopite or by calcareous schists with quartz, feldspar, muscovite, biotite or chlorite and epidote. Dark gray or silvery gray quartz, feldspar, biotite, muscovite, garnet schists appear on the west side of Crawford Point and the west side of Crawford Bay and are probably representative of the Hamill Group.

Cambrian Badshot Formation

The Badshot Formation is the best marker horizon in the Kootenay Arc. In the type area (Badshot Mountain, Ferguson Area) (Fyles and Eastwood, 1962) the Badshot Formation is a massive limestone with dolomitic and siliceous layers up to 305 m thick. In the map area it ranges from 15-100 m thick and is repeated several times by isoclinal folding and thrust faulting. The Badshot Formation has been correlated with the lower member of the Laib Group (Reeves member) by Little (1960) and with the Badshot Formation in the Rogers Pass area (Wheeler, 1963). It may grade into the Maitlen phyllite of the Metaline Quadrangle, Washington (Little, 1960). The Badshot Formation is placed in the Cambrian on the basis of these correlations, as the Reeves limestone contains archeocyathids which are also found in the Badshot Formation in the Rogers Pass area. Assuming the correlation to be valid, the ambiguity of the age of both the Badshot Formation and the overlying Lardeau Group are removed, placing both in the Cambrian and not in the pre-Cambrian Windermere Group as suggested by earlier workers (Walker, 1928; Walker and Bancroft, 1929; Rice, 1941).

In the map area, the Badshot Formation is represented by pure white, coarsely crystalline dolomitic marble, which often contains smaller amounts of diopside, tremolite and phlogopite. On the east side of Crawford Bay, the Badshot Formation lies in contact with a small pegmatite body, and within 9 m of the contact displays a spectacular range of pegmatitic crystals of diopside and tremolite up to 1.5 m long and 50-75 cm thick. The Badshot Formation is also correlated with the famous Bluebell Limestone, host of the Bluebell orebody.

Lardeau Group

The Lardeau Group lies firmly in the Cambrian and has been divided into six formations by Fyles and Eastwood (1962) and Fyles (1964). They are the Index, Triune, Ajax, Sharon Creek, Jowett and Broadview Formations. The author considers that only the Index Formation and possibly the Triune Formation are represented in the map area. Rocks of the Lardeau Group have been intensely deformed and possibly intruded by basic sills of Kaslo age, hence lithological differentiations are impossible to make with any degree of confidence. In the type area, the Index Formation is divided into a lower carbonaceous and siliceous argillite interbedded with limestones and slate, and an upper quartz muscovite-chlorite metavolcanic intercalated with limestone. No such division appears possible in the map area, as all types are complexly interfolded by tight isoclinal folds. On the west side of Kootenay Lake, the Princess and Early Bird Formations may correlate with the Triune Formation (Fyles, 1967). The lithology of the Lardeau Group in the map area is very similar to that of the Hamill Group and even more closely resembles that of the Milford Group. The author considers that the Lardeau Group may be separated from the Hamill Group by its amphibolite content and generally higher limestone content. Intercalated pods of amphibolite and limestone appear to be common in the rocks of the Lardeau Group. On this basis, Lardeau Group rocks appear to repeat within the envelope of the Badshot Formation in the northeast quadrant of the map and to be interfolded with the Hamill Group throughout the map area.

The Lardeau Group in the map area is represented by a large variety of rock types and mineral assemblages. Greenish banded calc-silicates and large amphibolite boudins are the most common rock types. Calc-silicates vary from 10 - 50% calcite + dolomite, and all contain diopside, tremolite-actinolite, hornblende, epidote, microcline and plagioclase with varying amounts of biotite. Minor chlorite occurs, and scapolite has developed in many samples. Amphibolites contain varying amounts of biotite, clinozoisite, chlorite and actinolite with or without garnet. Lower grade equivalents contain larger amounts of chlorite and actinolite. Interbedded with the above are thin layers of calcareous, micaceous schist and a few bands of pelitic schist containing garnet at higher grade. As the east side of the lake is approached, an increasing number of largely concordant pegmatites occur, and small to medium sized discordant dikes of aplite cut the various members.

Milford Group

Rocks of the Milford Group crop out in the western portions of the map area and are quite similar in lithology to those of the Lardeau Group. The Milford Group is difficult to distinguish because Kaslo Group rocks have been infaulted into it, producing patches of amphibolite almost indistinguishable from those in the Lardeau Group. The Milford Group appears to span a considerable amount of geologic time, being correlated outside of the map area with rocks of Carboniferous-Permian and Triassic age. Milford Group rocks appear in the Ferguson area (Fyles and Eastwood, 1962), as well as in the Duncan Lake area (Fyles, 1964) and may be found south of the map area (Rice, 1941; Little, 1960). The Milford Group consists of limestones interbedded with calcareous and non-calcareous schists and quartzites. In the Ainsworth-Kaslo area they are intruded by sills of Kaslo age (Fyles, 1967).

Milford Group rocks are represented by massive to thinly banded dolomitic limestones which appear blue-gray in fresh outcrop. Thin bands of rusty-weathering calcareous muscovite-biotite schist, locally garnetiferous, are found interbedded with the carbonates. Mineral assemblages are similar to those of Lardeau Group rocks with tremolite-phlogopite "gneisses" and diopside-actinolite-microcline-plagioclase-quartz banded gneisses. The Kaslo intrusives are biotite amphibolites, occasionally garnetiferous.

Kaslo Group

A thick series of andesitic volcanics and associated diorites occur in the type area of Slocan and Upper Arrow Lakes (Cairnes, 1928). They overlie rocks of the Milford Group in the type area, and are thus of probable Triassic age. In the present map area they are considered to be intrusive into the Milford Group, and are represented there by hornblende schists and gneisses.

Slocan Group

The Slocan Group is represented by a small outcropping in the extreme northwest corner of the map area. Rocks of the Slocan Group are interbedded gray and white, fine-grained crinoidal limestone, dolomite and slate or argillite overlying the Kaslo volcanics. The Slocan Group is also considered to contain some volcanics (Cairnes, 1928), but these do not extend into the map area. Fossil assemblages place the Slocan Group in the Triassic. No samples from the Slocan Group were obtained for this study.

Intrusive Rocks

The entire Kootenay Arc is sandwiched between large granitic, granodioritic and syenitic intrusives of Jurassic-Cretaceous and Tertiary age (Fig. 1). Little (1960) considered that rocks of the Kootenay Arc were wrapped around the Nelson Batholith, but examination of the work by Fyles and Eastwood (1962) and Fyles (1964, 1967) shows that the Arc extends well beyond the Kuskanax Batholith to the north, and correlation with rocks and structure in Washington extends the Arc well to the south of the Nelson Batholith. These large batholiths provide a barrier (or transition) between the Shuswap metamorphic complex to the west and the folded metasediments to the east. Extension of the Shuswap complex into the United States indicates that this is true for the whole of the known Arc.

The largest intrusives are composite batholiths of Jurassic-Cretaceous age. Intrusion of these batholiths has deformed the metasediments of the Arc and created metamorphic aureoles up to 1.4 km wide. The large batholiths are granodioritic, with granitic and sometimes more basic portions, often porphyritic with large phenocrysts of potassic feldspar. Smaller intrusives include the Crawford Bay Stock and numerous aplite and pegmatite bodies too small to map. The Crawford Bay Stock is described as a porphyritic biotite-granodiorite by Crosby (1968). Thin sections examined by the author indicate that it has syenitic affiliations and that some parts of the body are quartz-syenite.

The smaller aplite and pegmatite bodies are often syenitic (especially the aplites). These bodies may be either concordant or discordant, but the larger pegmatite bodies are largely concordant, while most of the aplites observed were discordant. Some of the smaller bodies have associated aureoles up to 10 cm wide. Many of the smaller bodies, and portions of the larger intrusives, have textures indicative of cataclasis.

STRUCTURE

Structure in the Kootenay Arc is complex in detail, but in general remains remarkably constant throughout the entire arc length. The structure is defined by N to NW trending, northward plunging isoclinal folds, with deviations from the trend in the vicinity of the batholiths. Axial planes are nearly vertical or dip to the west at high angles. This pattern of dip changes locally, and probably changes regionally as the curvature of the arc changes. For instance, in the Ferguson area, axial planes dip southwest at 70-80° (Fyles and Eastwood, 1962), whereas in the Metaline Quadrangle, dip of the axial planes is approximately 80° southeast (Park and Cannon, 1943). Faults trend in the same direction as the strike of the axial planes of the folds, except for radial folds which are related to the batholiths (Little, 1960).

Three phases of folding were recognized in the area by Crosby (1968). Phase I and Phase II folds are co-axial, with a third phase having axial planes approximately perpendicular to the first two. All authors working in the Arc agree that two phases of folding exist, but Fyles (1964, 1967) and Fyles and Eastwood (1962) do not recognize Phase III as such and group this type together with minor folds in the area to the north and south of the map area. There is some ambiguity in the definition of the phases of folding, especially in regard to scale. Phase I folds are defined by all authors as isoclinal, and can only be recognized by study of Phase II folds, but no Phase I closures have been observed. Phase II folds are more open than Phase I. Where refolded Phase I folds are present, they acquire the S shape of the Phase II folds.

Crosby (1968) defines Phase II folds as the smaller of the two, in direct contradistinction to Fyles (1964) who defines them as large antiformal or synformal folds. Crosby finds that Phase II folds may be defined in large outcrops by lineation, axes of minor folds and attitude of the first foliation. In the central Kootenay Arc, identification is more difficult due to poorer outcrop and difficulty with definition of local stratigraphy. The present author suspects that Phase I and II folds have been misidentified in portions of Crosby's work due to the above factors.

Unlike the Phase I and II folds, the minor folds (Phase III of Crosby, 1968) are readily identifiable in outcrop. They are crenulations of variable spacing along schistose beds, with axes dipping to the west.

General structural styles can be recognized, however, and will be briefly mentioned here since they have bearing on the genesis of the Arc. The structural style appears to change from more open isoclinal folds to the west to tight isoclinal folds in the east. Isoclinal folds may be recognized on both sides of the lake, but the west side is complicated by a series of faults and by the presence of the Nelson Batholith. Fyles (1967) considers that there is no complete stratigraphic section on the western margin of the area and describes the structure and stratigraphy in terms of four fault slices. Examination of his structural cross-sections shows complexly folded and sheared Kaslo and Milford rocks adjacent to the batholith with folds opening as the lake shore is approached. The rocks are folded into isoclinal folds interrupted by faults and distinguishable between fault slices only by careful stratigraphic mapping. On the eastern shore, the relatively less competent Lardeau rocks are overturned to the east, and folding becomes tighter as the eastern margin of the map area is approached. Tight isoclinal folds and thrust faults have repeated the Badshot and infolded the Hamill and Lardeau Groups. This style of folding resembles the "fan" type structures farther to the north. Part of the structural difference may be due to varying lithologies across the section and to the effects of the intrusion of the Nelson Batholith. These problems will be more fully discussed in the conclusions.

CHAPTER II

WHOLE ROCK CHEMISTRY AND METAMORPHIC MINERALOGY

INTRODUCTORY STATEMENT

Crosby (1968) defined metamorphic isograds based on classical index minerals found in the pelitic rocks from the Arc. On this basis he identified the chlorite, biotite, garnet, staurolite, kyanite and sillimanite isograds. In the course of this study, it became obvious that the metamorphic picture given by Crosby was in need of revision. The first problem lies in definition of isograds. Actual pelitic rocks are rare in the central Kootenay Arc; most micaceous schists examined contain modal calcite, placing the rock in a different chemical system from that of pelites. The second problem lies in the fact that the rocks are polymetamorphic and that a later retrogressive event has affected parts of the region studied. Retrogressive effects have caused misidentification of index minerals such as kyanite and sillimanite. Crosby (1968), in his modal analyses, lists up to 30% pseudomorphous kyanite and small (generally $< 1\%$) percentages of sillimanite from relatively few rocks. Pseudomorphs after cordierite are also mentioned. These rocks come from Riondel peninsula, from near the summit of Bluebell Mountain, from Woodbury Point and from the southwestern section of the map area near the lake shore. The author has examined about 400 thin sections and polished thin sections from the central Kootenay Arc and has failed to find sillimanite or kyanite on any regional scale. No cordierite has been identified. The two occurrences of sillimanite found by the author are from the immediate contact with the Crawford Bay Stock, and one occurrence of kyanite + staurolite from Woodbury Point is found sandwiched between two syenitic bodies. No rock found outside the aureoles of intrusive bodies has yielded any of the three higher grade index minerals.

The third problem lies with the superposition of the stratigraphy, structure and isograds. Both Crosby (1968) and Fyles (1967) recognized the fact that the isograds trend north-south, parallel to bedding, strike and axial planes of the folds. Because of the varied lithologies across section, one rock type cannot be used to define the entire series of metamorphic changes. The Lardeau Group rocks span the largest temperature-pressure (?) gradient, but they are composed mainly of calcareous and basic lithologies. Isograds, therefore, must be defined for many lithologies, and reactions are probably more indicative than index minerals.

SAMPLING PROCEDURE

An original aim of this project was to discuss chemical equilibrium in metamorphic rocks of moderate metamorphic grade. To do this, it was necessary to control as many natural variables as possible. Because the conditions of certain reactions differ from others on the basis of bulk chemistry, fugacity of volatiles, etc., the maximum chemical variation was sought in order to allow the broadest generalizations to be made. At the same time, it is desirable to choose an area where the intensive variables T and $P_{tot.}$ are constant for the range of chemical variation. An area 125 m square just north of Kootenay Landing was chosen for its chemical variability. Because little section is intersected, it is likely that T and $P_{tot.}$ would be the same for all samples collected. Some 108 samples were collected, about 65 of them in traverses across the small point (See Fig. 3 for sample locations). Care was taken to sample across "bedding" and across contacts with pegmatite and aplite bodies. Sample spacing is tight, so that all variations could be examined. All samples were thin-sectioned and examined carefully before choosing suitable assemblages for microprobe study. Forty-four assemblages were chosen for further examination, and coexisting phases within these slides were analyzed by electron microprobe.

In addition, it was necessary, because of the uncertainties found in the regional studies, to try and define metamorphic isograds and metamorphic reactions within the region. To this end, regional reconnaissance and collecting was undertaken. Two hundred rocks were collected in the region outlined in Fig. 2 (sample locations in Fig. 2), and several hundred specimens in the Cominco collection were examined. From all the rocks, 28 specimens were chosen for further analysis by electron microprobe. These samples were chosen with the following criteria in mind: 1) Pelitic rocks from all grades needed to be examined, since the greatest amount of quantitative data exists for these rocks. 2) Where possible, calc-silicate and amphibolite rocks were collected immediately adjacent to the pelites. Specimens of these rock types were collected near the pelitic rocks where they were not directly adjacent. 3) Rock types were chosen to be representative of assemblages found for the same or similar rock types at the same grade from the 200+ thin sections previously examined. 4) Samples were collected as far as possible from known large intrusives bearing visible contact aureoles, except where the assemblage was unique (as in 12WP-2, 2A and 11CBT-15). Rocks were unweathered and showed few, if any, signs of retrograde metamorphism.

Rocks analyzed from both the Point and the region are representative of all rock types found in the area with the exception of basic lamprophyre dikes. The following sections deal with the chemistry, mineralogy and petrology of these rocks. The treatment of analytical methods can be found in Appendix 1.

WHOLE ROCK CHEMISTRY

Because a great many studies of metamorphic petrogenesis lack comprehensive data on composition of the rock system in which the metamorphic minerals formed, conclusions concerning chemical variations with grade are always hampered by doubts as to the controls of bulk chemistry. Some circularity exists in any reasoning concerning chemical controls on mineral composition, since the rock composition is the result of the sum of the compositions of the mineral constituents. Ratios of major components may not be controlled by bulk composition alone, but may be influenced by the coexisting mineralogy, especially in systems smaller than a hand specimen or thin section.

Whole-rock compositions were obtained in two ways. Rocks from Kootenay Point were analyzed by X-ray fluorescence in the laboratory of J. G. Holland, Durham University (Table 1). Standards were included in the run to check the accuracy of the XRF data. The XRF data from Durham are not too satisfactory for quantitative analysis, and large errors are encountered in Al_2O_3, MgO and Na_2O values. Necessity dictates use of the data within this thesis, but they are useful only for

TABLE 1. XRF WHOLE ROCK SEMI-QUANTITATIVE ANALYSES - KOOTENAY POINT, B.C.

	1	2	3	4	5	6	7	8	9	10	11
Ox Wt	T2-6	T2-8	T1-6	205-95	T3-2a	T2-2	T3-2b	160-23	125-68E	T1-9	T1-9a
SiO_2	18.07	19.58	22.92	26.90	27.68	30.84	35.71	37.07	39.27	44.88	45.15
Al_2O_3	0.00	0.00	0.00	0.00	0.00	0.67	1.23	0.00	0.00	13.24	13.02
Fe_2O_3	1.77	0.77	0.80	0.29	0.29	1.80	5.00	1.06	2.61	13.37	13.09
MgO	23.63	23.32	22.41	23.37	24.52	23.94	17.25	35.32	23.49	14.74	12.93
CaO	31.98	30.56	30.06	28.89	28.26	25.68	28.39	13.95	22.71	10.23	10.52
Na_2O	0.00	0.00	0.00	0.00	0.00	0.00	0.00	0.00	0.00	0.83	1.13
K_2O	0.04	0.07	0.30	0.04	0.03	1.81	1.40	0.32	0.33	3.07	2.72
TiO_2	0.04	0.08	0.11	0.06	0.07	0.24	0.21	0.10	0.04	2.23	0.22
MnO	0.18	0.13	0.13	0.09	0.09	0.12	0.30	0.12	0.24	0.19	0.19
P_2O_5	0.19	0.17	0.17	0.16	0.13	0.12	0.19	0.08	0.12	0.37	0.41
Total	75.72	74.68	76.90	79.80	81.07	85.23	89.68	88.01	88.89	103.15	99.38

	12	13	14	15	16	17	18	19	20	21	22
Ox Wt	T2-18	240-137	56-20	T3-4	T2-3	375-140W	T4-8	T1-8	75-90	T4-4	T4-2
SiO_2	45.24	46.00	46.72	48.29	48.42	49.35	49.96	50.19	50.42	50.74	50.81
Al_2O_3	12.84	12.60	15.27	5.48	0.00	13.61	12.35	8.02	12.37	12.90	13.66
Fe_2O_3	4.94	13.50	5.18	3.52	2.18	13.08	14.02	6.11	4.65	15.53	11.23
MgO	18.22	14.55	19.32	28.16	20.46	10.86	8.32	23.44	17.56	7.96	8.90
CaO	11.19	11.26	8.15	10.05	21.73	11.46	11.57	11.08	10.82	10.66	10.14
Na_2O	0.57	0.99	0.83	0.00	0.00	1.85	1.60	0.25	0.71	1.73	0.88
K_2O	5.99	1.90	6.43	4.44	0.08	0.81	0.86	2.84	4.96	1.40	3.69
TiO_2	1.06	2.06	1.10	0.53	0.07	1.51	1.61	0.67	0.79	1.78	1.22
MnO	0.23	0.21	0.21	0.08	0.16	0.20	0.18	0.14	0.08	0.22	0.20
P_2O_5	0.06	0.37	0.05	0.05	0.10	0.16	0.23	0.06	0.08	0.22	0.16
Total	100.35	103.44	103.26	100.60	93.20	102.88	100.70	102.81	102.44	103.15	100.89

Raw data supplied by Dr. J. G. Holland, Durham University

TABLE 1 CONTINUED

	23	24	25	26	27	28	29	30	31	32	33
Ox Wt	55-20	190-120	T2-15	T3-5	199-146	205-50W	30-13E	215-70	T1-4	T2-5	T1-1
SiO_2	50.88	50.91	52.33	52.66	52.68	52.69	52.92	52.92	53.04	53.05	53.18
Al_2O_3	0.00	11.31	16.27	7.09	7.49	7.64	15.98	0.26	9.39	13.76	7.76
Fe_2O_3	4.33	6.65	11.86	5.23	5.09	3.29	11.81	6.15	5.51	7.55	3.98
MgO	20.28	12.58	9.20	26.41	21.41	28.61	9.92	21.63	14.59	11.48	22.27
CaO	21.39	10.76	5.32	7.45	13.36	6.58	5.58	16.78	12.37	7.42	11.39
Na_2O	0.00	0.43	2.19	0.00	0.42	0.04	1.96	0.00	0.25	0.47	0.00
K_2O	0.25	7.24	3.73	4.25	1.52	4.92	4.01	0.11	5.91	8.21	3.71
TiO_2	0.07	0.83	1.26	0.54	0.48	0.54	1.23	0.11	0.68	0.96	0.48
MnO	0.36	0.09	0.18	0.11	0.17	0.08	0.17	0.23	0.09	0.07	0.07
P_2O_5	0.10	0.05	0.12	0.05	0.09	0.09	0.13	0.08	0.06	0.06	0.16
Total	97.66	100.86	102.48	103.81	102.71	104.48	103.70	98.27	101.89	103.03	103.01

	34	35	36	37	38	39	40	41	42	43	44
Ox Wt	40-40E	198-146	T4-6	T2-4	115-45	105-101E	T2-9	T3-9	T3-12	T3-11	168-140
SiO_2	53.20	54.16	54.26	54.80	55.17	55.29	57.21	57.25	62.59	63.22	73.62
Al_2O_3	12.89	13.39	6.73	15.08	24.89	0.00	23.98	0.00	15.63	16.57	16.71
Fe_2O_3	7.36	6.07	6.58	5.20	3.54	2.74	0.17	3.24	6.25	6.46	0.45
MgO	10.45	11.96	21.24	12.72	6.73	26.04	1.68	25.40	3.52	3.23	0.23
CaO	10.43	8.38	12.15	6.21	4.74	12.83	5.80	15.74	3.43	3.19	1.14
Na_2O	0.99	0.43	0.63	0.31	4.93	0.00	6.45	0.00	1.01	0.94	4.32
K_2O	6.15	7.90	1.05	8.73	3.07	0.15	1.10	0.19	8.86	9.10	4.88
TiO_2	0.87	0.84	0.46	0.86	0.12	0.06	0.06	0.07	0.65	0.64	0.07
MnO	0.10	0.07	0.16	0.17	0.08	0.18	0.03	1.71	0.08	0.07	0.04
P_2O_5	0.07	0.05	0.12	0.05	0.06	0.07	0.07	0.08	0.18	0.17	0.04
Total	102.51	103.26	103.38	104.12	103.34	97.36	96.54	103.67	102.19	103.59	101.49

Raw data supplied by Dr. J. G. Holland, Durham University illustration of trends. Ratios of elements are not very accurate, especially with regard to Al_2O_3, but they should, when used in sufficient numbers, allow trends to be discerned. Further discussion of the accuracy of these results can be found in Appendix 1. Whole rock compositions were determined for the 28 regional rocks studied following the method of Friedman (1960) (Table 2). The procedure was modified to the extent that chemical analyses of minerals from thin sections were used in the calculation. An analysis of standard T4-8 was made as a check of accuracy. Comparison of results indicated that analyses are accurate to within ± 5% of the total for most major elements. Larger differences are noted for minor elements and for Na_2O and K_2O. See Appendix 1 for discussion of results. Modal analyses of both the regional metamorphic rocks and rocks from Kootenay Point may be found in Tables 3 and 4.

Rocks from the Point are, with a few exceptions, divisable into two categories on the basis of both Niggli values and comparison with the plots of Winkler (1967) (Fig. 4). The larger group, characterized using Niggli values as femic-calc-alkaline or femic silicate rocks, plot in the region delimited by Winkler as ultrabasic or basaltic rocks. The remaining large group of rocks are characterized by Niggli values as femic silicates, but the si value is very much lower than that for the other group, reflecting a greater amount of carbonate. Not all rocks in this second group are true carbonates, however, as examination of Table 4 will show. Several are more siliceous than a true carbonate, containing up to 80% tremolite, but the nature of the si calculation is such that al + c + alk + fm is used as a factor. Thus, high CaO, MgO, FeO rocks (such as would be expected of rocks containing calcite-

TABLE 2. CHEMICAL ANALYSES OF REGIONAL METAMORPHIC ROCKS

	1	2	3	4	5	6	7	8	9	10	11
	10BT-3	5LBT-3	8AT-18	5LBT-20	5LBT-15	4LBT-2	5LBT-17	10BT-4	5LBT-16	8AT-8	11CBT-7
SiO_2	7.64	10.88	15.37	17.76	23.28	29.21	29.27	33.64	41.63	44.46	44.88
TiO_2	0.02	tr	0.09	0.02	0.46	0.24	0.33	0.97	0.85	1.08	0.17
Al_2O_3	0.07	0.44	3.16	1.08	14.43	10.13	11.64	19.06	20.31	9.92	7.53
FeO	11.34	0.09	2.59	1.60	6.05	23.33	27.59	3.99	12.48	16.71	9.93
MnO	0.01	0.01	0.01	0.01	0.32	0.09	0.14	0.07	0.09	0.29	0.13
MgO	14.48	5.20	14.78	1.06	3.87	13.25	9.25	1.66	8.41	9.86	15.38
CaO	25.36	38.74	23.14	41.67	22.18	6.16	6.66	15.96	2.80	11.67	11.88
Na_2O	tr	0.02	0.39	0.03	0.58	0.28	0.80	1.96	1.25	1.99	1.19
K_2O	0.14	0.30	1.51	0.66	4.13	1.09	1.23	6.91	2.80	1.57	0.88
BaO	tr	tr	tr	tr	0.08	tr	0.06	0.15	0.06	0.01	0.01
Cl	tr	-	tr	tr	0.01	0.06	0.07	0.02	0.03	0.02	0.02
F	tr	-	0.10	tr	0.08	0.11	0.06	0.11	0.03	0.69	0.14
H_2O	0.02	0.04	0.26	0.17	3.41	4.95	4.47	1.75	7.03	0.93	2.40
CO_2	38.02	39.77	37.15	35.59	21.04	7.37	5.02	13.73	2.31	0.41	4.70
S	5.17	4.48*	0.87	0.49	-	6.03	6.19	-	-	-	1.37
Total	102.28	99.97	99.43	100.14	99.92	102.30	102.77	100.02	100.08	99.61	100.61

*Carbon

TABLE 2 CONTINUED

	12 5LBT-22	13 6CCT-1a	14 12WP-2a	15 6CCT-8	16 12WP-2	17 7RT-17	18 11CBT-16	19 6CCT-3	20 4LBT-1	21 10BT-17	22 10BT-9
SiO_2	46.22	46.93	47.62	48.86	51.16	55.07	55.08	56.96	56.97	62.99	65.23
TiO_2	3.30	1.66	2.20	3.55	0.96	1.54	1.81	0.54	0.24	0.85	0.04
Al_2O_3	9.87	13.34	18.20	11.46	21.23	15.20	13.91	8.04	15.77	17.07	5.97
FeO	14.03	14.54	12.97	14.05	9.49	12.81	15.38	4.51	2.33	5.82	4.98
MnO	0.22	0.04	0.44	0.19	0.04	0.15	0.15	0.08	0.01	0.07	0.11
MgO	6.49	9.30	4.75	6.67	4.03	3.35	3.51	6.57	2.59	2.97	7.85
CaO	10.40	7.60	8.96	11.16	2.52	2.92	1.67	13.14	7.89	2.24	10.77
Na_2O	1.60	0.97	1.82	1.52	3.57	2.06	0.58	0.65	0.54	2.19	0.29
K_2O	1.68	2.09	1.85	0.63	4.68	3.47	5.39	3.88	4.11	3.99	2.27
BaO	0.01	0.02	tr	-	0.16	0.10	0.09	tr	0.04	0.05	tr
Cl	0.27	0.03	0.01	0.07	0.04	0.23	0.09	tr	0.02	0.03	tr
F	0.07	0.05	0.09	0.02	0.17	0.04	0.11	tr	0.04	0.09	0.04
H_2O	1.23	2.56	1.21	1.54	2.27	0.72	1.56	0.62	2.88	2.41	0.81
CO_2	0.70	0.60	-	0.33	-	-	-	4.51	6.58	-	-
S	-	-	-	-	0.34	-	1.27	-	-	-	0.85
Total	96.09	99.73	100.12	100.05	100.66	97.66	100.60	99.50	100.01	100.77	99.01

TABLE 2 CONTINUED

	23	24	25	26	27	28
	6CCT-1	11CBT-15	7RT-7	10BT-11	10BT-13	10BT-8
SiO_2	66.25	66.80	67.09	69.43	71.87	79.44
TiO_2	0.72	0.33	0.15	0.15	0.20	0.57
Al_2O_3	6.46	16.58	11.96	16.58	3.35	9.35
FeO	6.59	4.21	2.47	0.80	2.32	3.39
MnO	0.09	0.02	0.04	0.03	0.02	0.07
MgO	4.68	1.82	2.71	0.38	1.61	0.84
CaO	1.55	0.62	8.45	1.95	10.38	1.19
Na_2O	1.41	2.92	1.40	5.89	0.42	3.49
K_2O	3.10	4.40	3.08	4.66	1.10	1.50
BaO	0.03	0.06	tr	tr	0.01	0.02
Cl	0.05	0.01	tr	tr	0.01	0.02
F	0.08	0.05	0.01	tr	0.22	0.05
H_2O	2.64	1.68	0.12	0.02	0.32	0.43
CO_2	-	-	0.37	-	8.59	-
S	-	-	-	-	-	-
Total	93.65	99.50	97.85	99.89	100.40	100.36

TABLE 3. MODAL ANALYSES OF REGIONAL METAMORPHIC ROCKS BASED ON 1200 COUNTS/SECTION

	Specimen	Hb	Tr-Act	Bi	Mu	Chl	Qtz	K-Feld	Plag	Scap	Cc	Dol	Magnesite	Di	Ep	Sph Opaque
1	10BT-3		0.2	0.6			8.0	0.4			15.1	67.6				8.2
2	5LBT-3				0.6		10.0	1.3			61.6	20.8				5.8
																graphite
3	8AT-18			7.8		0.3	7.2	4.8	4.3		7.4	66.9				1.3
4	5LBT-20		0.9	2.5			14.8	2.5	0.6		78.0	0.1				0.7
5	5LBT-15			7.4	32.3	9.7		tr	3.6		46.6				0.2	0.1
																0.2
																tour.
6	4LBT-2		13.8	12.3	tr	35.8	8.7		2.7			16.9				9.9
7	5LBT-17	19.9		13.5		32.7	6.6	0.1	5.3		7.8	3.8				10.1
																pyr
8	10BT-4			13.7	38.1	0.1		0.6	16.8		30.6		0.1			
9	5LBT-16			0.1	25.9	45.2	10.8	0.1	12.3		5.2					0.6
10	8AT-8	89.5		tr				2.5	4.4		1.0			tr		2.5
11	11CBT-7*		63.0	8.3					15.7		5.2		5.5	tr		2.2
12	5LBT-22	70.0	incl in Hb	2.5			9.8	4.4	6.7		0.8			tr	0.1	5.8
13	6CCT-1a	56.5		19.5			13.5	0.7	3.4			0.6	0.7			5.1
14	12WP-2a	25.4		21.8		0.2	9.5		27.8				11.4			3.9
													garnet			
15	6CCT-8	73.5					11.8	1.5	6.9		0.8		tr			5.4
													garnet			
16	12WP-2			18.3	6.1	2.2	42.1	1.6	28.0				1.3			0.5
													garnet			
17	7RT-17	2.6		38.4			23.6	0.1	27.8				6.5			1.0
													garnet			
18	11CBT-16		0.1	48.5	3.2		30.8	2.0	13.1				0.4			1.9
													garnet			
19	6CCT-3		28.3	0.3			15.1	27.5	4.7	0.1	10.1			7.6	5.2	1.0

*Partly destroyed by HF

TABLE 3 CONTINUED

	Specimen	Hb	Tr-Act	Bi	Mu	Chl	Qtz	K-Feld	Plag	Scap	Cc	Dol	Magnesite	Di	Ep	Sph Opaque
20	4LBT-1			0.1	37.7	7.6	34.0	0.3	5.8		14.5					
21	10BT-17			28.6	10.7		31.1		29.7							
22	10BT-9		18.0	0.3			30.6	16.3	6.1	1.7				22.9	2.8	1.3
23	6CCT-1			35.1	2.6	0.4	42.0	0.6	18.7						0.7	
24	11CBT-15			13.6	24.9	0.3	36.0	0.2	24.3			tr sill				0.7
25	7RT-7		4.4	0.4			31.1	21.3	22.8		0.8			14.8	4.2	0.3
26	10BT-11			0.4			13.0	30.4	52.6					3.3		0.3
27	10BT-13	1.9		8.5			64.1	1.0	5.8		18.0					0.2
28	10BT-8			12.3	0.7		57.1	0.3	29.6							

TABLE 4. MODAL ANALYSES OF METAMORPHIC ROCKS FROM KOOTENAY POINT BASED ON 1200 COUNTS/SECTION

	Specimen	Hb	Tr-Act	Bi	Mu	Chl	Qtz	K-Feld	Plag	Scap	Cc	Dol	Magne-site	Di	Ep	Sph Opaque
1	T2-6		32.2	0.3							4.3	63.1				
2	T2-8		15.6									75.1		9.3		
3	T1-6		19.1	1.1	tr			0.4			12.1	64.9	2.4			
4	205-95W		6.7								2.5	90.8				
6	T2-2		52.7	0.3							26.3	15.6	1.3	3.8		
7	T3-2b		87.1								0.3	11.2	1.3			
8	160-23E		0.2	37.7						0.9	0.1	49.1	12.1			
9	125-68E		99.3	0.5								0.1				0.2
10	T1-9b	69.1		25.1		0.2			0.3		2.8					2.5
11	T1-9a	65.0		23.5		2.2		1.3	2.6		1.5					3.8
12	T2-18	11.8		52.0				0.8	1.6	19.5	4.0			9.4	0.3	0.5
13	240-137E	77.4	14.3				1.3	0.3	3.2			0.1				3.3
14	56-20E			65.8			0.8	0.2	0.1	to 20	2.8	9.3		19.4		1.7
15	T3-4		28.0	37.0							35.0					
16	T2-3		17.8						0.2		26.3	5.0		50.7		
17	375-140W	72.1		5.2			0.1	0.3	21.0							1.3
18	T4-8	66.4		1.5			5.1	2.9	14.0						6.7	3.4
19	T1-8	87.4	11.8		tr						0.7	tr				tr
20	75-90E		0.6	34.0				4.8	16.4		0.5			43.3		0.5
21	T4-4	59.7		6.6		0.1	7.5	3.1	10.7		0.2				7.9	4.2
22	T4-2	44.3		18.6		0.5	2.1	15.8	5.4	5.7	0.9				3.7	3.0
23	55-20W		24.1	5.4							30.2	15.1		25.2		
24	190-120E	11.1		24.7			0.2	34.0	0.6		5.9			23.3		0.3
25	T2-15	26.2		42.1			8.9		22.4							0.3
26	T3-5		67.7	31.2				0.4		0.8						
27	199-146E		52.7	4.6							1.1	2.0		39.7		
28	205-50W		60.6	39.4												
29	30-13E	23.2		40.8			10.5	0.9	24.3							0.2
30	215-70W		73.3	2.6							1.7	20.4		2.0		

TABLE 4 CONTINUED

	Specimen	Hb	Tr-Act	Bi	Mu	Chl	Qtz	K-Feld	Plag	Scap	Cc	Dol	Magne-site	Di	Ep	Sph Opaque
31	T1-4			36.3				32.3	2.9					27.6		0.7
32	T2-5		8.3	42.3			0.1	27.6	2.6					19.2		
33	T1-1a		18.5	24.9				8.2	7.5					40.8		0.1
34	40-40E		1.5	27.9				33.1	3.7		1.5		0.2	31.3		0.7
35	198-146E	2.5		29.1			0.1	32.7	2.3		0.1			32.9		0.3
36	T4-6		80.1	9.6			1.1		8.1		1.1					
37	T2-4	0.4		33.0			0.1	32.0	2.5					31.1		0.9
38	115-45W		1.2	94.3				4.5	0.1							
39	105-101E		76.5	3.5							3.3	16.4				0.3
40	T2-9		1.5	46.6			2.4	0.2	47.4			0.1		1.9		
41	T3-9		84.1	12.9			0.1		0.3			1.9		0.1		0.7
42	T3-12	20.3		4.6			12.9	20.5	38.1						2.7	1.0
43	T3-11	11.3		17.5			12.1	9.3	44.1					0.6	4.3	1.0
44	168-140E			2.7			26.5	35.2	35.6							
	T1-5a (Hb-Bi)	20.6		27.2			2.3	4.6	17.7		0.9			24.8		2.0
	T1-5a (Aplitic)	5.9		4.3			15.4	40.9	29.4		0.6				2.5	0.9
	72-80E		46.7	11.5							9.4	31.8		0.4		0.2
	T3-12	26.2	4.5				5.6	56.7	2.7		0.1				2.9	1.3
	T2-18b	0.2		45.5			1.5	0.7	20.6	tr	1.2	1.1		26.2	0.2	2.9
	T2-10		0.9	16.2				0.5	0.2		0.1	58.6	23.6			
	T3-3		56.8	0.8							23.1	5.2	0.2	14.0		
	T1-5b	1.5		8.6			19.3	32.3	37.8							0.5

dolomite-tremolite and/or diopside) give very low si values. In these cases, mg is quite high, indicating the presence of magnesium silicates and dolomite. No true calc-silicates exist, there being not enough SiO_2 (or, in some cases, CaO) to produce a true calc-silicate assemblage. In the first group, by contrast, the mg value is lower, but more variable. The chief variation is in Al_2O_3 (Fig. 4). The rocks are grouped within a fairly narrow range of MgO + FeO; the remainder of their position being determined chiefly by Al_2O_3 (and CaO) variation. This variation is reflected in the modes, in which rocks lying closer to the A apex contain more feldspar or biotite (or hornblende) than those lying farther away. Those lying near the C-F base contain more tremolite-actinolite, diopside or carbonate and less feldspar or hornblende.

Six rocks do not fit into either of the first two groups according to the Niggli values. All but two lie within the fringe areas of the two groups. These rocks (18, 21, 38, 40, 42 and 43) are characterized either as calc-alumino-, alk-alumino- or calc-alk-aluminosilicates. Four of the six lie close to or in basalt-andesite group (18, 21, 42, 43).

Some rock compositions lie outside the ACF and AKF plots (8, 39, 44). The reason for this can be traced to the accuracy of the analyses. If a large error in Al_2O_3 occurs, and the error places the aluminum content below the real value, the A component of the ACF diagram becomes negative, placing the point below the C-F line. Points that plot outside the ACF diagram generally have negative A values. Those rocks falling outside the plot are generally high carbonate rocks, with low si values, similar to those plotting in Group 2.

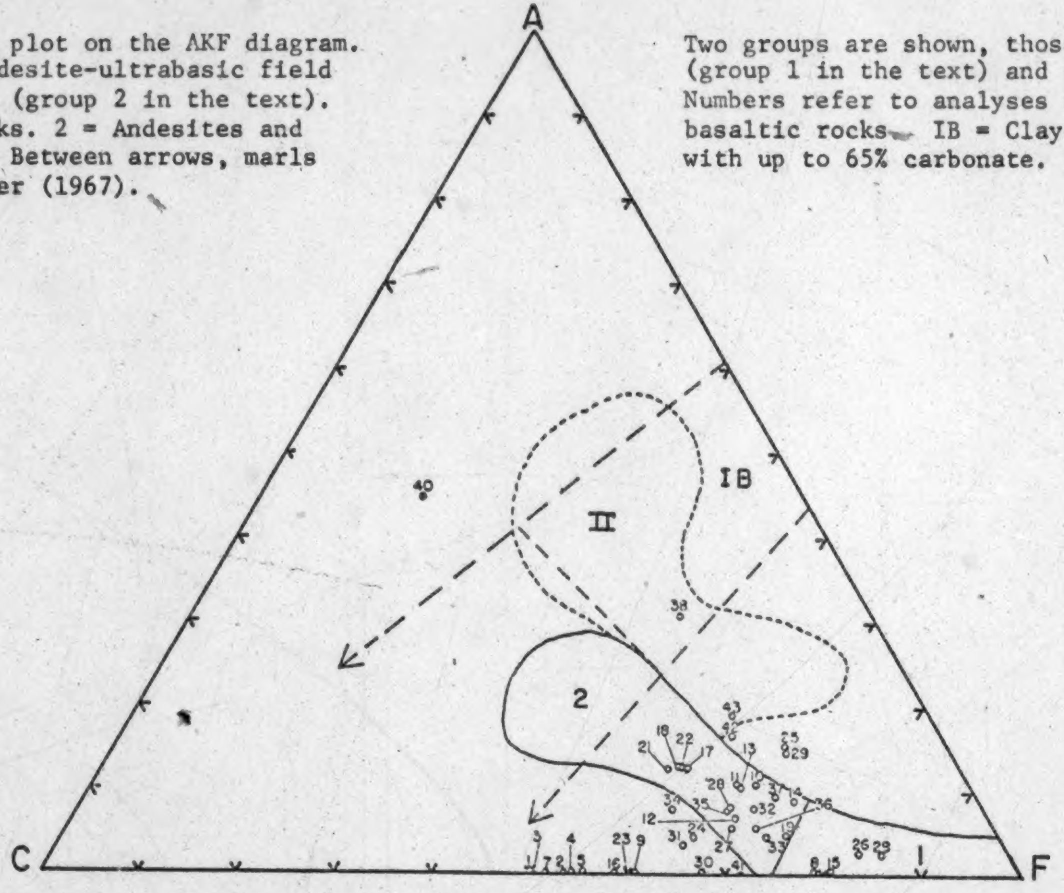

Fig. 4. ACF plot for rocks from Kootenay Point

Two groups are shown, those plotting in or near the basalt-andesite-ultrabasic field (group 1 in the text) and those plotting along the C-F edge (group 2 in the text). Numbers refer to analyses in Table 1. 1 = Ultrabasic rocks. 2 = Andesites and basaltic rocks. IB = Clays containing up to 35% carbonate. Between arrows, marls with up to 65% carbonate. II = Graywackes. Fields after Winkler (1967). Only 38, 40 and 43 plot on the AKF diagram.

Regional rocks, in contrast to those from the Point, are a considerably more heterogeneous group. Their compositions are represented on ACF and AKF diagrams (Fig. 5) and their modes are given in Table 3. The analyses are presented in Table 2. Comparing Fig. 5 with those of Winkler (1967), it can be seen that the rocks fall into all four fields represented. The largest number of rocks do not fall within any group, but approximate clay or clay-carbonate mixtures. The next largest group plots in the graywacke field, followed by ultrabasic and basaltic rocks and finally marls.

Using the Niggli values derived for these rocks, seven types may be recognized; eight when the si value is used. These seven types encompass nearly the entire range of silicate rocks given by Niggli (1954), including femic-calc-alkaline, femic silicate, calc-silicate, calc-alumino-silicate, alkali-calc aluminosilicates, alkali aluminosilicates and aluminosilicates. Generally, the rocks with low si values are femic, but have high mg values, as with the Point rocks. The rocks with higher si values have lower mg values. The carbonate-rich rocks are higher in mg generally, but some contain considerable iron, resulting in lower mg values. This iron is not held in the carbonates, but is held mainly in sulfides.

The chief compositional differences between the Point rocks and the regional rocks are silica and alumina content. They also differ in variability; a function of their sedimentary parentage. The rocks corresponding chemically to graywackes clearly derive from sediments, as do the high carbonate rocks, but those falling near or within the basalt-ultrabasic field may be derivatives of volcanic or mixed vol-

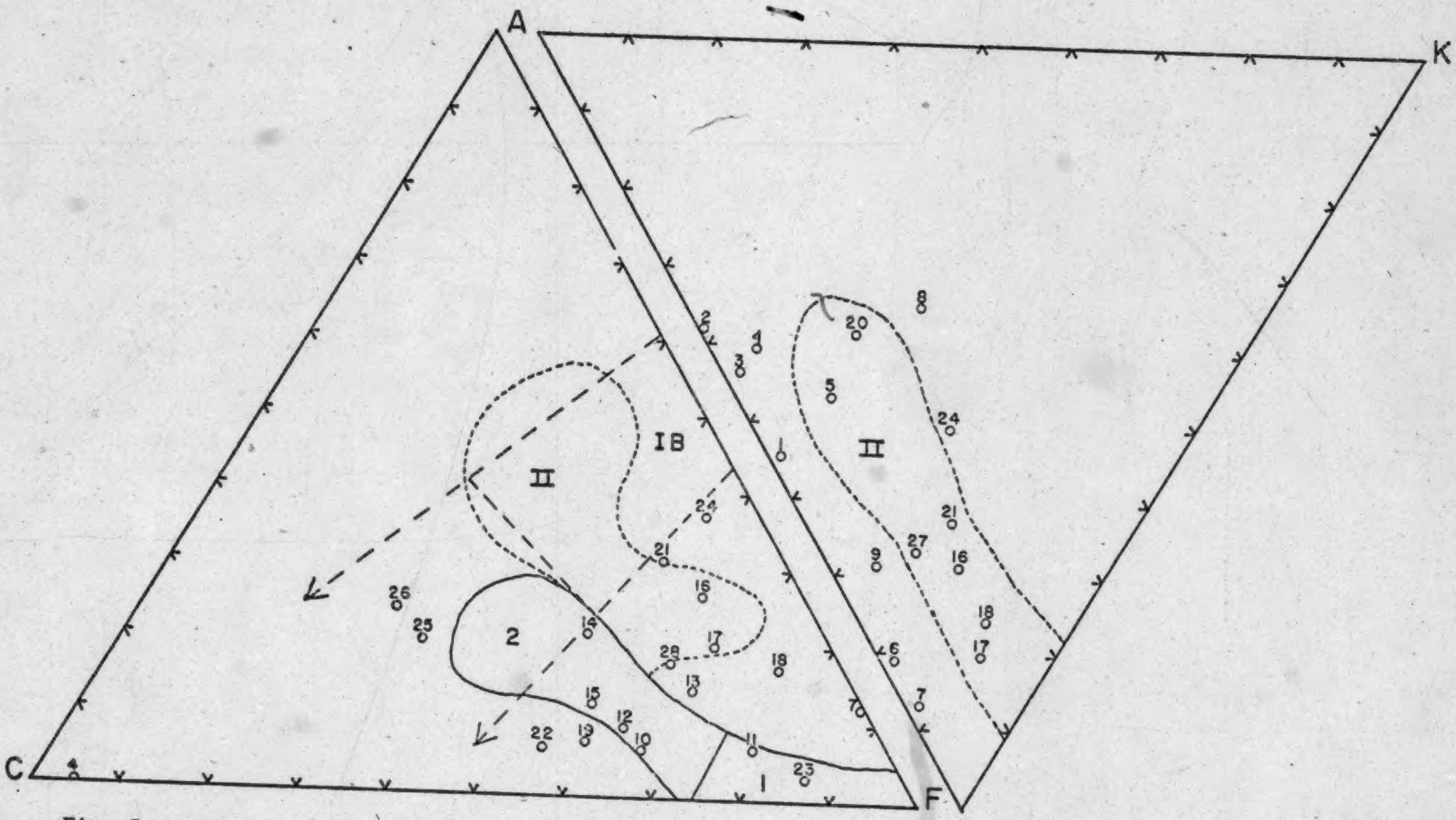

Fig. 5. ACF and AKF plots for regional metamorphic rocks

Numbers refer to analyses in Table 2. Fields are those described in Fig. 4.

canic and sedimentary rocks. The carbonates are never pure, always containing up to 30% detrital quartz and feldspar (seen only in the low grade rocks). Although several formations are identified in the area by Fyles (1967) and others, lithologies within any one formation may be much like those in another, chemically and petrographically. The chief problem lies in their lack of continuity either along the strike or across the stratigraphic section. This lack of continuity necessitates caution in defining metamorphic grade in the region.

In summary, the regional metamorphic rocks are found to be heterogeneous, indicative of diverse origins for the various rock types. Rocks from a restricted area show less variation, but define two distinct groups. The compositional variations indicated in this section will be applied in the next section dealing with metamorphic mineralogy in order to separate bulk rock compositional controls on mineral composition from other variables.

METAMORPHIC MINERALOGY

Muscovite

Muscovite is perhaps one of the best indicators of pressure-temperature conditions of metamorphism, in the absence of the classical index minerals andalusite, kyanite and sillimanite. Where index minerals are absent or multivariant and non-isochemical rock systems are present, muscovite provides perhaps the best indicator of metamorphic grade (see Butler, 1967). Work by Lambert (1959), Ernst (1963), Velde (1965, 1967b, 1968), Butler (1965, 1967), Brown (1967), Mather (1970), Ernst *et al*. (1970) and Cipriani *et al*. (1971) have established the relationships between phengite composition and pressure and temperature of metamorphism. Yoder and Eugster (1955a, 1955b), Velde (1965, 1967b), Iiyama (1964) and others have established stability ranges, extent of muscovite-paragonite solid-solution with temperature and composition of the fluid phase, and reaction curves for important metamorphic reactions. Brown (1967), Guidotti (1969), Wenk (1970) and others have discussed the relationship between muscovite composition, bulk rock composition and coexisting mineral phases. This volume of work has established definite patterns within which composition of white mica varies with temperature and pressure.

Velde (1967a, 1967b, 1968) and Butler (1967) believe that the composition of the rock does little to influence the composition of muscovite with respect to Si^{4+} and Al, and to a much lesser extent, Fe and Mg. Disagreement has been expressed by Brown (1967) and by Guidotti (1969), but both authors agree that systematic changes in Si, Al, Mg and Fe will take place with grade. In all cases studied, bulk rock composition seems to play a much more subdued role in establishing muscovite composition than for ferromagnesian minerals like biotite, but muscovite compositions cannot be shown to be completely independent of bulk rock composition in all cases. Guidotti (1969) has shown that muscovite compositional variation may be influenced by mineralogy, especially with respect to Al_2O_3 contents. He states that muscovites should only be used as grade indicators where they coexist with K-feldspar, a case sometimes found in pelitic rocks but not in rocks of glaucophane schist facies. Ernst et al. (1970) have demonstrated that systematic variations in white micas from the glaucophane schist facies can be related to different metamorphic environments, even in the absence of K-feldspar. Cipriani, et al. (1971), using several hundred analyzed muscovites, have related composition to temperature and pressure of formation.

Thirteen muscovites from regional metamorphic rocks within the central Kootenay Arc have been analyzed by electron microprobe for twelve elements. Two pairs from the same slide have been analyzed to check for variation within a single thin section. Analyses are presented in Table 5. All muscovites coexist with either chlorite or biotite or both, and all except 4LBT-1a, 4LBT-1b, 5LBT-15 and 10BT-17 coexist with K-feldspar, thus satisfying Guidotti's criteria for usage as an indicator of metamorphic grade (Guidotti, 1969). Low grade assemblages contain significant amounts of calcite or dolomite or both. 4LBT-1 contains 16.6% dolomite; dolomite contents of all other rocks are generally small (see Table 3 for modal analyses).

Inspection of Table 5 shows that the following generalizations can be made for the muscovites in this work. 1) An increase in silica is correlated with an increase in Mg and a decrease in Na and Al^{IV}. There appears to be a correlation between Fe and Si, with Fe rising as Si increases, but it is much less striking than the trend for Mg. Octahedral Al does not change significantly. Further detailed discussions concerning the compositional relationships between elements within the muscovites will be handled in the section on metamorphism, since these relationships can be shown to be related to metamorphic grade. Fig. 6 is a plot of muscovite compositions on a portion of the AFM diagram modified for total Fe as FeO. In addition to muscovites from the Kootenay Arc, muscovites from other metamorphic areas are plotted for comparison. The plot shows three trends of interest. 1) The field defined by the muscovites from the Sanbagawa (Shirataki) region of Japan

TABLE 5. ELECTRON MICROPROBE ANALYSES OF MUSCOVITES FROM REGIONAL METAMORPHIC ROCKS

Ox Wt	1 10BT-8(2)	2 11CBT-15	3 10BT-17	4 12WP-2a	5 10BT-8(1)	6 10BT-4	7 5LBT-15	8 6CCT-1	9 4LBT-2	10 5LBT-16
SiO_2	45.43	45.46	45.46	45.48	45.56	45.57	46.05	46.26	46.39	46.89
TiO_2	1.10	0.52	0.83	0.81	1.07	1.13	0.84	0.78	0.61	0.29
Al_2O_3	32.54	34.09	34.58	34.94	33.09	32.89	31.05	33.09	28.42	32.76
FeO	3.01	2.65	1.13	1.04	2.83	1.63	3.89	1.75	3.74	1.94
MnO	0.02	0.01	0.00	0.00	0.03	0.01	0.01	0.02	0.03	0.00
MgO	0.84	0.65	0.80	0.71	0.78	0.97	1.45	1.28	3.03	1.49
CaO	0.03	0.01	0.02	0.03	0.03	0.01	0.01	0.00	0.01	0.01
Na_2O	0.46	1.82	0.98	1.42	0.50	0.56	0.57	0.56	0.32	0.46
K_2O	10.46	8.74	9.94	8.91	10.61	10.36	10.33	10.34	10.27	10.56
BaO	0.15	0.19	0.31	0.00	0.17	0.22	0.23	0.27	0.05	0.21
Cl	0.03	0.01	0.00	0.00	0.01	0.02	0.02	0.00	0.00	0.00
F	0.09	0.01	0.00	0.00	0.09	0.11	0.10	0.00	0.00	0.04
Total	94.14	94.15	94.06	93.34	94.77	93.48	94.55	94.35	92.86	94.67
H_2O*	5.86	5.85	5.94	6.76	5.33	6.52	5.45	5.65	7.14	5.33
STRUCTURAL FORMULA ON THE BASIS OF 22 OXYGENS										
Si	6.209	6.154	6.145	6.135	6.184	6.228	6.299	6.254	6.429	6.322
Al^{IV}	1.791	1.846	1.855	1.865	1.816	1.772	1.701	1.746	1.571	1.678
Total tet.	8.000	8.000	8.000	8.000	8.000	8.000	8.000	8.000	8.000	8.000
Al^{VI}	3.450	3.593	3.654	3.691	3.396	3.526	3.305	3.527	3.072	3.528
Ti	.113	.053	.084	.077	.101	.116	.086	.079	.059	.029
Fe	.344	.300	.128	.117	.319	.186	.445	.198	.434	.219
Mn	.002	.001	0	0	.003	.001	.001	.002	.004	0
Mg	.171	.131	.161	.143	.157	.198	.296	.258	.626	.299
Total oct.	4.080	4.078	4.027	4.029	3.976	4.027	4.133	4.064	4.195	4.075
Ca	.004	.003	.003	.004	.004	.001	.001	0	.001	.001
Na	.122	.478	.257	.371	.131	.148	.150	.147	.086	.120
K	1.823	1.509	1.714	1.533	1.824	1.806	1.802	1.783	1.816	1.816
Total	1.950	1.988	1.974	1.908	1.959	1.956	1.955	1.930	1.903	1.938

*$H_2O$is determined by difference from 100%. This is a maximum value as Fe_2O_3 has not been determined. H_2O is not used in further calculations.

TABLE 5 CONTINUED

Ox Wt	11 4LBT-1(2)	12 5LBT-3	13 4LBT-1(1)
SiO_2	47.50	47.84	48.02
TiO_2	0.57	0.46	0.59
Al_2O_3	31.27	30.96	32.16
FeO	1.60	0.17	1.63
MnO	0.01	0.00	0.00
MgO	2.02	2.73	2.00
CaO	0.02	0.01	0.01
Na_2O	0.27	0.32	0.37
K_2O	10.43	10.42	10.35
BaO	0.14	0.23	0.11
Cl	0.00	0.00	0.01
F	0.09	0.00	0.09
Total	93.93	93.14	95.34
H_2O*	6.07	6.86	4.66

STRUCTURAL FORMULA ON THE BASIS OF 22 OXYGENS

Si	6.433	6.485	6.399
Al	1.567	1.515	1.601
Total	8.000	8.000	8.000
Al	3.425	3.432	3.449
Ti	.058	.047	.059
Fe	.181	.019	.182
Mn	.001	0	0
Mg	.408	.552	.397
Total	4.073	4.049	4.087
Ca	.003	.001	.001
Na	.071	.084	.096
K	1.802	1.802	1.759
Total	1.876	1.887	1.856

*H_2O determined by difference from 100%. This is a maximum value as Fe_2O_3 has not been determined. H_2O is not used in further calculations.

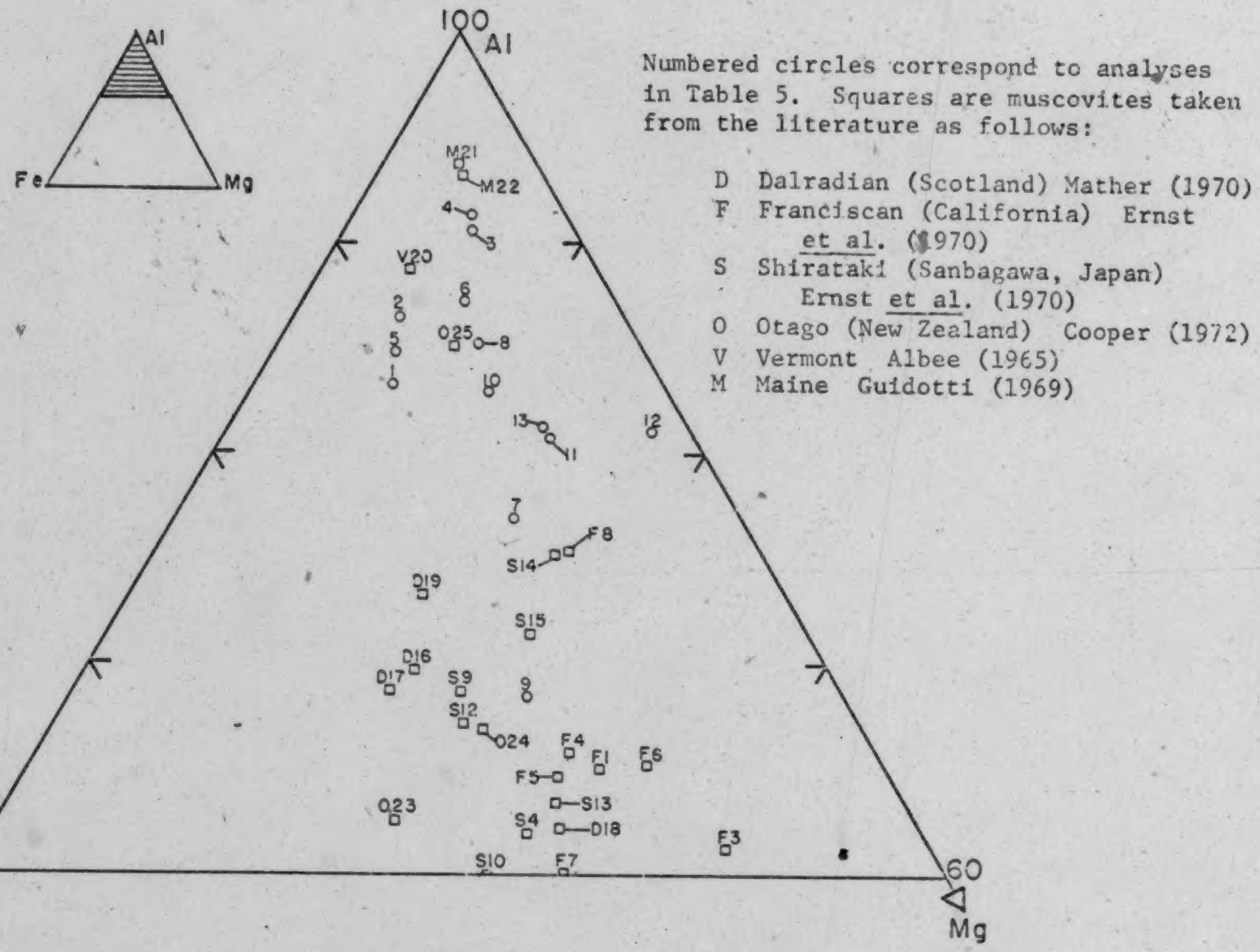

Numbered circles correspond to analyses in Table 5. Squares are muscovites taken from the literature as follows:

D Dalradian (Scotland) Mather (1970)
F Franciscan (California) Ernst *et al*. (1970)
S Shirataki (Sanbagawa, Japan) Ernst *et al*. (1970)
O Otago (New Zealand) Cooper (1972)
V Vermont Albee (1965)
M Maine Guidotti (1969)

Fig. 6. Portion of the AFM diagram for muscovites from regional metamorphic rocks

overlap the low-grade muscovites from the Kootenay Arc. 2) Muscovites from Otago, New Zealand and from the Scottish Dalradian overlap part of the range shown for the Kootenay muscovites, but both Dalradian and Otago muscovites are less magnesian. 3) Muscovites from the kyanite and sillimanite zones fall above the range shown for Kootenay muscovites.

Three muscovites deviate from the trend, 11CBT-15 (2), 10BT-8a, b (1,5) and 5LBT-3 (12). They more closely approximate the trend of Mather's muscovites. Sample 11CBT-15 is within the aureole of the Crawford Bay stock and has been reset by contact metamorphism. Because of this later event, the muscovite has lost Mg and gained Na, but Fe has apparently remained constant. 5LBT-3 comes from a rock which is very low in iron (0.06%). For this reason it has picked up considerably more magnesium in relation to iron, even though the magnesium in relation to iron is fairly low. There is no ready explanation for the behavior of 10BT-8a, b, however, as no nearby igneous body is present, and the rock composition is not radically different from the others lying within the trend.

Fig. 7 is an AKF plot for muscovites from the Kootenay Arc. Muscovite analyses from Mather (1970), Guidotti (1969) and Albee (1965) are plotted for comparison. This plot shows the familiar phengite trend illustrated by Lambert (1959) and later authors. Muscovites from the Kootenay Arc are phengites overlapping in composition those of Mather from the biotite zone and those of Albee from the kyanite isograd.

Variations in muscovite composition with rock composition are illustrated in Figs. 8 and 9. Fig. 8 illustrates the relationship

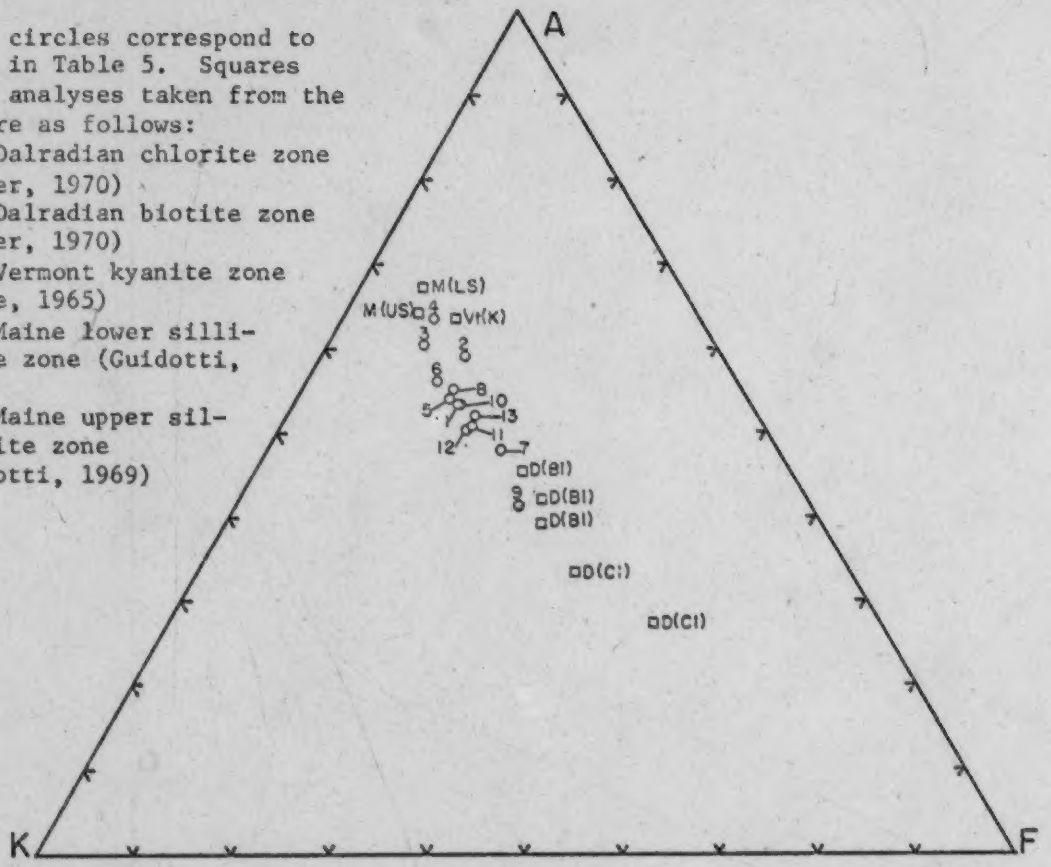

Numbered circles correspond to analyses in Table 5. Squares refer to analyses taken from the literature as follows:

D (Cl) Dalradian chlorite zone (Mather, 1970)

D (Bi) Dalradian biotite zone (Mather, 1970)

Vt (K) Vermont kyanite zone (Albee, 1965)

M (LS) Maine lower sillimanite zone (Guidotti, 1969)

M (US) Maine upper sillimanite zone (Guidotti, 1969)

Fig. 7. AKF plot for muscovites from regional metamorphic rocks

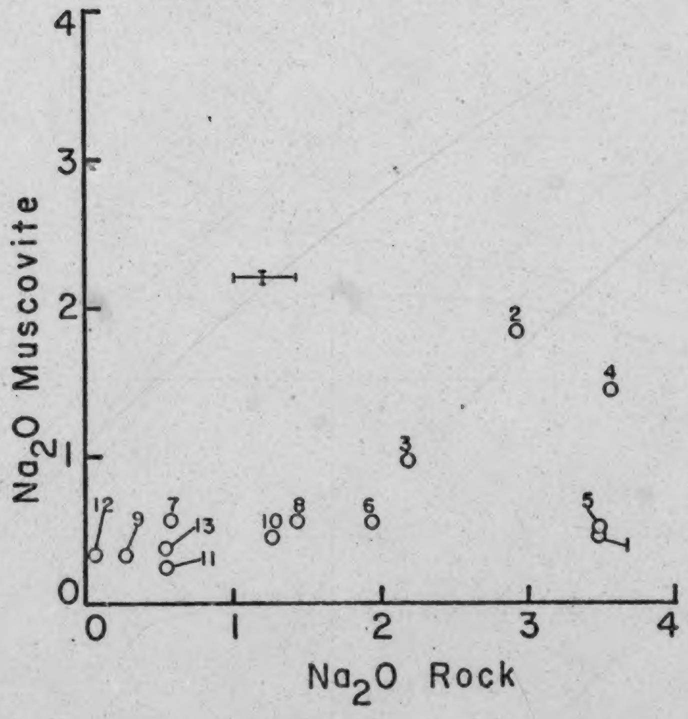

Fig. 8. Na_2O rock plotted against Na_2O in muscovite. Numbers correspond to analyses in Table 2.

Fig. 9a. FeO muscovite plotted against FeO rock

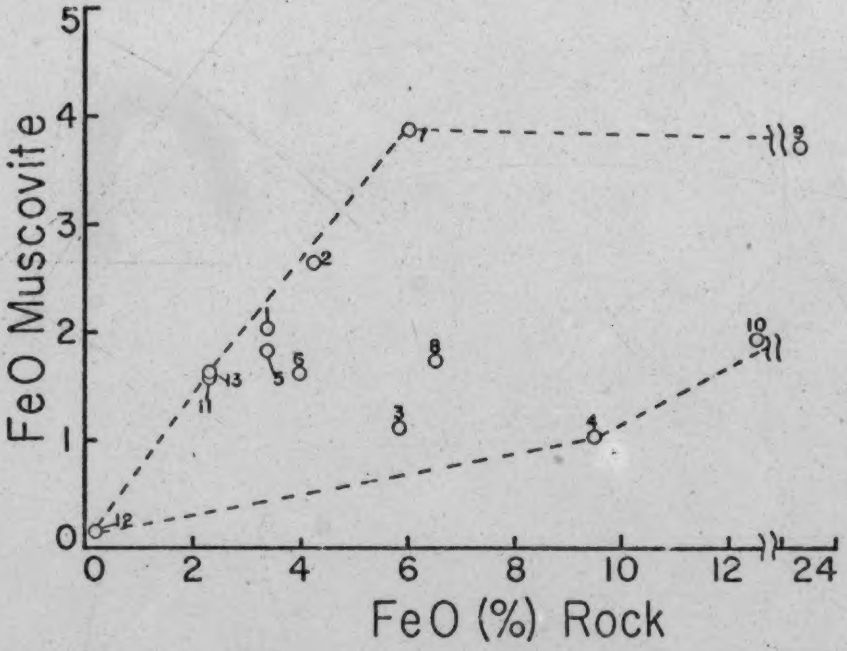

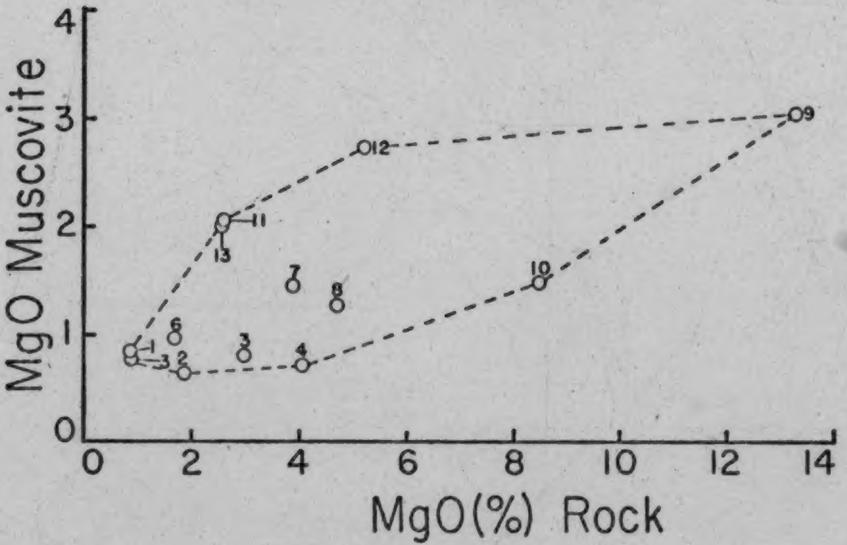

Fig. 9b. MgO muscovite plotted against MgO rock. Numbers correspond to analyses in Table 7.

between rock Na_2O and muscovite Na_2O. The correlation is positive, but only very slight dependence is indicated. Considerable scatter occurs at the higher values of Na_2O. Perhaps more pertinent to arguments yet to be developed is the relation between Fe, Mg and the respective rock values. Figs. 9a, b illustrate these relations. FeO in muscovite shows no relation to FeO in the rock, while MgO shows some correlation but considerable scatter. Mg/Fe ratios show a positive correlation, but with the same scatter shown in Fig. 9a, b. Any rock Mg/Fe ratio may result in different Mg/Fe ratios in the muscovite, thus only the most general correlation can be said to exist. No relation between SiO_2 in the rock and SiO_2 in muscovite can be found, thus supporting the findings of Velde (1967a, 1967b, 1968) and Butler (1967).

Biotite

Biotite is present in most rock types from the central Kootenay Arc. Textural relations are similar in all rock types. Biotite is usually the mineral giving the rock its foliation, but exceptions occur, especially in rocks containing scapolite or in rocks of lower grade. In the latter types, biotite cuts across foliation or is porphyroblastic. Porphyroblastic biotite is found most commonly in chlorite-muscovite-carbonate rocks, where the porphyroblasts may be ten times the size of the groundmass grains. Biotites in scapolite rocks are euhedral and fresh. They cut across lineations shown by amphiboles, or banding caused by alternating layers of feldspar and amphibole or diopside. Euhedral biotite grains may also be found superimposed over large amphibole grains.

Biotites from the region and the Point are generally subhedral, occasionally anhedral or euhedral. In some cases there are two generations of biotite (on textural grounds), one present as smaller subhedral grains, the other as large anhedral to subhedral porphyroblasts. The smaller grains may be poikilitically enclosed in amphibole or garnet. On the Point, biotite is found to form monomineralic pods or lenses. Biotite also forms "selvages" at contacts between small pegmatite bodies and the country rock.

Biotites range in color and pleochroism, but this range is not systematically correlated with grade or rock type. Chlorite-muscovite schists may yield biotites pleochroic yellow-green to olive, or yellow to brownish red or brown. Red biotites are more common along the east and west shore of the lake, where the metamorphism has reached a maximum, but they may occasionally occur at lower grades as well. Biotites from calc-silicate rocks are often nearly colorless, pleochroic to a very pale yellow. Optically they resemble phlogopite, but significant iron is present, making them magnesian biotites.

In relation to other minerals, biotite appears to be in textural equilibrium in most cases. Grain boundaries between amphibole, feldspar, or muscovite are usually smooth, and triple junctions often occur. In other cases, however, biotite is ragged, with serrated terminations. Many biotites have chlorite growing in cleavage traces, occasionally replacing more than half of the grain.

Biotites were analyzed from rocks representative of regional metamorphism of pelitic, amphibolitic and calc-silicic rocks, and all rock types present on Kootenay Point. In three sections, two biotites from different parts of the slide were analyzed to test for variation in biotite composition within single slide. Minerals coexisting with the biotites may be found in the modal analyses presented in Tables 3 and 4. Pertinent assemblages are listed on selected figures.

General chemistry: Major element chemistry for the 46 biotites studied is presented in Tables 6 and 7. Table 6 contains analyses of biotites from regional metamorphic rocks, and Table 7 presents analyses of biotites located on Kootenay Point. Biotites from regional metamorphic rocks were analyzed for 12 elements, including Ba, F and Cl, while biotites from Kootenay Point were analyzed for 11 elements by electron microprobe. Eleven trace elements were analyzed using bulk samples of eleven biotites especially selected and separated from the Kootenay Point suite. The trace element analyses will be presented in a later section. Biotites from the Kootenay Arc show deficiency in the Y-sites, based on calculation to 22 oxygens. Recalculation of the structural formula to 16 cations reveals that excesses usually occur in the Y-site, balanced by deficiencies in the X-site. The oxidation state of the iron as well as the presence of an element not analyzed contributes to the low totals where the total falls below 94%. Biotites with 6 - 7% water are not generally found; 4 - 5% is a more reasonable figure. Barium was not determined for biotites from the Point, but regional biotites may contain up to 0.43% of the oxide. Lithium may also be present in significant quantities.

The major elements are believed to be accurate to within ±3% of the amount shown, with Ti, Mn, Ba, Cl and F somewhat less accurate. Fluorine amounts are uncorrected for fluorescence, atomic number and absorption effects. (See Appendix 1 for further discussion.)

The biotites from the Kootenay Arc encompass the entire composi-

TABLE 6. ELECTRON MICROPROBE ANALYSES OF BIOTITES FROM REGIONAL METAMORPHIC ROCKS

	1	2	3	4	5	6	7	8	9	10
Ox Wt	5LBT-17	10BT-8	11CBT-15	11CBT-16	7RT-17	10BT-4	10BT-17	12WP-2a	12WP-2(2)	12WP-2(1)
SiO_2	33.24	34.43	34.49	34.74	34.79	35.04	35.10	35.32	35.69	35.93
TiO_2	1.71	4.06	1.35	3.53	2.71	3.58	2.47	1.64	2.30	2.22
Al_2O_3	15.25	17.35	18.08	17.12	16.24	18.20	18.77	19.17	16.16	16.62
FeO	22.07	24.61	19.05	24.62	24.75	21.94	18.50	10.01	21.97	21.65
MnO	0.09	0.46	0.11	0.28	0.10	0.33	0.24	0.04	0.07	0.11
MgO	13.06	6.08	10.92	6.83	7.51	7.07	9.38	10.44	10.13	10.04
CaO	0.02	0.04	0.08	0.03	0.03	0.03	0.01	0.06	0.01	0.00
Na_2O	0.08	0.08	0.15	0.07	0.10	0.11	0.13	0.27	0.15	0.15
K_2O	8.58	9.37	8.14	9.38	8.50	8.77	9.23	8.22	8.92	8.88
BaO	0.39	0.16	0.10	0.16	0.26	0.14	0.07	0.00	0.37	0.43
Cl	0.42	0.16	0.08	0.17	0.10	0.07	0.09	0.00	0.12	0.11
F	0.25	0.33	0.33	0.21	0.56	0.45	0.28	0.31	0.31	0.44
Total	95.16	97.14	92.88	97.15	95.65	95.73	94.27	94.50	96.20	96.59
H_2O*	4.84	2.86	7.22	2.85	4.35	4.27	5.73	5.50	3.80	3.41

STRUCTURAL FORMULA ON THE BASIS OF 22 OXYGENS

	1	2	3	4	5	6	7	8	9	10
Si	5.239	5.343	5.393	5.377	5.471	5.408	5.408	5.394	5.499	5.506
Al^{IV}	2.761	2.657	2.607	2.623	2.529	2.592	2.592	2.606	2.501	2.494
Total tet.	8.000	8.000	8.000	8.000	8.000	8.000	8.000	8.000	8.000	8.000
Al^{VI}	.072	.516	.725	.499	.481	.719	.817	.844	.433	.508
Ti	.203	.474	.159	.411	.320	.416	.286	.188	.266	.256
Fe	2.909	3.194	2.491	3.187	3.255	2.832	2.384	2.428	2.831	2.775
Mn	.012	.060	.015	.037	.013	.043	.031	.005	.009	.014
Mg	3.068	1.406	2.545	1.576	1.760	1.626	2.154	2.376	2.326	2.293
Total oct.	6.263	5.650	5.934	5.709	5.830	5.636	5.672	5.842	5.866	5.846
Ca	.003	.007	.013	.005	.005	.005	.002	.010	.002	0
Na	.024	.024	.045	.021	.030	.033	.039	.080	.045	.045
K	1.725	1.855	1.624	1.852	1.705	1.727	1.814	1.601	1.753	1.736
Total	1.752	1.885	1.682	1.878	1.740	1.765	1.855	1.691	1.800	1.780

*H_2O determined by difference from 100%. This figure is a maximum value as Fe_2O_3 has not been determined. H_2O is not used in further calculations.

TABLE 6 CONTINUED

Ox Wt	11 6CCT-1	12 6CCT-1a	13 4LBT-2	14 8AT-8	15 10BT-9	16 10BT-13	17 5LBT-20	18 8AT-18
SiO_2	36.04	36.39	38.02	38.25	38.30	29.60	40.08	40.09
TiO_2	1.85	1.61	1.77	1.23	2.11	1.05	0.74	1.11
Al_2O_3	16.44	16.71	16.75	13.72	15.87	14.56	14.75	16.24
FeO	16.86	17.53	16.93	16.72	11.48	18.43	8.64	8.76
MnO	0.24	0.07	0.14	0.21	0.12	0.14	0.00	0.00
MgO	12.08	12.76	13.05	14.53	16.63	11.56	20.64	19.63
CaO	0.05	0.00	0.00	0.02	0.01	0.02	0.08	0.00
Na_2O	0.25	0.11	0.03	0.05	0.03	0.01	0.05	0.08
K_2O	9.34	9.23	8.86	9.41	9.67	9.64	9.12	10.09
BaO	0.07	0.08	0.03	0.04	0.08	0.06	0.06	0.05
Cl	0.12	0.12	0.01	0.02	0.01	0.02	0.00	0.00
F	0.21	0.15	0.47	1.62	0.59	2.35	0.00	1.22
Total	93.56	94.78	96.15	95.81	94.32	97.56	94.15	97.27
H_2O*	6.44	5.22	3.85	4.19	5.68	2.64	5.85	2.73

STRUCTURAL FORMULA ON THE BASIS OF 22 OXYGENS

Si	5.564	5.541	5.662	5.842	5.673	5.989	5.828	5.740
Al^{IV}	2.436	2.459	2.338	2.176	2.327	2.011	2.172	2.260
Total tet.	8.000	8.000	8.000	8.000	8.000	8.000	8.000	8.000
Al^{VI}	.556	.540	.602	.285	.443	.584	.356	.480
Ti	.215	.184	.198	.141	.235	.119	.081	.120
Fe	2.177	2.232	2.109	2.129	1.422	2.331	1.051	1.049
Mn	.031	.009	.018	.027	.015	.018	0	0
Mg	2.780	2.896	2.897	3.297	3.671	2.606	4.473	4.189
Total oct.	5.759	5.862	5.823	5.879	5.786	5.658	5.961	5.837
Ca	.008	0	0	.003	.002	.003	.012	0
Na	.075	.032	.009	.015	.011	.006	.014	.022
K	1.839	1.793	1.683	1.828	1.827	1.860	1.692	1.843
Total	1.923	1.825	1.692	1.846	1.840	1.869	1.718	1.865

*H_2O determined by difference from 100%. This figure is a maximum value as Fe_2O_3 has not been determined. H_2O is not used in further calculations.

TABLE 7. ELECTRON MICROPROBE ANALYSES OF BIOTITES FROM KOOTENAY POINT

Ox Wt	19 T3-11	20 T4-4	21 T4-8	22 T3-12	23 T1-9a	24 375-140W	25 T4-2	26 240-137E(2)	27 T2-15	28 240-137E(1)	29 30-13E
SiO_2	35.93	36.16	36.30	36.90	37.10	37.25	37.31	37.32	37.47	37.67	38.17
TiO_2	2.06	2.04	1.66	1.91	1.72	1.87	1.47	1.65	2.59	1.74	2.32
Al_2O_3	15.14	15.13	15.29	14.45	15.81	16.07	15.99	16.10	15.11	16.12	11.85
FeO	18.69	17.57	17.99	20.12	14.01	15.97	14.74	13.53	18.30	13.07	17.76
MnO	0.17	0.18	0.20	0.19	0.14	0.14	0.23	0.13	0.24	0.11	0.18
MgO	11.05	11.64	12.00	11.29	14.73	13.36	13.92	15.16	12.04	15.96	12.90
CaO	0.25	0.06	0.08	0.07	0.20	0.00	0.14	0.00	0.09	0.06	0.03
Na_2O	0.07	0.11	0.10	0.54	0.32	0.10	0.09	0.13	0.16	0.35	0.02
K_2O	8.97	9.46	8.97	9.24	9.49	9.70	9.47	9.60	9.73	9.80	9.91
F	0.33	0.08	0.29	0.26	0.15	1.95	0.27	0.26	0.17	0.26	0.74
Cl	0.02	0.04	0.04	0.05	0.03	0.00	0.00	0.00	0.07	0.03	0.02
Total	92.68	92.41	92.93	94.52	93.40	96.41	93.62	93.86	95.96	95.17	93.80
H_2O*	7.32	7.59	7.07	5.48	6.30	3.59	6.38	6.14	4.04	4.83	6.20

STRUCTURAL FORMULA ON THE BASIS OF 22 OXYGENS

Si	5.645	5.639	5.665	5.696	5.625	5.636	5.675	5.629	5.667	5.602	5.939
Al^{IV}	2.355	2.361	2.335	2.304	2.375	2.364	2.325	2.371	2.333	2.398	2.061
Total tet.	8.000	8.000	8.000	8.000	8.000	8.000	8.000	8.000	8.000	8.000	8.000
Al^{VI}	.448	.420	.455	.324	.045	.502	.541	.491	.360	.428	.112
Ti	.243	.223	.180	.222	.196	.213	.168	.187	.295	.195	.271
Fe	2.456	2.291	2.329	2.597	1.776	2.021	1.875	1.707	2.315	1.626	2.311
Mn	.023	.024	.026	.025	.018	.018	.030	.017	.031	.014	.024
Mg	2.588	2.706	2.768	2.597	3.329	3.013	3.156	3.408	2.714	3.538	2.992
Total oct.	5.758	5.664	5.758	5.765	5.769	5.767	5.769	5.810	5.714	5.800	5.710
Ca	.042	.010	.013	.012	.032	0	.023	0	.015	.010	.005
Na	.021	.033	.030	.162	.094	.029	.027	.038	.047	.101	.006
K	1.798	1.882	1.771	1.819	1.835	1.872	1.837	1.847	1.877	1.859	1.967
Total	1.861	1.925	1.814	1.993	1.962	1.902	1.887	1.885	1.939	1.970	1.978

*H_2O determined by difference from 100%. This figure is a maximum value as Fe_2O_3 has not been determined. H_2O is not used in further calculations.

TABLE 7 CONTINUED

Ox Wt	30 T4-6(2)	31 190-120E(1)	32 190-120E(2)	33 T3-2b	34 198-146E	35 T3-9	36 T4-6(1)	37 T1-1	38 T1-8	39 T3-5
SiO_2	38.58	38.73	38.81	38.84	38.88	38.92	39.20	39.87	39.90	40.08
TiO_2	1.44	1.17	1.21	0.74	1.15	1.32	1.53	1.09	1.02	1.05
Al_2O_3	15.67	14.40	14.23	14.61	14.81	14.21	15.69	15.31	14.03	13.03
FeO	8.51	10.49	10.91	7.59	10.40	9.93	8.49	4.89	5.57	5.32
MnO	0.10	0.06	0.05	0.08	0.05	0.17	0.11	0.02	0.03	0.34
MgO	19.34	18.72	18.00	22.01	19.10	18.84	19.36	22.13	23.97	23.35
CaO	0.04	0.12	0.01	0.05	0.04	0.01	0.02	0.01	0.17	0.01
Na_2O	0.10	0.17	0.29	0.12	0.22	0.12	0.07	0.24	0.39	0.10
K_2O	9.47	10.18	10.27	9.96	10.08	10.19	9.57	10.41	9.93	10.04
F	0.49	0.51	1.04	0.51	0.63	1.16	0.43	0.47	0.58	0.75
Cl	0.03	0.04	0.15	0.11	0.03	0.01	0.02	0.02	0.01	0.14
Total	93.78	94.59	94.96	94.62	95.39	95.48	94.51	94.46	95.59	94.70
H_2O*	6.22	5.41	5.04	6.39	4.61	4.52	5.49	5.54	4.41	5.30

STRUCTURAL FORMULA ON THE BASIS OF 22 OXYGENS

	30	31	32	33	34	35	36	37	38	39
Si	5.687	5.750	5.791	5.739	5.719	5.78[illegible]	5.723	5.755	5.721	5.846
Al^{IV}	2.313	2.250	2.209	2.261	2.281	2.219	2.277	2.245	2.279	2.154
Total tet.	8.000	8.000	8.000	8.000	8.000	8.000	8.000	8.000	8.000	8.000
Al^{VI}	.409	.269	.293	.284	.286	.269	.422	.359	.091	.086
Ti	.160	.131	.136	.082	.127	.147	.168	.118	.110	.115
Fe	1.049	1.302	1.361	.938	1.279	1.234	1.037	.590	.668	.649
Mn	.012	.008	.006	.010	.006	.021	.014	.002	.004	.042
Mg	4.249	4.142	4.003	4.627	4.187	4.171	4.213	4.761	5.122	5.076
Total oct.	5.880	5.852	5.800	5.942	5.886	5.842	5.854	5.831	5.995	5.968
Ca	.007	.019	.002	.008	.006	.002	.003	.002	.026	.002
Na	.028	.049	.084	.034	.063	.035	.021	.067	.108	.028
K	1.780	1.928	1.955	1.877	1.891	1.931	1.783	1.917	1.816	1.868
Total	1.815	1.996	2.040	1.920	1.960	1.967	1.807	1.984	1.941	1.898

*H_2O determined by difference from 100%. This is a maximum value as Fe_2O_3 has not been determined. H_2O is not used in further calculations.

TABLE 7 CONTINUED

Ox Wt	40 205-50W	41 72-80E	42 56-20E	43 199-146E	44 T3-4	45 T2-2	46 105-101E
SiO_2	40.33	40.90	41.09	41.29	41.83	42.03	43.76
TiO_2	0.92	0.46	0.50	0.84	0.90	0.71	0.18
Al_2O_3	12.19	12.11	13.55	15.78	11.85	11.83	11.64
FeO	3.81	3.54	5.80	5.94	3.82	2.39	3.63
MnO	0.00	0.03	0.23	0.35	0.00	0.01	0.01
MgO	23.83	25.75	22.24	22.24	24.02	27.42	27.42
CaO	0.00	0.08	0.05	0.07	0.00	0.12	0.11
Na_2O	0.11	0.12	0.28	0.29	0.61	0.38	0.25
K_2O	9.94	9.48	10.36	10.21	10.04	10.19	9.91
F	2.24	1.19	2.22	0.89	0.59	0.75	1.33
Cl	0.00	0.00	0.02	0.02	0.27	0.03	0.03
Total	93.36	93.65	96.35	97.90	93.74	95.86	96.25
H_2O*	6.64	6.35	3.65	2.10	6.26	4.14	3.75

STRUCTURAL FORMULA ON THE BASIS OF 22 OXYGENS

Si	5.965	5.939	5.947	5.785	6.004	5.930	5.993
Al^{IV}	2.035	2.061	2.053	2.215	1.996	2.070	2.007
Total tet.	8.000	8.000	8.000	8.000	8.000	8.000	8.000
Al^{VI}	.090	.011	.258	.391	.009	.102	.084
Ti	.102	.050	.054	.089	.091	.075	.019
Fe	.471	.430	.702	.696	.459	.282	.425
Mn	0	.004	.038	.042	0	.001	.001
Mg	5.253	5.573	4.797	4.644	5.268	5.767	5.728
Total oct.	5.916	6.067	5.839	5.861	5.827	6.023	6.090
Ca	0	.012	.008	.011	0	.018	.017
Na	.032	.034	.079	.079	.170	.104	.068
K	1.875	1.756	1.913	1.825	1.839	1.834	1.772
Total	1.907	1.802	1.999	1.914	2.009	1.956	1.856

*H_2O determined by difference from 100%. This figure is a maximum value as Fe_2O_3 has not been determined. H_2O is not used in further calculations.

tional range of natural biotites given by Foster (1960) (Figs. 10, 11). Fig. 10 is a plot of biotites from the regional metamorphic rocks. Most biotites from regional metamorphic rocks are iron-biotites with a much smaller group of transitional magnesian biotites. The magnesian biotites coexist with tremolite-diopside-calcite and dolomite. Fig. 11 shows the compositional variation for biotites from Kootenay Point. The lower Mg group overlaps the group shown in Fig. 10. The compositional trends in biotite can be related to mineralogy, as can be seen from the zones delimited at the right of Fig. 11. Increasing Mg content is found in biotites coexisting with ep-hb, hb-cc-dol-act-di and tr-act-di-cc-dol respectively. The regional biotites do not show such sharp mineralogical dependence, but do show some dependence on grade.

The large compositional range of biotites makes examination of compositional controls within the biotite group possible. Such an examination is desirable from the standpoint of understanding the substitution scheme for biotites and understanding which elements are likely to be controlled primarily by bulk chemistry and which by changing conditions of formation.

The substitution scheme for biotites has been examined in detail by Foster (1960), Crowley and Roy (1964) and Deer, et al. (1966). Other contributions have been made by Wones (1967), Seifert and Schreyer (1971) and Reitan (1972). These investigations have defined substitutions involving octahedral and tetrahedral cations and have suggested relationships between X-site cations, anions and octahedral and tetrahedral cations. The following paragraphs will examine the relationships between X, Y and Z site cations and the F and Cl anions. The discussion will be qualitative, since structural parameters and amounts of

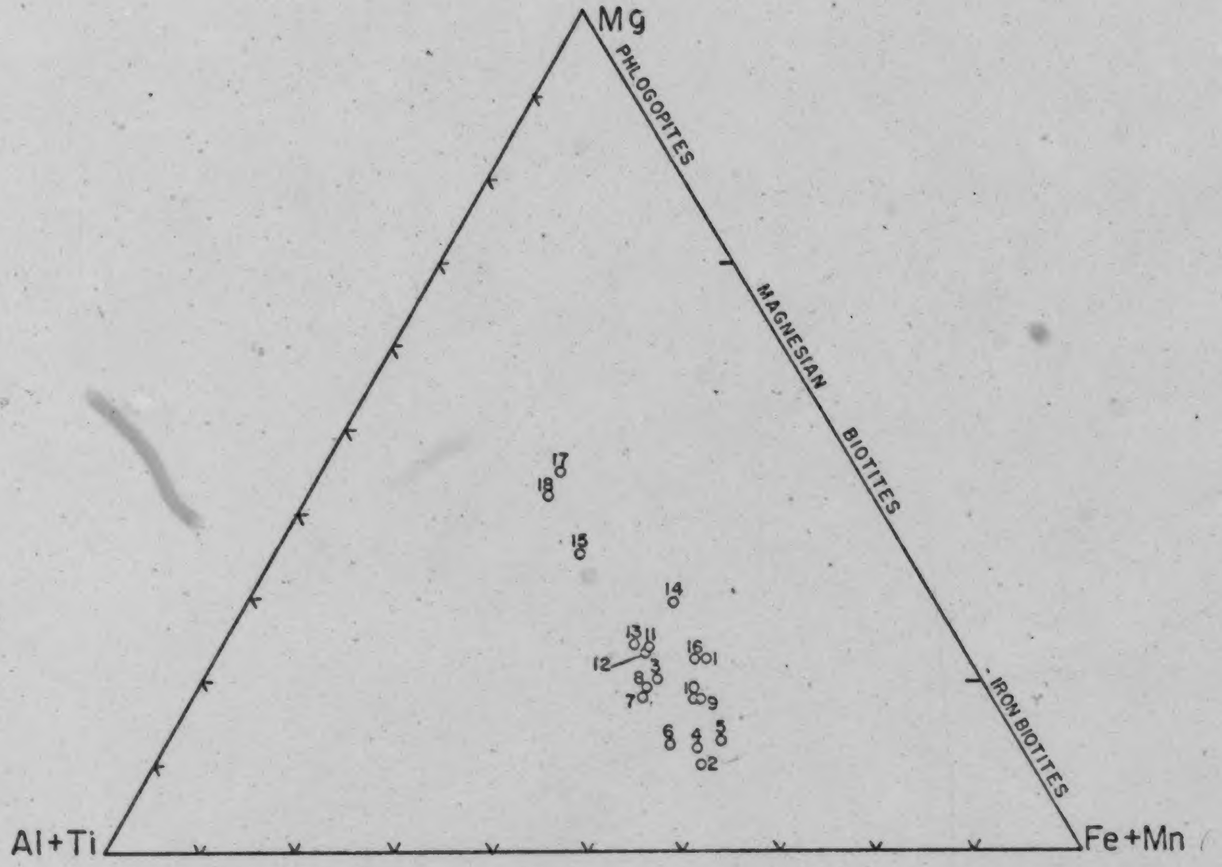

Fig. 10. AFM plot for biotites from regional metamorphic rocks. Biotite compositional ranges indicated along the right margin are taken from Foster (1960). Numbers refer to analyses in Table 6.

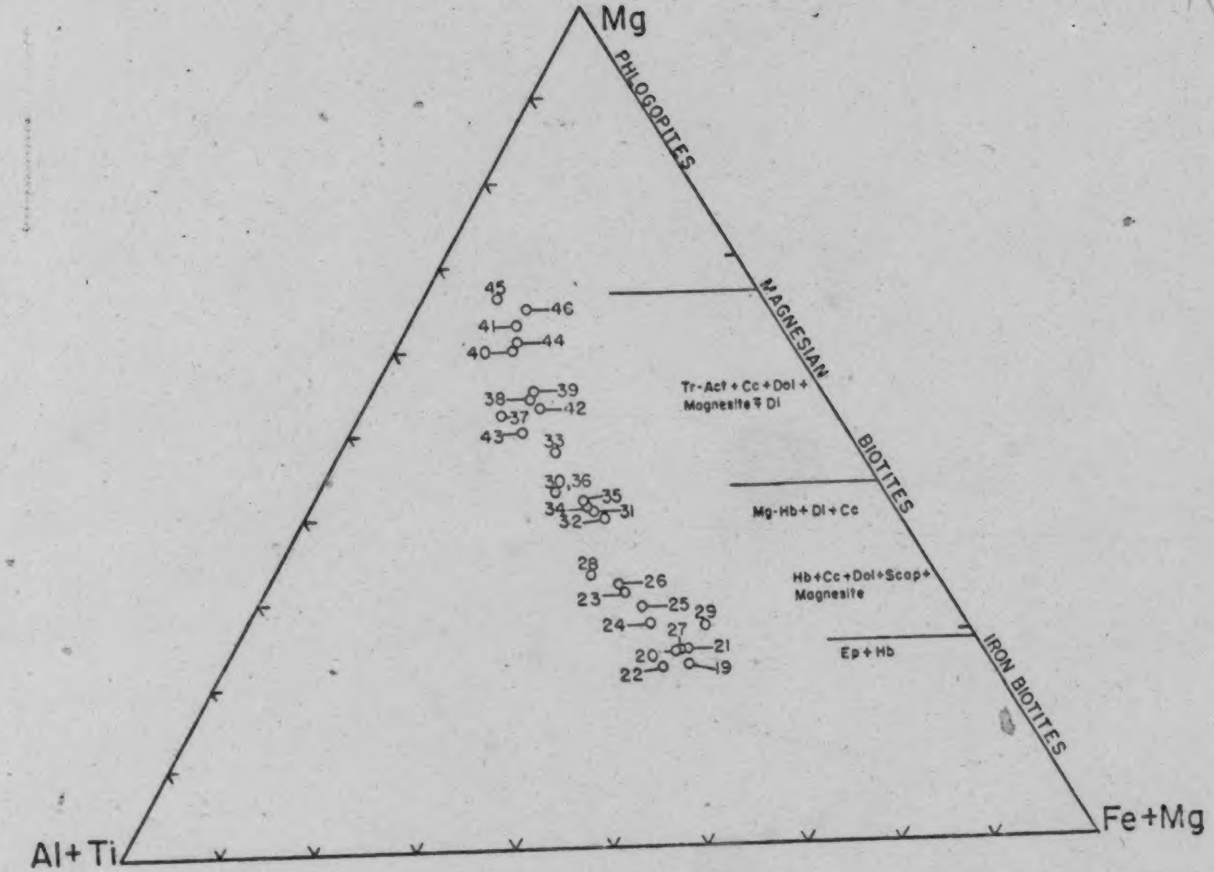

Fig. 11. AFM plot for biotites from Kootenay Point. Biotite compositional ranges as in Fig. 10. Mineral assemblages coexisting with the different biotites appear inside the right margin. Numbers refer to analyses in Table 7.

Fe^{3+} have not been determined, but the relationships should provide some insight into the relationships between the different cations.

Y-site cations: Replacement of Mg in phlogopite by R^{3+} ions, and replacement of Mg by Fe^{2+} on an ion for ion basis produces the different compositions of the biotite group (Foster, 1960). Foster (1960) considers that the $Fe^{2+} \rightleftharpoons Mg$ exchange proceeded independently of the $Mg \rightleftharpoons R^{3+}$ exchange based on absence of correlation between Fe^{2+} and amount of R^{3+} present. Wones (1967) considers $Mg \rightleftharpoons Al$ and $Al \rightleftharpoons Fe^{3+}$ substitution possible. Reitan (1972) suggests positive correlations between octahedral Al, tetrahedral Al and Fe/Fe + Mg; tetrahedral Al, Fe/Fe + Mg, Fe + Al^{VI}/Σoct and Al^{VI}/Σoct and negative correlations between octahedral Al, Σoct and Mg; tetrahedral Al and Mg, and no correlation between octahedral Al and Fe or tetrahedral Al and Fe.

Fig. 12 illustrates the relationship between Mg and Σ oct for all biotites studied. This relationship is the same as that found by Foster (1960), wherein a decrease in Y-site occupancy is correlated with increasing R^{3+} content. Figs. 13 and 14 plot tetrahedral Al against Ti, Fe, Mg and Fe/Fe + Mg and octahedral Al against Ti and tetrahedral Al. All other relationships between octahedral cations can be determined from these diagrams and the fact that octahedral Al shows the same trends as tetrahedral Al, but with more scatter. Both octahedral and tetrahedral Al rise with an increase in Σ oct. The trends for octahedral Al and Fe suggest that a correlation exists between $Fe_{tot.}$ and R^{3+}, and this fact, coupled with the negative trend for Mg, suggests that $Mg \rightleftharpoons R^{3+}$ and $Mg \rightleftharpoons Fe^{2+}$ substitutions may not be independent as suggested by Foster (1960). Their interdependence cannot be confirmed because no Fe^{3+} determinations have been made. These determinations

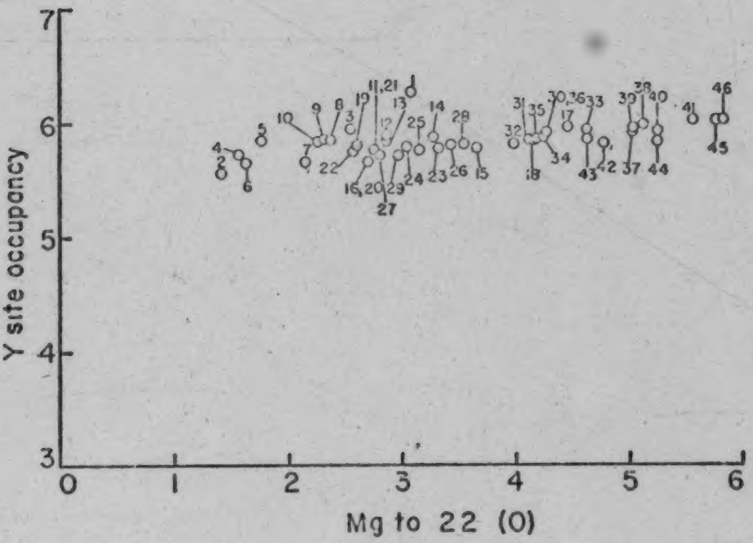

Fig. 12. Y-site occupancy (Σ oct) against Mg (calculated on the basis of 22 (O)) for all biotites. Numbers refer to analyses in Tables 6 and 7.

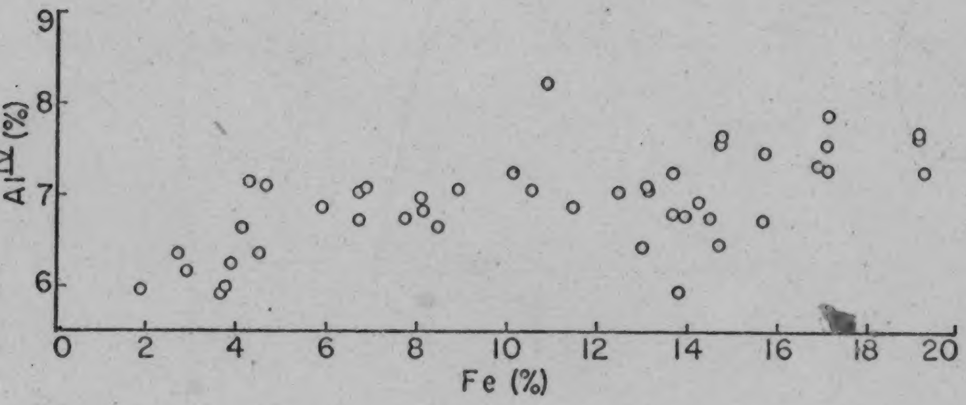

a

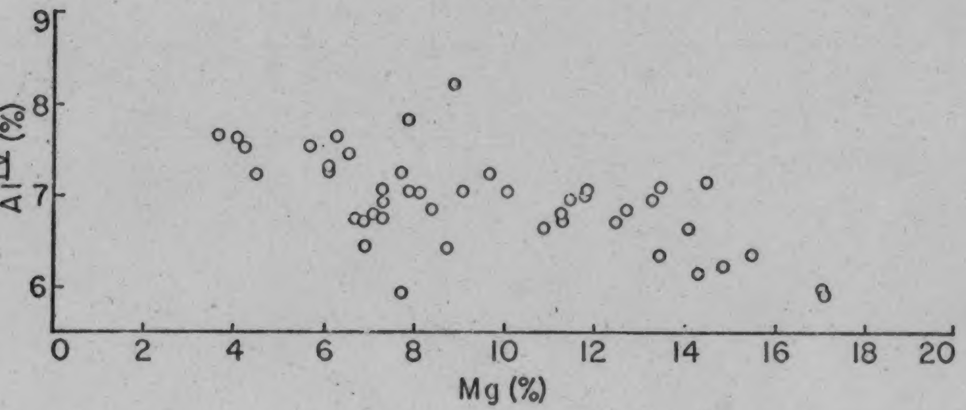

b

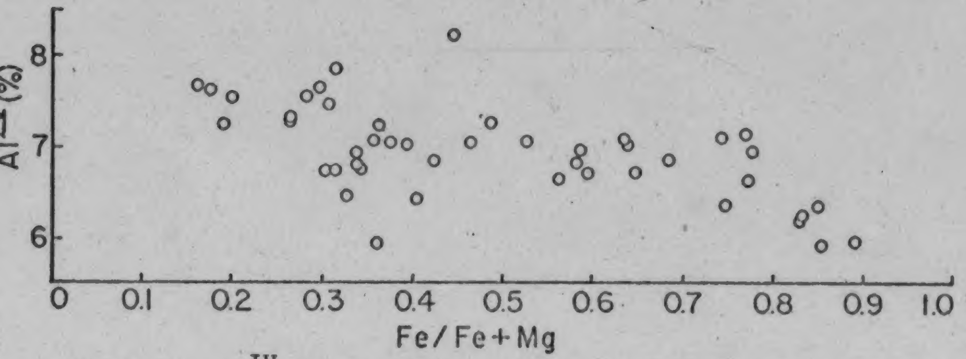

c

Fig. 13 a. Al^{IV} (%) against Fe (%), all biotites.

Fig. 13 b. Al^{IV} (%) against Mg (%), all biotites.

Fig. 13 c. Al^{IV} (%) against Fe/Fe + Mg, all biotites.

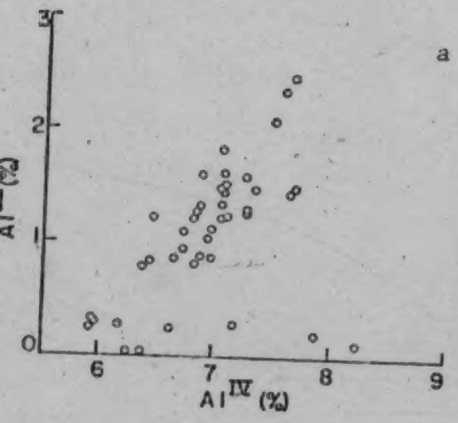

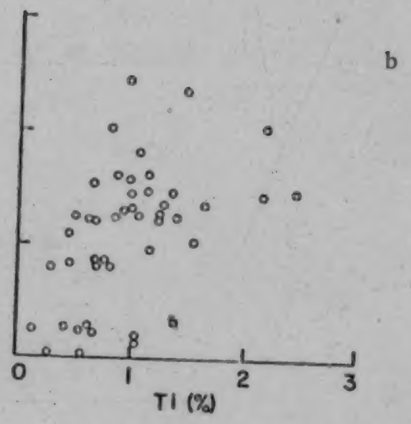

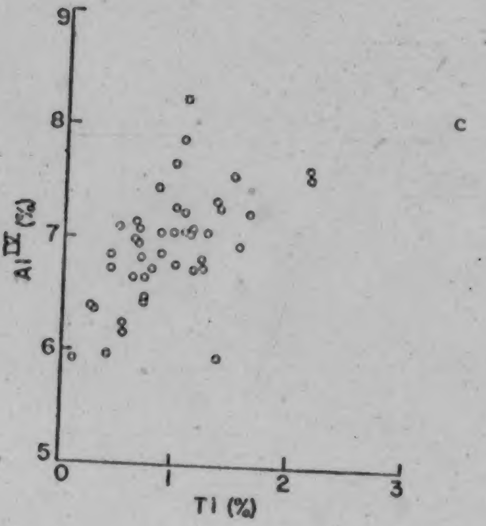

Fig. 14 a. Al^{VI} (%) against Al^{IV} (%), all biotites

Fig. 14 b. Al^{VI} (%) against Ti (%), all biotites

Fig. 14 c. Al^{IV} (%) against Ti (%), all biotites would be useful as the data from this study suggest coupled substitutions of $Al^{VI} + Fe \rightleftharpoons Mg$. Ti must also participate in this substitution, since it correlates positively with Al.

Z-site cations: The Z-site is normally occupied by Al^{3+} and Si, but some Fe^{3+} and Ti may also be present (Crowley and Roy, 1964; Deer et al., 1966). Si for Al exchange can be shown to take place in synthetic phlogopite up to Si_4Al_4 (Crowley and Roy, 1964). The substitutions in the site are coupled with octahedral cations, as has been demonstrated for muscovites. The correlations between tetrahedral Al and Fe, Mg, Ti and octahedral Al indicate coupled substitutions involving these cations.

Figs. 15 and 16 illustrate the correlation between Si and Mg/Al and Si and Al^{VI}. The two plots together indicate substitution involving $Mg + Si \rightleftharpoons Al$ (or $Mg + Si \rightleftharpoons 2Al$ as in muscovites). This substitution scheme is well known, but the plots of tetrahedral and octahedral Al against Fe, Ti and Mg indicate that the octahedral-tetrahedral exchange may involve related $Fe \rightleftharpoons Mg$ and $Al \rightleftharpoons Mg$ substitutions in the Y-site.

X-site cations: K, Na and Ca occupy the 12-fold X-site in micas, and their relation to octahedral and tetrahedral cations is not well understood. Foster (1960) suggested a relationship between K + Mg and Al^{3+}. Fig. 17 shows a positive relationship between K_2O and SiO_2 (wt %). This plot, coupled with those previously mentioned, suggests a relationship of the type postulated by Foster (1960). This relationship also indicates that X-site deficiency decreases with increased Si and Mg content (i.e., as biotite becomes more phlogopitic). This can be confirmed by glancing at Tables 6 and 7, noting that biotites with high Si content have the least amount of deficiency in the X-site.

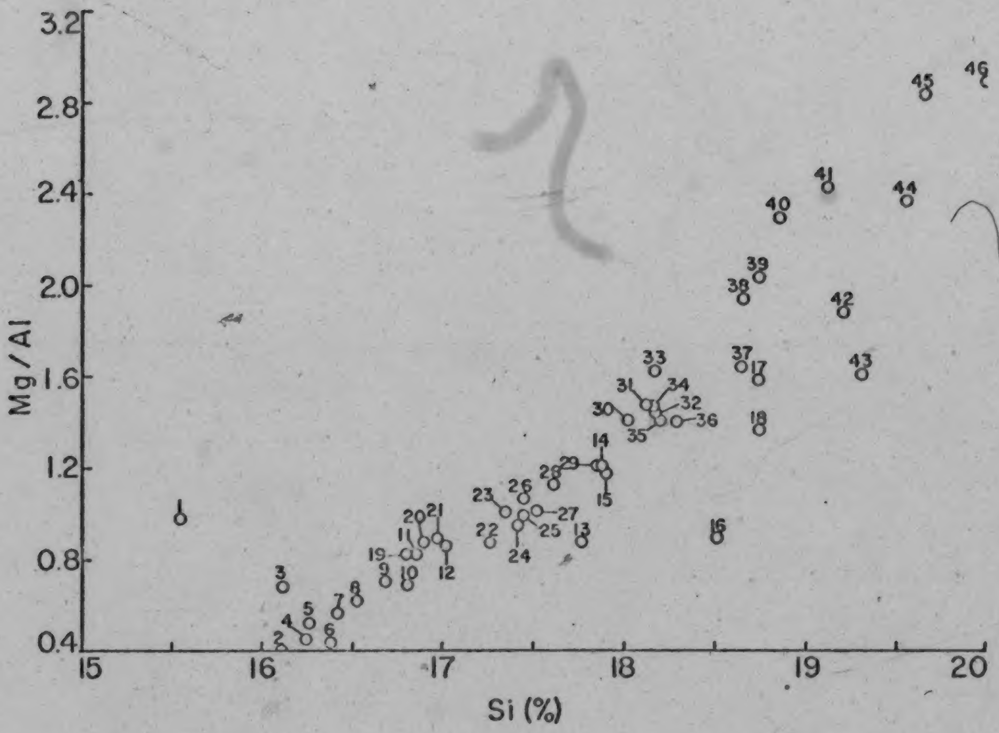

Fig. 15. Mg/Al plotted against Si (%) for all biotites analyzed. Numbers correspond to analyses in Tables 6 and 7.

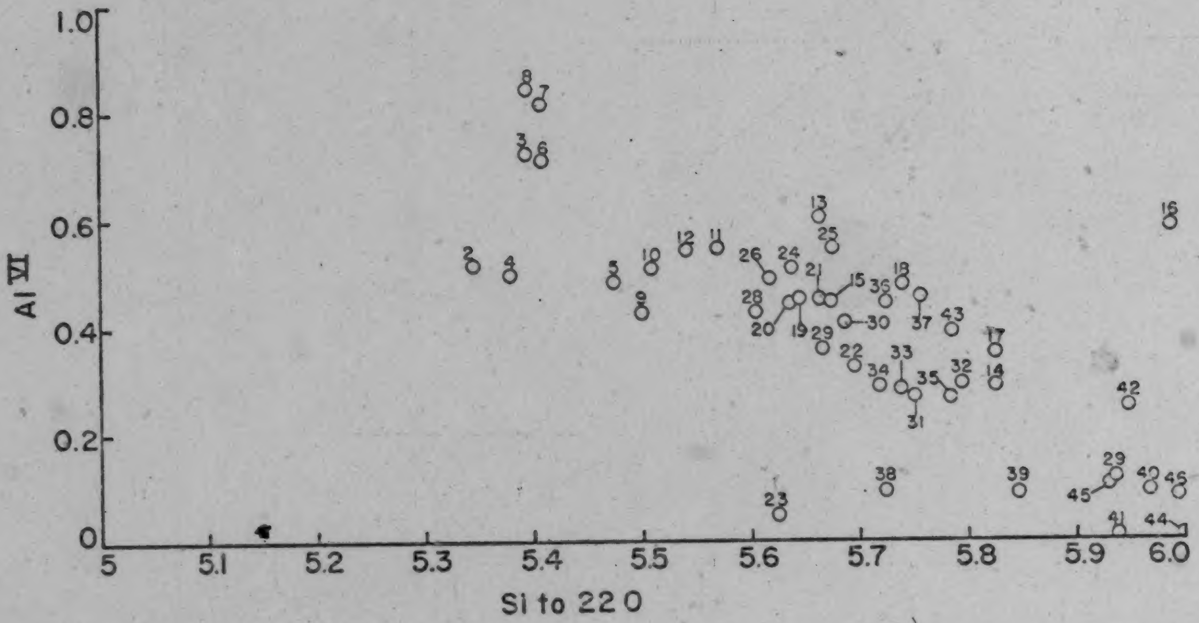

Fig. 16. Al^{VI} plotted against Si calculated on the basis of 22 oxygens, all biotites analyzed. Numbers correspond to analyses in Tables 6 and 7.

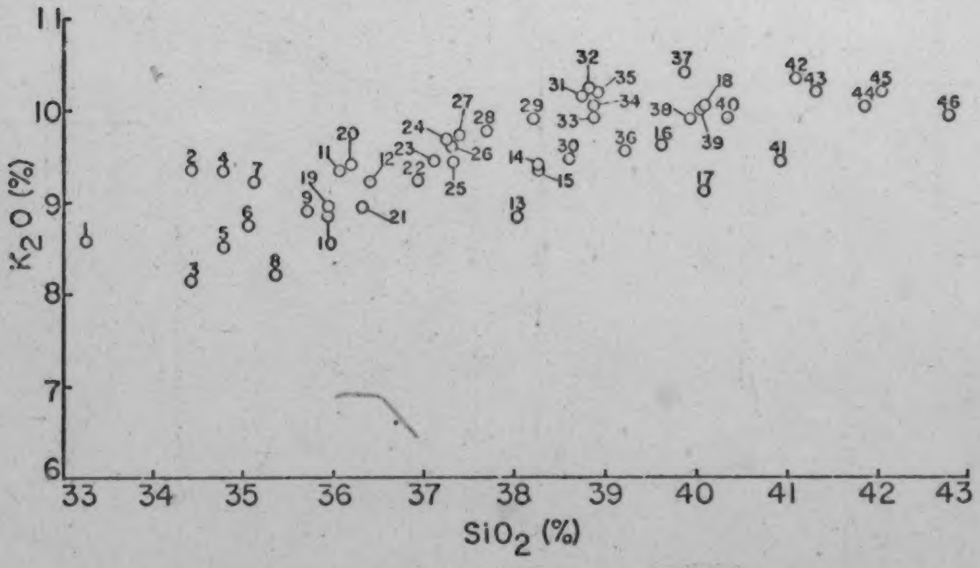

Fig. 17. K$_2$O (%) plotted against SiO$_2$ (%), for all biotites analyzed. Numbers correspond to analyses in Tables 6 and 7.

Anions: F + Cl may also be related to substitutions in other sites in biotites. In Fig. 18, F + Cl has been plotted against SiO_2 (wt %). This plot shows two trends. From SiO_2 33 to 38 wt %, a linear decrease in F + Cl is found. For values of SiO_2 beyond 38%, F + Cl jumps suddenly and shows a general increase. This break corresponds to the break in the trend for Mg/Al vs Si (Fig. 15). Consideration of these two plots leads to the hypothesis that more F + Cl will substitute in biotites with higher phlogopite content, rather than higher Ti content as suggested by Deer et al. (1966).

Biotite composition in relation to bulk chemistry: Bulk rock chemistry can be expected to influence the amounts of cations present in all sites by its influence on biotite composition. Bulk chemistry is known to influence Mg and Fe ratios in biotites, and other octahedral cations are affected. Mg/Fe ratios commonly vary according to bulk composition, grade and character of coexisting minerals in metamorphic rocks. Fig. 19a is a plot of Mg/Fe^{2+} in biotite against Mg/Fe^{2+} in the rock for biotites from the Point. The plot indicates a strong correlation between rock and mineral composition. The dependence of mineralogy on Mg/Fe rock ratios is further demonstrated by the limits for coexisting minerals shown along the top margin of Figure 19a. A regular succession from hornblende or hornblende-epidote bearing rocks through hornblende-actinolite to tremolite-diopside-calcite-dolomite is shown. Fig. 19b is a similar plot for biotites from the region. Fig. 20a demonstrates the dependence of Mg/Al ratios of biotites on rock Mg/Al for biotites from the Point, as well as indicating the successive disappearance of plagioclase and potassium feldspar with increased Mg/Al

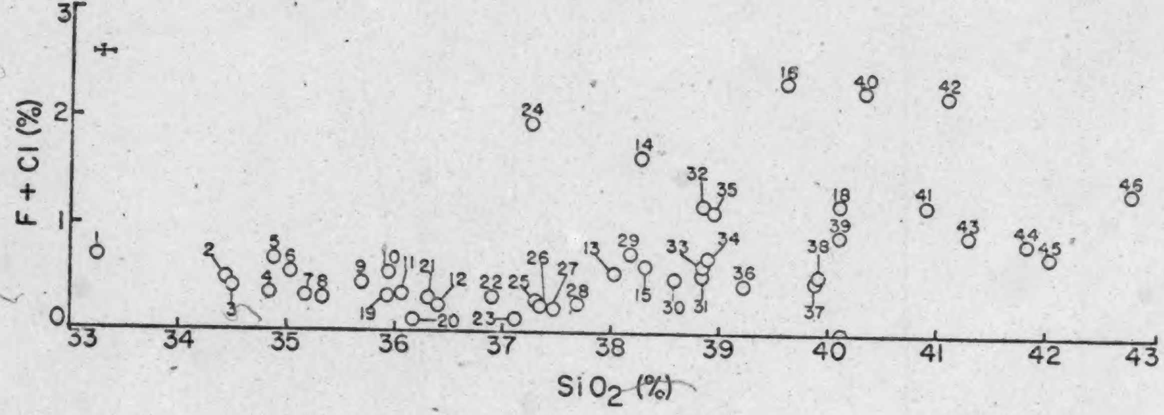

Fig. 18. F + Cl (%) against SiO_2 (%) for all biotites analyzed. Numbers refer to analyses in Tables 6 and 7.

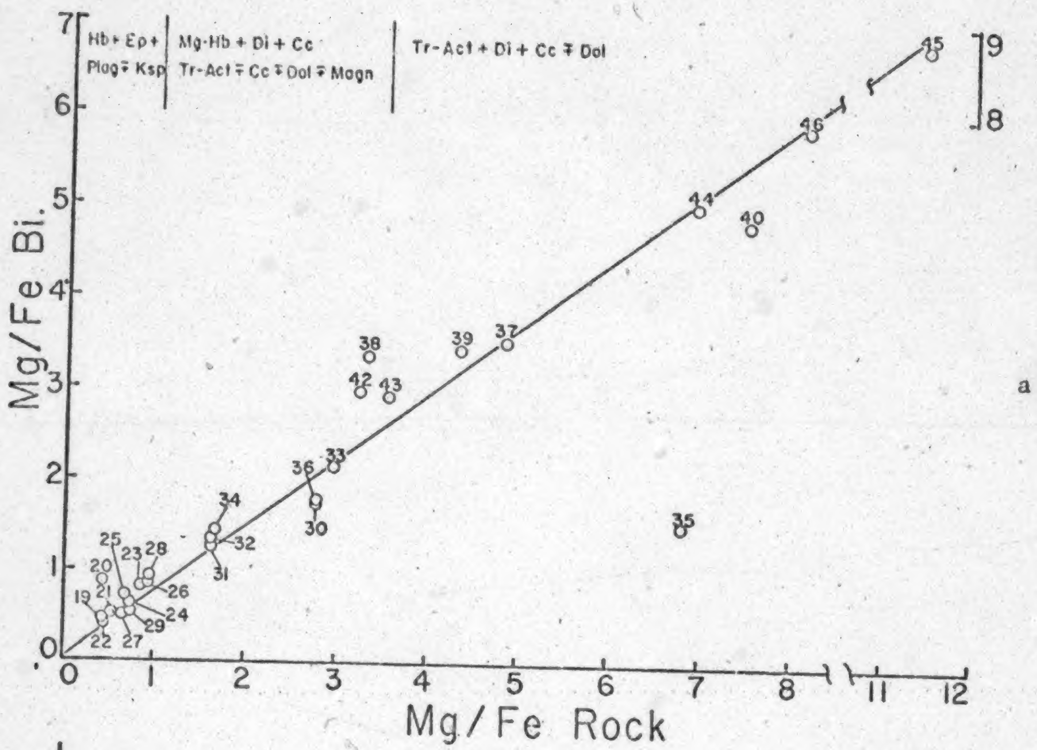

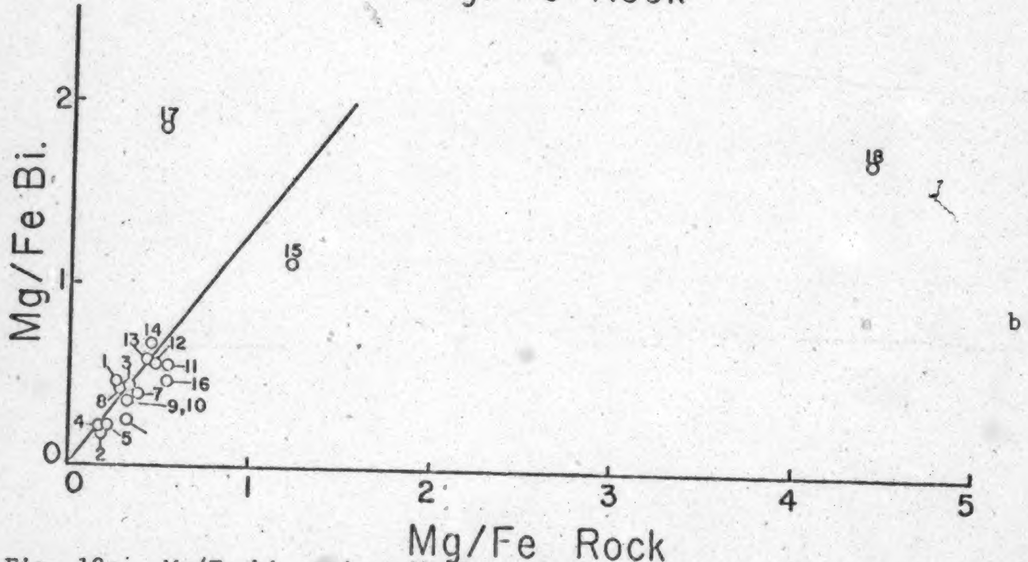

Fig. 19a. Mg/Fe bi against Mg/Fe rock for biotites from Kootenay Point. Coexisting minerals for various Mg/Fe ratios in rock are given along the upper edge.

Fig. 19b. Mg/Fe bi against Mg/Fe rock for biotites from regional metamorphic rocks. Minerals shown in Fig. 19a do not correspond to Fig. 19b.

Numbers refer to analyses in Tables 7 and 6 respectively.

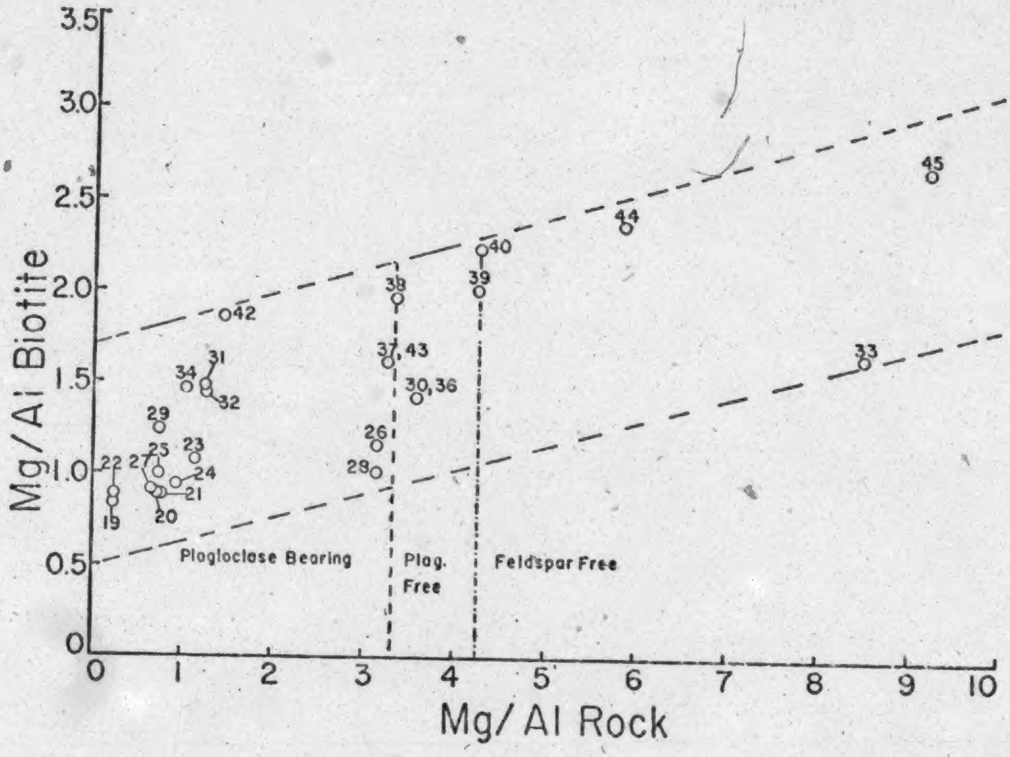

Fig. 20 a. Mg/Al biotite against Mg/Al rock for biotites from Kootenay Point. Feldspar fields given by dashed and dash-dot lines. Numbers refer to analyses in Table 7.

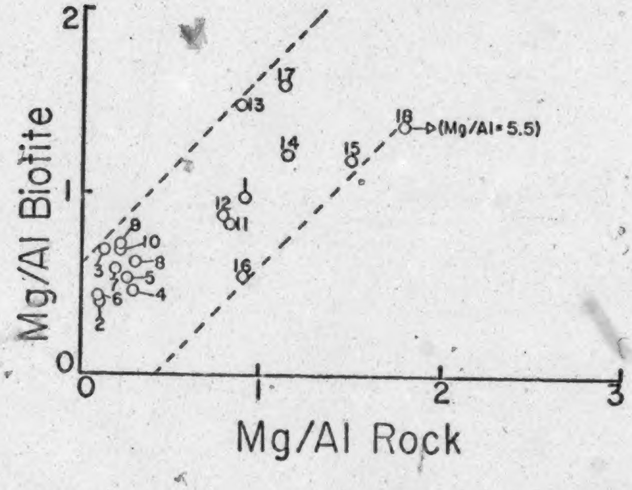

Fig. 20 b. Mg/Al biotite against Mg/Al rock for biotites from regional metamorphic rocks. Field corresponds to the plagioclase field of Fig. 20a. Numbers refer to analyses in Table 6.

ratio. More than one trend is shown on this plot. Within the plagioclase field, the biotites show a linear trend with a steep slope. A similar but less well defined trend is to be found between the margin of the plagioclase field and the feldspar-free field. The general trend is one of increasing Mg/Al ratio in biotite with increasing Mg/Al for the rock, but within fairly narrow Mg/Al rock limits, a steep linear (?) Mg/Al biotite, Mg/Al rock correlation exists. Fig. 20b, a plot of Mg/Al for regional biotites further illustrates the relationship over a small Mg/Al rock ratio variation. It is essentially congruent to the plot of Point biotites lying in the plagioclase field. This plot must be interpreted with more care, however, as it includes biotites from different metamorphic grades. Both plots indicate the interdependence of Mg, Fe and Al values (and hence octahedral occupancy) on rock composition.

Fig. 21a and 21b indicate the relationship between Ti in biotite and Ti in the rock and complete the demonstration of dependence of octahedral site composition on rock composition. Plots of SiO_2 in biotite against SiO_2 in the rock (not shown) indicate, contrary to Rimsaite (1964), that more siliceous biotites are not correlated with more siliceous rocks, at least with respect to biotites in the Kootenay Arc. No correlation between rock and biotite SiO_2 is found. The reasons for this lack of correlation are complex, in that, in very low silica rocks, biotite may be the only siliceous mineral. The biotites lowest in SiO_2 occur in fairly siliceous rocks. No relation exists between rock K_2O and biotite K_2O. Thus, both the interlayer cation K and the tetrahedral cation Si appear to be unrelated to bulk composition of the rocks under consideration.

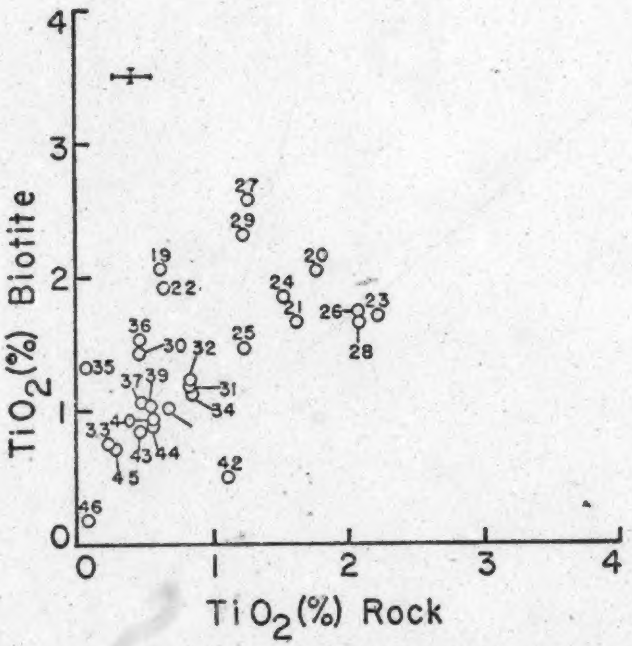

Fig. 21 a. TiO$_2$ biotite against TiO$_2$ rock for biotites from Kootenay Point. Numbers refer to analyses in Table 7.

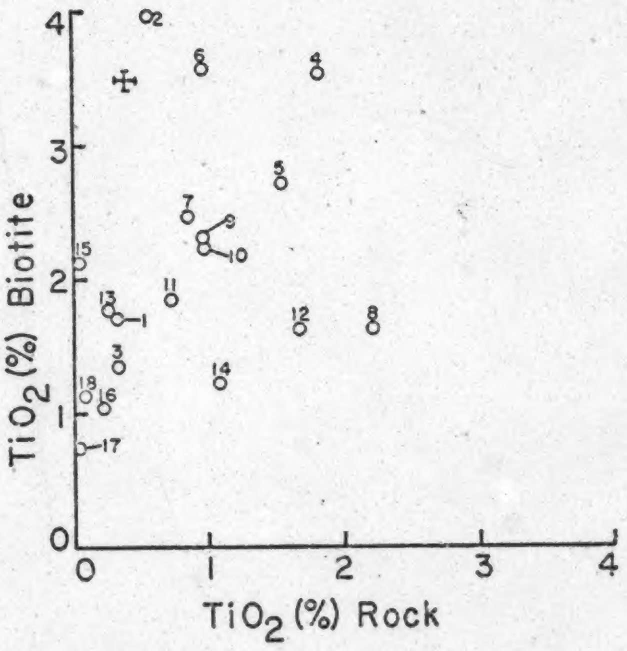

Fig. 21 b. TiO$_2$ biotite against TiO$_2$ rock for biotites from regional metamorphic rocks. Numbers correspond to analyses in Table 6.

Summary: Tetrahedrally coordinated cations are shown to be related to octahedrally coordinated cations and interlayer cations. Anions F and Cl are correlated with tetrahedral and interlayer cations. The octahedral cations Mg and Fe correlate strongly with bulk chemistry, but Ti and Al are less strongly influenced. Si is not related to rock composition, while Al is weakly correlated to Al in the rock. Interlayer cations are unrelated to rock composition.

The best indicators of grade would be Ti, K, Si or possibly Al, since they are less affected by rock composition, but they may depend on anion availability or octahedral substitutions which are strongly related to bulk chemistry. Mg and Fe contents are the least reliable, since they are strongly correlated with rock composition.

Chlorite

Chlorite is found at all metamorphic grades in the Arc, but is generally retrograde, forming as a result of alteration of biotite and garnet. Chlorite from the chlorite zone and from the biotite isograd is distinguishable optically from that formed by alteration. The regional assemblages in which chlorite is demonstrably stable on petrographic grounds are qtz-chl-phengite-cc, qtz-chl-tr-act-cc-dol or qtz-chl-bi-phengite ± cc. Rocks from the chlorite zone are rare; most rocks are transitional "biotite isograd" rocks in which a small amount of biotite has been formed. Chlorites coexisting with or without biotite are optically similar; pale green, pleochroic to yellow or pale yellow, with low birefringence colors, often brown at extinction. They do not show the blue anomalous extinction colors exhibited by chlorites (penninites) which result from alteration of biotite or garnet. Only

TABLE 8. ELECTRON MICROPROBE ANALYSES OF CHLORITES FROM REGIONAL METAMORPHIC ROCKS

Ox Wt	1 4LBT-1(1)	2 5LBT-17	3 5LBT-15	4 4LBT-1(2)
SiO_2	25.59	25.64	25.83	25.87
TiO_2	0.10	0.10	0.04	0.05
Al_2O_3	21.56	19.80	20.09	21.19
FeO	20.61	25.18	24.08	20.19
MnO	0.09	0.13	0.19	0.09
MgO	18.35	16.89	17.03	19.44
CaO	0.00	0.02	0.01	0.00
Na_2O	0.00	0.00	0.00	0.00
K_2O	0.07	0.12	0.05	0.04
BaO	0.00	0.02	0.02	0.00
Cl	0.01	0.06	0.03	0.14
F	0.10	0.04	0.04	0.09
Total	86.48	87.99	87.41	87.14
H_2O*	13.52	12.01	12.59	12.86

STRUCTURAL FORMULA ON THE BASIS OF 14 OXYGENS

Si	2.662	2.693	2.712	2.699
Al^{IV}	1.338	1.307	1.288	1.301
Total tet.	4.000	4.000	4.000	4.000
Al^{VI}	1.306	1.144	1.199	1.305
Ti	.007	.007	.003	.004
Fe	1.793	2.212	2.115	1.824
Mn	.008	.012	.017	.008
Mg	2.845	2.644	2.666	3.023
Ca	0	.002	.001	0
Na	0	0	0	0
K	.009	.016	.007	.005
Total	5.968	6.037	6.008	6.169

*H_2O is determined by difference from 100%. This is a maximum value as Fe_2O_3 has not been determined. H_2O is not used in further calculations.

four rocks contained suitable chlorite-grade or transitional assemblages, and chlorites in these rocks were examined by electron microprobe. Two different grains were examined in 4LBT-1. Results are presented in Table 8. All chlorites belong chemically to the ripidolite group, but an exact type cannot be established because ferric iron was not determined.

Fig. 22 illustrates the composition of chlorites from the Kootenay Arc in relation to chlorites from the Franciscan, Sanbagawa, Dalradian and Otago areas. The composition of the Kootenay chlorites overlaps that of the Sanbagawa district, and the edge of the field of the Dalradian chlorites.

Rock composition appears to affect the composition of chlorites with respect to Fe and Mg, but not with respect to Al_2O_3. Since there are few analyses, the relationships are tentative. The concentration of Mg in chlorite decreases with an increase in the concentration of Mg in the rock, while the amount of Fe increases with increase in Fe concentration in the rock. The variation between grains in 4LBT-1 (1,4) is greater than the variation in the entire group, suggesting that the trends are at best approximate. The reasons for this variation are obscure, but are probably related to areas of local variation in Mg and Fe within the thin section. Dolomite is found in patches and stringers throughout the rock and likely influences the local availability of Mg.

Amphiboles

Amphiboles are found in all rock types found in the central Kootenay Arc. Tremolites, actinolites and hornblendes can be identified optically. Tremolites are colorless, non-pleochroic and usually sub-

Fig. 22. AFM diagram for chlorites from regional metamorphic rocks. Plotted for comparison (squares) are chlorites from other metamorphic facies series.

D17-22 Dalradian (Scotland)
Mather (1970)
G1, 2 Goat Mountain, Calif.
Ernst _et al_. (1970)
024-27 Otago, New Zealand
Cooper (1972)
S Shirataki, Japan
Ernst _et al_. (1970)

Numbers refer to analyses in Table 8.

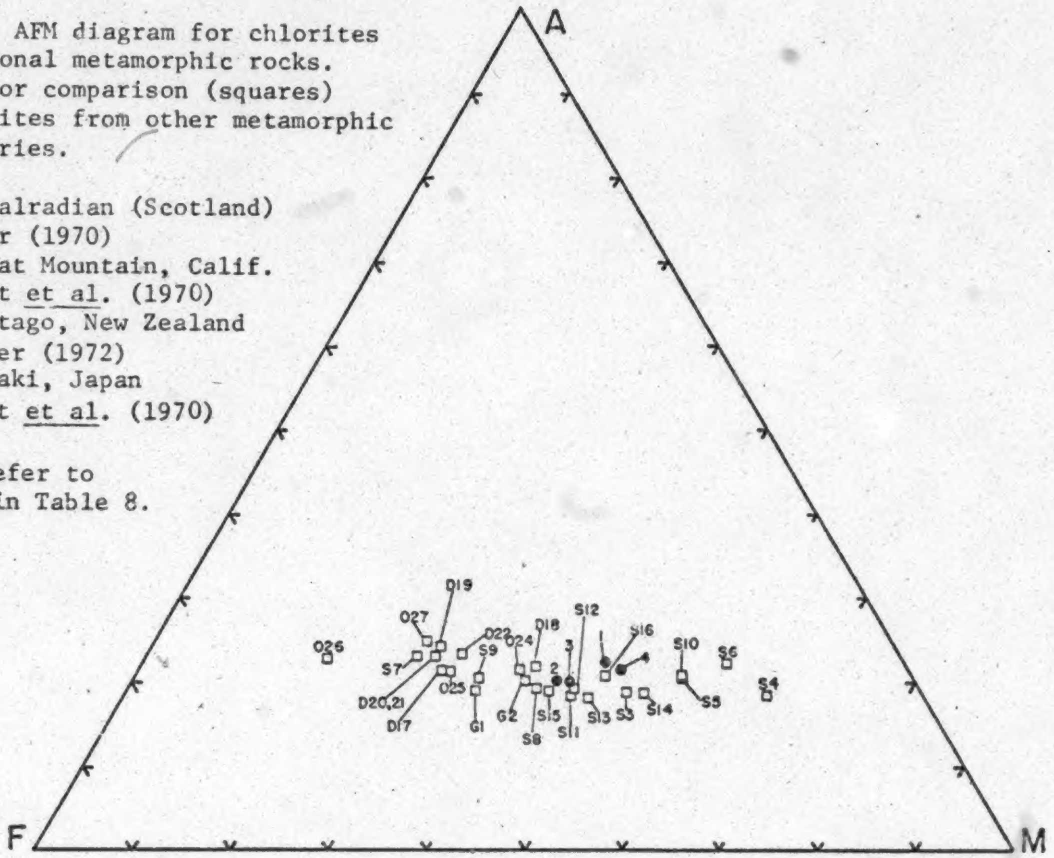

hedral or anhedral. They occur only in carbonate-bearing rocks, coexisting with diopside or magnesian biotite. No talc has been identified, despite finding rocks with "soapy" feel. Later microprobe analyses always confirmed the mica as a magnesian biotite. This lack of talc is probably due to the presence of iron and alumina in all tremolite-bearing rocks, and no pure, iron-free tremolites are found.

Actinolite (rather than tremolite) forms in rocks with somewhat higher iron content. It may be colorless, but it is usually pale green and pleochroic. In more basic rock types the mineral is distinctly blue. Actinolite coexists with diopside, biotite and often feldspar as well as quartz and carbonate. It also forms pods of large radiating crystals several centimeters long. These pods may be 95% or more actinolite. Actinolite also forms rims around hornblendes and patches within hornblende grains.

On textural grounds, both tremolite and actinolite often appear to be out of equilibrium with the rest of the mineral assemblage. Tremolite occurs in two generations in many rocks and frequently is found as a coarse grained anhedral grain surrounded by smaller, clearly younger, acicular masses. The larger, older grains are often shot through with blebby calcite and occasional dolomite. Actinolites and dolomites often grow with random orientation in a rock, although in banded calc-silicates from the region, they may be aligned parallel to the banding even when anhedral and corroded.

Hornblende, except where zoned, usually appears to be approaching textural equilibrium with the rest of the minerals in a section. Zoning of amphiboles is common in rocks from the Kootenay Arc. Hornblende, usually dark green or somewhat bluish-green, always forms the core,

TABLE 9. ELECTRON MICROPROBE ANALYSES OF AMPHIBOLES FROM KOOTENAY POINT

	1	2	3	4	5	6	7	8	9	10	11
Ox Wt	T4-4	T4-8	375-140W	30-13E	T3-11	T2-15	T1-9	240-137E	T4-2	T3-12	190-120E
SiO_2	41.01	41.37	41.49	42.49	43.14	43.68	43.68	44.10	45.55	46.73	50.45
TiO_2	1.12	0.89	1.42	0.78	0.57	0.97	1.34	1.22	0.49	0.32	0.12
Al_2O_3	12.73	12.69	15.40	13.77	11.70	10.77	11.97	12.28	9.18	6.88	3.63
FeO	16.90	17.37	13.69	15.11	18.22	15.88	13.27	12.40	14.97	16.12	6.48
MnO	0.29	0.27	0.26	0.65	0.24	0.36	0.25	0.23	0.33	0.26	0.17
MgO	8.78	9.31	10.43	10.35	9.54	11.05	14.21	12.42	12.66	12.13	18.20
CaO	11.77	12.02	11.28	11.28	12.01	11.82	11.02	11.56	12.09	11.42	12.05
Na_2O	1.34	1.25	1.11	1.17	1.16	1.23	1.64	1.41	0.82	0.99	0.59
K_2O	1.30	1.38	0.76	1.19	1.33	1.17	0.84	0.79	0.86	1.01	0.37
F	0.03	0.08	ND	0.43	0.04	0.09	0.09	0.10	0.27	0.07	0.15
Cl	0.07	0.07	ND	0.06	0.16	0.07	0.05	0.04	0.04	0.05	0.08
Total	95.31	96.70	95.84	97.28	98.11	97.09	98.36	96.55	97.26	95.98	92.29
H_2O*	4.69	3.30	4.16	2.72	1.89	2.91	1.64	3.45	2.79	4.02	7.71
STRUCTURAL FORMULA ON THE BASIS OF 23 OXYGENS											
Si	6.356	6.319	6.230	6.384	6.514	6.671	6.456	6.621	6.819	7.150	7.540
Al^{IV}	1.644	1.681	1.770	1.616	1.486	1.329	1.544	1.379	1.181	.850	.460
Total tet.	8.000	8.000	8.000	8.000	8.000	8.000	8.000	8.000	8.000	8.000	8.000
Al^{VI}	.682	.652	.955	.822	.596	.609	.540	.793	.440	.391	.183
Ti	.130	.102	.160	.088	.064	.111	.149	.137	.055	.037	.013
Fe	2.191	2.219	1.719	1.898	2.301	2.029	1.640	1.557	1.874	2.063	.810
Mn	.039	.034	.033	.083	.030	.046	.031	.029	.041	.033	.021
Mg	2.027	2.118	2.333	2.317	2.147	2.515	3.129	2.779	2.824	2.765	4.055
Total oct.	5.069	5.125	5.200	5.208	5.138	5.310	5.489	5.295	5.234	5.289	5.082
Ca	1.954	1.967	1.815	1.816	1.944	1.935	1.823	1.859	1.940	1.871	1.929
Na	.402	.370	.323	.342	.341	.364	.469	.412	.238	.293	.172
K	.257	.269	.146	.228	.257	.228	.159	.151	.163	.196	.070
Total	2.613	2.606	2.284	2.386	2.542	2.527	2.451	2.422	2.341	2.360	2.171

*H_2O is determined by difference from 100%. This is a maximum value as Fe_2O_3 has not been determined. H_2O is not used in further calculations.

TABLE 9 CONTINUED

Ox Wt	12 T1-8	13 T4-6(1)	14 199-146E	15 T1-1	16 DP-1	17 T3-2b	18 72-80E	19 125-68E	20 T2-6(2)	21 205-50W	22 T4-6(2)
SiO_2	50.80	52.38	52.91	53.87	54.71	54.77	54.96	55.50	55.50	55.65	55.74
TiO_2	0.41	0.28	0.42	0.11	0.03	0.53	0.01	0.00	0.04	0.00	0.09
Al_2O_3	6.74	5.59	6.53	4.09	1.68	3.65	0.39	0.37	0.50	0.54	2.56
FeO	4.44	5.74	4.24	3.14	1.14	4.37	1.74	1.71	1.55	1.84	5.10
MnO	0.10	0.16	0.39	0.04	0.01	0.17	0.24	0.15	0.16	0.11	0.14
MgO	19.14	19.61	19.58	19.90	22.12	20.56	22.54	22.84	23.64	22.90	21.07
CaO	12.36	12.69	12.47	12.72	12.38	13.22	12.91	12.77	13.87	12.78	13.17
Na_2O	0.92	0.76	0.91	0.59	0.13	0.26	0.06	0.13	0.11	0.13	0.39
K_2O	0.51	0.51	0.52	0.39	0.09	0.29	0.08	0.08	0.13	0.08	0.23
F	0.20	0.23	0.32	0.13	0.00	0.13	0.00	0.00	0.13	ND	0.17
Cl	0.02	0.13	0.00	0.05	0.00	0.01	0.00	ND	0.01	ND	0.02
Total	95.64	98.08	98.29	95.03	92.29	97.96	92.93	93.55	95.03	94.03	98.68
H_2O*	4.36	1.92	1.71	4.97	7.71	2.04	7.07	6.45	4.97	5.97	1.32

STRUCTURAL FORMULA ON THE BASIS OF 23 OXYGENS

	12	13	14	15	16	17	18	19	20	21	22
Si	7.353	7.351	7.438	7.476	7.874	7.632	7.909	7.924	7.909	7.907	7.697
Al^{IV}	.647	.649	.562	.524	.126	.368	.070	.063	.083	.091	.303
Total tet.	8.000	8.000	8.000	8.000	8.000	8.000	7.979	7.987	7.992	7.998	8.000
Al^{VI}	.502	.275	.519	.144	.159	.232	0	0	0	0	.114
Ti	.044	.030	.044	.012	.003	.006	.001	.003	.004	0	.010
Fe	.537	.674	.498	.365	.137	.509	.209	.137	.184	.219	.589
Mn	.013	.019	.047	.005	.001	.020	.029	.001	.019	.014	.016
Mg	4.129	4.102	4.104	4.324	4.745	4.270	4.835	4.745	5.020	4.848	4.335
Total oct.	5.225	5.100	5.212	4.850	5.045	5.037	5.074	4.886	5.227	5.081	5.064
Ca	1.916	1.908	1.879	1.891	1.909	1.973	1.991	1.953	2.118	1.946	1.948
Na	.259	.207	.248	.190	.036	.071	.016	.036	.030	.036	.104
K	.093	.092	.092	.069	.017	.051	.015	.014	.024	.014	.041
Total	2.268	2.206	2.219	2.150	1.962	2.095	2.022	2.003	2.172	1.996	2.093

*H_2O is determined by difference from 100%. This is a maximum value as Fe_2O_3 has not been determined. H_2O is not used in further calculations.

TABLE 9 CONTINUED

Ox Wt	23 T3-9	24 T2-2	25 T3-5	26 T3-4	27 T2-6(1)	28 105-101E
SiO_2	56.21	57.23	57.41	57.47	57.52	57.98
TiO_2	0.02	0.00	0.06	0.08	0.01	0.00
Al_2O_3	1.57	0.65	0.59	0.40	0.48	0.43
FeO	5.18	0.85	2.76	2.11	1.61	1.83
MnO	0.24	0.00	0.12	0.10	0.38	0.12
MgO	20.42	23.47	23.06	23.76	23.84	22.86
CaO	13.37	12.73	12.95	12.99	13.52	12.89
Na_2O	0.26	0.21	0.15	0.08	0.14	0.12
K_2O	0.19	0.02	0.12	0.09	0.16	0.05
F	0.00	0.22	0.07	0.07	0.13	0.15
Cl	0.38	0.02	0.10	0.01	0.01	0.00
Total	97.84	95.40	97.39	97.10	97.80	96.43
H_2O*	2.16	4.60	2.61	2.90	2.79	3.57

STRUCTURAL FORMULA ON THE BASIS OF 23 OXYGENS

Si	7.840	8.071	8.015	8.012	7.987	8.117
Al^{IV}	.160	0	0	0	.013	0
Total tet.	8.000	8.071	8.015	8.012	8.000	8.117
Al^{VI}	.098	.109	.097	.065	.065	.071
Ti	.002	0	.006	.008	.001	0
Fe	.604	.100	.323	.245	.186	.214
Mn	.028	0	.014	.012	.045	.014
Mg	4.244	4.932	4.799	4.938	4.934	4.771
Total oct.	4.976	5.141	5.239	5.268	5.231	5.070
Ca	1.999	1.923	1.937	1.940	2.011	1.931
Na	.071	.058	.041	.022	.038	.032
K	.035	.003	.021	.015	.029	.009
Total	2.105	1.984	1.999	1.977	2.078	1.972

*H_2O is determined by difference from 100%. This is a maximum value as Fe_2O_3 has not been determined. H_2O is not used in further calculations.

TABLE 10. ELECTRON MICROPROBE ANALYSES OF AMPHIBOLES FROM REGIONAL METAMORPHIC ROCKS

	29	30	31	32	33	34	35	36	37	38
Ox Wt	7RT-17	10BT-13	5LBT-22(2)	6CCT-8	12WP-2a	5LBT-17	6CCT-1a	8AT-8	10BT-9	5LBT-22(1)
SiO_2	39.25	41.12	41.77	42.78	42.86	43.43	43.76	43.99	52.85	53.14
TiO_2	0.44	0.62	0.95	1.35	0.77	0.41	0.31	0.43	0.11	0.09
Al_2O_3	16.39	12.36	10.98	12.59	13.73	13.56	16.36	9.51	3.87	3.20
FeO	23.34	22.45	20.59	18.68	19.32	19.84	12.54	18.47	8.50	14.00
MnO	0.22	0.31	0.33	0.25	0.21	0.21	0.04	0.32	0.18	0.28
MgO	4.83	6.66	8.87	8.86	8.05	8.53	11.22	10.90	18.14	15.39
CaO	11.53	13.29	11.69	11.26	12.67	10.63	11.49	11.44	12.51	12.30
Na_2O	1.48	0.00	1.27	1.49	1.78	1.75	1.15	1.77	0.42	0.42
K_2O	0.79	0.07	1.43	0.55	0.64	0.47	0.37	1.36	0.38	0.27
BaO	0.01	0.05	0.01	0.00	0.01	0.01	0.00	0.01	0.00	0.00
Cl	0.12	0.04	0.40	0.09	0.05	0.01	0.00	0.02	0.02	0.03
F	0.25	ND	0.10	0.03	0.08	0.07	0.04	0.77	0.18	0.10
Total	98.65	96.97	98.39	97.94	100.17	98.92	97.28	98.99	97.16	99.20
H_2O*	1.35	3.03	1.61	2.06	--	1.08	2.72	1.01	2.84	0.80

STRUCTURAL FORMULA ON THE BASIS OF 23 OXYGENS

	29	30	31	32	33	34	35	36	37	38
Si	6.024	6.364	6.353	6.442	6.350	6.470	6.378	6.646	7.547	7.608
Al^{IV}	1.976	1.636	1.647	1.558	1.650	1.530	1.622	1.354	.453	.392
Total tet.	8.000	8.000	8.000	8.000	8.000	8.000	8.000	8.000	8.000	8.000
Al^{VI}	.987	.618	.320	.675	.745	.852	1.188	.339	.199	.147
Ti	.050	.072	.109	.153	.085	.047	.033	.049	.013	.009
Fe	2.995	2.906	2.617	2.352	2.393	2.472	1.529	2.333	1.015	1.676
Mn	.029	.041	.042	.031	.026	.026	.005	.041	.022	.034
Mg	1.104	1.538	2.010	1.991	1.779	1.892	2.438	2.454	3.860	3.283
Total oct.	5.165	5.175	5.098	5.202	5.028	5.289	5.193	5.216	5.109	5.149
Ca	1.896	2.204	1.903	1.817	2.009	1.605	1.793	1.853	1.913	1.886
Na	.437	0	.374	.437	.511	.502	.324	.517	.116	.116
K	.153	.014	.278	.106	.121	.089	.069	.262	.068	.048
Total	2.846	2.218	2.555	2.360	2.641	2.286	2.186	2.632	2.097	2.050

*H_2O is determined by difference from 100%. This is a maximum value as Fe_2O_3 has not been determined. H_2O is not used in further calculations.

TABLE 10 CONTINUED

	39	40
Ox Wt	7RT-7	6CCT-3
SiO_2	54.31	54.90
TiO_2	0.05	0.02
Al_2O_3	2.96	2.05
FeO	15.52	10.23
MnO	0.16	0.14
MgO	16.55	17.59
CaO	12.57	12.77
Na_2O	0.30	0.22
K_2O	0.24	0.18
BaO	0.00	0.00
Cl	0.00	0.00
F	0.16	ND
Total	102.85	98.10
H_2O*	--	1.90

STRUCTURAL FORMULA ON THE BASIS OF 23 OXYGENS

	39	40
Si	7.542	7.777
Al^{IV}	.458	.223
Total tet.	8.000	8.000
Al^{VI}	.027	.118
Ti	.005	.002
Fe	1.803	1.212
Mn	.020	.017
Mg	3.425	3.715
Total oct	5.280	5.064
Ca	1.869	1.937
Na	.080	.059
K	.043	.033
Total	1.992	2.029

*H_2O is determined by difference from 100%. This is a maximum value as Fe_2O_3 has not been determined. H_2O is not used in further calculations.

while actinolite is present as a rim, as patches within the amphibole, or as separate grains coexisting with zoned amphiboles. The textural relationships of the zoned amphiboles are described by Winzer (1973) (Appendix 4).

Hornblende coexists with biotite, epidote, feldspar, garnet, and quartz, but not with diopside, It is usually subhedral and often poikilitic, enclosing biotites, feldspars and quartz. A few hornblendes have very fine, colorless cummingtonite exsolved within the central portion of the grain, but this has only been observed where the amphibole is zoned. No other varieties of amphibole have been found in any of the rocks studied.

All amphiboles studied are calcic or subcalcic; most belonging to the series actinolite-pargasitic hornblende. Twenty-eight amphiboles from different rock types from Kootenay Point were analyzed and are presented in Table 9. Table 10 consists of 12 amphiboles from regional metamorphic rocks. The range of compositions in terms of A-site occupancy and tetrahedral Al is illustrated in Fig. 23. The larger number of amphiboles studied fall near the actinolite corner, between Al^{IV} 0 and Al^{IV} 0.7 with the smaller group clustering between hornblende and pargasitic hornblende. Some amphiboles plot off this trend, with a suggestion of a series along the hornblende-actinolite join: 6CCT-1a (35), 375-140 (3), 7RT-17 (29), one tschermakitic amphibole, 10BT-13 (30) and 8AT-8 (36), an edenitic amphibole. Tielines join pairs of amphiboles coexisting in a single thin section: T4-6A 1,2 (13,22); 5LBT-22 A,B (31, 38). These amphiboles indicate solvi and miscibility gaps in the series and will be discussed later.

Perhaps more useful from the standpoint of classification is

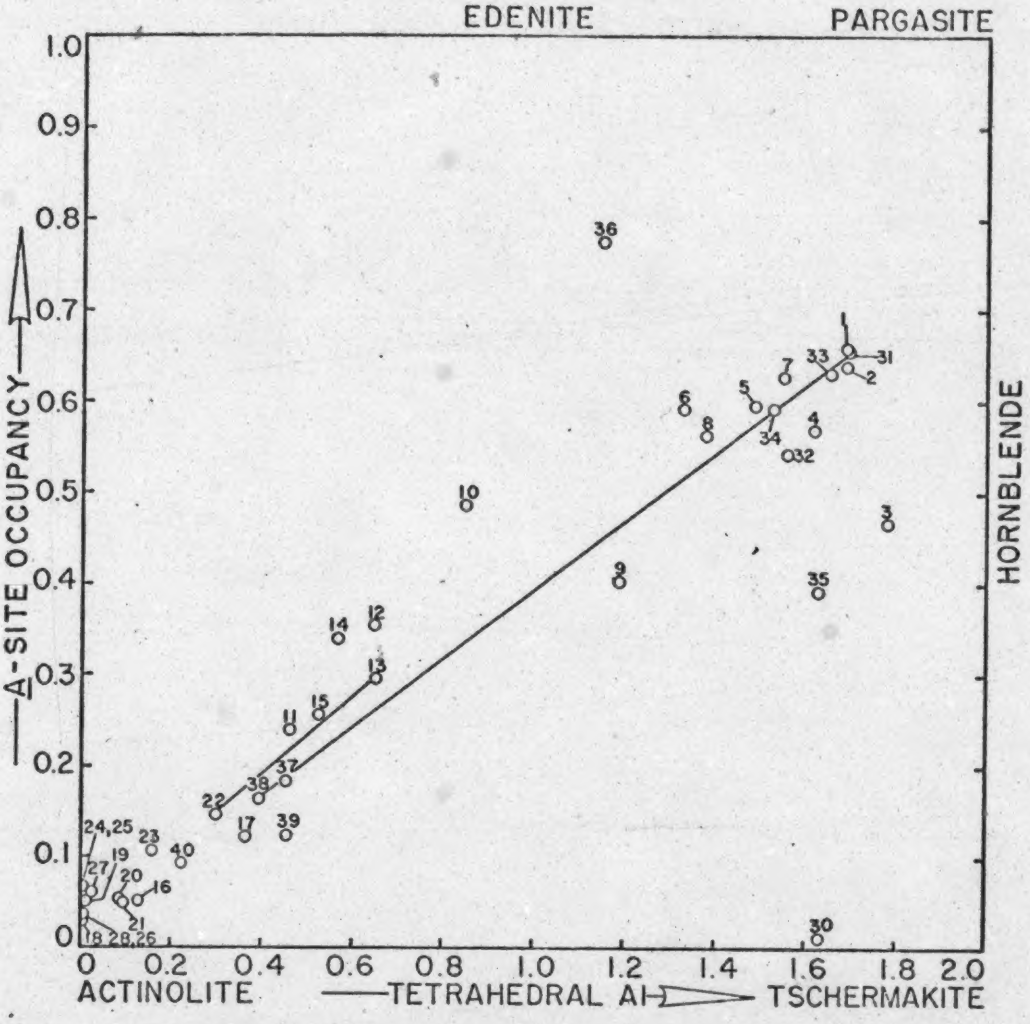

Fig. 23. A - site occupancy against tetrahedral Al for all amphiboles analyzed. Numbers correspond to analyses in Tables 9 and 10. A - site occupancy is calculated as Na+K, as ferrous iron has not been determined.

Leake's plot (Leake, 1968) for calciferous and sub-calciferous amphiboles (Fig. 24). By this classification, the larger group of Kootenay amphiboles are tremolites, some quite near the ideal tremolite composition, with a few tremolitic hornblendes. The more basic amphiboles are tschermakitic or pargasitic hornblendes, with three edenitic hornblendes and two tschermakites. Four amphiboles plot as magnesio-hornblendes. Four amphiboles, 24, 25, 26 and 28 lie outside the plot, with $Si > 8$. The reason for this is most likely error in the analysis.

Examination of both plots together reinforces the impression of a compositional gap between the tschermakitic and pargasitic amphiboles (hornblendes) and the actinolites. The greater number of actinolites are aluminous, and a miscibility gap lying between pargasitic hornblende/aluminous actinolite has been proposed by Read (1973) and also by Winzer (1973) (Appendix 4). The amphiboles examined by Winzer are zoned pargasitic hornblendes with aluminous actinolite rims.

Solid solution appears possible between aluminous actinolite-actinolite and pargasitic hornblende-aluminous actinolite, but the two series are separated by a miscibility gap located near $Al^{IV} = 0.7$, $\Sigma A = 0.35$. The degree of separation between coexisting pairs within the same slide, or zoned amphiboles with a sharp break between rim and core, marks the width of the solvus between aluminous actinolite-actinolite and aluminous actinolite-pargasitic hornblende. Fig. 23 illustrates both minimum and maximum widths for the solvus. Between 10 and 12 the gap is about 0.2 structural formula units wide in Al^{IV}. The maximum width is about 0.8 structural formula units, Al^{IV}. The range of solid solution is given by the range of values on both sides of the gap, but caution must be used in this interpretation as the amphiboles from the

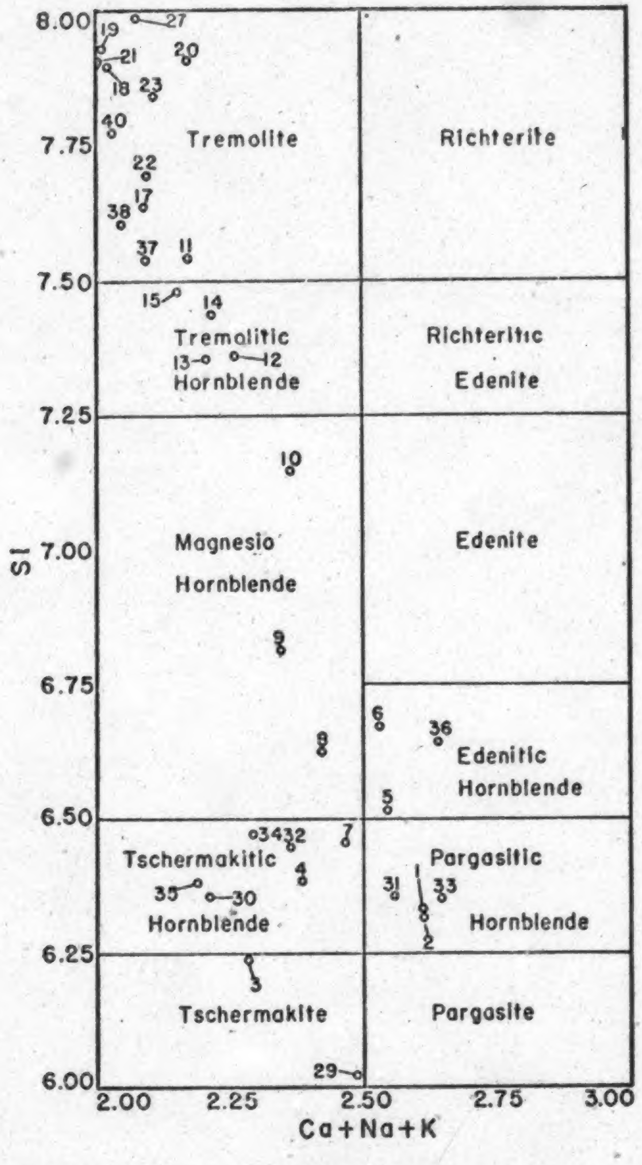

Fig. 24. Classification of analyzed amphiboles. Plot and compositional fields after Leake (1968). Numbers correspond to analyses in Tables 9 and 10. Numbers 24, 25, 26, 28 and 39 fall outside the range of Si or Ca + Na + K (Structural).

region form at varying temperatures and pressures. The amount of Al_2O_3 present in an amphibole depends to some extent on the amount of Al_2O_3 present in the rock, as will be discussed shortly, but the formation of amphiboles with specific amounts of Al^{IV} and Na + K appears to depend largely upon physical conditions of formation.

Leake (1965) suggested that a relationship existed between Al^{IV} and the maximum amount of Al^{VI} that would be present in the amphibole lattice. He further suggested that high pressure favored higher octahedral Al in amphiboles, based on behavior of other minerals with octahedral Al sites and octahedral Al values in amphiboles coexisting with kyanite, jadeite and glaucophane. Fig. 25 is a plot of Al^{IV} vs. Al^{VI} for all amphiboles studied in the Kootenay region. They show considerable range, and all except 6CCT-1a (35) fall below the maximum Al^{VI} permissible. This trend is produced by at least two factors, rock composition and physical conditions of metamorphism. Al/Mg + Fe rock against Al/Fe + Mg amphibole ratios show that amphibole Al/Fe + Mg ratios generally correlate positively with Al/Fe + Mg ratios. The dependence of Al also is related to K and Na values (as K + Na values increase with Al values, see Robinson, Ross and Jaffe, 1971) and is complexly related to the rock mineralogy, notably plagioclase (Leake, 1965, 1968). Fig. 23 illustrates the interdependence of Na + K and tetrahedral Al. Comparison of the analyses with the traces given in Winzer (1973, Appendix 4) will show that the same substitution scheme operates in the amphiboles from the Kootenay region as operates for the zoned amphiboles from Kootenay Point, as well as for gedrites (Robinson, Ross and Jaffe, 1971).

In order to know the dependence of Al in any structural site on

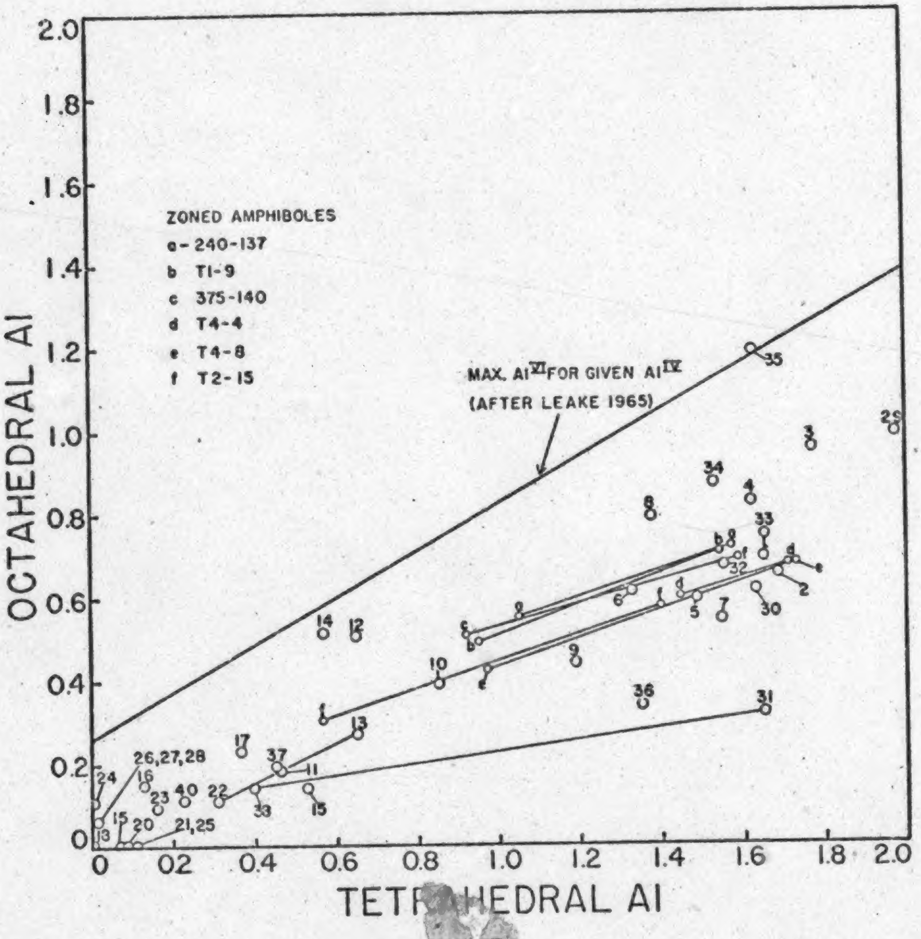

Fig. 25. Octahedral Al plotted against tetrahedral Al for all amphiboles analyzed. Tielines join coexisting amphiboles and core-rim compositions for zoned amphiboles described by Winzer (1973, Appendix 4). Numbers refer to analyses in Tables 9 and 10. Heavy diagonal line refers to the maximum amount of octahedral Al for a given amount of tetrahedral Al (after Leake, 1965).

external conditions, amphibole compositional dependence on rock composition must be discussed. Internal conditions are generally not discussed, as rock compositions are not often determined. Regardless of the mineralogical determinant for rock composition, amphibole compositions cannot be compared usefully without the rock analyses, as the next figures will show. When Al^{IV} and Al^{VI} are plotted against Al/Mg + Fe ratio in the rock, only a general positive relationship is noted. Plots of Fe/Fe + Mg rock against Fe/Fe + Mg amphibole for both Point and region indicate linear positive relationships between the two ratios (Figs. 26 a, b). One can establish that complex relationships involving positive and negative correlations between MgO and FeO exist for different amphiboles, and that these relationships are different when grade is added as a third variable. Fig. 27a plots FeO against rock FeO for amphiboles from the Point and shows two interesting things. First, as expected, increasing FeO in the amphibole is correlated generally with increasing FeO in the rock, but two distinct fields are present, and the relationships within these fields are different. At lower FeO values, actinolites and tremolites are found, and with some scatter, they show a direct positive relationship with rock FeO. MgO plots (not shown) show, on the other hand, a less well-defined case. The tschermakitic, pargasitic and edenitic hornblendes correlate positively with increased MgO content, but with considerable scatter. The opposite is true for amphiboles from the region. There is no well defined correlation for FeO, but MgO in amphibole shows a positive correlation with MgO in the rock (Fig. 27b). These two plots suggest a control independent of rock composition, at least for MgO in actinolites and to some extent FeO in hornblendes. The hornblendes decrease in iron with increase in

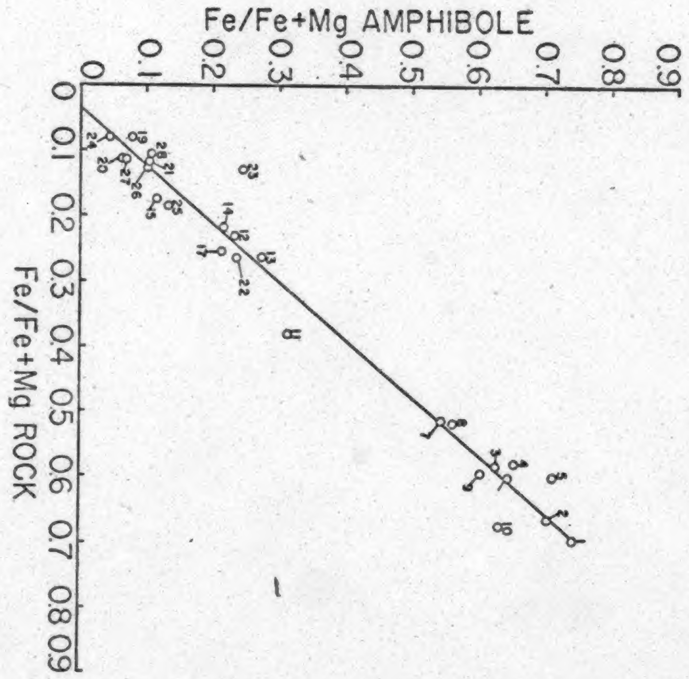

Fig. 26 a. Fe/Fe + Mg rock against Fe/Fe + Mg amphibole for amphiboles from Kootenay Point. Numbers correspond to analyses in Table 9.

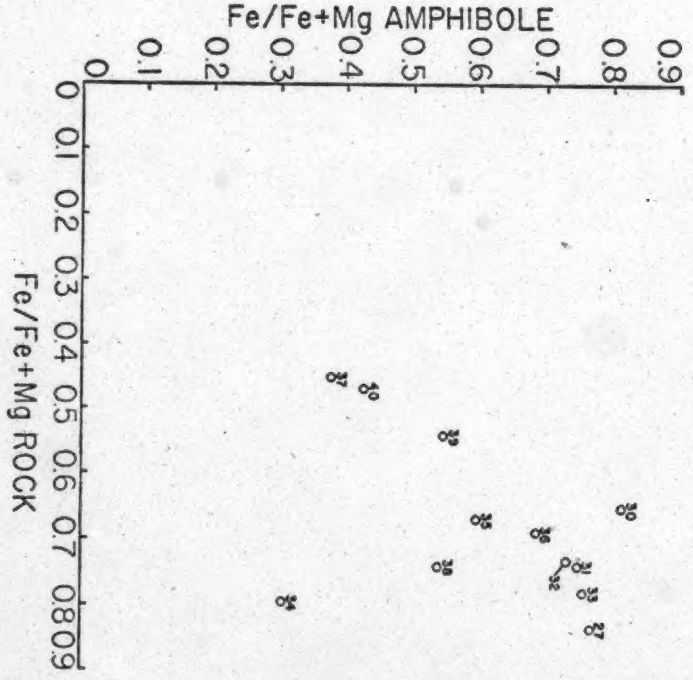

Fig. 26b. Fe/Fe + Mg rock against Fe/Fe + Mg amphibole for amphiboles from regional metamorphic rocks. Numbers correspond to analyses in Table 10.

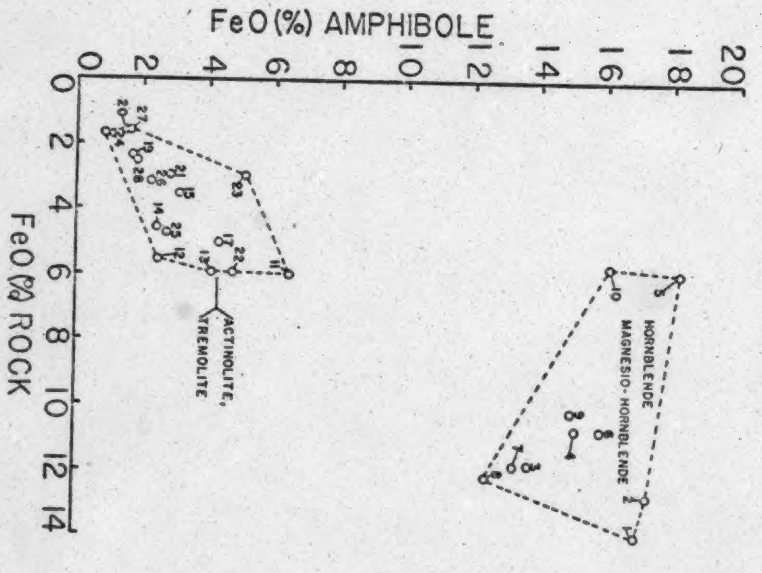

Fig. 27 a. FeO % amphibole against FeO % rock for amphiboles from Kootenay Point. Numbers correspond to analyses in Table 9.

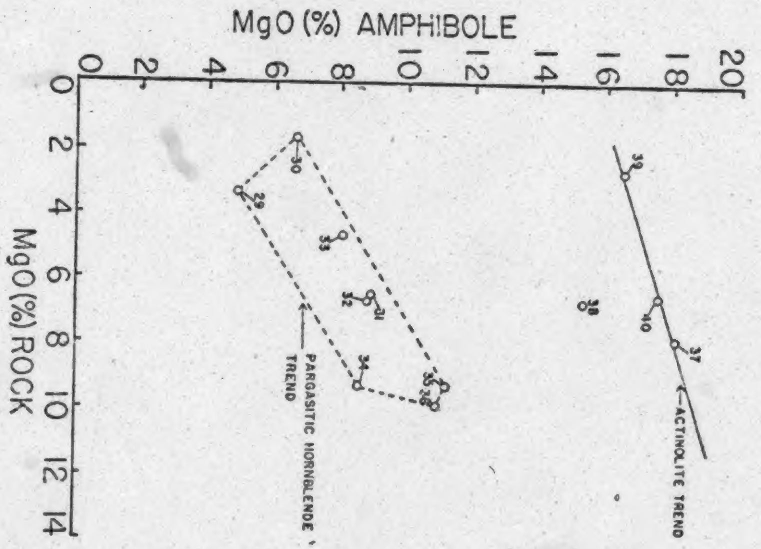

Fig. 27 b. MgO % amphibole against MgO % rock for amphiboles from regional metamorphic rocks. Numbers correspond to analyses in Table 10.

rock FeO, while with increased rock MgO, they gain some MgO. Tremolites, on the other hand, gain FeO with increasing rock FeO and may gain MgO as well, but they respond to MgO in a more complicated way. These relationships further suggest that different coupled substitutions occur in the tremolites compared with hornblendes.

Figs. 28 a,b are plots of TiO_2 in the rock against TiO_2 in amphiboles. The trends are distinctly different. Fig. 28a, for amphiboles from the Point, shows a definite positive trend, while those from the region (Fig. 28b) do not show a similar, well-defined trend. There is a suggestion of an increase with rock TiO_2, but only for the last three samples. Comparison with Fig. 27 indicates that Fe and Ti are linked in a lattice substitution scheme, but where temperature and pressure vary as well as composition, the link seems to be suppressed. Further discussion of these variables will be presented in the metamorphism section.

Pyroxene

Pyroxene occurs in siliceous carbonates and calc-silicates from the Kootenay region. Pyroxene is found with calcite, dolomite and tremolite in siliceous carbonates, and with actinolite, actinolitic-hornblende or magnesio-hornblende, epidote and biotite in the more mafic calc-silicates and "amphibolites". All pyroxenes found are clinopyroxenes, and no orthopyroxenes appear. The assemblages diopside-enstatite-(or hypersthene) hornblende or diopside-hornblende are absent, except for 5LBT-22, which contains zoned amphiboles and salite.

Pyroxenes in the Kootenay Arc appear in a few different textural relations. In rocks from the Point, they occur as pale green crystals up to several centimeters across, or as green or white crystals several

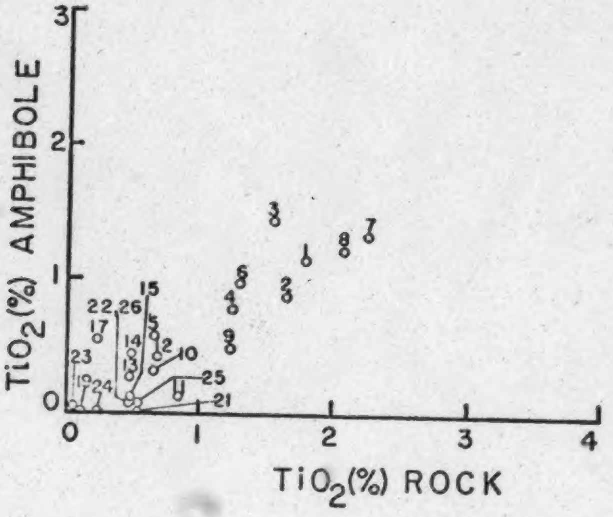

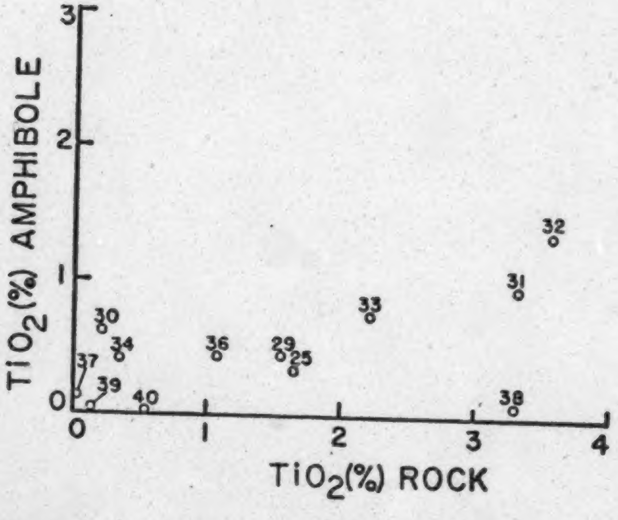

Fig. 28 a. TiO_2 amphibole against TiO_2 rock for amphiboles from Kootenay Point. Numbers correspond to analyses in Table 9.

Fig. 28 b. TiO_2 amphibole against TiO_2 rock for amphiboles from regional metamorphic rocks. Numbers correspond to analyses in Table 10.

millimeters across. In thin section, the larger grains tend to be poikilitic, enclosing actinolite, tremolite or magnesian biotite. The larger grains are generally subhedral and sometimes anhedral or blebby. Smaller grains are often equant and euhedral to subhedral, occasionally growing together as aggregates. In regional rocks pyroxene textural relations are similar, but in some rocks they occur in bands with actinolite, microcline and phlogopite and usually appear less stable. Smaller grains are anhedral and blebby. In both regional and Point rocks, pyroxene can commonly be found in a reaction relationship with actinolite and carbonate.

Twenty-one pyroxenes were analyzed by electron microprobe for nine elements. Thirteen were collected from Kootenay Point, and of the thirteen analyzed, four are from one thin section. Eight pyroxenes from regional rocks were analyzed, of which two were taken from the same thin section. The analyses are presented in Tables 11 and 12. Molecular end-members are calculated for $CaSiO_3$-$FeSiO_3$-$MgSiO_3$-Na_2SiO_3, but only the end members for $CaSiO_3$-$FeSiO_3$-$MgSiO_3$ are plotted on a pyroxene quadrilateral (Fig. 29). Pyroxenes from the Kootenay Arc lie along the join diopside-hedenbergite, most being either diopside or salite, using the classification of Deer, Howie and Zussman (1966). All except 10BT-11 (1), a ferrosalite, plot near the maximum permissible $CaSiO_3$ content. All contain from just less than 1 to 2% jadeite (based on the Na calculation). Sample 10BT-11 (1) contains 6.5% jadeite component. All pyroxenes deviate from the ideal diopside-salite-ferrosalite composition in that they contain significant aluminum. Almost two-thirds of the pyroxenes studied contain more octahedral aluminum than tetrahedral aluminum;

TABLE 11. ELECTRON MICROPROBE ANALYSES OF PYROXENE FROM REGIONAL METAMORPHIC ROCKS

	1	2	3	4	5	6	7	8
Ox Wt	10BT-11	5LBT-22	8AT-8	10BT-9	6CCT-3	7RT-7	11CBT-7(1)	11CBT-7(2)
SiO_2	50.50	51.66	52.23	52.52	52.85	53.07	53.15	53.40
TiO_2	0.07	0.07	0.02	0.04	0.05	0.04	0.03	0.02
Al_2O_3	1.49	1.44	0.70	0.71	0.95	1.05	0.50	0.39
FeO	17.00	12.27	10.87	5.51	8.56	9.73	8.30	9.14
MnO	0.59	0.39	0.44	0.29	0.17	0.20	0.08	0.08
MgO	7.39	10.91	11.38	15.22	12.97	12.45	13.33	13.25
CaO	19.89	23.25	23.85	24.33	23.50	23.99	24.42	24.39
Na_2O	1.79	0.41	0.68	0.17	0.33	0.32	0.16	0.13
K_2O	0.07	0.07	0.11	0.07	0.08	0.07	0.07	0.09
Total	98.78	100.46	100.29	98.87	99.46	100.93	100.04	100.87
STRUCTURAL FORMULA ON THE BASIS OF 6 OXYGENS								
Si	1.987	1.960	1.978	1.967	1.987	1.978	1.988	1.942
Al^{IV}	.013	.040	.022	.033	.013	.022	.012	.017
Total	2.000	2.000	2.000	2.000	2.000	2.000	2.000	1.959
Al^{VI}	.056	.024	.009	.000	.029	.024	.010	0
Ti	.002	.002	0	.001	.001	.001	.001	0
Fe	.559	.389	.344	.173	.269	.304	.259	.278
Mn	.020	.012	.014	.009	.005	.007	.002	.002
Mg	.434	.617	.642	.850	.726	.692	.743	.718
Ca	.838	.945	.968	.977	.946	.958	.979	.950
Na	.137	.030	.050	.013	.025	.023	.012	.010
K	.004	.003	.005	.003	.003	.003	.003	.004
Total	2.050	2.022	2.032	2.026	2.004	2.012	2.009	1.962
%Ca	42.60	47.71	48.28	48.57	48.12	48.50	49.11	48.60
Mg	22.02	31.14	32.05	42.28	36.94	35.01	37.30	36.73
Fe	28.41	19.65	17.18	8.59	13.68	15.35	13.03	14.22
Na	6.97	1.50	2.50	.56	1.26	1.14	.56	.45

TABLE 12. ELECTRON MICROPROBE ANALYSES OF PYROXENE FROM KOOTENAY POINT

	9	10	11	12	13	14	15	16	17
Ox Wt	40-40E(3)	40-40E(2)	40-40E(4)	198-146E	190-120E	T2-5b	40-40E(1)	T2-4	T2-18
SiO_2	52.29	52.38	52.70	53.74	53.92	53.96	54.41	54.43	54.62
TiO_2	0.24	0.08	0.05	0.10	0.08	0.06	0.06	0.07	0.03
Al_2O_3	0.65	1.13	1.01	1.43	1.51	0.64	1.39	0.81	0.53
Cr_2O_3	0	0.01	0.01	0.01	0.01	0.02	0.00	0	0.02
FeO	6.10	6.61	6.55	4.97	5.40	5.46	6.42	4.29	3.52
MnO	0.18	0.15	0.16	0.12	0.14	0.13	0.14	0.13	0.28
MgO	14.49	13.98	14.42	15.50	14.85	14.92	14.30	15.98	16.19
CaO	23.64	24.59	24.61	24.61	23.80	24.27	24.36	24.67	25.16
Na_2O	0.33	0.28	0.29	0.33	0.49	0.28	0.28	0.24	0.26
Total	98.42	99.23	99.80	100.82	100.21	99.75	101.37	100.62	100.61
STRUCTURAL FORMULA ON THE BASIS OF 6 OXYGENS									
Si	1.985	1.964	1.964	1.963	1.980	1.994	1.984	1.985	1.989
Al^{IV}	.015	.036	.036	.037	.020	.006	.026	.015	.011
Total tet.	2.000	2.000	2.000	2.000	2.000	2.000	2.000	2.000	2.000
Al^{VI}	.014	.014	.009	.025	.064	.022	.034	.020	.012
Ti	.007	.002	.001	.003	.002	.002	.002	.002	.001
Cr	0	0	0	0	0	0	0	0	.001
Fe	.192	.207	.204	.152	.166	.169	.196	.131	.107
Mn	.006	.005	.005	.004	.004	.004	.004	.004	.009
Mg	.812	.781	.801	.844	.813	.822	.777	.868	.879
Ca	.952	.988	.982	.963	.937	.961	.952	.964	.981
Na	.024	.021	.021	.024	.035	.020	.020	.017	.019
Total	2.007	2.018	2.023	2.015	2.021	2.000	1.985	2.006	2.009
%Ca	48.07	49.48	48.93	48.57	48.01	48.74	48.95	48.66	49.45
Mg	41.00	39.13	39.89	42.56	41.67	41.68	39.97	43.85	44.27
Fe	9.68	10.38	10.17	7.66	8.51	8.56	10.07	6.60	5.40
Na	1.25	1.02	1.00	1.22	1.81	1.01	1.01	.88	.88

TABLE 12 CONTINUED

	18	19	20	21
Ox Wt	T1-4	75-90E	56-20E	T2-8
SiO_2	54.74	54.74	55.41	55.76
TiO_2	0.10	0.06	0.05	0.04
Al_2O_3	0.74	1.15	0.89	0.13
Cr_2O_3	0.02	0.01	0.01	0.01
FeO	4.73	3.12	2.77	0.50
MnO	0.13	0.12	0.08	0.06
MgO	15.77	16.35	16.76	18.71
CaO	24.46	24.99	24.67	25.46
Na_2O	0.31	0.22	0.36	0.08
Total	100.99	100.77	101.01	100.74
STRUCTURAL FORMULA ON THE BASIS OF 6 OXYGENS				
Si	1.990	1.982	1.995	1.997
Al^{IV}	.010	.018	.005	.003
Total tet.	2.000	2.000	2.000	2.000
Al^{VI}	.022	.031	.033	.003
Ti	.003	.002	.001	.001
Cr	.001	0	0	0
Fe	.144	.094	.084	.015
Mn	.004	.004	.003	.002
Mg	.855	.883	.899	.999
Ca	.953	.969	.952	.977
Na	.022	.016	.025	.006
Total	2.004	1.999	1.997	2.003
%Ca	48.29	49.42	48.54	48.92
Mg	43.31	44.99	45.88	50.01
Fe	7.29	4.81	4.26	.75
Na	1.11	.78	1.32	.32

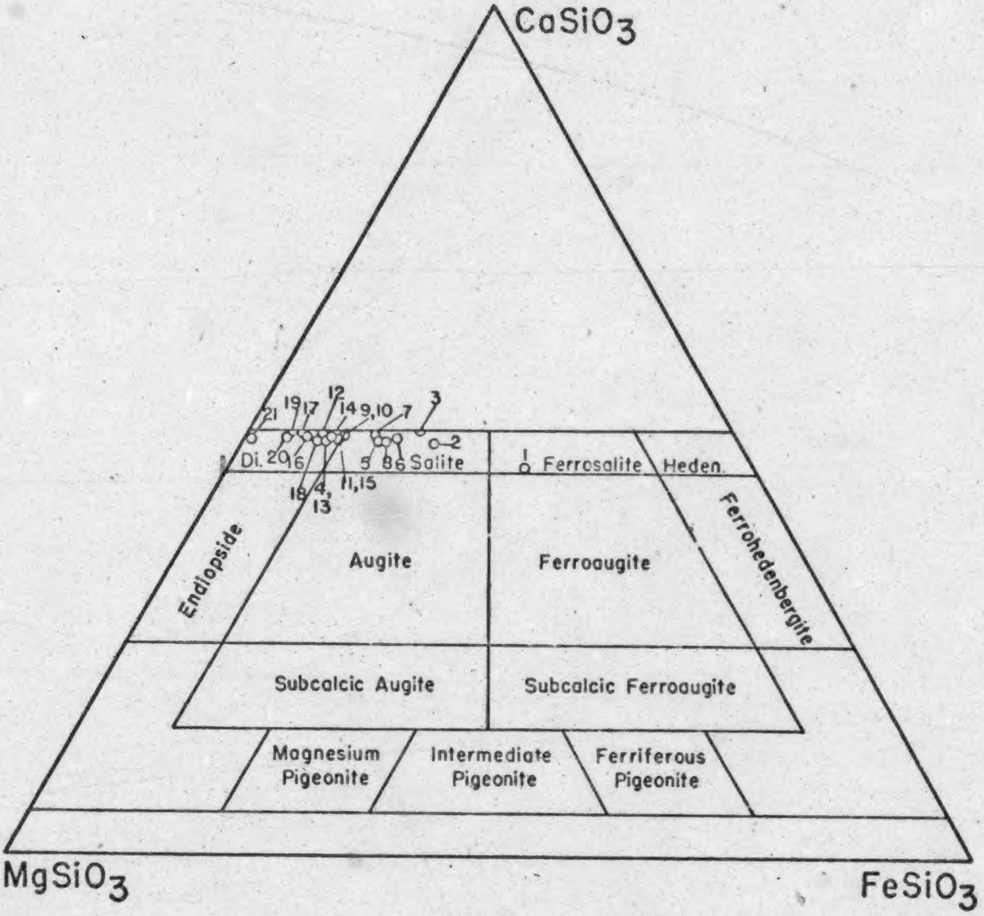
CaSiO$_3$
21
19
17
12
14
9,10
7
3
2
Di.
20
16
5
8
6
Salite
18
4,
13
11,15
1
Ferrosalite
Heden.
Endiopside
Augite
Ferroaugite
Ferrohedenbergite
Subcalcic Augite
Subcalcic Ferroaugite
Magnesium Pigeonite
Intermediate Pigeonite
Ferriferous Pigeonite
MgSiO$_3$
FeSiO$_3$

Fig. 29. The pyroxene quadrilateral, after Deer et al. (1966). All pyroxenes analyzed are plotted as numbered circles. Numbers correspond to analyses in Tables 11 and 12.

the significance of this occurrence will be discussed later.

The grouping of pyroxenes on an ACF plot (not shown) is quite close and is a result of the lack of significant solid solution of soda or alumina in the system. The pyroxenes studied are dependent on rock composition for their Fe/Fe + Mg ratios, as can be seen from Fig. 30. Rocks from Kootenay Point form an almost linear relationship when Fe/Fe + Mg ratios are compared, indicating that the composition of the rock was the prime control, grade being equal. Pyroxenes from the region show more scatter, with only two lying on the line determined by pyroxenes from the Point. Al/Mg + Fe ratios for pyroxenes and rocks show no systematic variations.

Epidote

Paragenesis of the epidote group in the Kootenay rocks is complex. In no rock studied can it be said that epidote group minerals are stable. They are usually found to be in a reaction relationship with one or more of the following: amphibole, calcite-plagioclase-quartz or possibly diopside. Epidote group minerals occur in rocks of varied compositional type, from pelitic or calc-pelitic rocks to amphibolites. Chemical data for epidote-group minerals is limited to four thin sections and five analyses. Two analyses are from basic rocks (one-or-two amphibole gneisses) (T3-11b, T4-8b) of Kootenay Point, the other three from two regional metamorphic rocks, both calc-silicates. Analyses are presented in Table 13.

Examination of Table 13 reveals that the epidote group minerals analyzed are low in "pistacite" content (calculated as moles--octahedral $Fe^{3+}/Al + Fe^{3+}$, all Fe as Fe^{3+}). They range from $Ps_{9.28}$ -

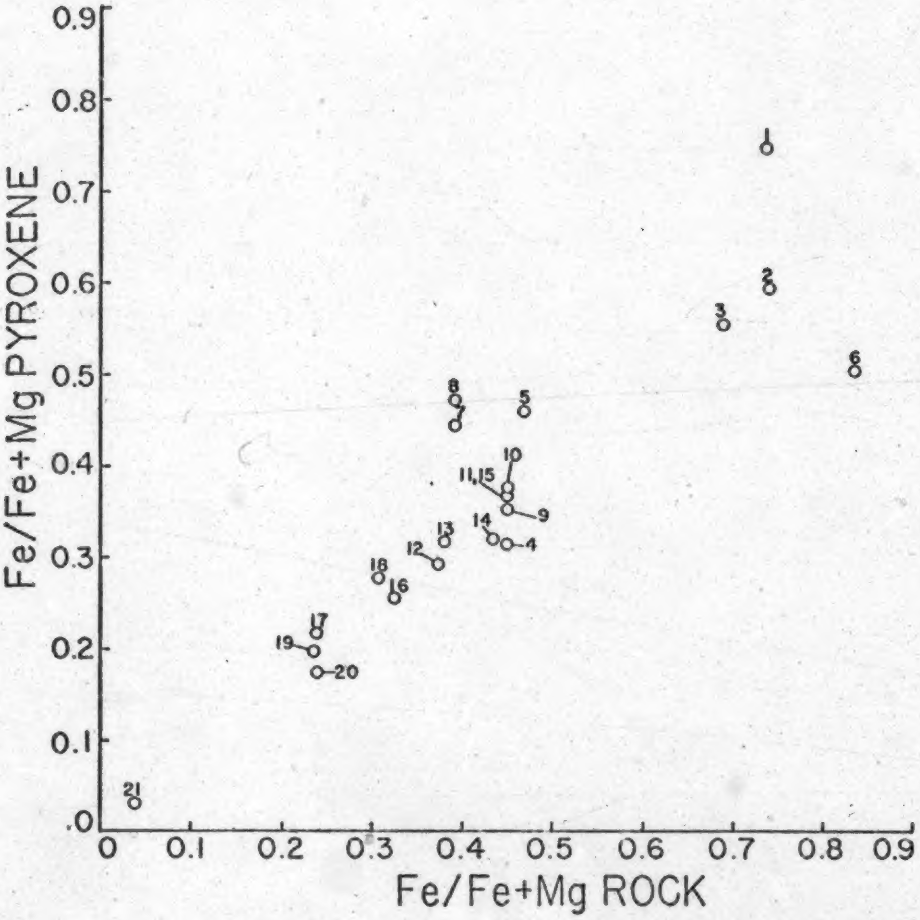

Fig. 30. Fe/Fe + Mg pyroxene plotted against Fe/Fe + Mg rock for all pyroxenes analyzed. Scatter is caused by pyroxenes from regional metamorphic rocks which do not fall along the line defined by pyroxenes from the Point. Numbers correspond to analyses in Tables 11 and 12.

TABLE 13. ELECTRON MICROPROBE ANALYSES OF EPIDOTES

	1	2	3	4	5
Ox Wt	T3-11	T4-8	11CBT-7	7RT-7(2)	7RT-7(1)
SiO_2	37.06	37.99	38.11	38.96	39.02
TiO_2	0.18	0.11	0.16	0.05	0.08
Al_2O_3	24.11	25.92	25.46	30.29	29.11
Fe_2O_3	11.70	9.79	10.11	4.85	5.68
MnO	0.13	0.08	0.03	0.04	0.06
MgO	0.21	0.09	0.09	0.04	0.05
CaO	21.41	23.72	26.52	24.03	23.88
Na_2O	0.01	0.00	0.00	0.00	0.00
K_2O	0.09	0.07	0.07	0.08	0.08
Cl	0.01	0.04	ND	ND	ND
Total	94.91	97.81	100.55	98.34	97.96
H_2O*	5.09	2.19	--	1.66	2.04

STRUCTURAL FORMULA ON THE BASIS OF 12.5 OXYGENS

	1	2	3	4	5
Si	3.015	2.993	2.950	2.989	3.015
Al	0	.007	.050	.011	0
Total	3.015	3.000	3.000	3.000	3.015
Al	2.327	2.399	2.272	2.728	2.665
Fe^{3+}	.716	.580	.589	.280	.330
Total	3.043	2.979	2.861	3.008	2.995
Ti	.011	.007	.009	.003	.005
Fe^{2+}	--	--	--	--	--
Mn	.009	.005	.002	.003	.004
Mg	.025	.011	.010	.005	.006
Ca	1.866	2.002	2.199	1.975	1.977
Na	.002	0	0	0	0
K	.009	.007	.007	.008	.008
Total	1.922	2.032	2.227	1.994	2.000
Ps	23.67	19.43	20.23	9.28	11.08

*H_2O is determined by difference from 100%. Total Fe as Fe_2O_3. H_2O is not used in further calculations.

ND = Not Determined

$Ps_{23.67}$. T4-8b and T3-11b are optically identifiable as epidote, with $2V{\sim}80^{o}$, opt (-), and definite pleochroism. The others are clinozoisites (colorless, pleochroism faint or absent, $2V{\sim}60$ opt (+)). Both groups show anomalous interference colors, although epidotes from lower grade epidote-actinolite assemblages show normal colors.

Epidote group minerals are compositionally complex, being able to incorporate large amounts of rare-earths and other trace elements into the lattice. Examination of the minerals studied shows that generally low totals are encountered, except for 11CBT-7. The low totals can be produced by 1) a certain amount of water (up to 1 (OH) per formula unit) or 2) by the presence, in large amounts, of rare-earths or other trace elements. Up to 2% H_2O is encountered (Deer, Howie and Zussman, 1966), which is enough to account for the totals of 7RT-7A and B, but not enough for T3-11b and T4-8b. T3-11b is especially low, and the low Ca suggest high rare earth content (undetermined). Structural formulae (calculated with all Fe as Fe^{3+}) are good, with the exception of 11CBT-7 which has a bit too much calcium. No error is indicated in the raw data, but calcite is present in several epidote grains, possibly producing above normal calcium counts.

Clinozoisite shows considerable variability within a single slide, a variance suspected from optical data. 7RT-7 (1) and (2) have quite different Al/Mg + Fe ratios. Iron-poor epidotes and clinozoisites observed in thin sections from rocks at lower and higher grades are often zoned, with iron-rich cores and iron-poor (non-pleochroic) rims. Also, two epidote group minerals will appear in the same slide. In 7RT-7, the two are probably related to different volume chemistries during formation, but in other slides a pleochroic epidote coexists with a non-pleochroic clinozoisite. Neither can be said to have been in stable equilibrium, however.

Strens (1964) postulated a miscibility gap between Ps_{13} and Ps_{24} in the epidote-clinozoisite series from the Borrowdale Volcanics. Holdaway (1965) also postulated a gap in the series for rocks formed at lower temperature. Chemical analyses of epidotes from the Kootenay rocks do not confirm the gap postulated by Strens, since pistacite contents of 19 - 23 are found. The coexistence of two epidotes, as well as zoned epidotes, could indicate the presence of a miscibility gap. No chemical data were taken on these complex lower grade epidotes, however, so the presence of a gap cannot be confirmed.

There is a distinct change in paragenesis and amount of epidote as one moves from the lower-grade eastern assemblage towards the higher-grade assemblages along the lake shore. The low-grade assemblage, which appears stable is an epidote-actinolite-hornblende-sphene-calcite assemblage. The epidote, pleochroic colorless to straw yellow, is subhedral and often poikilitically enclosed in anhedral actinolite. The actinolite, pleochroic α colorless to $\beta = \gamma$ pale green or bluish-green, contains numerous inclusions of calcite. Variations of the low grade paragenesis are 1) hornblende, zoned or with patches of actinolite coexisting with actinolite and epidote, or clinozoisite, or both. (Biotite, usually green, may also be present); 2) banded calc-silicates with muscovite-calcite-epidote-quartz and biotite. Feldspar or quartz-rich bands alternate with epidote-rich bands. These are true calc-silicates, derived from shaley or sandy marls. At higher grades, epidote diminishes in importance within the slide. In the actinolite-calcite-quartz rocks, a greater amount of hornblende forms and epidote becomes embayed or granular. It is often poikilitically enclosed within the hornblende. Plagioclase increases in An content, and clinozoisite increases in importance, while the epidote becomes iron-poor. In the calc-silicates (where clinozoisite appeared to be more abundant than epidote) epidote (and clinozoisite) disappear or decrease in importance while actinolite and diopside begin to form. At the highest grades, clinozoisite coexists with hornblende or with diopside, but not in apparent textural equilibrium. It is always anhedral and deeply embayed and appears in the process of being absorbed by either hornblende, tremolite-actinolite or diopside.

One other paragenesis of interest is that in pelitic rocks. In this paragenesis, clinozoisite occurs as very small grains in muscovite-biotite-plagioclase-quartz-K-feldspar "schists". It is commonly observed to be breaking down to muscovite and plagioclase.

Feldspar

Feldspar occurs in all but the most calcareous rock types in the Kootenay Arc. It occurs as anhedral grains, usually untwinned at lower grades, becoming progressively more complexly twinned as grade increases. Plagioclase feldspars at higher grades are often zoned with higher An cores and lower An rims. A few cases of reverse zoning have been observed optically, but this type of zoning has not been confirmed by later microprobe analysis.

Potassium feldspar is also anhedral and usually untwinned at the lower grades. At higher grades, microcline twinning develops. All potassium feldspar is either untwinned or optically identified as microcline. Microcline twinning may cover the entire grain or be pre-

TABLE 14. PARTIAL ELECTRON MICROPROBE ANALYSES OF FELDSPAR

KOOTENAY POINT, B.C.

		K_2O	Na_2O	CaO	Or	Ab	An
1	T1-5	0.18	8.16	4.95	1.09	74.08	24.83
2	T2-15	0.22	8.58	5.61	1.23	72.57	26.20
3	115-45W	0.28	9.37	6.36	1.41	71.71	26.88
4	T2-9(1)	0.25	8.24	5.99	1.43	70.32	28.25
5	T2-9(2)	0.28	7.89	6.70	1.56	67.01	31.43
6	T4-8	0.20	7.04	7.58	1.13	61.99	36.88
7	75-90E	0.23	7.19	7.87	1.30	61.51	37.20
8	240-137E	0.16	7.66	8.76	0.82	60.78	38.40
9	T4-4b	0.18	6.75	8.61	1.06	58.04	40.90
10	375-140W	0.14	6.48	9.54	0.79	54.71	44.50
11	240-137E	0.13	6.50	9.64	0.71	54.58	44.72
12	168-140E	14.81	1.43	0.02	87.14	12.77	0.10
13	T2-5a	15.04	1.25	0.03	88.66	11.21	0.13
14	198-146E	14.81	1.17	0.05	89.03	10.73	0.24
15	190-120E	14.71	1.15	0.05	89.20	10.56	0.24
16	T1-4	14.92	1.09	0.01	89.92	10.02	0.06
17	T3-11	15.19	1.07	0.06	90.10	9.61	0.29
18	T2-4	15.39	0.94	0.01	91.51	8.46	0.03

TABLE 15. ELECTRON MICROPROBE ANALYSES OF FELDSPAR FROM REGIONAL METAMORPHIC ROCKS

	19	20	21	22	23	24	25	26	27	28
Ox Wt	5LBT-20(2)	5LBT-20(1)	11CBT-16	7RT-7	11CBT-7	6CCT-8	7RT-17	6CCT-3	10BT-13	6CCT-1(2)
SiO_2	43.96	44.04	51.80	55.33	56.58	57.34	59.13	59.36	59.40	60.00
TiO_2	0.00	0.00	0.00	0.00	0.00	0.01	0.02	0.00	0.00	0.01
Al_2O_3	34.86	35.79	30.83	29.22	27.07	27.28	25.78	25.88	26.06	25.68
FeO	0.03	0.00	0.10	0.04	0.09	0.04	0.04	0.03	0.02	0.05
MnO	0.03	0.03	0.02	0.00	0.00	0.00	0.00	0.00	0.00	0.01
MgO	0.01	0.01	0.01	0.01	0.01	0.01	0.02	0.01	0.00	0.01
CaO	18.85	19.29	13.26	11.67	9.11	9.22	7.32	7.70	7.77	7.34
Na_2O	0.75	0.52	3.90	5.26	6.68	6.24	7.62	7.03	7.10	7.31
K_2O	0.08	0.05	0.15	0.17	0.18	0.16	0.21	0.22	0.21	0.04
Total	98.58	99.73	100.06	101.69	99.72	100.31	100.12	100.23	100.56	100.44

STRUCTURAL FORMULA ON THE BASIS OF 32 OXYGENS

	19	20	21	22	23	24	25	26	27	28
Si	8.246	8.168	9.406	9.852	10.204	10.250	10.556	10.569	10.548	10.640
Al	7.706	7.821	6.593	6.131	5.755	5.749	5.423	5.432	5.453	5.368
Total	15.952	15.989	15.999	15.983	15.959	15.999	15.979	16.001	16.001	16.008
Ti	0	0	0	0	0	.002	.002	0	0	.002
Fe	.006	0	.016	.006	.014	.006	.006	.004	.002	.008
Mn	.004	.004	.002	0	0	0	0	0	0	.002
Mg	.005	.005	.004	0	0	.004	.004	0	0	.004
Ca	3.787	3.834	2.580	2.226	1.760	1.766	1.400	1.468	1.477	1.396
Na	.275	.189	1.371	1.815	2.333	2.163	2.636	2.424	2.441	2.517
K	.020	.011	.033	.038	.042	.038	.047	.049	.049	.008
Total	4.097	4.043	4.006	4.085	4.149	3.979	4.095	3.945	3.969	3.937
Ab	6.680	4.640	34.430	44.500	56.450	54.540	64.560	61.510	61.570	64.170
An	92.850	95.070	64.700	54.560	42.550	44.540	34.270	37.230	37.230	35.600
Or	.470	.290	.870	.950	1.000	.920	1.170	1.270	1.200	.230

TABLE 15 CONTINUED.

Ox Wt	29 8AT-18	30 10BT-17	31 12WP-2	32 6CCT-1(1)	33 8AT-8	34 6CCT-3	35 10BT-4	36 10BT-9	37 5LBT-17	38 7RT-7	39 8AT-8
SiO_2	61.68	61.63	61.85	62.17	64.32	64.42	64.67	64.73	64.95	64.96	65.07
TiO_2	0.00	0.01	0.01	0.02	0.00	0.02	0.00	0.00	0.00	0.01	0.01
Al_2O_3	24.09	24.29	24.71	24.73	18.33	18.37	21.76	18.08	22.11	18.53	22.37
FeO	0.01	0.02	0.06	0.04	0.03	0.01	0.00	0.02	0.05	0.02	0.06
MnO	0.00	0.00	0.00	0.00	0.00	0.00	0.00	0.00	0.00	0.00	0.00
MgO	0.00	0.01	0.01	0.01	0.00	0.00	0.00	0.01	0.00	0.00	0.00
CaO	5.24	5.56	6.17	6.08	0.00	0.02	2.37	0.00	3.17	0.02	3.13
Na_2O	8.63	8.34	8.17	8.01	0.72	0.94	10.65	0.70	9.78	0.92	9.79
K_2O	0.29	0.15	0.14	0.04	15.64	15.16	0.33	15.35	0.11	15.23	0.27
Total	99.94	100.01	101.12	101.21	99.04	98.95	99.78	98.89	100.17	99.70	100.71

STRUCTURAL FORMULA ON THE BASIS OF 32 OXYGENS

Si	10.958	10.934	10.870	10.900	11.987	11.987	11.440	11.870	11.420	11.993	11.394
Al	5.045	5.081	5.120	5.111	4.025	4.028	4.538	3.908	4.581	4.033	4.616
Total	16.003	16.015	15.990	16.011	16.012	16.015	15.978	15.778	16.001	16.026	16.010
Ti	0	.002	0	.002	0	.002	0	0	0	.002	.002
Fe	.002	.002	.009	.006	.004	.002	0	.004	.008	.004	.009
Mn	0	0	0	0	0	0	0	0	0	0	0
Mg	0	.004	.004	.004	0	0	0	.005	0	0	0
Ca	.996	1.056	1.162	1.143	0	.003	.448	0	.598	.003	.588
Na	2.972	2.870	2.784	2.722	.263	.340	3.652	.249	3.336	.328	3.327
K	.066	.033	.032	.032	3.716	3.600	.073	4.534	.024	3.585	.059
Total	4.036	3.967	3.991	3.909	3.983	3.962	4.173	4.792	3.966	3.922	3.974
Ab	73.660	72.450	70.000	69.880	6.540	8.600	87.460	5.200	84.280	8.400	83.690
An	24.710	26.690	29.210	29.310	0	.100	10.670	0	15.100	.100	14.790
Or	1.630	.860	.790	.800	93.460	91.300	1.780	94.800	.620	91.500	1.520

TABLE 15 CONTINUED

	40	41	42	43	44	45
Ox Wt	5LBT-22	11CBT-15	10BT-11	5LBT-15(1)	5LBT-15(2)	10BT-8
SiO_2	65.51	65.98	66.61	68.32		
TiO_2	0.00	0.01	0.00	0.00		
Al_2O_3	18.62	21.65	21.03	20.49		
FeO	0.15	0.02	0.07	0.02		
MnO	0.01	0.01	0.00	0.00		
MgO	0.02	0.00	0.00	0.00		
CaO	0.03	2.57	1.95	0.86	0.42	4.07
Na_2O	2.82	10.29	10.57	11.50	14.38	11.93
K_2O	12.54	0.14	0.27	0.14	0.12	0.33
Total	99.69	100.67	100.51	101.34	14.91	16.33

STRUCTURAL FORMULA ON THE BASIS OF 32 OXYGENS

Si	11.988	11.532	11.651	11.817	11.870	
Al	4.014	4.461	4.335	4.179	3.908	
Total	16.002	15.993	15.986	15.996	15.778	
Ti	0	0	0	0		
Fe	.024	.002	.011	.004		
Mn	.002	.002	0	0		
Mg	.005	0	0	0		
Ca	.005	.482	.364	.161		
Na	1.000	3.490	3.584	3.856		
K	2.927	.032	.062	.032		
Total	3.963	4.008	4.021	4.053		
Ab	25.430	87.190	89.390	95.300	97.880	82.870
An	.150	12.030	9.110	3.940	1.580	15.620
Or	74.420	.780	1.500	.760	.540	1.510

sent in patches, often as "ghost" twins which appear fuzzy and ill-defined.

Myrmekitic intergrowths of quartz and feldspar are present throughout the Kootenay Arc. Myrmekite occurs where microcline and plagioclase are in contact, and quartz is present. It occurs in rocks containing scapolite, in plagioclase-rich amphibolites and in calc-silicates, but appears absent from calc-pelitic or pelitic rocks.

Plagioclase is usually dominant over potassium feldspar, except where diopside is present. In this case, microcline occurs, and is dominant over plagioclase. In rocks containing diopside, both plagioclase and K-feldspar may be present in significant percentages.

Forty-six feldspars, inclusing twelve of the orthoclase-albite group and 34 of the plagioclase series, were analyzed either partially or completely by electron microprobe. Eighteen partial analyses were made on rocks from Kootenay Point, the remaining twenty-eight from regional metamorphic rocks.

Table 14 lists partial analyses for feldspars from Kootenay Point. Only the characterizing elements Ca, Na and K were determined. The remaining elements were calculated from stoichiometry during the adjust program used for correction. Molecular percentages Ab-An-Or are given in the table. Table 15 presents analyses for 28 feldspars from regional metamorphic rocks. Barium was not determined, but it is probably present in greater or lesser amounts in the feldspars from the region. Two of the analyses were for three elements only.

Where two identifiable feldspars were present, both were analyzed. The two feldspars were usually plagioclase and microcline or untwinned

K-feldspar. The presence of two plagioclases in some thin sections was confirmed optically. Thin sections were stained with cobaltinitrate prior to point counting to discriminate between K-feldspar and plagioclase.

Potassium feldspar: All K-feldspars analyzed are microcline, or grains showing patches of microcline twinning in otherwise optically homogeneous grains. Analyses indicate that, for rocks from the region, the microcline plots within the maximum microcline composition given by Deer, et al. (1966). However, these microclines cannot be called maximum microclines without substantiation by X-ray. Sample number 5LBT-22 (21) shows considerably more albite substitution than the others. This sample exhibits an odd paragenesis. Two amphiboles, epidote and plagioclase (albite), as well as a greenish clinopyroxene (?) coexist with the microcline (Winzer, 1973, Appendix 4). The two amphiboles are interpreted to result from a retrograde reaction forming actinolite rims around pargasitic hornblende cores (as well as forming separate actinolite grains). The retrograde reaction involves liberation of sodium, which goes into plagioclase increasing the albite content.

The feldspar ternary diagrams (Figs. 31 and 32) illustrate that very little of the anorthite molecule is present in these microclines. Fig. 31, a plot of all feldspars from Kootenay Point, indicates a range in albite content in microclines of from 8 to 13%. The system is not excessively high in soda, however, but significant amounts of scapolite are found in 168-140E (12) and T2-5a (13). The other rocks contain no scapolite.

Plagioclase: In the last ten years, it has been recognized that metamorphic plagioclases do not show complete solid solution between the

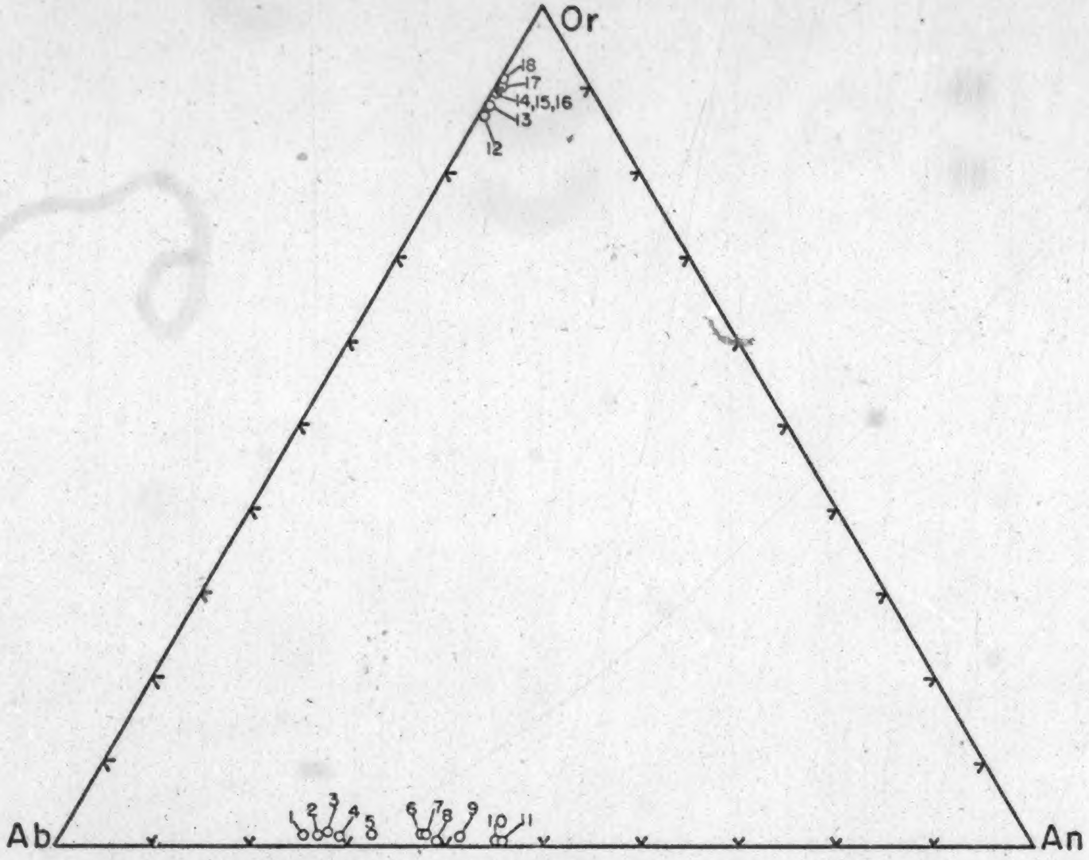

Fig. 31. Ab-An-Or triangular plot for feldspars from Kootenay Point. Numbers correspond to analyses in Table 14.

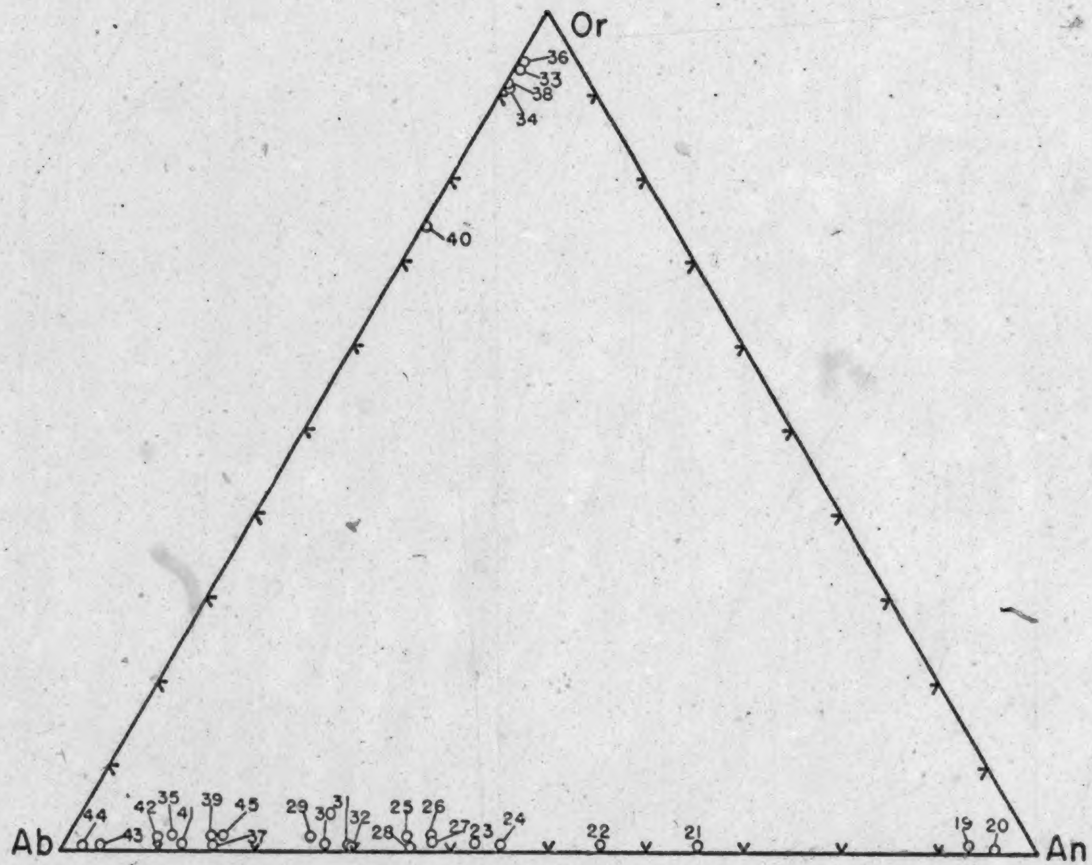

Fig. 32. Ab-An-Or triangular plot for feldspars from regional metamorphic rocks. Numbers correspond to analyses from Table 15.

two end-members albite and anorthite (Christie, 1962; Evans, 1964; Crawford, 1966; Hunahashi, et al., 1968; Barth, 1969; Leake, 1970; Cooper, 1972; Smith, 1972). The more recent authors (Crawford, 1966; Hunahashi, et al., 1968; Cooper, 1972) have empirically demonstrated shape and location of solvi in the series, mainly the peristerite solvus between An_{0-25}. Smith (1972) has produced a tentative phase diagram putting temperature and pressures on feldspar formation and giving positions and shapes for three solvi in the system.

No attempt was made to undertake a detailed statistical analysis of feldspars in the Kootenay rocks. Optical and electron probe reconnaissance work indicates that two plagioclases occur in rocks of hand specimen size from all over the region. Usually, an untwinned plagioclase will coexist with a twinned plagioclase of higher An content. Because of the difficulty of distinguishing the untwinned albite from the quartz, the untwinned albite is often overlooked, and was not analyzed by electron probe. Untwinned plagioclase can be distinguished from untwinned orthoclase by cobaltinitrate stain, but only through 2V or refractive index measurements may the untwinned plagioclase be distinguished from quartz.

Regional reconnaissance from lower to higher grades will reveal the shape of the peristerite solvus if rock composition does not significantly influence the composition of the plagioclase, or if the position of the gap is not influenced significantly by rock composition. The work of Crawford (1966), Hunahashi, et al. (1968) and Cooper (1972) indicate that the peristerite gap exists regardless of composition when the temperature and pressure conditions are such that the solvus is intersected. It would seem logical that rock composition and paragenetic history would determine the composition of the unmixed plagioclase, and further cooling would result in intersection of one of the solvi in the series. With prograde metamorphism, the situation would work in reverse, but would likely be considerably more complicated because a high-An unmixed plagioclase will not nucleate. Instead, plagioclase on either side of the gap may nucleate at the same time.

Figs. 31 and 32 indicate the compositional range and forbidden areas for plagioclases from the Kootenay Arc. The only gaps are in the high An group, between An_{45}-An_{55} and An_{55}-An_{90}, but this does not negate presence of other gaps, because beam movement will integrate microscopic intergrowths in an unmixed plagioclase. All plagioclases studied have some substitution of the $KAlSi_3O_8$ molecule (up to 2%). Plots of Ca/Al, Na/Al, K/Al and CaO/Na_2O in the rock against An content of the plagioclase reveal no direct compositional dependence between feldspar and rock. Instead, the feldspars tend to cluster around certain anorthite contents regardless of rock ratios. For instance, seven lie between An_1 and An_{15}, with a gap between An_5 and An_{11}. The bulk of the plagioclases fall between An_{26} and An_{45}, essentially the area between the An-rich limb of the peristerite solvus and the An-poor limb of the Bøggild gap. Within these ranges, Ca/Al and K/Al ratios in the rocks may vary by a factor of 10, Na/Al by a factor of 3. The data do not eliminate compositional control, but they do suggest that external conditions of formation (P,T at least) exerted more influence on plagioclase composition.

Scapolite

Scapolite is restricted to metamorphic rocks, but may occur at all grades and in a wide variety of assemblages. Until recently, little was known about the structure and stoichiometry of the scapolite series, but work by Shaw (1960a,b) and Evans, et al. (1969) has established working parameters for judging the range and reliability of scapolite analyses. Two schools of thought have emerged regarding the origin of scapolite in metamorphic rocks. One group (White, 1959; Hietanen, 1967; Ramsay and Davidson, 1970) subscribes to conditions of origin which are essentially isochemical and with varying fugacities of the volatiles Cl, CO_2 and SO_4. The other group has presented a metasomatic origin for scapolite (Shaw, et al., 1963a,b; Shaw, et al., 1965; Marakushev, 1964). Recent papers (Haughton, 1971; Ekstrom, 1972) discuss scapolite paragenesis in equilibrium with plagioclase, contradicting earlier statements by Shaw that no relationship exists between plagioclase and scapolite composition in the same rock. The paragenesis of scapolite is complex. Marialitic scapolites may form by either isochemical metamorphism of halite-bearing beds or by Na-K metasomatism. Meionite would appear to be metasomatic. However, its formation by isochemical metamorphism can not be ruled out. Scapolite in a rock almost certainly reflects changes in the fugacity of Cl, SO_4 and CO_2.

Nine scapolites in five thin sections from Kootenay Point were analyzed for seven elements by electron microprobe (see Table 16). All scapolites analyzed fall near the composition of mizzonite (Me_{70}, Shaw, et al., 1965), ranging from $Me_{68.2}$ - $Me_{74.8}$. All are high carbonate meionites, but T4-4a (4) and 199-146E (6) contain considerable SO_4.

Structural formulae are calculated on the basis of 12(Al + Si) x 10^3 after Evans, et al. (1969). Comparisons with Evans' scapolites are generally good, but some differences occur. Evans, et al. (1969) believe that the ideal structural formula should calculate near 4000 for W (Ca + Na + K). The range is 3927-4068, but Shaw (1960) reports

TABLE 16. ELECTRON MICROPROBE ANALYSES OF SCAPOLITE FROM KOOTENAY POINT

	1	2	3	4	5	6	7	8	9
Ox Wt	T4-2(3)	T4-2(2)	T4-2(1)	T4-4	T2-18(2)	199-146E	56-20E(2)	56-20E(1)	T2-18(1)
SiO_2	45.07	45.28	46.02	46.26	46.43	46.52	47.28	47.49	48.11
Al_2O_3	27.75	28.05	27.49	24.62	27.26	28.52	26.25	26.95	26.33
CaO	15.37	15.96	16.25	16.23	17.81	16.31	18.27	17.82	18.31
Na_2O	3.81	3.68	3.84	3.48	3.34	3.99	3.26	3.37	3.38
K_2O	0.23	0.26	0.25	0.25	0.18	0.27	0.20	0.20	0.23
SO_4	0.58	0.41	0.70	4.19	0.06	2.38	0.05	0.05	0.06
Cl	0.27	0.27	0.31	0.08	0.18	0.36	0.18	0.23	0.26
Total	93.08	93.91	94.86	95.11	95.26	98.35	95.49	96.11	96.68
CO_2 diff.	6.92	6.09	5.14	4.89	4.74	1.65	4.51	3.89	3.32
ATOMIC PROPORTIONS ($\times 10^3$) ON A BASIS OF (Si + Al) = 12									
Si	6954	6935	7042	7375	7092	6967	7253	7191	7294
Al	5046	5065	4958	4625	4908	5033	4747	4809	4706
Ca	2540	2620	2664	2772	2915	2617	3003	2891	2974
Na	1139	1093	1139	1076	988	1158	975	991	993
K	46	52	48	52	36	52	38	39	45
S	56	39	67	418	6	223	5	5	6
Cl	70	71	81	21	47	91	48	58	67
C	1458	1274	1074	1064	989	337	945	804	687
W	3725	3765	3851	3900	3939	3827	4016	3921	4012
Me%	68	70	69	71	74	68	75	74	74

ranges for microprobe analyses of 3900-4120 and for wet chemical analyses 3754-4326. The scapolites presented here range from 3725-4016. Using Evans' criteria, 199-146E (6) and all scapolites from section T4-2 are deficient in Ca + Na + K. Low analytical totals for T4-2 (2) and (3) may indicate a deficiency, but totals for T4-2 (1) and 199-146E (6) seem reasonable. Sr was usually present in trace amounts. Other unanalyzed elements such as Mg, Ba or Fe may be present in significant amounts, thus giving low totals. Another deviation is in the sum of the volatiles. Evans, et al. (1969) feel that Cl + C + S should sum to 1000, but previous work, as well as their own, indicates a range of from 261-1153. Scapolites from Kootenay Point show a range of 651-1584 (Cl + C + S). This part of the structural formula is sensitive to small errors in analysis of major elements because CO_2 is determined by difference and has a very large atomic proportion. For the above reasons, T4-2 (1), (2) and (3), and possibly T4-4a (4) give large excesses for volatiles. CO_2 determined for other scapolites may be as high as 4.8%. Thus, all but T4-2 (1), (2) and (3) have reasonable amounts of CO_2, while T4-4A has considerable sulfur. Figs. 33a, b, c and d illustrate structural formulae trends for atoms Si plotted against Ca and Na + K, Cl against Ca and C + S against Ca. The plots illustrate the problems discussed above and suggest that the analyses fall into two groups, those with Si in excess of that required for the amount of Ca or Na + K present, and those deficient in Si for the amount of Ca or Na + K present. The evidence is inconclusive, as the "deficient" scapolites plot near the line given by Shaw (1960). The plot of C + S against Ca illustrates the dependence of C on the analytical total and is not as instructive as the other two plots. The comparisons suffer from the fact that the analyses of Evans et al. (1969) do not contain data on metamorphic grade. Thus they cannot

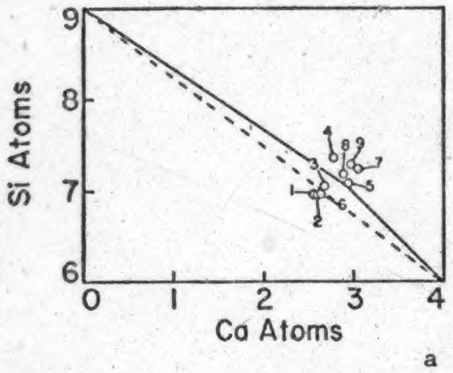

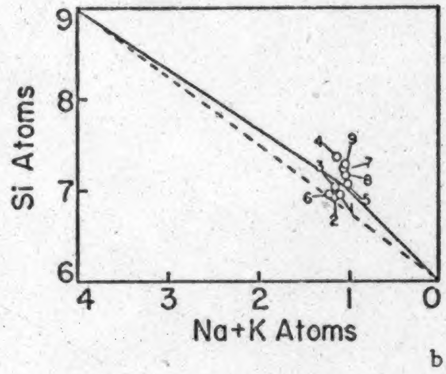

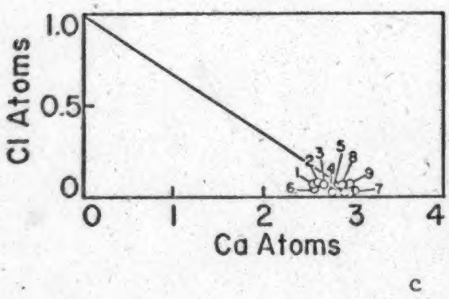

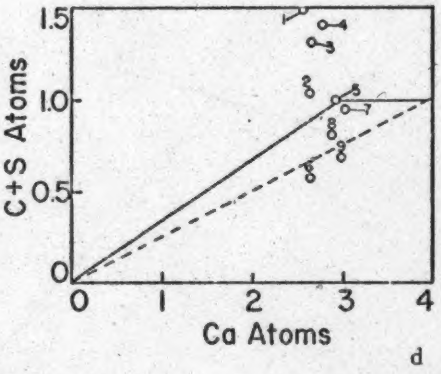

Fig. 33 a. Si atoms plotted against Ca atoms for all scapolites analyzed.

Fig. 33 b. Si atoms plotted against Na + K atoms for all scapolites.

Fig. 33 c. Cl atoms plotted against Ca atoms for all scapolites.

Fig. 33 d. C + S atoms plotted against Ca atoms for all scapolites.

Dark line after Evans et al. (1969), dashed line indicates previous trend. Numbers refer to analyses in Table 16.

be compared to Kootenay scapolites. However, the Kootenay analyses exhibit some error. An error in the standards is possible but does not explain the two groupings of scapolites, since the same standards were used for both. The differences, at least, are real and reproducible within each group.

Scapolite in the Kootenay area occurs in different parageneses. The assemblages for the analyzed scapolites are as follows:

(4)	T4-4A	Hornblende-plagioclase (An$_{40}$)-quartz-biotite-clinozoisite-scapolite
(5,9)	T2-18	Diopside-plagioclase An$_{34-28}$, An$_5$-biotite-calcite-dolomite-quartz-scapolite-sphene
(6)	199-146E	Tremolitic hornblende-Aluminous actinolite-diopside-biotite-calcite-dolomite-scapolite
(1,2,3)	T4-2	Actinolitic hornblende-biotite-epidote-clinozoisite-microcline-albite-quartz-scapolite
(7,8)	56-20E	Scapolite-diopside-biotite-calcite-dolomite quartz-sphene

Other scapolite bearing assemblages from the Kootenay region are:

29-36	Hornblende-quartz-plagioclase-K-feldspar-biotite-sphene-chlorite-epidote-scapolite
18-4	Quartz-biotite-plagioclase-muscovite-calcite dolomite-scapolite
3/8-3	Quartz-plagioclase (An$_{15}$)-K-feldspar (?)-scapolite-biotite-muscovite-epidote
5LBT-20	Calcite-dolomite-quartz-plagioclase-scapolite-diopside-tremolite
9CBT-2	Diopside-actinolite-plagioclase (An$_{40}$)-scapolite-Mg biotite-sphene-quartz
9CBT-6	Calcite-dolomite-diopside-actinolite-plagioclase-microcline-epidote-scapolite-phlogopite-quartz (possibly magnesite)

There are similarities between all parageneses. First, all scapolites, regardless of their location, grade, or rock type are meionitic. Second, where diopside and scapolite occur together, they are accompanied by calcite-dolomite and either quartz or an amphibole with a high tremolite content. Third, the scapolite is usually seen to be replacing plagioclase, and if more than one plagioclase is present, replaces the plagioclase with the higher anorthite content. Fourth, meionite contents are higher by up to 40% than the anorthite content of the plagioclase they are replacing, and higher by up to 70% than the An content of the plagioclases they coexist with (usually albite). Fifth, scapolites occur in calc-silicates or amphibolites but do not occur in pelites. Sixth, where amphibole is present with scapolite, the amphibole is almost always zoned.

A typical scapolitized rock has 5-10% scapolite in anhedral irregular grains up to 6 mm long. In the same thin section, less irregular, anhedral, poikilitic grains of scapolite and scapolitized feldspar cores both appear. Both textures indicate growth of scapolite following crystallization of the main minerals in the rock. Magnesian or ferromagnesian silicates are usually anhedral, blebby and poikilitic, with the amphiboles generally fresher than the pyroxenes. Amphiboles are often zoned, with a continuous change from darker green cores to bluish-green rims. The amphibole is usually hornblende at the core, with increasing actinolite towards the rim. Pyroxene is small, rounded and often embayed. The exception to these general disequilibrium textures is found in biotite. Biotite is euhedral to subhedral, forming fresh flakes often present as a randomly oriented matte superimposed on all other minerals. It is poikilitically enclosed in amphibole and scapolite. Epidote and clinozoisite are anhedral and irregular, often poikilitic, enclosing small rounded quartz grains, and seem to have been in the process of being actively incorporated into amphibole and diopside.

Feldspar, where present, provides more interesting textures. Both feldspars may be present, but where they are, microcline is dominant. The plagioclase present is usually untwinned albite, but where scapolite is minor, twinned feldspars up to An_{40} are present. Myrmekitic intergrowths of quartz and feldspar are common. The plagioclase may be zoned or patchy, with several irregular zoned regions inside a single grain. Anorthite rich cores are often replaced by scapolite.

In the diopside-scapolite rocks, calcite and dolomite are found in apparently stable coexistence with quartz. In sample 56-20E, very little feldspar is present, and the rock is really composed of a few large sieve-like grains of scapolite poikilitically enclosing anhedral diopside, euhedral biotite, calcite, dolomite and quartz. The carbonates and quartz are rounded anhedral grains. Carbonate sometimes occurs in stringers between quartz, diopside and scapolite.

The petrographic evidence indicates that scapolite is replacing feldspar in the rocks from the Kootenay Arc. Textures of minerals in the slides suggest reactions affecting major ferromagnesian minerals, but suggest also the stable coexistence of calcite-dolomite and quartz. The composition of the scapolites indicates that they formed under very high P_{CO_2}, low f_{Cl} and variable f_S. The paragenesis of scapolite will be discussed in more detail in the next chapter.

Carbonates

Calcite, dolomite and magnesite are present in rocks from the Kootenay Arc. Calcite-dolomite and dolomite-magnesite are found in stable coexistence with one another, but calcite and magnesite are not; as would be expected from phase relations among the carbonates at moderate to high pressures (Goldsmith, 1960; Goldsmith and Graf, 1960; Goldsmith and Heard, 1961; Goldsmith, et al., 1962; Rosenberg, 1967, 1968).

A variety of textures is presented by the carbonates. At the lower grades, calcite predominates in the rocks studied, but dolomite is usually present. Quartz, feldspar and mica (muscovite or biotite) are usually present in the more acidic rocks; chlorite, epidote and actinolite, with quartz and feldspar, in the more basic rocks. The lower grade carbonates are usually rounded, anhedral, sometimes embayed grains with smooth boundaries to neighboring carbonates (whether calcite or dolomite). The calcites are cloudy or dusty looking and are usually twinned. The dolomites, on the other hand, are usually smaller, more rounded, untwinned and clear. Both carbonates appear to coexist stably with quartz and feldspar.

At the higher grades, a considerably greater variety of textures is encountered. Both calcite and dolomite are coarser than at lower grades. They may be present as separate grains, apparently coexisting stably, since boundaries are smooth and "triple point" junctions appear. Calcite may enclose ragged, irregular dolomite, or vice versa, or calcite may be present as stringers and blebs between dolomite grains. No true, oriented, exsolution textures are seen, but some of the blebby grains appear to have exsolved from the larger host carbonate. Many carbonate grains enclose silicate phases, usually tremolite or magnesian biotite, but also quartz and feldspar. At higher grades, quartz and feldspar occur, again apparently stably, with calcite and dolomite. Scapolite may also coexist with both carbonates as mentioned in the last section. In some cases, where inclusions of biotite or tremolite are found in dolomite, alizarin red stain reveals a rim of calcite separating the dolomite from the silicate. The grain is otherwise homogeneous. This texture is taken to indicate that the silicate has leached Mg (and possibly Fe) from the host dolomite during its formation. Another interesting texture consists of numerous blebs of dolomite enclosed within large tremolite crystals. Calcite may also be enclosed in tremolite, but it is usually present in lenses outside the grains, or mixed with smaller fresher grains of subhedral tremolite. In some cases, the blebs show preferred orientation along cleavage. The larger tremolite grains appear to be breaking down.

Magnesite, recognized only in rocks from the Point, has a different habit from calcite or dolomite, occurring as aggregates of small anhedral rounded grains mixed with nearly colorless biotite and very small flakes of graphite. The aggregates appear as irregular pockets, rather than as veins or stringers. The biotites within these aggregates are usually anhedral and ragged or wispy, whereas biotites in the same slide from the dolomite areas are subhedral and generally fresher in appearance.

Sixteen carbonates from Kootenay Point (Table 17) and nine calcites from the central Kootenay region (Table 18) were analyzed by electron microprobe. Carbonates cannot be distinguished from one another without staining. Since staining ruins the polished surface of a probe section, areas were chosen and grains picked for analysis by reconnaissance. Only three elements were determined on carbonates from the Point, nine on carbonates from the region. The absence of dolomite analyses from the region does not reflect the absence of that mineral, but rather its presence in such small amounts that it was not easily found during reconnaissance with the microprobe. Later staining turned up dolomite in many of the regional rocks (see modal analyses, Table 3). No siderites or ankerites were found in any of the rocks studied.

Examination of the structural formulae calculated on the basis of

TABLE 17. ELECTRON MICROPROBE ANALYSES OF CARBONATES FROM KOOTENAY POINT, B.C.

Ox Wt	55-20W(1)	55-20W(2)	40-8E(1)	40-8E(2)	105-101E(1)	105-101E(2)	T1-6c(1)	T1-6c(2)
CaO	28.95	50.59	28.84	0.22	30.18	29.82	30.10	51.86
FeO	0.33	0.24	0.33	1.21	1.52	1.52	0.39	0.27
MgO	19.69	2.43	21.94	49.80	19.80	19.74	21.32	1.91
Total	48.97	53.26	51.11	51.23	51.50	51.06	51.81	54.04
CO_2	51.03	46.74	48.89	48.77	48.50	48.94	48.19	45.96
STRUCTURAL FORMULA ON THE BASIS OF 6 OXYGENS								
Ca	.935	1.752	.939	.007	.991	.977	.988	1.811
Fe	.009	.006	.009	.030	.039	.039	.009	.008
Mg	.884	.117	.994	2.050	.909	.900	.973	.092
Total	1.828	1.875	1.942	2.087	1.939	1.916	1.970	1.911
C	2.086	2.063	2.029	1.956	2.031	2.042	2.015	2.044

Ox Wt	T2-10(1)	T2-10(2)	T2-3a	T2-2	160-23E(1)	160-23E(2)	215-70W	205-95W
CaO	0.53	0.30	53.65	29.35	29.64	0.23	51.59	30.39
FeO	1.24	1.35	0.19	0.57	0.15	1.13	0.46	0.19
MgO	47.01	47.68	0.45	19.64	20.75	44.29	2.05	20.30
Total	48.78	49.33	54.29	49.56	50.54	46.65	54.10	50.88
CO_2	51.22	50.67	45.71	50.44	49.46	53.35	45.90	49.12
STRUCTURAL FORMULA ON THE BASIS OF 6 OXYGENS								
Ca	.015	.009	1.883	.948	.964	.007	1.802	.991
Fe	.029	.032	.006	.015	.004	.027	.014	.006
Mg	1.987	2.023	.022	.883	.938	1.861	.100	.922
Total	2.031	2.064	1.911	1.846	1.906	1.895	1.916	1.919
C	1.984	1.968	2.045	2.077	2.047	2.052	2.042	2.041

TABLE 18. ELECTRON MICROPROBE ANALYSES OF CALCITE - REGIONAL METAMORPHIC ROCKS

Ox Wt	5LBT-3(1)	5LBT-3(2)	5LBT-17	10BT-13	6CCT-3	5LBT-20	8AT-18	11CBT-7	7RT-7
SiO_2	0.05	0.04	0.04	ND	0.01	0.00	0.00	0.01	0.28
TiO_2	0.00	0.00	0.01	ND	0.00	0.00	0.01	0.00	0.00
Al_2O_3	0.04	0.02	0.02	ND	0.02	0.01	0.02	0.03	0.06
FeO	0.03	0.05	2.08	ND	0.30	0.26	0.40	0.28	0.42
MnO	0.02	0.02	0.64	ND	0.15	0.01	0.07	0.04	0.16
MgO	1.38	1.10	1.32	ND	0.24	0.41	0.62	0.27	0.26
CaO	52.29	53.71	49.05	52.70	52.66	53.37	52.51	53.10	52.82
Na_2O	0.01	0.00	0.00	0.00	0.00	0.00	0.00	0.00	0.00
K_2O	0.07	0.09	0.07	0.14	0.07	0.06	0.06	0.07	0.06
Total	53.89	55.03	53.24	52.83	53.45	54.12	53.68	53.81	54.07

STRUCTURAL FORMULA ON THE BASIS OF 6 OXYGENS

Si	.002	.002	.002	0	0	0	0	0	.008
Ti	0	0	0	0	0	0	0	0	0
Al	0	0	0	0	0	0	0	0	.002
Fe	.001	.002	.057	0	.008	.006	.010	.006	.010
Mn	.001	.001	.018	0	.004	0	.002	.002	.004
Mg	.067	.053	.063	0	.010	.020	.029	.012	.012
Ca	1.825	1.894	1.708	1.828	1.837	1.871	1.834	1.857	1.853
Na	0	0	0	0	0	0	0	0	0
K	.001	.002	.002	.003	.002	.002	.002	.002	.002
Total	1.897	1.954	1.850	1.831	1.861	1.899	1.877	1.879	1.891
C	2.057	2.022	2.076	2.086	2.070	2.050	2.061	2.061	2.056

6 (0), and the totals for the oxides indicates immediately that almost all the carbonates studied are deficient in Ca + Mg + Fe. Occupancies range from 1.828-2.064, and only the magnesites show occupancies over 2.000, the ideal value. Deer, et al. (1966) report values from 1.99-2.02. Several possible reasons exist to explain these low totals. First, in carbonates from the Point, neither Mn, Ba or Sr were determined for any of the carbonates. Mn can be present in amounts of 3% or more in calcites and dolomites, but Sr and Ba should be insignificant. The carbonates from regional metamorphic rocks have little Mn, however, (to .64%), and there is no real reason to expect higher values for the carbonates from the Point. The second reason involves the possibility of wavelength shift giving different peak positions for Ca and Mg on standards and in the samples. The standards used were both silicates (wollastonite for Ca, olivine for Mg and Fe). The difference in bonding energies for the respective elements between standard and sample could be enough to give a peak shift resulting in lower apparent concentrations, especially for Mg. A third possibility is that the beam volatizes the sample. Care was taken to move the beam quickly over the specimen, and beam current was kept low (0.1 microamp). However, low totals indicate that some volatilization could have occurred. The final reason is error in the standard. Errors in Mg in the standard olivine used would introduce disproportionate errors in magnesite, because the sample has a Mg concentration about 20% higher than the standard. Even a small standard error would give an enhanced error for Mg in the sample. Calcium values are similar. Thus, the error multiplication would be less.

Sphene, Staurolite and Garnet

Sphene is ubiquitous in amphibolites from the Kootenay Arc, being present in amounts up to 6% (see modal analyses, Tables 3,4). It is also present in calc-silicate rocks and occurs as an accessory in nearly all rock types. In the amphibolites, sphene occurs as euhedral to subhedral crystals up to 6 mm long. In calc-silicate rocks it is often "granular", present in aggregates of smaller rounded grains, or occurs as large (5 mm) irregular, rounded grains. In a few cases, sphene has yellowish cores of rutile. Five sphenes from amphibolites (5LBT-22, 8AT-8, 6CCT-8) and calc-silicate rocks were analyzed for nine elements (Table 19). Sphenes from the amphibolites have higher Al_2O_3 + FeO contents than those from the calc-silicates, and generally lower titanium. Calcium is higher in the calc-silicate sphenes. These differences probably reflect availability of the major cations, and partitioning, especially of Ti, between the major phases. The presence of hornblende or biotite would be important in determining the availability of sites for Ti.

Staurolite has been found in only one small area of the central Kootenay Arc. It occurs as anhedral, yellowish, faintly pleochroic porphyroblasts in a rock containing two "porphyroblasts" of kyanite in a matrix of quartz, feldspar, muscovite and biotite, and as small euhedral crystals in another location in the same area. Other thin sections from the same hand specimen contain garnet, mostly highly corroded and absorbed into the matrix of quartz, feldspar, biotite and muscovite. Six elements were determined on one of the grains (Table 19), confirm-

TABLE 19. ELECTRON MICROPROBE ANALYSES OF SPHENE AND STAUROLITE

	Sphene					Staurolite (Partial Analysis)	
	5LBT-22	11CBT-7	8AT-8	6CCT-8	T4-4		12WP-2a
SiO_2	30.34	29.92	30.06	30.25	30.11	SiO_2	27.54
TiO_2	37.97	39.36	36.59	40.85	38.01	TiO_2	0.41
Al_2O_3	2.33	1.89	2.47	1.17	1.03	Al_2O_3	53.92
FeO	1.08	0.53	1.62	0.36	0.54	FeO	12.48
MnO	0.06	0.00	0.09	0.09	0.10	MnO	0.13
MgO	0.01	0.01	0.04	0.01	0.03	MgO	1.61
CaO	28.39	28.18	27.07	27.88	29.02		
Na_2O	0.02	0.01	0.02	0.00	0.01		
K_2O	0.08	0.08	0.08	0.08	0.08		
Cl	ND	ND	ND	ND	0.02		
Total	100.27	99.99	98.05	100.68	98.96		96.09
IONS TO 19.5 OXYGENS						IONS TO 48 OXYGENS	
Si	3.815	3.762	3.863	3.771	4.018	Si	8.063
Al^{IV}	.185	.238	.137	.172	-	Al	18.603
Total tet.	4.000	4.000	4.000	3.943	4.018	Ti	.090
Al^{VI}	.160	.042	.237	-	.162	Fe	3.055
Ti	3.351	3.474	3.300	3.574	3.169	Mn	.032
Fe	.114	.056	.174	.038	.060	Mg	.702
Mn	.006	0	.010	.010	.011		
Mg	.002	.002	.008	.002	.006		
Total oct.	3.633	3.574	3.729	3.624	3.408		
Ca	3.825	3.797	3.727	3.724	4.149		
Na	.005	.002	.005	0	.003		
K	.013	.013	.013	.013	.014		
Total	3.843	3.812	3.745	3.737	4.166		

ming the presence of staurolite. Adding 2% H_2O to the total brings it up to 98%, indicating analytical deficiency, but elements such as zinc were not determined.

Garnet is present in amphibolites or pelitic and calc-pelitic rocks, but absent from calc-silicates. Garnet also occurs in the fine-grained microgranites (aplites) and some pegmatites from the area. Dodds,(unpbl. M.Sc. thesis, 1965) reported on garnet from schists, amphibolites and igneous rocks in the central Kootenay Arc. He found that garnet from amphibolites was richer in the grossular and pyrope molecules than those of the schists or igneous bodies. He noted that changes of CaO, MgO, MnO and FeO with grade were slight, and that values of CaO, MgO, FeO and MnO were similar whether the sample came from the sillimanite or biotite zone of Crosby (unpbl. Ph.D. thesis, 1960). Dodds further noted the absence of garnet from some amphibolites which were located quite near garnetiferous bodies. He was not able to explain this phenomenon fully, as he had no analyses for coexisting minerals in any of the amphibolites. The present author has found the same phenomena, but it appears that garnet forms in amphibolites containing pargasitic or tschermakitic hornblende. "Amphibolites" containing magnesio-hornblende or tremolitic hornblende are free of garnet. Another peculiar garnet paragenesis was noted in core from exploration hole 2114 (Cominco-Bluebell Mine). Here a small bed of amphibolite a few feet thick is in contact above and below with biotite-muscovite-quartz-feldspar gneiss. Garnet is present in amounts of $>$ 20% near the contacts, but dies off to nil at the center of the body. Grain size decreases from a few millimeters to 1 mm before disappearing altogether. Contacts between the gneiss and the amphibolite are sharp.

Garnet from the central Kootenay Arc shows a variety of textures which range from nearly euhedral (in all rock types) to anhedral, blebby grains or aggregates well on the way to be being consumed by other minerals in the rock. The garnet is generally filled with inclusions. Most appear to have grown in place, displacing the surrounding material so that foliation bends around the grain. In some cases, mica outlines the garnet perfectly; in others "selvages" of plagioclase, quartz and K-feldspar separate the garnet from the mica minerals (see also Dodds, 1965). Some garnet is stretched, often elongated to four times its width, but few appear to be "rolled".

Five garnets, in four rock specimens, were analyzed by electron microprobe. The analyses are presented in Table 20. Totals from these garnets are somewhat high, reflecting zoning in the grains. They range in composition from almandine 61.5-77.1, grossular 26.0-12.1. However, the two amphibolite garnets (12WP-2 and 6CCT-8) show significantly higher almandine contents than those of Dodds. Part of this difference is due to the probable presence of andradite ($CaO + Fe_2O_3$). The amount cannot be calculated because Fe^{3+} cannot be determined on the 'probe. Spessartine and pyrope components are small but variable. Spessartine is higher in the amphibolite garnets than in the schist garnets; pyrope shows the reverse.

The advent of the electron microprobe has prompted more detailed studies of mineral composition on the microscale, and few minerals have shown more surprises than garnet. Early studies by Hollister (1966, 1969), Atherton and Edmunds (1966) and later work by Atherton (1968), Edmunds and Atherton (1971), Fediukova and Vejnar (1971) and Kurat and Scharbert (1972) have established that garnet from regional and contact

TABLE 20. ELECTRON MICROPROBE ANALYSES OF GARNET

Ox Wt	7RT-17(2)	11CBT-16	12-WP-2	7RT-17(1)	6CCT-8
SiO_2	37.50	37.50	37.76	37.89	38.10
TiO_2	0.01	0.15	0.21	0.02	0.11
Al_2O_3	21.27	20.99	21.43	21.31	21.39
FeO	33.36	31.89	31.87	31.84	25.76
MnO	1.23	1.31	2.10	1.40	2.55
MgO	3.46	2.86	2.45	3.10	2.69
CaO	6.73	7.07	6.62	4.98	10.91
Na_2O	0.01	0.00	0.03	0.01	0.01
K_2O	0.05	0.01	0.08	0.04	0.06
Total	103.64	101.87	102.55	100.59	101.59

IONS TO 24 OXYGENS

Si	5.842	5.908	5.922	6.010	5.949
Al	.158	.092	.078	0	.051
Total	6.000	6.000	6.000	6.010	6.000
Al	3.748	3.806	3.884	3.984	3.886
Ti	.001	.017	.023	.002	.012
Total	3.749	3.823	3.907	3.986	3.898
Fe	4.346	4.202	4.180	4.224	3.364
Mn	.162	.175	.279	.188	.337
Mg	.803	.672	.573	.733	.626
Ca	1.123	1.194	1.113	.846	1.825
Na	.003	0	.009	.003	.003
K	.010	.002	.016	.008	.012
Total	6.447	6.245	6.170	6.002	6.167
Alm	74.5	73.9	74.0	77.1	61.5
Spess	2.8	3.0	4.9	3.4	6.1
Pyr	7.7	6.6	5.7	7.5	6.4
Gr	15.0	16.4	15.4	12.1	26.0

N.B. These analyses are from arbitrarily selected homogeneous areas within the garnet and therefore do not necessarily reflect the average composition of the grain.

metamorphic rocks is commonly zoned, and that zoning reflects growth conditions at the time of formation. The work of these authors has led to unravelling of physical conditions in polymetamorphic rocks.

Garnet from the central Kootenay Arc is zoned. Several grains were chosen for traverses by electron microprobe. Two were analyzed quantitatively at stations 10 and 20 microns apart. Several grains were traversed using a Rikadenki three pen recorder. Comparison of these results for four elements (Fe, Mn, Mg and Ca) indicates at least three types of garnet zoning. Examples of the three types are given in Figs. 34 - 36.

The first type, illustrated by 7RT-17 (Fig. 34), gives a relatively simple trace. The major zonation across the 2112 micron traverse is in calcium and magnesium. Calcium changes slowly from a low of about 4.6% (uncorrected) to a high of about 7%. The changes in magnesium and iron are opposite the calcium trend. The Mn trace shows little change until the margins of the grain are reached, whereupon a sharp rise occurs. The garnets from 7RT-17, a garnetiferous biotite-quartz-feldspar gneiss with minor blue-green actinolitic hornblende, are large and nearly rectangular in shape. They contain large inclusions of biotite (aligned within the garnet in the same direction as the rock foliation), quartz and feldspar. Smaller garnets are scattered throughout.

The second type of garnet zoning is illustrated by traces for 12WP-2a (Fig. 35a and 35b). Two garnets are presented, one large, the other about 1/3 the size of the first. The smaller of the two is a somewhat corroded grain showing four good crystal faces. It is free of inclusions. The larger has good crystal form, but many inclusions of quartz, feldspar and biotite. The garnets coexist with hornblende. Some of the hornblende grains are optically zoned, with olive green cores and bluish-green rims. Some separate blue-green actinolite grains appear as well. The zoning traces are more complex than those of 7RT-17. First, calcium and iron show pronounced variation on either side of the center of the grain. The zoning for the two elements is antipathetic, and is reflected to some extent in the Mg trace as well. Mn, on the other hand, does not show a similar trace. For the larger grain, the Mn curve resembles a depletion curve placed off-center. Mn rises again towards the grain margin. This trend is clearer in the smaller grain, which one could imagine as being the larger grain cut off at the Mn peak. The trace is similar to that of the right hand portion of the larger grain.

The third, and most complex type of zonation is demonstrated by the trace for 11CBT-16 (Fig. 36). This garnet comes from a porphyroblastic biotite-quartz feldspar schist which contains only three or four highly corroded garnet grains. The garnet chosen for traversing is part of a knotty glomeroporphyroblast which outlines a larger original garnet. About half of the garnet has been replaced, and many inclusions occur in the remaining portion. The complex trace does not result from traversing inclusions, however, since the station plots agree with the intensity trace. The garnet would appear to be a series of smaller grains which have coalesced, but not "homogenized". Each smaller section shows a similar trend, enriched Mg, Fe and depleted Ca, with Mn sharply enriched near the edges. In the "between" grains portion, grossular (Ca) and spessartine (Mn) components show very sharp rises, with concomitant drop in almandine and pyrope.

One factor is constant for all garnets; Mn does not show a symmetrical depletion pattern, and it is always sharply enriched at the edge or near-edge areas. Most authors agree that an increase in Mn near the edge indicates growth under conditions of falling temperature, and it is difficult to see how a simple Rayleigh fraction model can fit a Mn enrichment at the margins.

Zoning in the Kootenay garnets arises from complex interactions between the garnet and its coexisting minerals. In view of the zoning found within the garnets, it is not surprising that those studied by Dodds failed to show systematic trends in bulk composition with grade. The petrogenesis of the Kootenay garnets will be discussed in the next section.

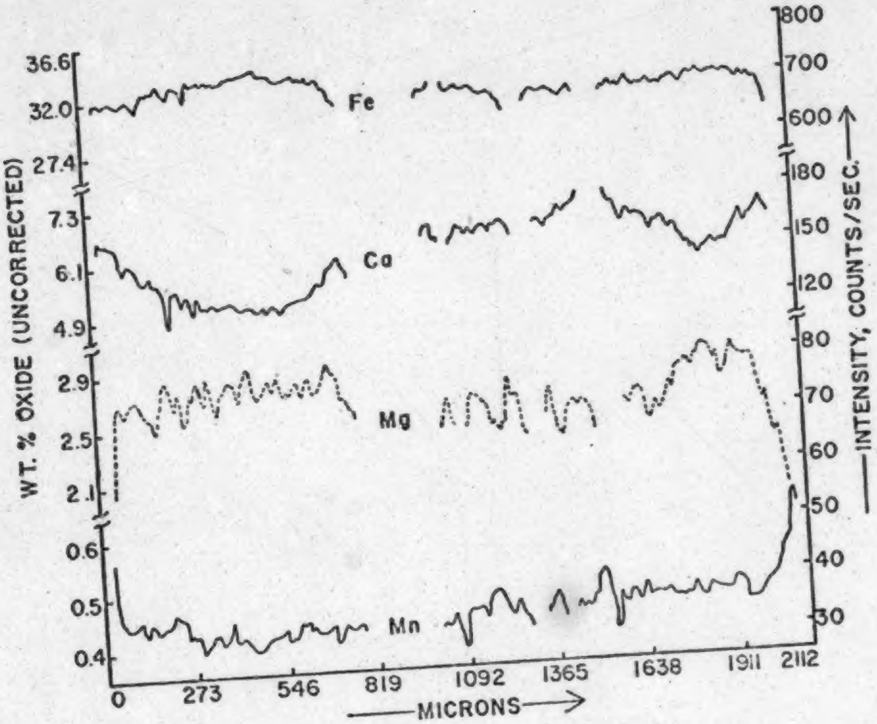

Fig. 34. Zoning trends for 7RT-17, a Type I garnet. Intensity in counts per second, wt % oxide, uncorrected. Dashed line is used on figures 34 through 36 in order to distinguish Mg from Mn.

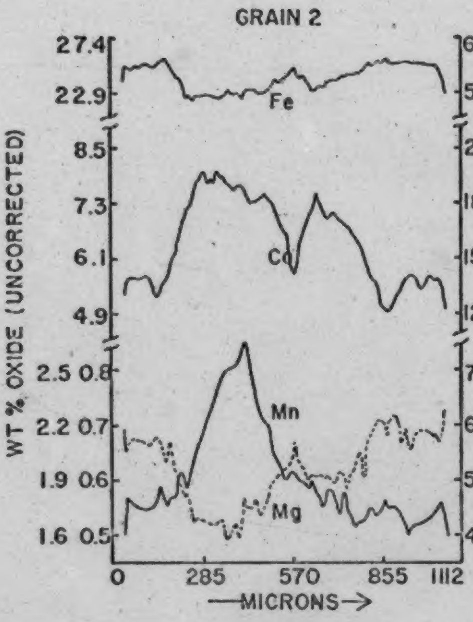

Fig. 35 a. Zoning trends for 12WP-2a, a Type II garnet.

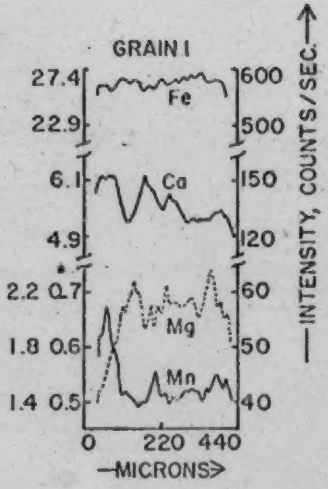

Fig. 35 b. Zoning trends for a smaller Type II garnet from 12WP-2a.

Intensities in counts per second, wt % oxide uncorrected. Inner scale MnO; outer scale MgO.

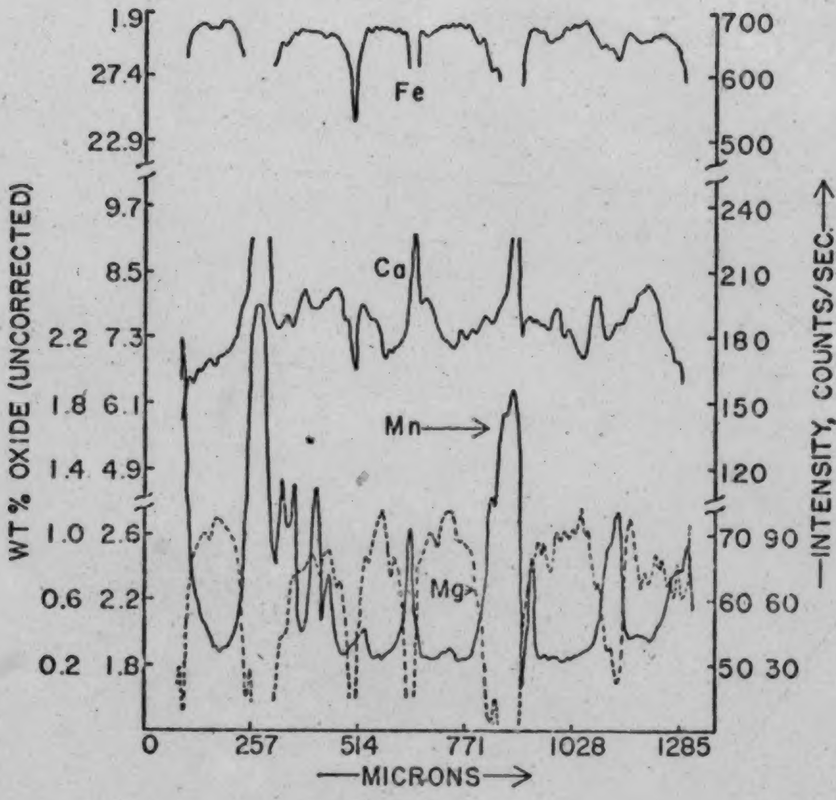

Fig. 36. Zoning trends for 11CBT-16, a Type III garnet. Intensities in counts per second (inner scale MgO; outer scale MnO). Wt % oxide uncorrected.

CHAPTER III

METAMORPHIC PETROLOGY

The degree and type of metamorphism in the central Kootenay Arc presented by Crosby (1968) is in need of revision. Barrovian zones of metamorphism, determined by the first appearance of certain index minerals, do not precisely reflect temperature and pressure of metamorphism. Modern interpretations are based on the identification of reaction isograds within field settings. Several examples exist of the successful application of this type of study (Albee, 1965; Mather, 1970; Guidotti, 1970; Cooper, 1972). Unfortunately, in order to successfully complete a detailed study of isograds, the area must be well mapped and contain rocks of similar chemistry cropping out over long distances. Neither criterion is met in the central Kootenay Arc. Outcrop is not usually more than 10-20%, and well exposed rocks are confined to shorelines, creekbeds and roadcuts. The rapid change of lithology along strike and across the section causes large variations in the composition of the rock system so that continuity of one rock composition is almost impossible to establish.

Another commonly used manner of characterizing metamorphic facies is that of mineral assemblages, summarized by Turner (1970). Winkler (1967) has outlined temperature and pressure regions in which certain assemblages are stable. The problem with this approach is that most of the quantitative work on pressure and temperature at which assemblages are stable is limited to rocks of pelitic composition. Reactions producing characteristic assemblages in siliceous dolomites are also well quantified. Very little work of a quantitative nature has been done on rocks of intermediate or basaltic composition, or on rocks which would be classified as calc-silicates, "dirty" siliceous limestones or calcareous pelites. Unfortunately, the last three rock types abound in the central Kootenay Arc, and the first two are virtually absent.

Another method of establishing the effects of metamorphism is to study systematic changes in minerals. Systematic changes may often be correlated with changes in grade, and may, in comparison with the same minerals from similar rock types in other areas, be used to define the metamorphic environment in the area chosen for study.

This last method, and that of assemblages, will be used in this study to define the type and extent of metamorphism in the Kootenay Arc, and to compare the metamorphism in this area with that of other metamorphic belts in the world in order to deduce the evolution of this part of the Kootenay Arc. The mineral groups which show systematic changes will be discussed first, in the same order as they were presented in the mineralogy section. These minerals will then be related to one another to deduce reactions in progress and to attempt to quantify the conditions under which these reactions are taking place.

A grade index for the central Kootenay Arc must first be defined. Earlier work by Crosby (1968), Fyles (1967), Livingstone (unpbl. M. Sc. thesis, 1968), Ransom (pers. comm., 1972, 1973) and work by the author establishes the fact that the degree of metamorphism increases from east to west, at least as far as the west side of Kootenay Lake. From the west side of the lake toward the contact aureole of the Nelson batholith, metamorphic grade falls according to Fyles (1967) and Crosby (1968).

This decrease in metamorphic grade was based on the interpretation of both kyanite and sillimanite isograds lying near the lake shore. Rocks containing sillimanite have been found by the writer only in the contact zone of the Crawford Bay Stock. Livingstone (unpbl. M. Sc. thesis, 1968) reports one section containing sillimanite in a fine-grained muscovite aggregate from the north shore of Riondel peninsula. Samples collected from this area by this author are sillimanite free, and Ransom (pers. comm., 1972, 1973), a mine geologist at Riondel, reports no sillimanite. Kyanite is restricted to a small pod within ten feet of the contact with a large syenitic body on Woodbury Point. Retrograded kyanite extends about 15 meters from the body, but is not found elsewhere to the north or south, despite rocks of favorable composition. These observations suggest that neither zone exists in regional extent, and interpretations of decline in metamorphic grade within the area west of the lake shore to the contact aureole of the Nelson may be in error.

Given the situation outlined, a grade index may be defined by measuring the distance from the east side of the map sheet to any given sample location to the west, with the reasonable assumption that as one goes farther west, grade increases. Rocks lying at the extreme eastern edge of the map area are in the chlorite zone or at the biotite isograd. One problem in adopting this method of indexing the rocks is that isograds may be folded, or may not be parallel to the map edge. All structural trends in the area are generally north-south, however, and there is no field evidence for folded or deformed isograds. The grade index is read in kilometers west of the map edge. Maximum grade lies along the western shore of the lake or under the lake itself.

Muscovite

Some muscovite paragenetic relations have been discussed in the last section. However, it is worth elaborating on the changes in texture with increasing metamorphic grade. Low grade muscovites such as those coexisting with chlorite, actinolite or epidote and the minor biotites of the lower grade rocks are similar in habit. These muscovites are fine-grained subhedral flakes, often bent, giving the rock its foliation. The muscovites often show both foliations in a section, being bent by f_2. Glomeroporphyroblasts composed mainly of muscovite also occur at lower grades, and muscovite can be seen to be an alteration product of rounded, presumably detrital, grains of feldspar. The grain size of muscovite increases with grade, but it reaches its maximum size very quickly (between points 3 and 4) and does not change significantly in size thereafter. Glomeroporphyroblasts consisting largely of muscovite occur at all grades as a result of retrograde metamorphism of feldspar and of kyanite on Woodbury Point. Muscovite is almost always intimately associated with biotite at higher grades, although in some rocks it occurs in layers of practically pure muscovite alternating with layers of biotite and feldspar + quartz + muscovite + biotite.

Cipriani et al. (1971) have produced several diagrams indicating the relation between substitutions of Mg-Fe, Mg-Na, Fe-Na, Fe-Si and Na-Si and temperature and pressure of formation. Their work is empirical, comparing a large group of muscovites from different parageneses, and it does not take into account variations in partial pressures of oxygen, CO_2 or water. Nevertheless, systematic trends do appear.

Muscovites from the Kootenay Arc follow some of the trends established by Cipriani et al. (1971), but not others. In general, muscovites from the Kootenay Arc do not fall into the fields defined for the different metamorphic grades delimited on their plots. Especially Fe-Mg, Fe-Na and Fe-Si are aberrant, although for Fe-Si and Fe-Mg, the general trend with increasing temperature is followed.

Muscovites from the Kootenay Arc have been plotted on the diagrams of Cipriani et al. (1971) to establish their relation with compositional fields found in the study of white micas from several other localities. Fig. 37 is a plot of Mg vs Na in structural formula units. It can be considered as roughly coinciding with P (Mg increasing) and T (Na,(paragonite) increasing). The plot indicates the relative range of P and T indicated for Kootenay muscovites, as well as indicating the possibility that two sets of muscovite exist.

Fig. 38 is a plot of silica in structural formula units against the extent of silica content found by Cipriani et al. (1971). The spread for rocks from the Arc is not great and does not seem to be compatible with the grade indicated by Cipriani et al. (1971) on the basis of assemblage and other criteria of grade from rocks of the Kootenay Arc. As both Si and Na content in muscovite are considered to be indicators of temperature, a plot of Si against Na was constructed (Fig. 39). This plot eliminates some of the problems of plotting Mg against Na or Si, since Mg-content is sensitive to pressure. The trend here is perhaps more indicative of temperature change in the Kootenay Arc, especially when compared with micas from the Moine Schists, Maine and Vermont. The trend is systematically towards lower Si and higher Na contents with grade. Kootenay muscovites fall between chlorite zone and kyanite zone assemblages with the exception of 11CBT-15. A further indication of grade dependence has

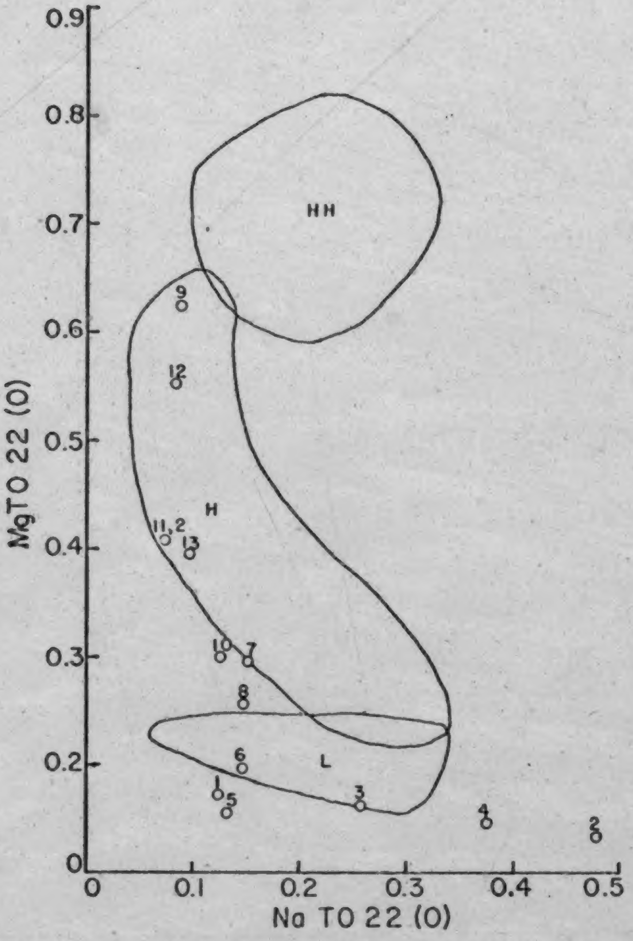

Fig. 37. Mg (structural) plotted against Na (structural) for muscovites from regional metamorphic rocks. Fields are those given in Cipriani et al. (1971). HH - very high pressure (glaucophane schists); H - high pressure; L - low pressure.

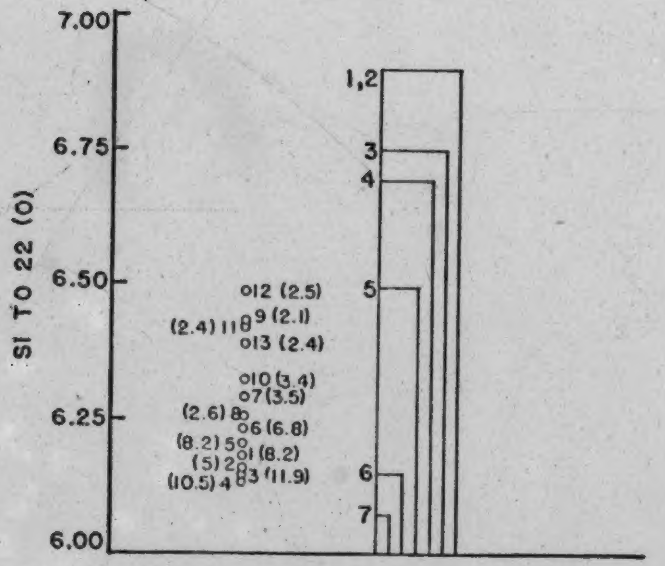

Fig. 38. Si (structural) in muscovites from regional metamorphic rocks plotted against comparison ranges from Cipriani *et al.* (1971). Numbers refer to zones: 1, 2) chlorite-biotite; 3) almandine; 4) staurolite; 5) kyanite; 6) sillimanite; 7) sillimanite-orthoclase

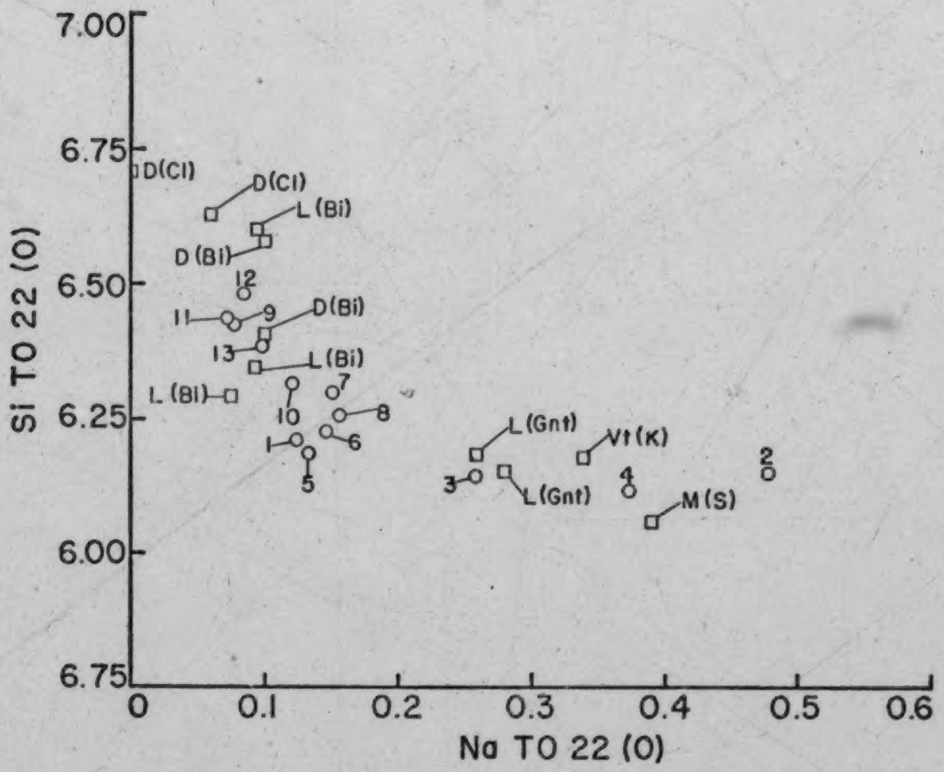

Fig. 39. Si (structural) against Na (structural) for muscovites from regional metamorphic rocks. Samples plotted for comparison are as follows: D (Cl) Dalradian, chlorite zone (Mather, 1970); D(Bi) Dalradian biotite zone (Mather, 1970); L (Bi) Moine Schists (Lambert, 1959); L (Gnt) Moine Schists, garnet zone (Lambert, 1959); Vt (K) Vermont Kyanite zone (Albee, 1965); M(S) Maine sillimanite zone (Guidotti, 1969). Numbers refer to analyses in Table 5.

been given by Butler (1967) for multivariant rocks. Fig. 40 gives a plot of Fe total (as FeO) against Al_2O_3 wt. % in muscovite. Fields of stability are defined by solid lines. The fields defined by Butler (1967) must be looked at with some care, since not all his muscovites coexist with K-feldspar. 5LBT-3 falls outside the plots because of its exceptionally low Fe content. It can be seen immediately that this plot is only useful for rocks from Barrovian-type assemblages, because for micas subjected to higher pressures, Mg content will affect total iron present in the muscovite. Also, K-feldspar must coexist with muscovite in order to be certain that Al_2O_3 values for muscovite are dependent only on T and P. The range of stable compositions for chlorite and biotite zone should be extended. Butler (1967) mentions that the fields delineated are approximate. Examination of Butler's plots shows chlorite assemblage micas plotting into the almandine field, but not the staurolite field.

Examination of the calculated structural formulae given in Table 5 shows a deficiency in the X-site for all muscovites analyzed. This deficiency has been reported elsewhere (Cipriani et al., 1971), but it has been suggested that the deficiency decreases with grade. Variations in octahedral and tetrahedral Al are also said to occur with grade. Systematic changes are not well demonstrated by any of the three variables from muscovites in the study area, although both Al^{IV} and Al^{VI} increase slightly with grade. The lowest X-site occupancies are found in muscovites of the lowest grade, but scatter at higher grades encompasses nearly the entire range. The sum of the octahedral site cations does not vary with grade, indicating that the substitution scheme $2R^{3+} \rightleftharpoons R^{2+} + Si$ works without filling empty octahedral site positions as suggested by

Fig. 40. Plot of FeO (%) against Al_2O_3 (%) for muscovites from regional metamorphic rocks (after Butler, 1967). Comparison samples are the same as for Fig. 39. Fields are those of Butler (1967).

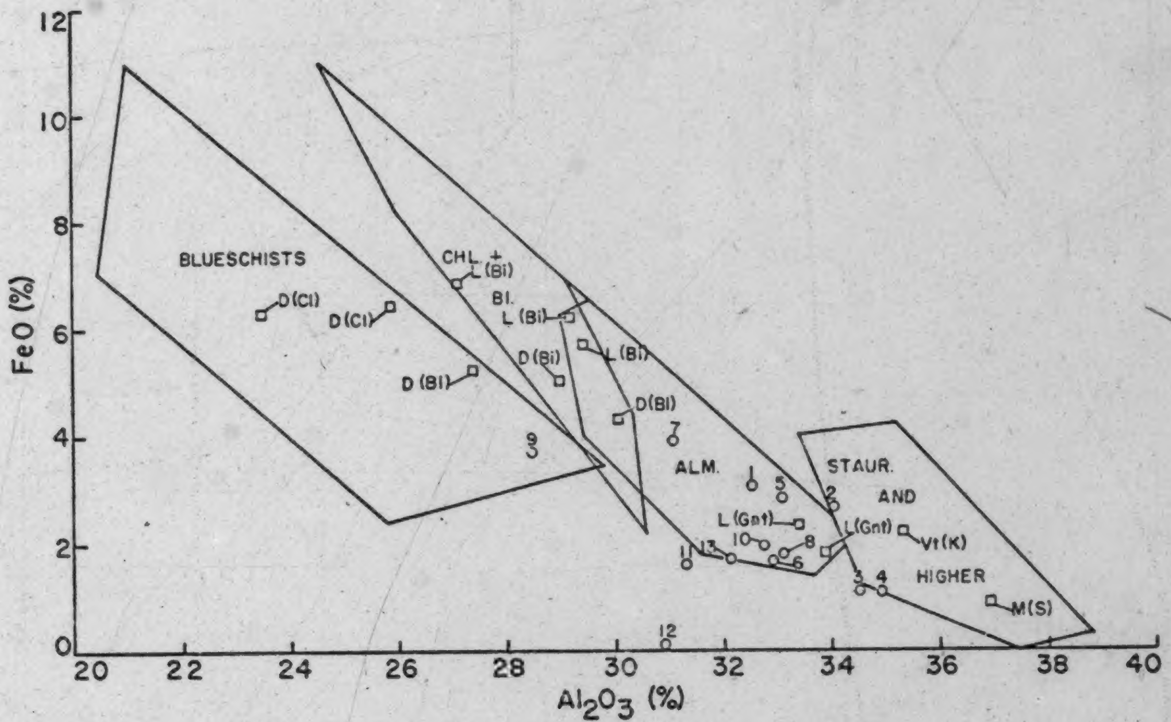

Foster (1956).

Despite the problems mentioned, examination of the figures and comparison of Kootenay muscovite compositions with those of other areas reveals several trends which are of value in reconstructing the regional metamorphic history of the central portion of the Arc. First, examination of Fig. 6 indicates that the muscovites from the Arc fall in a high pressure series intermediate between Sanbagawa and Barrovian (or Otago) varieties. Pressure estimates for the Sanbagawa (Shiratakí) belt are from 4-7 kb, and intersection of part of the Franciscan trend with the lowest grade mica from the central Kootenay Arc indicates that the upper portion of the pressure range for the Sanbagawa rocks would be favored. That the entire series is of higher pressure origin is also suggested by a comparison of Barrovian and Otago micas with the Kootenay low grade micas. The Kootenay muscovites plot closer to the Al-Mg side of the AFM triangle, providing an extension of the Franciscan and Sanbagawa trends to higher temperature.

Second, paragonite content (Na) and silica content of muscovites may be used as estimates of temperature (Fig. 39) when plotted along with muscovites from other localities. The silica-iron plot of Cipriani et al. (1971) is not wholly reliable for these micas, probably due in part to the effect of pressure on the position of the mica with respect to the Fe axis. Figs. 39 and 40 illustrate the range of temperature (grade) and compare the Kootenay rocks with rocks from other metamorphic areas. These plots also illustrate the variability of temperature-dependent and composition-dependent index minerals on the development of mineralogy coexisting with muscovite. For example, the Moine schists contain biotite, but muscovite has Si and Na contents indicative of lower temperatures (#661, Lambert, 1959), whereas muscovites of Mather's chlorite zone plot in the same range as Kootenay muscovites coexisting with chlorite. The trend for muscovites from garnet, kyanite and sillimanite zones indicates that the partitioning of Si and Na with increasing temperature is similar in different areas and does not seem to be greatly influenced by pressure. It has already been demonstrated that rock composition has little influence on these two elements. Fig. 39 illustrates the change of Na content with grade and illustrates the unusual position of muscovite from a rock very close to the contact with the Crawford Bay Stock. Muscovites in this rock show blastesis and are growing across normal foliation, indicating late postkinematic growth. A small amount of fibrolite is present in the section. The Na content of the mica, then, reflects a later thermal event and is not part of the regional pattern. 12WP-2A from Woodbury Point also falls outside the trend shown by the remainder of muscovites from the area. The explanation is somewhat more difficult, since no large stock exists in the area. The rock was collected from a schist between two syenite dikes of considerable extent and contains kyanite-staurolite and garnet. The aluminosilicate may also be a thermal phase (it occurs as a porphyroblast), as suggested in the previous section.

Plots involving Fe and Al are less reliable indicators of grade, although trends are generally adhered to. The best example is that of Al_2O_3 and FeO plotted by Butler (1967) for Ardnamurchan (Fig. 40). Using this plot, most Kootenay rocks fall into the Almandine zone, a conclusion in some cases clearly contravened by assemblage and examination of the other plots. Fe and Mg can be demonstrated to decrease with grade, but the systematics of this decrease are probably controlled by total pressure, mineralogy, and possibly variations in partial pressure of volatiles such as CO_2, O and H_2O.

We can conclude with reasonable certainty that the muscovites indicate a high pressure, moderately high temperature suite of metamorphic rocks. We may also conclude that the highest grade reached was equivalent to the staurolite zone, as suggested by the data shown on Figs. 6, 40 and 41.

Biotite

No transition between chlorite zone and biotite zone rocks may be defined over any large area in the Kootenay region. The two low-grade assemblages present are distinctly different and cannot be related in detail from chlorite zone to biotite zone. Biotites in lower grade pelitic rocks are pleochroic pale yellow to reddish-brown and occur in two habits within the same section. The biotite is intimately intermixed with muscovite, usually forming small grains present in cleavage traces, and it also occurs as porphyroblasts which cut across foliation. In this form the biotite is often poikiloblastic, enclosing quartz, feldspar and muscovite grains. The poikiloblasts are often brown or olive green. Chlorite is present in these rocks but is not necessarily intimately associated with biotite. K-feldspar is usually present in small amounts detectable only by staining.

The second lower grade assemblage involves more basic rocks, with associated minerals chlorite, calcite or dolomite, quartz, epidote, actinolite and magnetite. Biotite is the same color in these rocks, pleochroic yellowish brown to rusty reddish-brown. In the basic rocks, biotite is intimately associated with chlorite and may be found growing in cleavage traces of chlorite. Rutile and sphene may also be present, although rutile, where present, occurs in very small amounts.

Rocks containing calcite and dolomite, feldspar and muscovite are always biotite-free in these low grades. All three assemblages are intermixed spatially. Biotite-free two-carbonate rocks may be found farther east than rocks of pelitic composition containing biotite, and vice-versa. The same observation holds for biotites found in more basic assemblages. For this, and the other reasons mentioned, no biotite isograd can be defined in the map area.

All major and minor elements in biotites from the regional rocks were plotted against the grade index. No systematic relationship could be found between grade and K_2O, Na_2O, MnO, octahedrally and tetrahedrally coordinated aluminum or Mg/Al ratio. The SiO_2 plot shows a slight tendency for higher silica biotites to be present in higher grade rocks, but scatter in the diagrams makes any conclusion tenuous. Aluminum (Al^{IV}) shows almost no change with grade. Fluorine and chlorine show no well defined trends, but fluorine is somewhat more enriched in higher grade rocks than in lower grade rocks, and a definite fluorine anomaly is indicated on the west shore of the lake by high fluorine values for 8AT-18, 8AT-8 and 10BT-13. This pattern is in general agreement with the work of Munoz and Eugster (1969) where fluorination of hydroxylated minerals is found to be favored by an increase in temperature. The anomalously high fluorine values for the samples mentioned may be due to the presence of thermal waters in the general area, but no data exist to test this hypothesis. The high fluorine content may also be related to high "phlogopite" content, as more phlogopitic biotites contain more fluorine (see Fig. 18).

Ti, Mg, Fe and the Mg/Fe ratio in biotites do show dependence on grade. Ti, Mg, Fe and the Mg/Fe ratio for biotites from the region are plotted against the grade index in Fig. 41. Magnesium can be seen to decrease to a low lying between points 8 and 10, with iron showing the opposite trend. The Mg/Fe ratio shows a very linear decrease to the region of point 8, with an increase beyond showing somewhat more scatter. The trends shown here are opposite to those found in some metamorphic rocks (Engel and Engel, 1960; Snelling, 1957). Increase in Fe with increasing grade has been reported by De Vore (1955), Miyashiro (1953, 1958) and Ghose (1968). The plot is anomalous from another standpoint, which will be mentioned here but which will become clearer as systematic variations in other minerals are considered. The inflection point for all four plots occurs between points 8-10, whereas field evidence and that of the muscovites indicates that the culmination of metamorphism should occur between points 12 and 13. If the Mg, Fe, Mg/Fe and Ti trends are solely dependent on metamorphic grade, then the evidence presented in the plot suggests falling grade west of Kootenay Lake. However, dependence of Mg, Fe, Ti and the Mg/Fe ratio on rock composition was shown in the last section. The Mg/Fe ratios for biotite are clustered, except for rocks containing actinolite, diopside and carbonate. The close dependence of the biotite Mg/Fe ratio on rock composition suggests some control of the ratio by rock composition. The TiO_2 plot shows considerable scatter and also some control by rock composition. Examination of Fig. 42, a plot of Fe/Fe + Mg ratios for all rocks from the region shows the same trend as that shown in Fig. 41. There is a strong suggestion, then, that the Fe, Mg and Mg/Fe ratio is controlled by the bulk rock composition, providing the Mg/Fe ratio in the rock is not

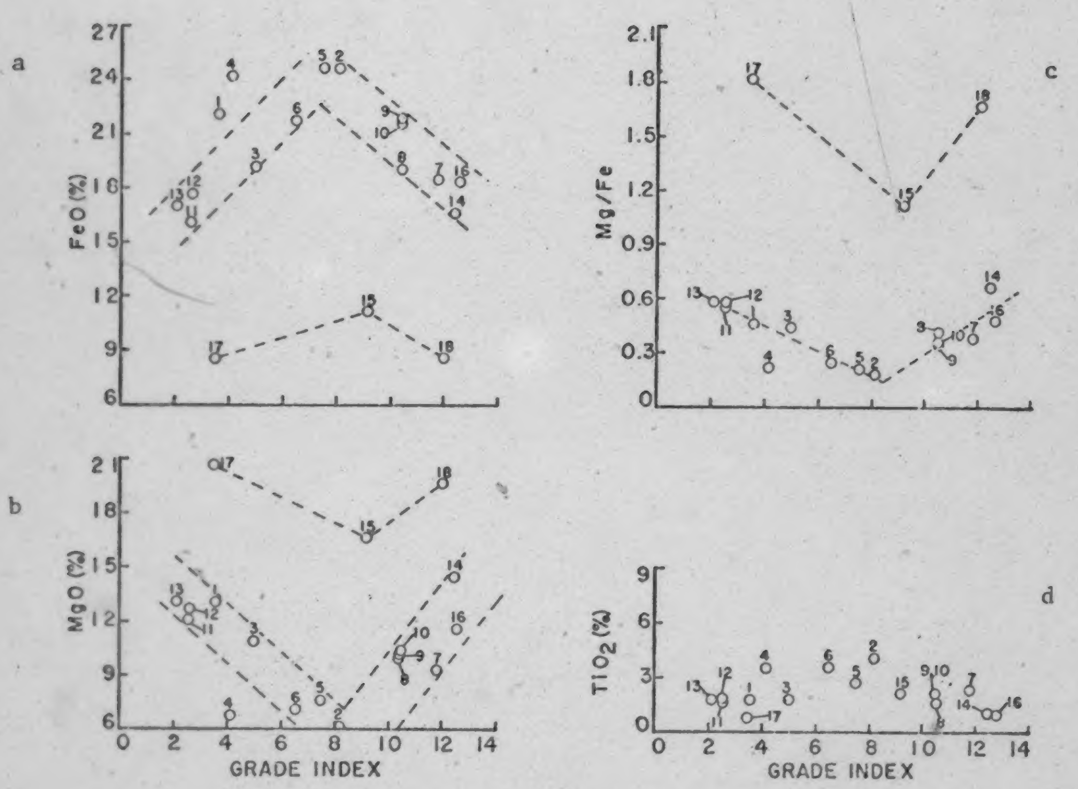

Fig. 41 a. FeO% against grade index, biotites from regional metamorphic rocks.

Fig. 41 b. MgO% against grade index, biotites from regional metamorphic rocks.

Fig. 41 c. Mg/Fe ratio plotted against grade index, biotites from regional metamorphic rocks.

Fig. 41 d. TiO$_2$% against grade index, biotites from regional metamorphic rocks.

Numbers correspond to analyses in Table 6.

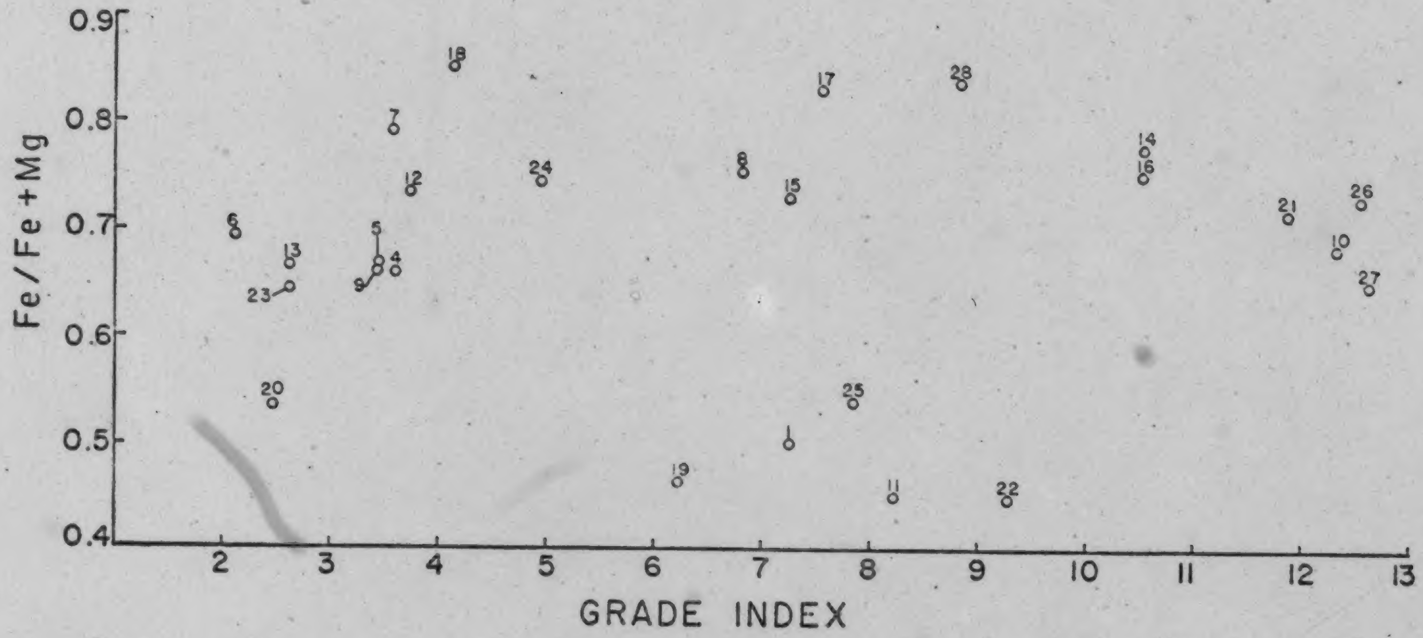

Fig. 42. Fe/Fe + Mg (rock) plotted against grade index, regional metamorphic rocks.

defined entirely by the Mg/Fe ratios and contents of the biotite. If they are, it is obvious that a statement to the effect that rock composition controls biotite composition is circular or based on the assumption that the pre-biotite rock did not change in composition with increase in metamorphism. More will be said about this problem later. Increased Ti may indeed be favored by higher temperature, but no firm statement can be made for biotites from the central Kootenay Arc. Both temperature and compositional effects could be operating.

The disappearance of magnetite from chlorite-muscovite rocks suggests that it may be a source for iron in biotites, as well as a source for titanium, since Ti may be high in magnetite. Systematic changes in modal amounts of minerals cannot be used as indicators of products and reactants because the variations are so great that any trends are masked.

Assemblages in more basic rocks are more difficult to interpret, since the source for K_2O becomes a real problem. Often, there is only a trace of K-feldspar, but considerable biotite is present.

Two carbonate, biotite-free rocks are more easily interpreted, because although all the ingredients are present to form biotite, the magnesium (and possibly some of the iron) would have to come from dolomite. Reactions involving dolomite involve liberation of CO_2. The reasoning is circular, but it may be implied that P_{CO_2} is too high in these rocks to allow the reaction to proceed at temperatures found in the low grade rocks.

Chlorite

The similarities of structure in the mica group and between the micas and chlorite suggest that some relation between intensive variables and composition might be expected for chlorite as well as for muscovite. In the earlier mineralogy section, chlorites were plotted on an AFM diagram (Fig. 22), along with chlorites from other regions. Although the correlations are not nearly as good as those of the white micas, some relationship does exist between composition and metamorphic conditions. The higher pressure, moderate thermal gradient rocks of the Sanbagawa (Shirataki) produce chlorites with higher molecular amounts of magnesium and generally lower amounts of aluminum than rocks from the lower pressure moderate thermal gradient rocks of the Dalradian and Otago. Further, chlorites from zone I of Shirataki are somewhat more magnesian than those of zones II and III, suggesting expulsion of magnesium with rising temperature. Otago chlorites show this trend also, but Dalradian chlorites are variable. That pressure and temperature exert the dominant control is suggested by the fact that bulk compositions of rocks taken from the literature do not vary greatly. However, great caution must be used in interpreting these trends. Perhaps more important is coexisting mineralogy, especially where biotite is concerned. The position of the Kootenay chlorites is within the Sanbagawa trends, suggesting similar pressures, if not temperatures, of formation. Such a position is reinforced by the trend of muscovites shown in the last section.

Some compositional variation with grade is indicated. Inspection of the data (Table 8) shows the following: 1) Tetrahedral Al shows no change with grade, but Al^{VI} and Mg both decrease with increasing grade. 2) Fe increases with increased grade. 3) Total Al decreases with increasing grade, the decrease apparently resulting from decreasing octahedrally coordinated aluminum supplanted by Fe. Thus, chlorite becomes more iron-rich with increasing metamorphic grade, at least in the lower grades.

Amphiboles

Amphiboles do not, in general, show systematic optical variation with grade. Amphiboles are identifiable either as actinolites, tremolites or hornblendes optically, but no significant textural changes are undergone except where zoning is encountered. Low grade assemblages contain either actinolite-chlorite or actinolite-chlorite-epidote, higher grade assemblages, hornblende-biotite or hornblende-clinozoisite. More magnesian assemblages contain diopside and actinolite. Some systematic trends may be discerned in amphiboles, however.

As was illustrated in the last section, amphibole composition with respect to octahedral cations is dependent on rock composition. Various authors (Leake, 1965a, b, 1968; Kostyuk and Sobolev, 1969) have suggested that amphibole compositions may be related to grade. Leake (1965) suggested that Ti should increase with grade, but warned against use of this element unless the rock contained rutile, sphene or ilmenite indicative of Ti saturation. Leake (1965) also indicated that an increase in octahedrally coordinated aluminum would correspond to increasing pressures of metamorphism, and that a maximum amount of Al^{VI} was possible for any given Al^{IV} content. Kostyuk and Sobolev (1969) take a statistical approach to the problem, as did Leake (1965a, b, and 1968). Kostyuk and Sobolev (1969) compare the compositions of amphiboles from different metamorphic facies, claiming on the basis of statistical analyses that amphiboles from different facies may be identified in this manner.

Several amphibole variables were plotted against grade for rocks from the central Kootenay Arc. No systematic variation with grade was found for any variable except Mg in actinolites, which was found to increase with grade, but only on the basis of four data points. No trends at all were discernible within the hornblende series, including Ti which shows no significant trend with increasing grade.

Fig. 43 is an illustration of the variance between Al total (structural) and Fe/Fe + Mg (the f value of Kostyuk and Sobolev, 1969). Comparison of this plot with that of Kostyuk and Sobolev (1969, p. 72) shows that amphiboles from the same grade in the amphibolite facies (unnumbered dots) plot within the fields defined for greenschists and winchites, and for amphibolite facies rocks of different composition as well as hornblendes from granites. Recalling Fig. 25, discussed in the mineralogy section and comparing with Fig. 3 of Kostyuk and Sobolev (1969, p. 74), it may be seen that the octahedral and tetrahedral aluminum values encompass rocks of greenschists, winchites, glaucophane schists, granulites, kyanite-bearing rocks and amphibolite facies rocks.

The absence of systematic changes with grade, and the groupings of amphiboles on plots of the type given by Kostyuk and Sobolev (1969) illustrate several points, both about the metamorphism in the Central Kootenay Arc and about the use of amphiboles as indicators of metamorphic grade. First, the lack of compositional variation could be due to several factors. The first is that there is no great temperature gradient across the area studied. That there is a gradient has been illustrated by the muscovites, but the indication from the study of the micas is that the regional gradient was not great. Temperature measurements have been made using the

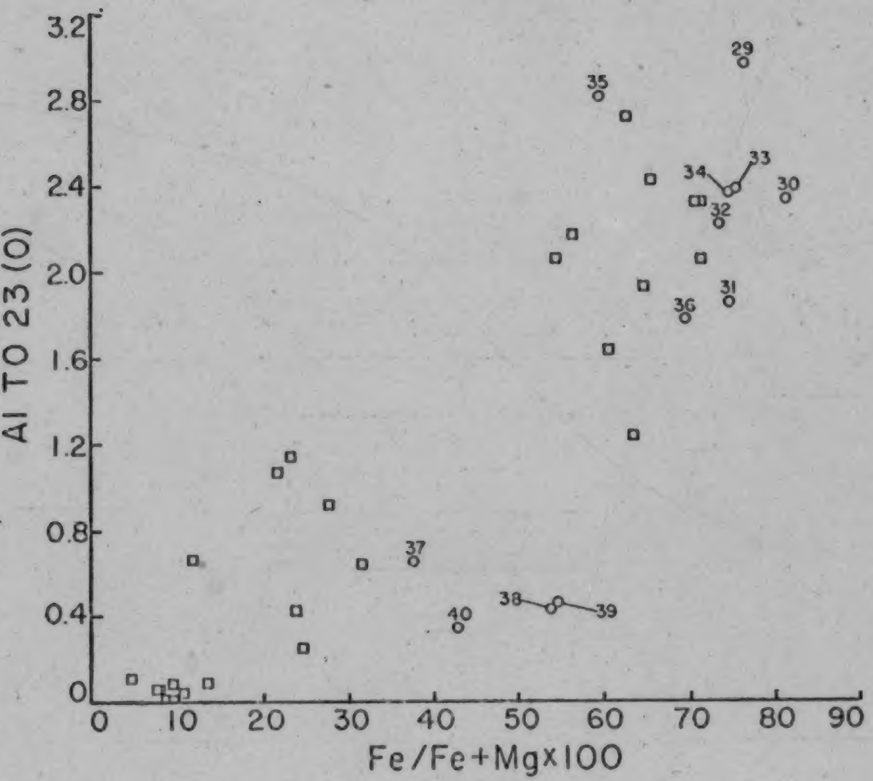

Fig. 43. Al total (structural) plotted against Fe/Fe + Mg for amphiboles from regional metamorphic rocks. The Fe/Fe + Mg ratio is the f value of Kostyuk and Sobolev (1969). Unnumbered points are amphiboles from Kootenay Point.

calcite-dolomite geothermometer, and they indicate a difference of about 130°C between points 2 and 10. These temperature measurements will be discussed in more detail later.

The second reason for lack of definable variation is that variations in rock composition mask temperature-induced variations. The scatter in compositional trends from regional rocks may be explained by temperature effects, but the two cannot be separated.

The third, and perhaps most interesting reason lies in the crystal-chemistry of the calcic amphibole group. Miscibility gaps within the group have been proposed by several authors (Klein, 1969; Cooper and Lovering, 1970; Cooper, 1972, Winzer, 1973, see Appendix 4). For amphiboles in the Kootenay Arc, the gap lies somewhere in the region of Al^{IV} 0.7-0.8, as illustrated by zoning in amphiboles from the Point, and as illustrated by pairs from the region (Fig. 25). Kostyuk and Sobolev (1969) did not take into account the effect of a miscibility gap on the distribution of amphibole compositions in plots like those of Fig. 25 and 43. Four variables are involved in determining the position of an amphibole on a plot such as in Fig. 43: T, P, composition and the width of the solvus for hornblende-actinolite or pargasitic hornblende-aluminous actinolite. Composition and thermal history will determine the position of an amphibole on these plots. This explains the groupings of dots on Fig. 43, and the reason that so many paragenetic groups are included. A fifth variable that cannot be discounted is whether the amphibole has attained equilibrium at the pressures and temperatures to which it was subjected. This important factor will be discussed more fully later on.

The two plots do indicate something about the metamorphism in the

Kootenay Arc, despite the foregoing restrictions. Fig. 25 is an indicator of pressure during metamorphism. It indicates that amphiboles formed under conditions of fairly high pressure but does not indicate alone, or in conjunction with Fig. 43, what the thermal conditions were at the time.

Another interesting factor can be determined from examination of Figs. 23 and 25. Because the rim "actinolites" or actinolitic hornblendes are a small portion of the volume of the whole rock and because they seem to interact only with the minerals nearest them (Winzer, 1973, Appendix 4), we may state that they are examples of amphiboles formed in a rock of known composition (the composition of the core hornblende and remaining minerals in the rock). We know, then, the original rock composition and the parent amphibole composition. The tielines joining rim and core are rotated towards the maximum line of Leake (1965), and the compositions of the rim actinolites lie in the zone of calcic amphiboles from glaucophanitic schists, thus indicating the possibility that the rim amphiboles formed under conditions of higher pressure than the core hornblendes.

Pyroxene

Pyroxene, like biotite, shows an odd inflection around point 9. Fe/Fe+Mg ratios plotted for pyroxenes from the regional rocks (Fig. 44) show a trend opposite that of the whole rock trend and opposite that of biotite. This trend suggests that the pyroxene becomes increasingly magnesian with increasing grade, and where it coexists with biotite competes with that mineral for the available magnesium in the rock. This trend is the same as that for actinolite, suggesting that Fe must be expelled, presumably to go into biotite where present. Al/Mg + Fe ratios show the

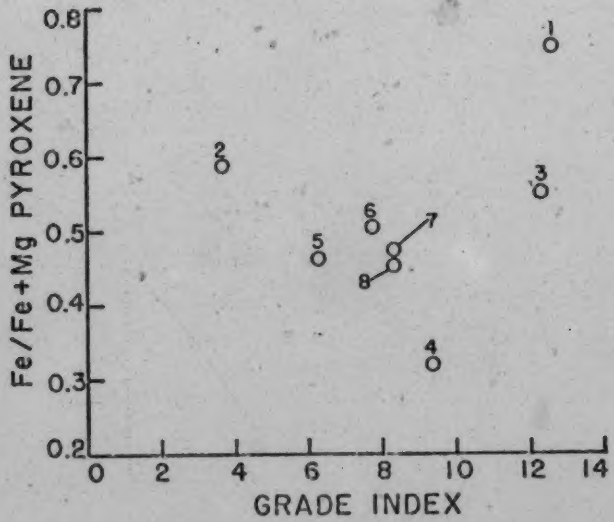

Fig. 44. Fe/Fe + Mg pyroxene plotted against Grade Index for pyroxenes from regional metamorphic rocks. Ratio decreases to point 9, then increases sharply.

same trend as Fe/Fe + Mg, but with even more scatter. Relations involving Al are probably similar to those in amphiboles, being related to feldspar where present.

Pyroxene compositions show the general effect of pressure, as well as being strongly dependent on rock composition with respect to Mg and Fe. The presence of octahedrally coordinated aluminum is indicative of formation under high pressure (Yoder, 1950a,b; Coleman and Clark, 1968; Dobretsev, 1968; Makanjuola and Howie, 1972). The diopsides and salites studied are higher in Al_2O_3 than those of the Biwabik (Bonnichsen, 1968) or of the Glen Urquhart area (Francis, 1958, 1964) although they are nearer to the Glen Urquhart area in composition. They are similar to pyroxenes from the Grenville province of Ontario (Shaw et al., 1963a, b). Systematic analyses of metamorphic clinopyroxenes are notably absent from the literature, hence they do not as yet serve as indicators of grade. Temperature and pressure does affect the composition of pyroxene (Dobretsev, 1968). Thus it is worth looking at metamorphic pyroxenes as possible indicators of metamorphic grade.

Epidote

Systematic chemical analyses for epidote group minerals were not undertaken, due to scarcity of proper rocks. Rocks donated by Cominco later in the course of this work contained iron epidote and actinolite, but clinozoisite is the common mineral in the rocks studied. Lower grade rocks lying along the eastern margin of the map area contain epidotes, which, by their birefringence, color and pleochroism are iron epidotes. Assemblages, with grade index, are as follows:

Grade Index	Assemblage
.7	Ep + act + cc + sphene + apatite
1.1	Chl + ep + qtz + carb + bi + mt
3.1	Musc + plag + ep + An 15 + qtz + mt + hem
3.2	Act + ep + bi + mic + plag + Ab-olig + qtz + mt + hem
3.4	Hb + act + ep + cc + plag (An_{57}) + qtz + sphene
4.3	Hb + act + ep + mic + plag (An_{58}) + qtz + carb + bi + sphene

Rocks from the Point and the higher grade areas of the region bear colorless, non-pleochroic epidotes with low pistacite contents, closely resembling clinozoisites chemically. These epidote group minerals coexist with hornblende, diopside and actinolite and are found in scapolite-bearing rocks. They are more complex than the lower-grade epidotes in that they often appear zoned, and show compositional variance within the same slide. The zoned epidotes have epidote cores and clinozoisite rims, with sharp demarcation between the two. In the higher grade rocks, epidote group minerals are present in small amounts (generally), but may reach 10%. Examination of the assemblage data given above and the analyses for "epidotes" from the Point and higher-grade regional rocks indicates systematic changes with grade. Two chemical groupings exist to complicate the matter, calc-pelites and metabasic rocks, both bearing epidote. The metabasic rocks show the most distinct trend, with the lowest grade assemblage consisting of ep-act without hornblende, or ep-act-albite-oligoclase and biotite, while the higher grade rocks contain hornblende and plagioclase of higher An content. Also of interest is the absence of magnetite and hematite as grade increases. Rocks from the Point contain graphite and are devoid of magnetite or hematite, all iron minerals being present as sulfides. The graphite and low pistacite content of epidotes from the Point indicates low f_{O_2}, and the magnetite and hematite in the iron-epidote rocks indicates higher f_{O_2} (Strens, 1964; Holdaway, 1965, 1966, 1972; Boettcher, 1970; Cooper, 1972). Thus, we may establish that conditions become more reducing from lower grade rocks to higher grade rocks within the region. Further discussion of volatile partial pressures will be made somewhat further on.

Plagioclase

The complexities of the plagioclase series render simple interpretations of metamorphic changes with grade of dubious validity. However, work by Evans (1964), Crawford (1966, 1972) and Cooper (1972), among others, have turned up consistent distributions of feldspar compositions with grade. The existence of the peristerite gap and its closure with increasing metamorphic grade in contact and regional metamorphic rocks have been demonstrated by the aforementioned authors.

Fig. 45 is a plot of the composition of all plagioclases analyzed by electron microprobe from rocks in the Kootenay Arc against the grade index. It must be emphasized that these are not coexisting plagioclases, but come from different rock samples. Samples 1-11 all come from the Point, from similar rock types. As was discussed earlier, rock composition does not seem to exert a primary control on plagioclase composition. Thus, it is likely that either temperature and pressure and/or coexisting mineralogy exert the primary controls.

Plotted on Fig. 45 are the positions of the Peristerite, Bøggild and Hüttenlocher gaps after the data of Smith (1972). It is immediately obvious that plagioclases of all grades plot along the margins of the

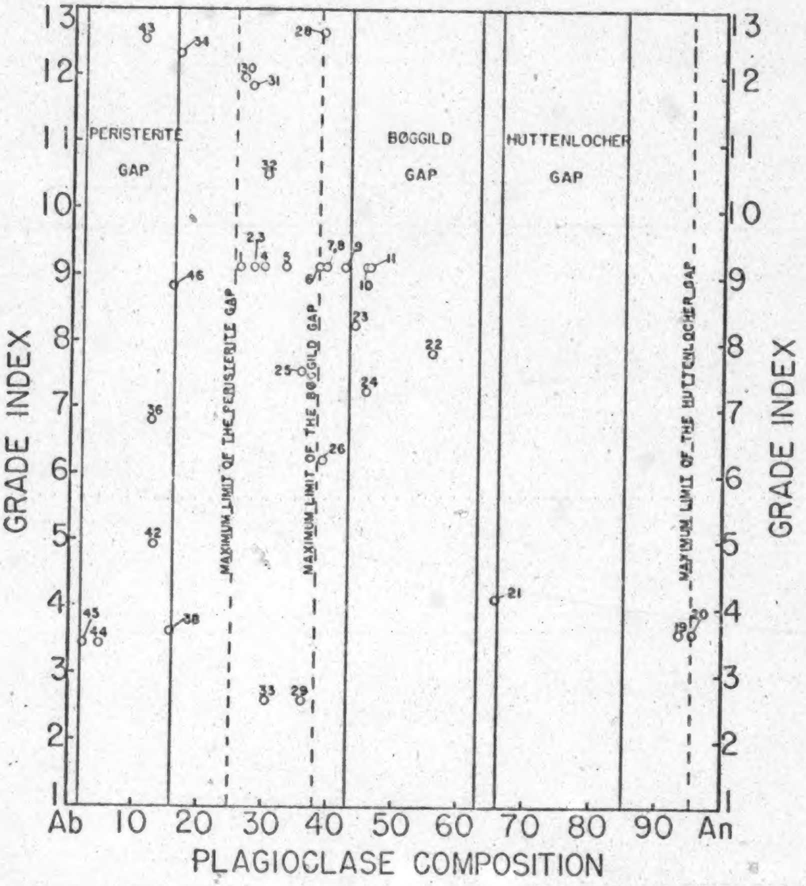

Fig. 45. Plot of plagioclase composition (An content) against grade index for all plagioclases from regional metamorphic rocks and rocks from the Point. Numbers correspond to analyses in Tables 14 and 15. Position of the Peristerite, Bøggild and Huttenlocher gaps after Smith (1972).

peristerite gap and that at higher grades (notably from the Point), feldspars plot within the region of the Bøggild gap. Because the beam is moved around the feldspar grain during analysis, an unmixed plagioclase may go undetected and plot within one of the gaps. The bulk of the plagioclases analyzed fall between the solvi, although five fall within the Bøggild solvus, indicating that they were either formed at temperatures above it or represent a disequilibrium state. The data are not consistent, at higher grades, with those of the zone between the almandine and staurolite isograds (Crawford, 1966; Smith, 1972).

Reconnaissance optical studies reveal many rocks at all grades which contain more than one plagioclase, but firm conclusions may not be reached without further study of plagioclase compositions by electron microprobe. This work is suggested to further quantify temperatures of formation of Kootenay metamorphism.

The lack of truly consistent results is due to lack of complete systematic data on feldspars from the Kootenay Arc. Further complicating factors are retrograde reactions involving feldspar such as those forming zoned amphiboles. The feldspar problem is also tied to the epidote problem, since reactions involving epidote and actinolite or chlorite forming hornblende produce anorthite. Before discussing this problem in more detail, it is perhaps valuable to discuss the carbonates, for they provide temperature data and data pertaining to the fugacity of CO_2 in rocks from the Arc, important factors in the production of oligoclase and feldspar of higher An content during metamorphic reactions.

Carbonates

Calcite, when coexisting with dolomite in the presence of sufficiently high P_{CO_2} to stabilize both carbonates, may be used as a thermometer (Goldsmith and Graf, 1960; Goldsmith and Heard, 1961; Rosenberg, 1967, 1968; Goldsmith and Newton, 1969). Certain stipulations must be met, and some extrapolations made (Hörmann and Morteani, 1972). First, $MnCO_3$ must be present in negligible amounts. For the use of Goldsmith and Newton's (1969) curve, $FeCO_3$ should be absent or present in small amounts. The effects of MnCO3 on subsolidus relations in the carbonates have not been worked out. $FeCO_3$ serves to decrease temperatures (i.e., more $FeCO_3$ is present in solution at lower temperatures than $MgCO_3$) when present with $MgCO_3$. In order to use the unique polybaric curve of Goldsmith and Newton (1969), P_{CO_2} must be demonstrably high enough to have stabilized both carbonates.

Several coexisting carbonates from the Kootenay region were analyzed by electron microprobe. Coexisting calcite and dolomite were analyzed from the Point, but only calcite from regional rocks was analyzed, although later staining of sections demonstrated the presence of dolomite. As was mentioned in the mineralogy section, the carbonates appear to be in textural equilibrium. In five sections, two carbonates were found to coexist with either quartz or tremolite. It is difficult to determine the stability of tremolite, as all sections containing tremolite show signs of textural disequilibrium. Quartz appears stable in the presence of both carbonates in lower and higher grade rocks. The presence of either silicate with calcite and dolomite is indicative of high P_{CO_2}, probably $P_{CO_2} = 0.9\text{-}1.0$ ($P_{CO_2} = P_{tot.}$)(Skippen, 1971), thus satisfying one of the requirements for use of the curves. $MnCO_3$ is negligible in all carbonates analyzed for that element, and there is no reason to suspect that carbonates from the Point should contain greater amounts. In comparison with $MgCO_3$, $FeCO_3$ is present in small amounts, with the exception of 5LBT-17. Thus, most criteria are filled allowing the use of the magnesian calcite-dolomite geothermometer. The five sections selected are: 5LBT-3, 5LBT-17, 55-20W, 215-70W and T1-6c. 5LBT-3 and 5LBT-17 are from low grade chlorite-muscovite-biotite schists; the remaining three carbonates come from the Point.

Two temperatures were obtained for 5LBT-3, with a spread of 35°C. This spread is probably due to variations in chemistry due to inhomogeneities smaller than a thin section, or they could be due to disequilibrium. To arrive at a temperature for 5LBT-17, the same extrapolation as that of Hörmann and Mortiani (1972) was used. The interpretations of the remaining three are straightforward, as neither contains much iron. The temperatures derived are:

Low-grade		Kootenay Point	
5LBT-3A	428°C	55-20W	533°C
5LBT-3B	393°C	T1-6c	488°C
5LBT-17	423°C	215-70W	500°C

The unique polybaric curve of Goldsmith and Newton (1969) is shown in Fig. 46. One further caution must be exercised. As all carbonate analyses are low from the structural standpoint, it is possible that errors are present in the $MgCO_3$ and $FeCO_3$ components. These errors should be small, since the large comparison errors will be in Ca. Temperatures should be taken as ±30°C, about twice the error given by Goldsmith and Newton (1969).

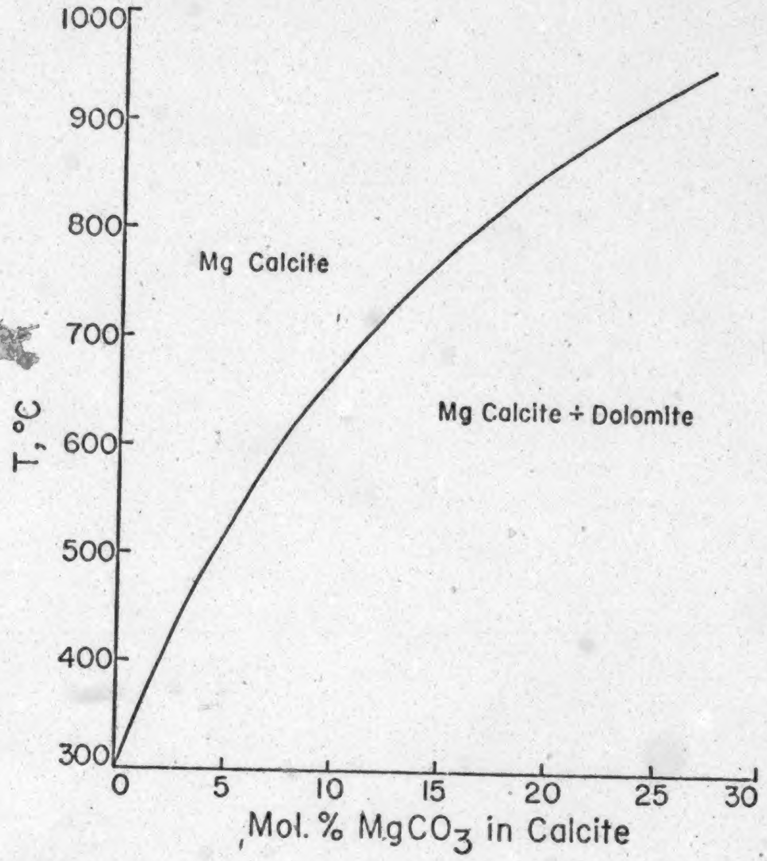

Fig. 46. Unique polybaric curve for magnesian calcite coexisting with dolomite, after Goldsmith and Newton (1969).

Garnet

Partitioning of magnesium and iron between garnet and biotite has been discussed by Livingstone (1968). Livingstone's distribution coefficients can only be used to indicate relative change with grade, since the methods used to obtain Mg/Mg + Fe ratios for garnet and biotite produce large uncertainties. Correlation between garnet composition and metamorphic zones delimited by Crosby (1968) for the central Kootenay Arc were discussed by Dodds (1965). Dodds found that correlation was poor, but he did not have enough evidence to revise existing isograds.

No extensive work was undertaken on garnets from the central portion of the Kootenay Arc, since the study of Dodds (1965) established with certainty the compositional ranges of garnets from three of the rock types present. Electron microprobe traces were undertaken to establish zoning trends and have been discussed earlier. The metamorphic implications of the zoning trends are now discussed.

The sharp rise in MnO at the margins of garnets can be interpreted in three ways. Edmunds and Atherton (1971) believe that increase in MnO is caused by falling growth rate as supersaturation is relieved. Falling growth rate changes the effective distribution coefficient. Kurat and Scharbert (1972), in a study of zoned garnets from Moldanubicum granulites, arrived at the conclusion that the increase in MnO was due to garnet growth during a period of falling temperature. Grant and Weiblen (1971) arrive at a model involving resorbtion of initially homogenized garnet coupled with decreasing outer shell radius and decreasing temperature to explain increase of MnO at the margin. The latter two studies were made on garnets from granulite facies rocks or second sillimanite zone rocks.

The paragenesis of the Kootenay garnets allows discrimination between the hypothesis of Edmunds and Atherton (1971) and the hypotheses of Kurat and Scharbert (1972) and Grant and Weiblen (1971). Rocks from the central Kootenay Arc containing garnet show evidence of retrogression. Garnets from amphibolites coexist with hornblendes which are zoned (see also Dodds, 1965). Actinolite rims are formed on hornblendes from rocks containing zoned garnet, wherein the rim is enriched in MnO (6CCT-8). Selvages of plagioclase, biotite, quartz and occasionally actinolite are reported by Dodds (1965) to surround garnets in some amphibolites. These selvages are clearly retrograde, as no orthopyroxene is formed in the rocks (Dodds, 1965). Garnets from schists also show an enrichment in MnO at the rim. Retrograde effects may be established in schists as well. 12WP-2 contains corroded kyanite porphyroblasts surrounded by muscovite and containing small euhedral staurolite crystals. Larger corroded staurolite crystals occur in adjacent sections. It is probable, then, that garnets grew under conditions of decreasing temperature during formation of the rim, but the data available do not indicate whether or not they formed according to the model of Grant and Weiblen (1971). Garnets with selvage rims suggest resorbtion of garnet, but no zoned garnets with selvage rims were studied by this author.

K_{Mn} for garnet cores and rock were calculated for zoned garnets, as were $K_D^{Mg/Fe}$ for biotite-garnet pairs. The results are inconclusive. K_{Mn} for all but 12WP-2 are about 8; 12WP-2 calculates to 52.5. $K_D^{Mg/Fe}$bi-gnt gives values of .23-.34 for 7RT-17, 11CBT-16 and .17 for 12WP-2. Both distribution coefficients fit a staurolite zone interpretation for 12WP-2, but the others are found in granulite facies rocks or plutonic rocks. These values cannot be easily compared, however, because higher CaO garnets do not show the same trends as lower CaO garnets with increasing metamorphic grade (Lyons and Morse, 1970).

Phase Relations and Metamorphic Reactions

The preceding discussion brings to light a number of important factors relating to a definition of the conditions of metamorphism in the central Kootenay Arc. Briefly noted, they are:

1) In the study area, no sharply defined transition exists between chlorite and biotite zone for any rock type.

2) In chlorite, Mg and Al^{VI} decrease and Fe increases with grade.

3) The change in metamorphic grade indicated by changes in muscovite composition is small.

4) The change between biotite zone rocks and rocks containing garnet or hornblende occurs in the eastern quarter of the map area.

5) Compositional changes in minerals such as garnet, hornblende, biotite and pyroxene are not systematic in rocks above the garnet or hornblende "isograds".

6) Iron epidote is found in lower grade rocks, aluminous epidote or clinozoisite at higher grades.

7) The peristerite gap is not completely filled anywhere in the area, but the Bøggild gap appears closed at the eastern shore of the lake.

8) Temperatures obtained indicate a difference of 100-150°C

9) Garnet compositions are consistent for biotite and garnet zones, but not for higher grades of metamorphism.

10) A regional retrogressive event is suggested by garnet and amphibole zonation and by retrogression of kyanite on Woodbury Point.

Fig. 47 and 48 illustrate phase relations in calcareous and non-calcareous pelites from the region. The diagrams do not illustrate the exact relationship between rock composition and mineralogy, because the ACF and AKF faces of the ACKF tetrahedron are projected onto the flat plane of the paper. Rock compositions are calculated for either ACF or AKF and are plotted in whichever triangle they fall. The projection is used to illustrate coexistence of K-feldspar, calcite-dolomite and plagioclase with the other phases present. Two rocks plot outside the defined fields (10BT-4, 6CCT-1), probably due to the projection, but possibly because of error in the rock analysis.

The phase relations in calcareous pelites from the central Kootenay Arc illustrate changes in coexisting phases with increasing grade. At lower grades, chlorite-phengitic muscovite-calcite-K-feldspar and plagioclase coexist with or without biotite. The presence of both assemblages suggests that: 1) the area containing muscovite-chlorite and muscovite-biotite-chlorite assemblages is at or below the conditions of the biotite isograd; 2) the reaction forming biotite involves chlorite and phengite combining to form biotite, less phengitic muscovite, and more iron-rich chlorite by the following reaction:

1) 2Phengite + high Mg/Fe chlorite + 5 quartz → biotite + lower Mg/Fe chlorite + less phengitic muscovite + XH_2O

Such a reaction would be consistent with trends of chlorite and muscovite compositions across the region prior to the appearance of garnet. The reaction cannot be quantified further due to lack of data.

The entrance of garnet in the Kootenay rocks marks the exit of sta-

Fig. 47. Phase relations for calcareous and non-calcareous pelites from chlorite (?) through garnet zones. Heavy arrows mark change of composition with grade.

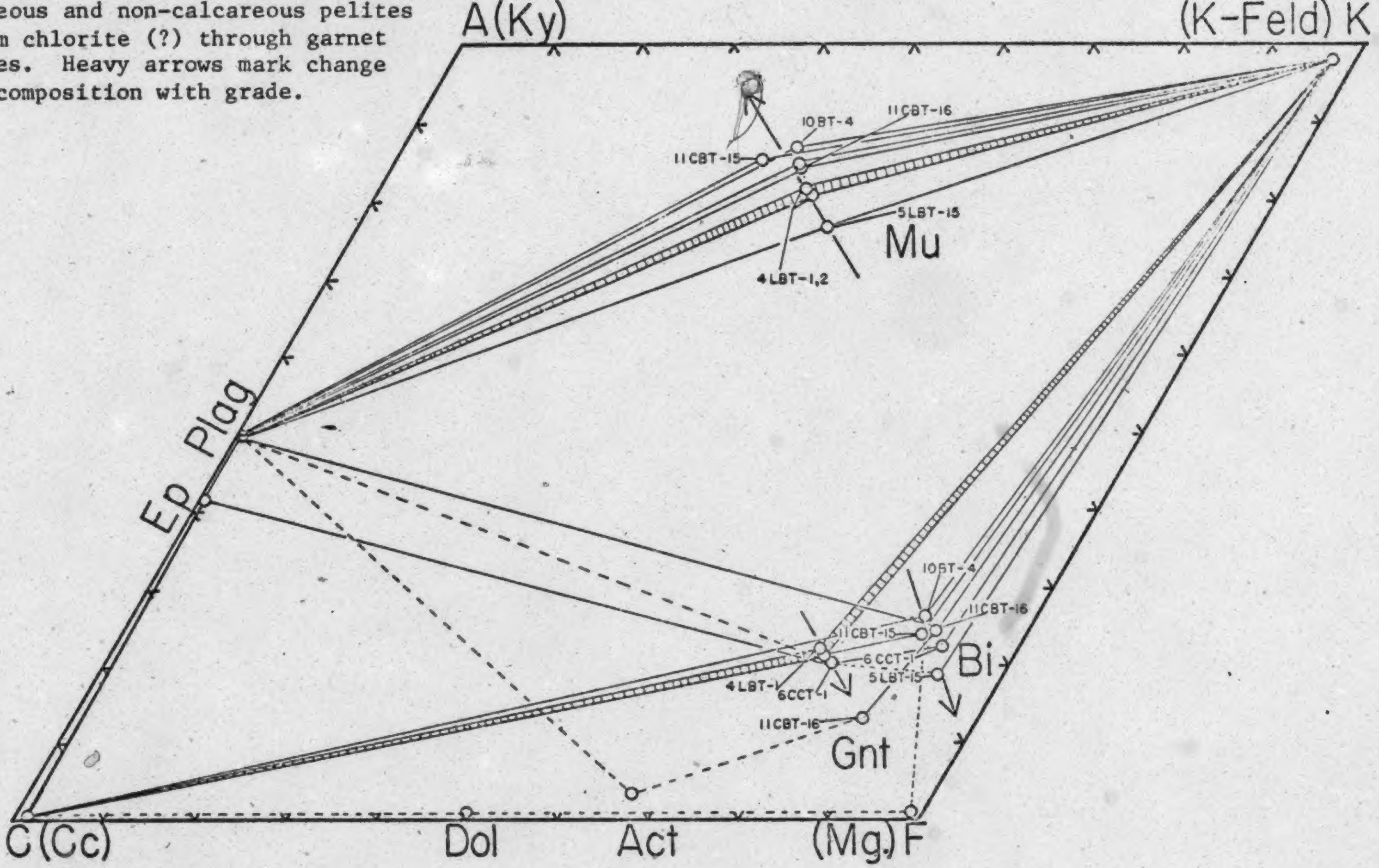
A(Ky)
(K-Feld) K
Plag
Ep
C(Cc)
Dol
Act
(Mg.) F
Mu
Bi
Gnt
10BT-4
11CBT-16
11CBT-15
5LBT-15
4LBT-1,2
10BT-4
11CBT-16
11CBT-15
6CCT-1
5LBT-15
4LBT-1
6CCT-1
11CBT-16

Fig. 48. Phase relations for rocks containing kyanite and staurolite from Woodbury Point. Dashed lines indicate uncertainty regarding stability of phases present.

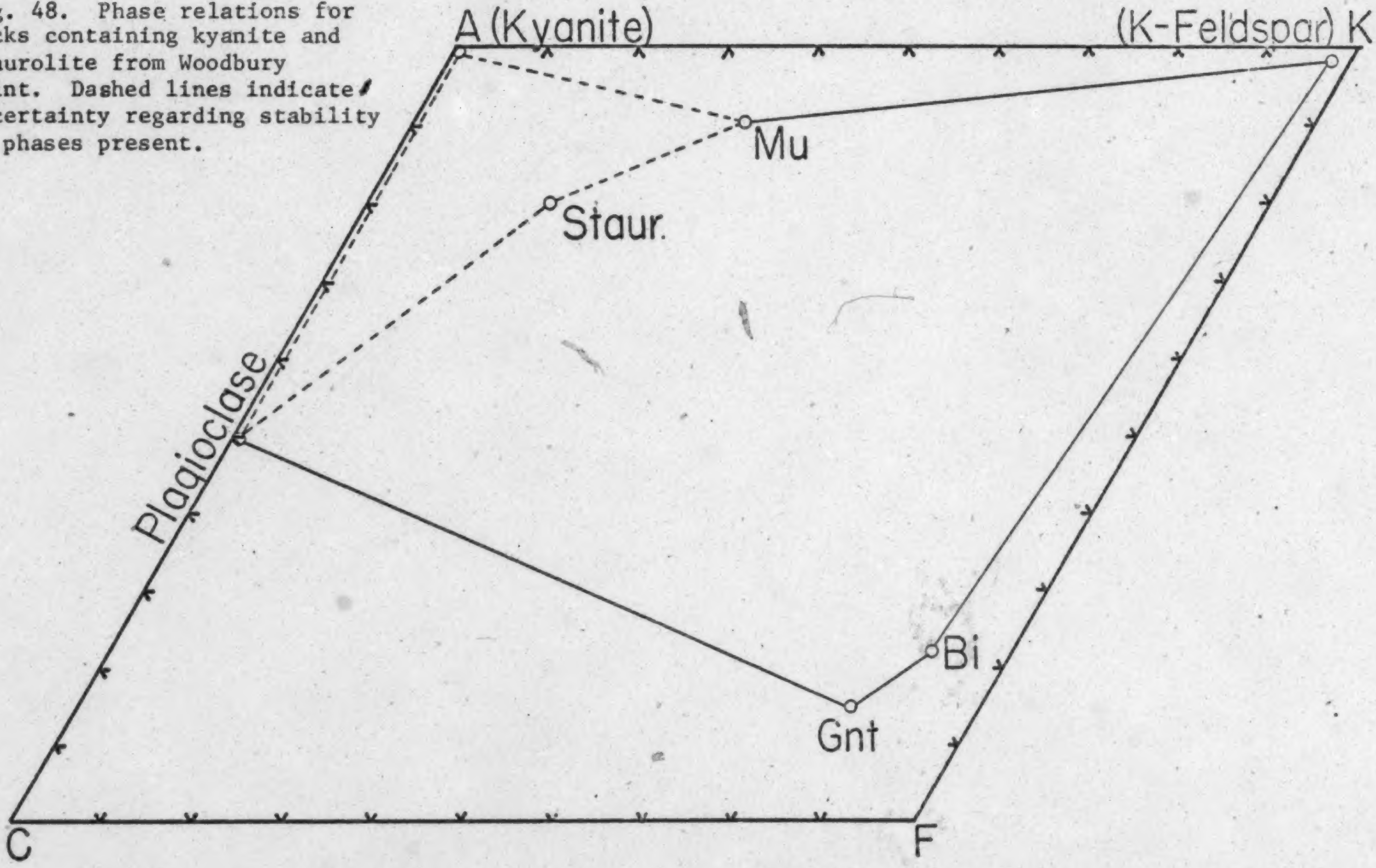
A (Kyanite)
(K-Feldspar) K
Mu
Staur.
Plagioclase
Bi
Gnt
C
F

ble prograde chlorite from the assemblages given in Fig. 47. In calcareous pelites, the incoming of garnet correlates with absence of carbonate, thus breaking both the chlorite-biotite and the calcite-chlorite tielines. One exception occurs (29-14), but the garnet in this rock is clearly unstable and is breaking down to biotite, chlorite, quartz and feldspar. This rock lies within the biotite-chlorite-muscovite field.

The assemblages are:

1) Chlorite-muscovite-calcite-quartz-K-feldspar-plagioclase-magnetite (ilmenite) ± biotite

2) Biotite-quartz-K-feldspar-muscovite-garnet-plagioclase-magnetite (ilmenite)

The garnets in assemblage 2 are intimately associated with ilmenite, magnetite, quartz, biotite and a very small amount of muscovite. A few grains of yellowish chlorite are found associated with biotite where garnet is not present, and considerably more muscovite is found mixed with biotite in areas where garnet is absent. These relations suggest that chlorite and muscovite are reactants and biotite a product of the garnet-forming reaction. A few grains of plagioclase are also associated with garnet. Textural relations must be used with some care, because retrogression has occurred in many rocks containing garnet.

Using compositions of minerals from garnet-free rocks of lower grade and garnet-bearing rocks of higher grade, a reaction of the following form can be written:

2) Phengitic muscovite + 1.33 chlorite + calcite + 2.65 quartz + 2 ilmenite or magnetite $\rightarrow$ Biotite + garnet + .161 calcic plagioclase + CO_2 and XH_2O

This reaction was balanced for major elements using analyses of muscovite from 5LBT-15, chlorite from 5LBT-17 (both close to the transition to garnet-bearing rocks), garnet from 11CBT-16, biotite from

11CBT-16, and calcite from 5LBT-17. The reactions were written using anhydrous formulae. XH_2O is used among the reactants since the amount of water produced is uncertain. The difficulty with the reaction is the necessity for Fe, Ti, and Mn. No analyses have been made of oxide phases, but analyses from Deer, et al. (1966) for ilmenite may be used to balance the equation. Magnetite will supply enough Fe and Ti, but leaves a shortage of Mn. Jones (1972) proposed a reaction involving ferroan dolomite as a source of Mn. Carbonates from this region do not contain enough Mn to form garnet with the amount of Mn present. Ilmenite is present in low grade rocks and occasionally in higher grade rocks, but the highest proportion of iron bearing minerals are sulfides. Further work on all opaque phases is necessary to further quantify reactions of this type.

The reaction proposed is a simple form of what is probably a more complex case. First, muscovite is present in rocks from both sides of the reaction isograd, as is plagioclase. Muscovite becomes less phengitic above the isograd, while plagioclase increases in anorthite content. The second observation is consistent with the reaction. The first may also be consistent as long as muscovite is not present in significant amounts adjacent to growing garnet. Reactions 1 and 2 may well be coupled, one occurring in one small volume of rock, the other in an adjacent volume. This suggestion would be in line with optical observations, but further work across the isograd would be needed to confirm it. Further quantification of this reaction will be difficult in the central Kootenay Arc because of lack of control on outcrop.

The reaction produces a very iron-rich biotite, consistent with increasing iron content of biotites in the region with increasing metamorphic grade. This reaction alone cannot explain the trend, however, as it is by far more common to have biotite without garnet, even at higher grades. The increase in iron content of biotites at higher grades may be tied to consumption of iron oxides, as they are decidedly less prevalent at higher grades.

Reaction 1 takes place at around 400°C as indicated by the calcite-dolomite geothermometer. Reaction 2 occurs between 400 and 500°C, but a more precise calibration is not possible. Temperatures nearer 430°C are more likely on field evidence (11CBT-16 and other rocks containing similar assemblages lie within 2 or 3 km of 5LBT-17. The temperature derived for 5LBT-17 was 423°C.)

These temperatures compare favorably with those of Mueller and Schneider (1971) for garnets formed in the Stavanger area of Norway. In their rocks, temperatures range from 400°-590°C between zones I and III. The paragenesis of garnet from zone II more closely approximates the paragenesis of garnet from the central Kootenay Arc. Temperatures suggested by Mueller and Schneider (1971) for zone II garnets lie between 475°-525°C at P=3-5 kb. However, they do not mention reactions involving carbonate. Reaction temperatures proposed by Jones (1972) for production of almandine from the Horsethief Creek Group in the Esplanade range of British Columbia are 365°C at P=3.9 kb. The reaction proposed for the production of garnet in the central Kootenay takes place at higher total pressure than either of the above reactions, but temperatures appear to be somewhat lower than for the Stavanger areas.

The last assemblage indicated for pelitic or calc-pelitic rocks is illustrated in Fig. 48. This assemblage is difficult to evaluate, because it is uncertain whether staurolite is actually stable. The presence of euhedral staurolite crystals associated with retrograded kyanite suggests that staurolite is stable. The assemblage is:

Biotite + muscovite + quartz + garnet + staurolite + plagioclase. The reaction producing this assemblage cannot be pieced together from existing data, since only one sample containing staurolite has been found in the study area. Two reactions producing staurolite are considered (den Tex, 1971):

a) 8 chloritoid + 7.5 $Al_2SiO_5 \rightleftharpoons$ 15 staurolite + .5 quartz + H_2O

b) chlorite + muscovite $\rightleftharpoons$ staurolite + biotite + quartz + H_2O

Both occur between 515-600°C, between 2 and 20 kb P = Ptotal. The first reaction is unlikely, since no chloritoid has been found in the entire region. However, the textural relationships do suggest the involvement of kyanite. The second reaction is possible, but no stable chlorite is seen to exist in other staurolite-free assemblages from this area. The main problem is the supply of iron biotite coexisting with the staurolite. Reaction temperatures for the production of staurolite are consistent with those found across the lake on Kootenay Point.

In the more basic rocks from the region, definition of even approximate reactions producing biotite are a problem. Most lower grade rocks contain epidote, actinolite, chlorite, carbonate and feldspar, often both plagioclase and K-feldspar. 4LBT-2 contains a trace of muscovite. Biotite occurs in small amounts in the lower grade rocks, becoming a major constituent only after the formation of hornblende. Biotite appears with K-feldspar in basic metaigneous (?) rocks. Biotite may form by reactions involving carbonate, chlorite and muscovite in basic metasediments.

The most important reactions involving basic rocks are those producing hornblende or diopside. As was mentioned in the discussion involving epidotes, lower grade assemblages contain epidote-actinolite± biotite±calcite±albite-oligoclase-microcline±quartz, and higher grade assemblages carry hornblende-actinolite-epidote-clinozoisite-An_{38-57} plagioclase-calcite-quartz±biotite±sphene. The assemblage change, coexistence of actinolite and hornblende + epidote, and the sharp rise in An content of plagioclase strongly suggests a reaction involving epidote + actinolite or epidote + chlorite + calcite to form hornblende + plagioclase of higher An content. Two reactions can be postulated:

3) 2Fe epidote + .6Al-actinolite + 1.2 low An plagioclase + .71 ilmenite $\rightleftharpoons$ Al epidote + hornblende + higher An plagioclase + .7 sphene + .2 Ab + 1.5 quartz

4) Fe epidote + .75 chlorite + .6 low An plagioclase + 2 calcite $\rightleftharpoons$ Al epidote + hornblende + 2.5 quartz + $2CO_2$ + XH_2O

Both reactions are complex and are difficult to balance for certain elements. Reaction 3 requires consumption of epidote in a ratio of 2 : 1 to provide enough aluminum for the formation of hornblende, aluminous epidote and plagioclase with higher An content. Iron is also required, again for the formation of hornblende. Because of the large amount of epidote consumed, Ca is left over, to be combined with excess Si and Ti in ilmenite to form sphene. These exchanges are all consistent with observed mineral assemblages, except for the small amounts of ilmenite-magnetite found in all rocks. The major problem involves Na given off by the consumption of low An plagioclase. Na must either leave the system, or form albite. K also poses a problem, which is even greater, as it is needed in the hornblende, and no K containing phases occur among the reactants. The formation of Ab and a plagioclase with more anorthite content is not inconsistent with feldspars on either side of the three solvi in the series. This still leaves the problem of K. The other possibility is that the reaction is allochemical and involves a K rich aqueous solution which exchanges K for Na, forming hornblende and taking off the excess Na. Reaction 4 may be balanced as is, with suitable epidote composition and with suitable plagioclase composition (albite with a significant amount of potassium). In the presence of potassium and aluminum in sufficient quantities, biotite would form as well. However, no significant amounts of K-feldspar or muscovite are present in the lower grade rocks. This problem will be discussed further presently.

These two reactions are supported by the decline in epidote across the "isograd" and the replacement of actinolite by hornblende in rocks of suitable composition. In calcareous rocks containing chlorite instead of actinolite, the epidote-chlorite tieline would be broken by completion of the reaction. In actinolite-epidote rocks the only change is in the position of the hornblende-epidote actinolite-epidote tieline. However, if calcite is not present in excess, this mineral will disappear during the course of the reaction breaking the hornblende-calcite and calcite-epidote tielines. Sphene appears as a new phase.

The form of these reactions is different from those proposed by Cooper (1972) for metamorphism of basic rocks of the Haast Schist group of Southern New Zealand, wherein calcite is not involved and epidote disappears from the rock during the reactions. That epidote remains can be seen by examining Tables 3 and 4. Examination of Table 13 shows that epidote analyses were not carried out on rocks below the hornblende "isograd". Therefore, compositional comparisons are based on optical differences between epidotes from actinolite-epidote and chlorite-epidote assemblages and those of the higher grade rocks.

These reactions are important because they clearly define a reaction isograd in the area which spatially closely coincides with the garnet isograd defined for more pelitic rocks. Both pelitic and basic rocks above (further west than) the hornblende "isograd" may contain garnet. Garnet production in basic rocks is another problem that cannot be clearly resolved within the study area on the basis of the data available. The presence of Al-epidote in hornblende-biotite rocks at higher grades, and the lack of it in garnetiferous amphibolites suggests a reaction involving Al-epidote to produce garnet with the grossular contents indicated in the Kootenay region. Such reactions are possible when epidote and clinozoisite are found in the presence of plagioclase, but they are dependent on the fugacity of oxygen in the rock (Holdaway, 1972). The reactions producing hornblende in basic rocks from the Haast Schist Group (Cooper, 1972) also take place at the almandine isograd, indicating that the two isograds may be coincident in other metamorphic belts, as well as indicating similarities between the two areas.

In rocks with higher magnesium content, the garnet and hornblende isograds coincide with the formation of diopside in rocks containing actinolite, dolomite and calcite. Any rock above or along the zone indicated by the garnet and hornblende isograds may contain diopside + tremolite-actinolite ± calcite ± dolomite ± magnesite ± quartz ± K-feldspar ± plagioclase ± Al-epidote ± biotite ± scapolite (Tables 3, 4, Appendix 3). Tremolite is not common from rocks in the central Kootenay Arc. Actinolite is by far the more prevalent mineral. Rocks from the Point contain tremolite and the reaction:

5) Tremolite + 3calcite + 2quartz $\rightleftharpoons$ 5diopside + $3CO_2$ + H_2O

can be seen in progress. This reaction occurs at temperatures from 400-540°C (Skippen, 1971, Fig. 9) at varying P_{CO_2}. Using the independent temperature measurements for calcite-dolomite formation on the Point, mole fraction CO_2 can be variously estimated at between 0.3 and 0.8 for the reaction. The pure reaction given above is not common anywhere in the Arc, however. Biotite is almost always present, and microcline is a common constituent in calc-siliceous rocks, along with plagioclase. Furthermore, reaction relationships seen in thin section indicate that tremolite or actinolite and diopside are being formed at the same time in some rocks. Staining of carbonate by alizarin red solution reveals a halo of calcite surrounding the tremolite, indicating that the growing tremolite depletes the dolomite of magnesium. In low grade rocks, quartz crystals are enclosed in dolomite, indicating that the reaction:

6) 5Dolomite + 8quartz + $H_2O \rightleftharpoons$ tremolite + 3calcite + $7CO_2$ takes place with rising temperature. Concurrent with this reaction, consumption of tremolite and the production of diopside occurs as indicated by reaction 5. Reaction 5 occurs between 520-540°C at higher mole fractions of CO_2, but the temperature of formation has been demonstrated to be independent of CO_2 above X_{CO_2} - .2 (Winkler, 1967). Reaction 6 has not been evaluated experimentally, but probably takes place at somewhat lower temperatures.

Textural evidence supports the occurrence of both reactions and may help to explain rocks in which tremolite occurs in two habits. Larger subhedral and sometimes euhedral tremolites and actinolites are formed by reaction 6 at lower temperatures, but the fields of stability of both tremolite and diopside overlap in the area, partly due to varying PCO and partly due to the fact that the system is complicated by the presence of aluminum and iron. Smaller, fibrous tremolites and corroded tremolite porphyroblasts develop in rocks where reaction 5 has begun. A number of rocks containing both dolomite and calcite show both reactions taking place simultaneously.

Assemblages containing diopside + tremolite-actinolite + calcite, dolomite or calcite + dolomite alone are not common in any set of rocks from the Kootenay Arc. Rocks containing pure tremolite and diopside are nonexistent. Most assemblages contain high magnesium biotite (not phlogopite), microcline and plagioclase with varying amounts of quartz in addition to diopside and actinolite. These assemblages indicate that K, Al and Fe were also present in the system.

An immediate problem arises when lower and higher grade rocks are compared. Rocks lying below the hornblende and garnet isograds contain significantly less K-feldspar + biotite (12%) than rocks lying above the isograds (18.3%). Thus, no lower grade rock is available which can isochemically produce the amounts of microcline and biotite present in the higher grade rocks. The potassium problem also occurs in basic rocks (reaction 3). The possibility of forming biotite by potassium metasomatism in the central Kootenay Arc was raised by Dodds (1965) and Livingstone (1968), but no quantitative data were provided. The data presented in this study provide some supporting observations for metasomatic introduction of various cations. First, biotite does not always parallel foliation in regional or Point rocks. It may grow across foliation or be randomly oriented in thin section. As was mentioned previously, this random texture is common in rocks containing scapolite. The second fact, noted by Crosby (1968), is that amphibolites from the central Kootenay Arc often contain considerable amounts of microcline and biotite, more than expected if a rock of basaltic composition was the source. Amphibolites in the Kootenay Arc may originate by metamorphism of sediments or by metamorphism of tuffs mixed with detrital material, a factor which would cause variable amounts of microcline and biotite to be present. Bulk chemistry plots indicate that the rocks lie in basalt, andesite or ultrabasic compositional fields, indicating that they could be derived from igneous rocks. Reactions may be written to explain zoning in amphiboles without recourse to the addition of extra components (Winzer, 1973, Appendix 4). However, zoning may be a late stage, post metasomatic effect.

Diopside-actinolite-carbonate rocks containing large amounts of biotite and microcline cannot be produced from rational sedimentary or igneous rock compositions without addition of at least K_2O. Biotite in these rocks is quite often random in orientation and conspicuously subhedral in form, as compared to other minerals.

That migration of cations took place may be illustrated by examining the map of Kootenay Point (Fig. 3). Several pods, lenses and irregularly shaped bodies of monomineralic or almost monomineralic rock exist in this small area, which is similar to other outcrops of the same extent throughout the higher grade portions of the area. The monomineralic areas are usually actinolite or biotite and may range in size from bands one centimeter thick to pods or lenses one meter or more thick and several meters long. Within such monomineralic areas, the mineral is randomly oriented in sprays or mattes. Thin section examination reveals that 95% of the slide consists of the mineral in question, with small amounts of other minerals common to the area.

The presence of scapolite further confirms the migration of fluids. Scapolite replaces plagioclase in some rocks, or grows independently in others, poikilitically enclosing biotite, diopside, amphibole and quartz as well as accessory minerals.

These factors, added to the enrichment of potassic minerals above the hornblende and garnet isograds, provide sufficient independent evidence to suggest that at least potassium has been added to rocks of higher grade, but not all rocks appear to be equally affected. For instance, there is less reason to suspect that calc-pelites have had K_2O added at higher grades. Some amphibolites would also appear to have undergone isochemical metamorphism. The large compositional variability of rocks from the central Kootenay Arc could be explained by metasomatic introduction of material into certain rock types, such as siliceous magnesian carbonates.

In contrast, the variations can also be explained by sedimentary facies change. This argument can be supported to some extent by observing that the hornblende and garnet isograds lie close to the inferred contact between Horsethief Creek Group rocks and the Hamill formation in the southern portion of the map area and Hamill and Lardeau Formations in the north. Most of the samples from the central and western portions of the map area come from the Lardeau Formation, but some from the southwestern portion are from the Milford Group. Using this argument, the rock composition would be said to control the assemblages found.

Against the above are the following arguments: 1) In the northeastern portion of the map area, the isograds do not conform to the contact, and as was mentioned in the discussion of geologic setting, Lardeau Formation and Hamill Group rocks are infolded in this region. 2) The presence of scapolite and random orientation of biotite with the textures described earlier, suggest independently the introduction of material. 3) The presence of monomineralic zones suggests independent migration of material, as it is impossible to find a parental rock with actinolite or biotite composition.

With these arguments in mind, we can reconsider the reactions taking place in actinolite-diopside-microcline-plagioclase-biotite rocks as involving essentially inert components CaO, MgO, FeO, Al_2O_3 (?) and SiO_2 (?) and more mobile components K_2O and Na_2O. Coupled reactions involving the breakdown of actinolite in the presence of quartz, water and dolomite, with mobile K would form biotite and pyroxene. Reactions involving the breakdown of plagioclase in the presence of dolomite would form scapolite and biotite, liberating Al_2O_3 for the formation of microcline. Further discussion of these reactions will be saved for the last section following discussion of chemical equilibrium.

Status of CO_2

The status of CO_2 is of interest in any metamorphic area. Zen (1961) discussed the possibility that CO_2 might be an "internal value component" in some metamorphic rocks. Winkler (1967) discussed variable molecular proportions of CO_2 in metamorphosed siliceous limestones. Evidence for the value of X_{CO_2} in rocks from the Kootenay Arc comes from the assemblages present. If calcite and dolomite are present with quartz or tremolite, in an area where the temperature can be shown to be high enough to cause a reaction to take place, then the molecular amount of CO_2 must be high. The diagrams of Skippen (1971) indicate that, for T = 530°C, $X_{CO_2} = 0.8$ at $P_{CO_2} + P_{H_2O} = 2$ kb. Inspection of Table 4 indicates one case of tremolite-actinolite-calcite-dolomite-diopside coexisting with biotite (T2-18b). There are more numerous cases of tremolite-calcite-dolomite-diopside with biotite and scapolite, or with plagioclase, but without quartz. The first assemblage suggests X_{CO_2} - 0.95 at P_{CO_2} + P_{H_2O} = 2 kb. However, it is not an invariant assemblage, thus any exact definition of X_{CO_2} is not possible.

Two assemblages containing both carbonates, biotite, quartz and microcline or plagioclase, but lacking diopside (10BT-3) or diopside and tremolite (8AT-18) can be found in Table 3. These assemblages would only fail to react if P_{CO_2} were high enough to prohibit the decarbonation reaction.

Further corroborative evidence that P_{CO_2} was high in some rocks lies in the presence of high carbonate meionites in assemblages from the Point and from regional rocks. Scapolites from the region were not analyzed, but they are optically similar to those from the Point. These scapolites have quite low Cl contents, variable S and high CO_2. The fact that their composition was unrelated to plagioclase composition, but was fairly uniform regardless of assemblage, indicates that their paragenesis is related to P_{CO_2}. The evidence indicates that scapolite formed at high P_{CO_2}.

However, other assemblages are found which do not contain both carbonates, or which contain assemblages like tremolite-calcite-diopside with biotite or feldspar but no quartz or diopside-quartz with some calcite. These assemblages suggest that decarbonation reactions were able to proceed, thus implying a lower P_{CO_2}. The low P_{CO_2} rocks lie within 150 m of those with high P_{CO_2} indicated. Thus the effect cannot be one of temperature. The data indicates that P_{CO_2} varies from rock to rock, and thus is not controlled from the external environment, making it an internal value component and suggesting that some rocks are closed to CO_2. Putting this statement another way, CO_2 is internally buffered in some rocks but not in others. The mole fraction CO_2 is likely significant in most rocks from the central Kootenay Arc, simply because of the presence of carbonate in nearly all rocks. Equilibrium coexistence of carbonate with silicates other than quartz, calcite and dolomite is not well understood, but it is likely that P_{CO_2} must remain at fairly significant levels to stabilize carbonate in the presence of feldspars and chlorite in relation to phlogopite or hornblende respectively, but at a sufficiently low level to prevent low temperature dissociation of muscovite.

Status of Oxygen

The crossing of the hornblende isograd correlates with the disappearance of magnetite and hematite from most rocks in the central Kootenay Arc and correlates with the appearance of low iron, high aluminum epidote. The change from iron epidotes to aluminous epidotes is correlated with change from oxidizing to reducing conditions (Holdaway, 1972). Opaque minerals in rocks above the hornblende and garnet isograds are mainly sulfides; pyrite, pyhrrotite, chalcocite and chalcopyrite, with carbonates containing considerable graphite. Graphite occurs throughout the central portion of the Kootenay Arc, in low and in higher grade rocks. The presence of graphite indicates low oxygen fugacity, but exact oxygen fugacities depend on T and P_{CO_2} (Nokleberg, 1973). The data indicate a change from oxidizing to reducing conditions across the hornblende and garnet isograds. Systematic work on sulfide phases, present in all rock types, would allow further quantification of oxygen fugacity, and it is recommended that such work be undertaken in future studies within the Kootenay Arc. It would be of considerable use in quantification of reactions suggested earlier.

Pressure-Temperature Conditions of Metamorphism in the Central Kootenay Arc

Pressures during metamorphism in the Kootenay Arc were high, probably between 6 and 8 kb for the range of temperatures indicated. Of this pressure, P_{H_2O} was less than P_{total}, and in some rocks $P_{total} = P_{CO_2}$. Pressures derived from comparisons of muscovite, chlorite and amphibole compositions indicate a facies series between Barrovian and Glaucophane schist.

Thermal gradients in the region are fairly low, as indicated by lack of large changes in composition for muscovite, amphibole, biotite and pyroxene with change in grade, and by temperatures derived through the use of the calcite-dolomite geothermometer. Another indication of low thermal gradients may be found by comparing distribution coefficients for hornblende-biotite, amphibole-pyroxene and biotite-muscovite. $K_D\ Mg^{Act\text{-}Di}$, $K_D\ Fe^{Act\text{-}Di}$ and $K_D\ Fe^{Bi\text{-}Mu}$ are the only distribution coefficients showing systematic changes with grade. $K_D\ Fe^{Act\text{-}Di}$ increases in a linear manner from 0.85 - 1.75 with grade increase, $K_D\ Mg^{Act\text{-}Di}$ decreases from 1.25 to 0.55 over the same interval. The change in $K_D\ Mg^{Act\text{-}Di}$ is non-linear. $K_D\ Fe^{Mu\text{-}Bi}$ decreases from 0.16 to 0.03 from low to high grades. The plot of $K_D\ Fe^{Mu\text{-}Bi}$ shows considerable scatter and is non-linear. All other distribution coefficients for all other octahedrally coordinated cations show random distribution of K_D with grade. It is reasonable to assume that they do so because of lack of strong thermal gradients, but lack of equilibration or effect of other cations on partition relations must be sonsidered. The latter two reasons will be discussed more fully in the last chapter.

Only two isograds can be mapped consistently over any distance in the central Kootenay Arc. These are the garnet and hornblende reaction isograds defined by reactions 2, 3 and 4 respectively. The two lie about 1.5 km apart in the southern half of the map area, but may coincide in the northeastern section of the region. The tremolite isograd is also present, but is not parallel to the others, an occurrence found in other areas (Hutcheon and Moore, 1973). This isograd cannot be mapped in the area. Reaction temperatures for these isograds lie between 430 and 500°C. Temperatures above the isograd did not rise significantly over 530 C, based on the incoming of staurolite and on the calcite-dolomite geothermometer. Comparison with the almandine isograd in the Haast Schist Group (Cooper, 1972) and with the hornblende isograds of the Bessi-Ino district in Japan (Banno, 1964) and the oligoclase isograd of the Haast Schist Group (Cooper, 1972) indicates that the position of the isograds is similar to those in the Haast Schist Group. The hornblende isograd in the central Kootenay Arc is reached before the almandine garnet isograd. Furthermore, the reaction producing hornblende in the central Kootenay Arc involves epidote-actinolite or chlorite-epidote and albitic plagioclase rather than albite-actinolite-chlorite, and the amphibole produced is more calcic. Na_2O contents are generally higher than K_2O contents, approaching 2% in some cases, but they are not as high as those found in the lower temperature-higher pressure regions of the Bessi-Ino district. This is probably a function of temperature in the

Kootenay Arc, but it may also be a function of somewhat lower pressures. Soda contents of amphiboles produced in the reactions presented in this study are slightly higher than those from the Haast Schist Group. It is more difficult to evaluate the significance of the reaction producing garnet in the Bessi-Ino district in comparison with that of the central Kootenay Arc. The main differences appear to be the presence of biotite in central Kootenay Arc, and the differences in MnO content between both garnets. Amounts of MnO in garnet are strongly related to oxygen fugacity in some rock types, but may be unrelated to metamorphic grade (Müller and Schneider, 1971). As no temperatures are given by Banno (1964), direct comparison is not possible, but the impression given is that the production of almandine occurs at higher temperatures in the Kootenay Arc.

The order of isograds differs from the Dalradian of Scotland in that hornblende appears before garnet, but the picture is not complete because the biotite isograd cannot be defined in the map area. The two isograds may nearly coincide, as was indicated earlier by coupled reactions involving phengite and chlorite producing biotite and garnet in the same rock. The indication of all data available is that the metamorphic facies series is intermediate between the Barrovian and the Glaucophane schist facies.

CHAPTER IV

CHEMICAL AND ISOTOPIC EQUILIBRIUM

The problem of chemical equilibrium in metamorphic rocks is important, since most discussions of temperature or pressure regimes of metamorphism presuppose that minerals in the rocks in question have reached a state of true equilibrium. The nature of this equilibrium and the degree of attainment of equilibrium have been the subject of considerable discussion (Thompson, 1955; Korzhinskii, 1957, 1966, 1967; Kretz, 1959, 1960; Weill and Fyfe, 1964, 1967; Moxam, 1965; Blackburn, 1968; Saxena, 1969a, and others). Discussions of chemical equilibrium involve use of the phase rule, textural relationships, interpretation of the geometry of joining tie lines of coexisting minerals (Zen, 1961) and the use of partition diagrams (Kretz, 1959, 1960; Moxam, 1965; Saxena, 1966, 1968a, b, 1969b; Gorbatschev, 1969; Kwak, 1970; Lyons and Morse, 1970, and others). A considerable number of papers use one of the above methods to determine how closely the system has approached equilibrium.

Two basic problems complicate the study of equilibrium in metamorphic rocks. The first is that all factors of equilibrium in a system at the time of metamorphism are not known. The second is that a natural metamorphic system is, because of changing conditions, one which has not reached a stable or "steady state" equilibrium. The first problem leads to circularity of reasoning in applications of thermodynamic parameters to metamorphic rocks. One easily appreciated example is the evaluation of temperature based on the presence of certain phases. The determination of temperature usually necessitates some assumptions about the nature of volatile components which are said to have been present. This problem can be diminished to some extent by direct measurement of composition of fluid inclusions, or by using a thermometer which is based on simple subsystems which are relatively less affected by changes in the larger system. The second problem is much more difficult, since it involves reaction kinetics and necessitates deviation from assumptions of classical thermodynamics related to evaluation of metamorphic reactions. An example is the study of metamorphic reactions in experimental systems. Here all equilibria are based on reversible reactions, usually in closed systems with simple mineralogy. In a natural system, however, reactions proceed irreversibly.(Korzhinskii, 1957). Because of the irreversible nature of natural reactions, the concept of local or mosaic equilibrium has been erected to allow handling of reactions in the dynamic state (Korzhinskii, 1957, 1970; Thompson, 1955, 1970).

In order to study the concept of equilibrium in metamorphic rocks and to demonstrate effects of incomplete equilibrium or disequilibrium, a small area of the Central Kootenay Arc was selected for concentrated study. This area was chosen because of its small size, allowing T and $P = P_{total}$ differences to be ignored and because of wide variation in chemical composition, texture and mineralogy. This variation, within very narrow PT limits, allows compositional controls of such variables as partition coefficients to be determined.

Many of the rocks studied contain textural evidence of disequilibrium. These textures are: 1) Zoned minerals: garnet, epidote, amphibole and plagioclase feldspar; 2) Ragged or irregular boundaries on minerals: garnet, biotite, feldspars, amphiboles and epidote, as well as carbonates; 3) Presence of incompatible mineral assemblages at temperatures apparently beyond their reaction limits: dolomite, calcite and quartz; tremolite, calcite and dolomite.

Other rocks, often in direct contact with rocks showing examples of the above, have textures which would be interpreted as indicative of equilibrium. Minerals are optically unzoned, boundaries are smooth with many "triple junctions" indicative of boundary adjustment to equilibrium conditions (Spry, 1969) and no incompatible phases are present. These rocks are separated from those showing disequilibrium textures by sharp boundaries. Thus, both texturally equilibrated and non-equilibrated rocks coexist side by side under the same conditions of temperature and total pressure.

APPLICATION OF THE PHASE RULE

Adherence to the phase rule is a necessary but not sufficient condition for an assemblage at equilibrium (Zen, 1961). The Gibbs Phase Rule was derived for essentially static systems, but Korzhinskii (1957) demonstrated that the phase rule could be derived for and applied to systems undergoing dynamic change. It has also been demonstrated that the phase rule may be applied to systems containing mobile components (Thompson, 1955, 1970; Korzhinskii, 1957, 1970) thus extending its possible use to open systems.

Accurate definition of inert and mobile components must first be made before application of the phase rule is possible. Differentiation between inert and mobile components is one of the greatest problems in the application of the phase rule to metamorphic rocks. The identification of mobile components depends upon recognition of an open or a closed system at the time of formation of the mineral assemblage. We are immediately confronted with the necessity of making assumptions as to the nature of the system at the time of formation. Some of the assumptions concerning K_2O and CO_2 have already been discussed. H_2O and CO_2 have been considered mobile by many investigators, but Zen (1961) raised the question of CO_2 being an internal value component. Fluid inclusion work suggests that CO_2 may exist as a separate phase (Smith and Little, 1959; Takenouchi and Kennedy, 1965 and Roedder, 1972). H_2O can reasonably be considered mobile in rocks bearing hydrous phases, but the actual composition of the fluid phase may introduce more mobile or inert components into the system.

Definition of the number of independent inert components is another difficult problem. Korzhinskii (1957, p. 13) states that: "....the number of independent components is the smallest number of those chemical constituents whose combination (addition or subtraction) can give the compositions of all possible phases in the system, including phases of variable composition." He goes on to define inert and perfectly mobile components as those components whose masses or molar amounts are equilibrium factors of the system (inert components) or whose chemical potentials, activities and concentrations in one of the phases (including partial vapor pressures) are equilibrium factors of the system (perfectly mobile component).

Using the assemblages without incompatible phases (See Table 4), the phase rule can be applied to rocks from Kootenay Point. Comparison of Fe/Mg ratios for biotite, pyroxene and amphibole in single sections indicates that these two elements cannot be treated as one component. CaO, Al_2O_3, Na_2O, K_2O and SiO_2 are the other major components, but where sphene is present as a separate phase, TiO_2 cannot be considered as an accessory component, and must be used as another independent component. Using Gibbs' rule, the variance of systems from the Point is between 2 and 8, with only two divariant assemblages (T2-18, T4-2). The remainder are trivariant, quadrivalent or multivariant. It is interesting to note that the two divariant assemblages are scapolite-bearing. If we use the Korzhinskii rule $J_{in} + J_{ex} = C + 2$, where J_{in} are the independent intensive parameters T, P, $\mu_i \ldots \mu_j$ and J_{ex} the extensive parameters (equivalent to phases) defined for the system at equilibrium, the variance described above becomes the maximum number of intensive parameters. As T and P for the system are constant, the variance is the maximum number of mobile components present *provided the system is in equilibrium.* Thus, the phase rule alone cannot tell us if the rocks being studied are in equilibrium. If we make the assumption that they did reach equilibrium, the phase rule would indicate some information about the number of possible mobile components in the system.

PARTITION STUDIES

Another possible approach to the problem of defining chemical equilibrium in a rock system is to study the partitioning of major and trace cations between coexisting phases. If a system has reached chemical equilibrium, then everywhere within that system, the chemical potential of each ion must be the same. Or, if stoichiometric requirements result in different chemical potentials for the same element in different phases, ΔG must be at a minimum (Albee, 1965). If these criteria are not satisfied, reactions and rearrangement of phases and components are possible. The dependence of partitioning of elements on equilibrium factors of a system is given in the following relationship (Ramberg and De Vore, 1951; Kretz, 1959):

$$\frac{X_i}{1-X_i} \cdot \frac{1-X_j}{X_j} = e^{\frac{-\Delta G}{2RT}} = K_D$$

where X_i and X_j are the mole fractions of the element in phase i and phase j respectively, G is the free energy, R is the gas constant, and T the temperature. This relationship defines the distribution coefficient (K_D) which should be constant for any set of mineral pairs which have attained equilibrium at constant T and P. This is so because the relationship is derived from the expressions defining the chemical potential of an element in each phase: $\mu_i{}^a = \mu_i^o + RT\ln f X_i{}^a$

$$\mu_i{}^b = \mu_i^o + RT\ln f X_i{}^b \quad ,$$

and $\mu_i{}^a = \mu_i{}^b$ at equilibrium. The equation also illustrates the dependence of the distribution coefficient on T, where T affects μ differently in the two phases (Saxena, 1968). The distribution coefficient has potential as a thermometer. However, f, the activity coefficient, must be defined for real, non-ideal systems before any thermometer can be put to use, and this has proved generally impracticable.

Mineral pairs of different composition coexisting in different rocks may be used to define the distribution coefficient graphically by plotting the concentrations of the element in question. The points will describe a curve or a straight line (at more dilute concentrations) passing through the origin with slope equal to K_D. For dilute solutions, the relations takes the form $$K_D = \frac{X_i{}^a}{X_i{}^b}$$ (Kretz, 1960).

Plots of $X_i{}^a$ against $X_i{}^b$ should provide a graphical illustration of the degree of equilibration of a system, providing the distribution coefficients are independent of crystallographic factors or other elements, and provided T was constant during formation of the mineral pairs. Trace elements are particularly sensitive indicators of equilibrium, since, at low concentrations, small changes in chemical potential will produce large variations in the distribution coefficient.

Twenty-three pairs of coexisting amphiboles and biotites from rocks located on Kootenay Point were analyzed by electron microprobe. Two pairs from the same thin section, located less than 10 mm apart were also analyzed. Four pairs contain phases incompatible with each other and show disequilibrium textures (T2-2, 105-101, 72-80 and T3-2b). Two others (T1-8, 199-146) contain trace amounts of "incompatible" phases, but show textures indicative of equilibrium. Eleven pairs were further analyzed for eleven trace elements, Ga, Li, Cr, Cu, Co, Zn, Ni, Mn, Rb, Sr and Ba. A Rb-Sr mineral isochron was derived for the twenty-two minerals in these eleven pairs, and nine of the biotites were dated by the potassium-argon method. The latter work was done in order to correlate isotopic changes and changes in the age of minerals with possible varying degrees of equilibration. Trace element data are presented in Table 21, Rb-Sr isotope data are presented in Table 22, and K-Ar isotope data in Table 23. Major element values are taken from Tables 6 and 9. Error limits for trace element and isotope data are presented in Appendix 2.

TABLE 21. TRACE ELEMENT CONCENTRATION (PPM) IN MINERAL PAIRS FROM KOOTENAY POINT

	Sample	Ga	Li	Cr	Cu	Co	Zn	Ni	Mn	Rb	Sr	Ba
1	T1-9 (Hb)	11	30	687	16	29	95	190	1242	15	70	221
	T1-9 (Bi)	15	292	792	24	35	181	261	680	635	36	926
2	T4-2 (Hb)	29	53	724	23	32	162	75	2666	35	69	62
	T4-2 (Bi)	15	356	651	29	35	236	141	1613	739	27	440
3	30-13E (Hb)	16	32	213	25	34	95	32	1649	12	23	37
	30-13E (Bi)	30	291	329	13	60	139	217	1282	450	9	829
4	T3-12a (Hb)	42	59	182	9	23	132	102	1633	17	22	8
	T3-12a (Bi)	57	374	199	8	31	124	79	1018	394	16	735
5	205-50W (Tr)	6	8	22	4	3	54	5	665	23	30	526
	205-50W (Bi)	21	85	69	2	3	41	8	196	1012	2	1003
6	240-137E (Hb)	17	22	720	4	41	91	292	1349	15	92	140
	240-137E (Bi)	15	347	745	28	56	147	325	899	476	62	3674
7	T4-6a (Act)	8	14	36	2	6	59	6	980	6	36	11
	T4-6a (Bi)	26	330	66	4	3	167	5	585	498	20	810
8	T2-15 (Hb)	18	14	199	6	13	49	18	2156	15	27	22
	T2-15 (Bi)	22	263	284	16	67	136	60	1375	497	11	536
9	T1-1 (Act)	7	12	27	8	4	56	11	310	10	162	38
	T1-1 (Bi)	24	287	166	6	20	78	68	337	368	75	3815
10	199-146 (Act)	11	39	49	19	6	140	18	983	48	208	48
	199-146 (Bi)	25	270	58	12	6	247	11	774	720	92	871
11	T1-8 (Act)	9	11	46	3	4	72	8	754	24	84	25
	T1-8 (Bi)	17	152	58	5	16	140	14	462	612	15	926

TABLE 22. Rb-Sr ISOTOPIC DATA FOR MINERAL PAIRS FROM KOOTENAY POINT

Sample	Rock Type	Mineral	Rb, ppm	Sr^N, ppm	Rb^{87}/Sr^{86}	Sr^{87}/Sr^{86}
T2-15	Andesitic Amphibolite	Iron-Biotite	496.5	11.1	129.73	.8256
T4-6	Basaltic Amphibolite	Magnesian-Biotite	498.1	19.7	73.05	.7607
30-13E	Andesitic "Amphibolite"	Iron-Biotite	450.0	9.0	144.31	.8437
240-137E	Biotite Amphibolite	Magnesian-Biotite	476.1	61.7	22.32	.7251
205-50W	Biotite "Amphibolite"	Magnesian-Biotite	1011.9	2.2	1330.10	1.5920
199-146	"Calc-silicate"	Magnesian-Biotite	720.3	92.0	22.66	.7321
T1-9	Andesitic Bi Amphibolite	Fe-Mg Biotite	634.8	35.7	51.38	.7594
T1-1	"Calc-silicate"	Magnesian-Biotite	368.1	74.4	14.31	.7244
T1-8	Biotite Amphibolite	Magnesian-Biotite	612.0	14.5	122.10	.8068
T4-2	Andesitic Bi-Scap Amphibolite	Iron-Biotite	739.1	27.1	78.70	.7601
T3-12	Calc-silicate	Iron-Biotite	393.7	16.1	70.82	.7843
T1-1	"Calc-silicate"	(Tremolitic Hornblende) Actinolite	10.2	162.2	.18	.7138
T1-8	Biotite Amphibolite	(Tremolitic Hornblende) Actinolite	24.3	84.0	.84	.7144
199-146	"Calc-silicate"	(Tremolitic Hornblende) Hornblende	48.2	207.3	.67	.7142
205-50W	Biotite "Amphibolite"	Tremolite	22.8	29.7	2.23	.7143

TABLE 22 CONTINUED

Sample	Rock Type	Mineral	Rb, ppm	Sr^N, ppm	Rb^{87}/Sr^{86}	Sr^{87}/Sr^{86}
240-137	Biotite Amphibolite	Magnesio-Hornblende (zoned)	14.5	92.0	.46	.7052
30-13E	Andesitic. "Amphibolite"	Tschermakitic Hornblende	12.3	23.3	1.52	.7234
T4-6	Basaltic Amphibolite	(Tremolite-Tremolitic Hb) Actinolite (zoned)	5.5	35.8	.45	.7138
T4-2	Andesitic, Bi-Scap. Amphibolite	Magnesio-Hornblende	35.3	68.5	1.49	.7111
T4-2	Andesitic, Bi-Scap. Amphibolite	Magnesio-Hornblende	35.3	43.9	2.33	.7115
T3-12	Calc-Silicate	Magnesio-Hornblende	17.3	22.2	2.26	.7492
T2-15	Andesitic Amphibolite	Edenitic Hornblende (zoned)	15.3	27.2	1.63	.7250
T1-9	Andesitic Bi-Amphibolite	Tschermakitic Hornblende (zoned)	14.5	70.3	.60	.7062

^{87}Rb: $\lambda = 1.39 \times 10^{-11} yr^{-1}$

Rb abundance $^{85}Rb/^{87}Rb$ atomic = 2.591

TABLE 23. K-Ar ISOTOPIC DATA FOR MICAS FROM KOOTENAY POINT

Sample	K_2O percent	Ar^{40r} cc. STP	$\frac{Ar^{40r}}{Ar^{40}\text{ tot.}}$	Age m.y.
205-50W	9.90	1.718×10^{-5}	0.88	52 ± 3
T4-2	8.06	1.396 "	0.68	52 ± 3
T1-1	9.06	1.665 "	0.82	55 ± 3
T3-12	7.92	1.319 "	0.50	49 ± 3
T1-9	8.78	1.508 "	0.75	51 ± 3
199-146E	8.20	1.282 "	0.59	47 ± 3
T2-15	9.05	1.518 "	0.65	50 ± 3
30-13E	8.52	1.640 "	0.78	57 ± 3
T4-6	8.96	1.700 "	0.53	57 ± 3
T1-8	9.39	1.633 "	0.63	52 ± 3

$K^{40}/K = 0.000119$ atomic

K^{40}: $\lambda_\beta = 4.72 \times 10^{-10}\ yr^{-1}$

K^{40}: $\lambda_e = 0.585 \times 10^{-10}\ yr^{-1}$

PARTITIONING OF MAJOR AND MINOR ELEMENTS

Concentration of elements in biotites and amphiboles are generally calculated as atoms of element divided by Σ Fe + Mn + Mg + Ti, after Kretz (1959); Moxam (1965). Calculation of concentrations is a problem, since sites are not equivalent in the amphibole group and may not be equivalent in the biotites. An octahedrally coordinated element competing for a site can be considered to occupy any of four sites in amphibole; M_1, M_2, M_3 and M_4. The M_4 site, however, is filled with Ca or Na in the calcic and subcalcic amphiboles, leaving only three sites available for significant substitution. For ions with affinities for Mg, Mn, Ti or Fe, the three sites are considered to be equally available, unless a relationship exists between the element or its partition coefficient and an element existing in another site. Octahedrally coordinated Al is the usual element showing relationships to Ti, Mg or Fe. Among the major and significant minor cations, only Ti appears related to any other element, this being octahedral Al. Calculating concentration as the element over Σ oct + Al^{IV} makes little difference in the plots, however. Alkalis also present difficulties, as the site for K in amphibole is not always present (or occupied). Here, concentration is calculated as K (Rb or Ba)/Ca + Na + K. However, this calculation may not always be correct.

Iron

The partition diagram for iron (Fig. 49a) shows two groupings. One group is characterized by K_D = 0.96 and contains the hornblendes including zoned pargasitic hornblende (240-137, T2-15, T3-12a, 30-13E). With the exception of T3-12a, pairs containing zoned amphiboles fall very close to the line defining the distribution coefficient. The dichotomy representing the miscibility gap in the amphibole series is well represented in this plot. For the tremolitic and actinolitic amphiboles (be (below $Fe/\Sigma\ oct = 0.4$), the distribution is considerably more erratic. T4-6(1) and T4-6(2) (located less than 10 mm apart) show quite different distribution coefficients. The difference between the distribution coefficients is outside the error range of the analysis and reflects crossing tielines, interpreted by Zen (1961) as indicating disequilibrium. The conclusion drawn from this diagram is that equilibrium with respect to iron was closely approached in rocks containing hornblende-biotite pairs, regardless of zoning, but was not established in actinolite-biotite or tremolite-biotite pairs. The plot of Al^{IV} amphibole/Al^{IV} biotite (Fig. 49b) shows no relationship to $K_D Fe^{Bi-Hb}$ other than to indicate two groups of amphiboles (actinolite and hornblende). Within each group, the general conclusion is that $K_D Fe^{Bi-Act}$ is smaller (closer to 1 in this case) than is $K_D Fe^{Bi-Act}$, but both groups show complete scatter with no real trends indicated. Plotting the actinolite group as $Fe/\Sigma\ oct + Al^{VI}$ decreases the scatter in Fig. 49a somewhat, but the relationships still hold. No change occurs in the hornblende group, suggesting some control by Al at lower Fe concentration.

Magnesium

In contrast to iron, the magnesium plot (Fig. 50) shows less scatter for the actinolite group and somewhat more scatter for the hornblende, but the general indication is for a closer approach to apparent equilibrium for this element in both groups. Samples 190-120 and T3-9 are conspicuously outside the trend, in agreement with the iron plot, indicating

Fig. 49 a. Partition diagram for Fe.

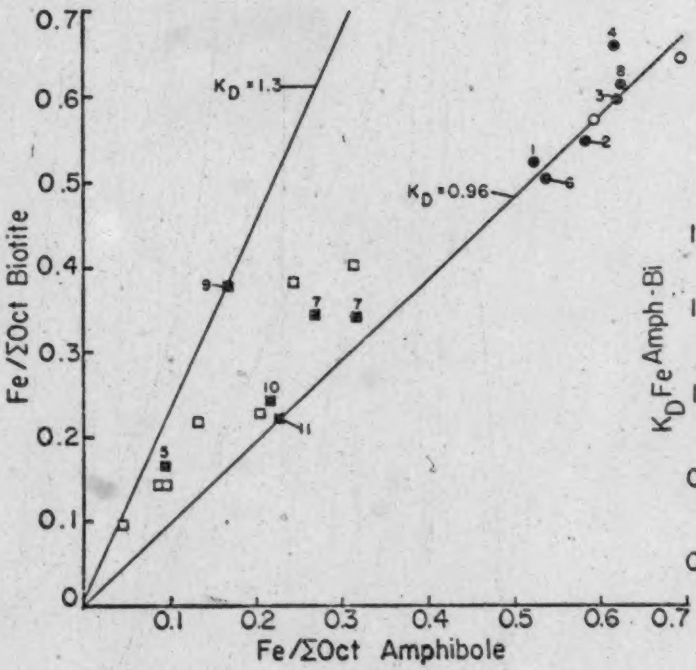

Fig. 49 b. Al^{IV} Amphibole/Al^{IV} Biotite plotted against $K_D Fe_{\text{Amph-Bi}}$ for 22 pairs.

K_D is the reciprocal of that shown in Fig. 49a. Symbols and numbers as in Fig. 49a.

K_D = 1.3 calculated for number 9.

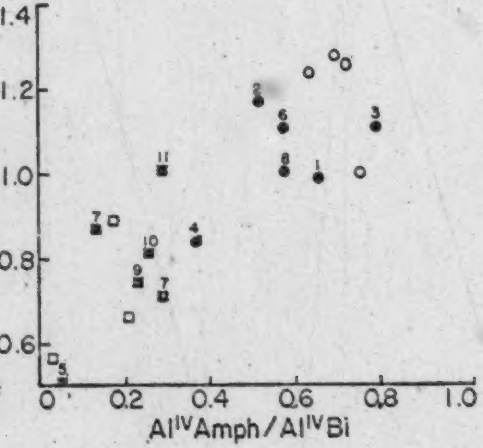

Circles - hornblendes; squares - actinolites.

Filled symbols indicate samples on which further trace element and isotopic work has been done.

Numbers refer to analyses in Table 21.

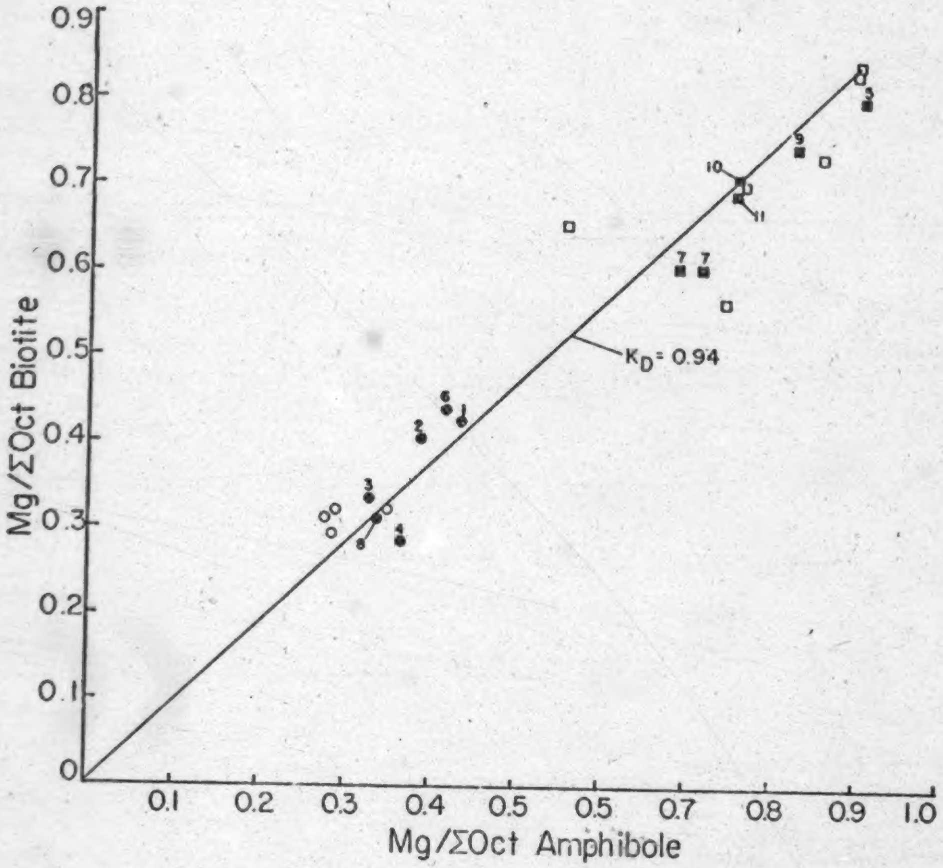

Fig. 50. Partition diagram for Mg. Symbols and numbers as in Fig. 49. Unnumbered, unfilled square lying above the line is 190-120, that lying below is T3-9. Both are near #7.

that both elements are disequilibrated in these two specimens. There is a suggestion that K_DMg is higher for hb-bi pairs than for act-bi pairs. However, the scatter in hb-bi is too large to be certain. Scatter among the hornblende group could be due to zoning (which produces large changes in Mg), but only T2-15 and 240-137 are conspicuously zoned (See Winzer, 1973, Appendix 4).

Manganese

The Mn plot (Fig. 51a) again appears to show two groupings, although not all members of the iron or magnesium groups plot in the same Mn group. The actinolites generally plot in a scattered group with a small K_D. Sample 30-13 could belong to this group, but may be disequilibrated due to zoning. Some samples do not belong to either group. It has been suggested (Saxena, 1968) that Ca in amphibole influences $K_D\text{Mn}^{\text{amph-bi}}$. Ca ions to 23 oxygens were plotted against $K_D\text{Mn}^{\text{amph-bi}}$. Again the samples divide into two groups, but no relation between or within groups can be found. No relationship exists between Mn and other elements, suggesting that deviations from the pattern are due to incomplete equilibration of the pairs. Among the pairs, those with actinolite show more scatter, but a majority of pairs fall near the mean K_D, indicating relatively close approach to apparent equilibrium.

It is interesting to compare a plot of PPM Mn (bi against coexisting hb) determined by atomic absorption with the plots of Fig. 51a (Fig. 51b). The linear nature of this plot is striking, with three samples deviating significantly (30-13E, T4-2 and 205-50W). The position of T4-2 on this plot is odd, as it falls close to the line in Fig. 51a. The deviation of 30-13E is to be expected. 205-50W does not appear on Fig. 51a as Mn

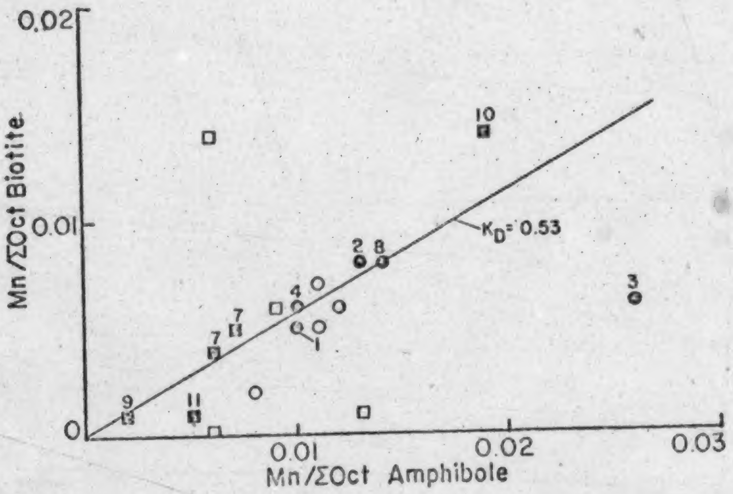

Fig. 51 a. Partition diagram for Mn from microprobe analyses. Symbols and numbers as in Fig. 49. K_D calculated for number 8.

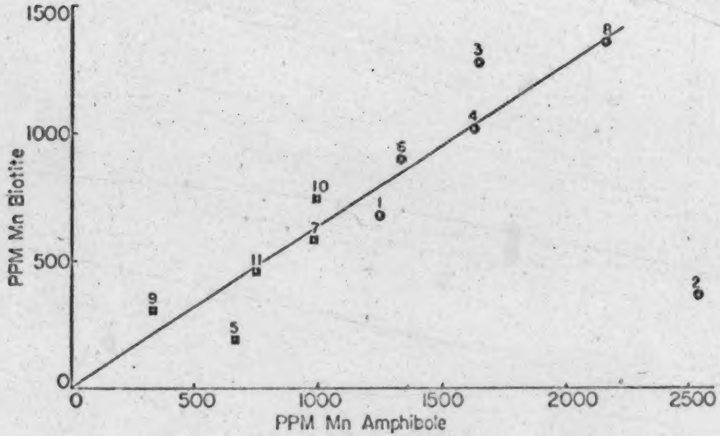

Fig. 51 b. PPM Mn biotite plotted against PPM Mn amphibole from bulk samples. Symbols as in Fig. 49.

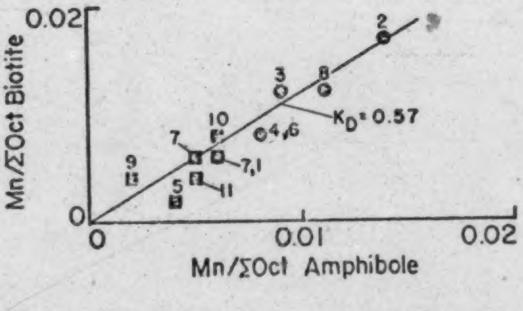

Fig. 51 c. Partition diagram for Mn from bulk analyses. Symbols and numbers as in Fig. 49. K_D calculated for number 7.

concentration was below the detection limits of the microprobe. Fig. 51c is a plot of Mn/Σ oct for amphibole and biotite using the bulk separates. $K_D\text{Mn}^{\text{bi-amph}}$ is slightly higher than for the microprobe results, but the distribution looks quite similar, suggesting that Mn distributions within small domains have the same K_D as the bulk samples, indicating similar approach to equilibrium on microscale and macroscale for this element. Because the concentrations of the other major cations are determined only for closely coexisting minerals, the concentration diagram (Fig. 51c) is not strictly comparable. Two separate lines of evidence suggest that Mn may equilibrate in larger volumes of rock. T4-6(1) and (2) show quite similar $K_D\text{Mn}$ (Fig. 51a), and traces for zoned amphiboles indicate virtually no change in Mn across strongly zoned amphiboles (Winzer, 1973, Appendix 4).

Titanium

Ti/Σ oct is plotted for amphibole and biotite in Fig. 52a. Complete lack of correlation is found with K_D ranging from 0.8 - 15. Al^{IV} Amphibole/Al^{IV} Biotite was plotted against $K_D\text{Ti}^{\text{amph-bi}}$ to test for correlation between tetrahedral Al and Ti distribution (Fig. 52b). The plot is equivocal. Up to $K_D\text{Ti} = 0.4$, a linear relationship exists between $K_D\text{Ti}^{\text{amph-bi}}$ and tetrahedral Al. Beyond this point, no relationship exists. It is possible that all plotted points show complete scatter above $K_D\text{Ti}^{\text{amph-bi}} = 0.3$. Comparing the two plots, there is no certain relationship between $K_D\text{Ti}^{\text{amph-bi}}$ and tetrahedral Al, and scatter in the distribution of Ti cannot be completely explained by control of this element in either actinolites or hornblendes. No other elements show any correlation with Ti, indicating that Ti has not equilibrated. Similar scatter has been found by Moxam (1965); Saxena (1968), Gorbatschev (1969), and Annersten and Ekstrom (1971). Moxam (1965) ascribed this scatter to inclusions of rutile in biotite or amphibole, but the microprobe analyses rule out this possibility. Gorbatschev (1969) found similar scatter in his amphibole-biotite pairs (also analyzed by electron microprobe) and concluded that despite some dependence on octahedral Al, the titanium did not equilibrate. A third possibility does suggest itself, however. If the mineral pairs in question do not exchange Ti with each other, but depend on consumption of another phase, then Ti is determined by the other phase, and the distribution coefficient of each pair is a function of the behavior of Ti in another phase. In rocks from Kootenay Point, sphene is common in rocks containing hornblende. There does not seem to be a relationship between $K_D\mathrm{Ti}^{hb\text{-}bi}$ and rocks containing or devoid of sphene. In areas where $K_D\mathrm{Ti}$ is determined, the presence of rutile, sphene, ilmenite or magnetite should be recorded. Enough data from widely spaced and differing areas might allow this problem to be solved.

Aluminum

No rationally interpretable distribution of either octahedral or tetrahedral Al was found between biotites and amphiboles studied on Kootenay Point. This finding is in contrast to that of Annersten and Ekstrom (1971) wherein a fairly strong positive relationship was found for rocks from a metamorphosed iron formation at approximately the same grade.

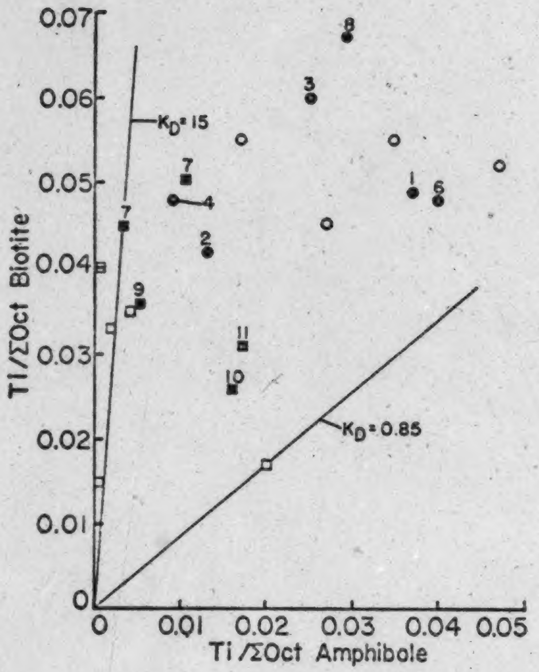

Fig. 52 a. Partition diagram for Ti.

Symbols and numbers as in Fig. 49.

K_D = 15 calculated for number 7.

K_D = 0.85 calculated for intercepted square.

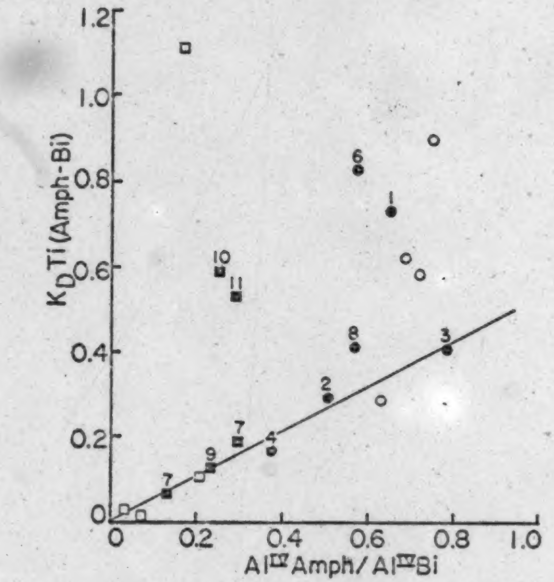

Fig. 52 b. Al^{IV} amphibole/Al^{IV} bi plotted against $K_D{}^{\text{Amph-Bi}}\text{Ti}$. K_D is the reciprocal of that shown in Fig. 52 a. Symbols and numbers as in Fig. 49.

TRACE ELEMENTS

Gallium

Gallium may substitute in positions occupied by either iron or aluminum (Goodman, 1972). Plots of gallium against iron and gallium against aluminum for biotites and amphiboles from Kootenay Point do not show good correlation in the actinolite group and their coexisting biotites, but some positive correlation is found for Ga-Fe in hornblendes and their coexisting biotites. Figs. 53a and 53b show gallium in PPM for amphibole plotted against biotite (53a) and concentration of gallium in amphiboles against biotites (calculated as Ga/Ga + Al + Fe). This plot is erratic, indicating that Ga is not equilibrated between the two minerals, since the scatter does not appear to be caused by control of another element. The scatter is well outside the error range of determinations.

Lithium

Lithium may be found either in tetrahedral or octahedral sites. Its size and charge indicate that it would be found in sites occupied by Fe, Mg, Al or Ti. Li plotted against the above elements yields no relationships between them. Lithium was also plotted against K and Na, again without producing any significant associations. Fig. 54 illustrates the distribution of lithium. It is strongly fractionated into biotites, probably due to the availability of octahedral sites for monovalent cations. $K_D^{\mathrm{amph-bi}}\mathrm{Li}$ is calculated from Li/Σ oct less Ti. The variation is considerable, due to the high slope of the line. No definite conclusions can be reached with respect to equilibration of lithium, but considerable scatter exists in the plot. The distribution is more orderly than that of gallium, suggesting, perhaps, a closer approach to equilibrium.

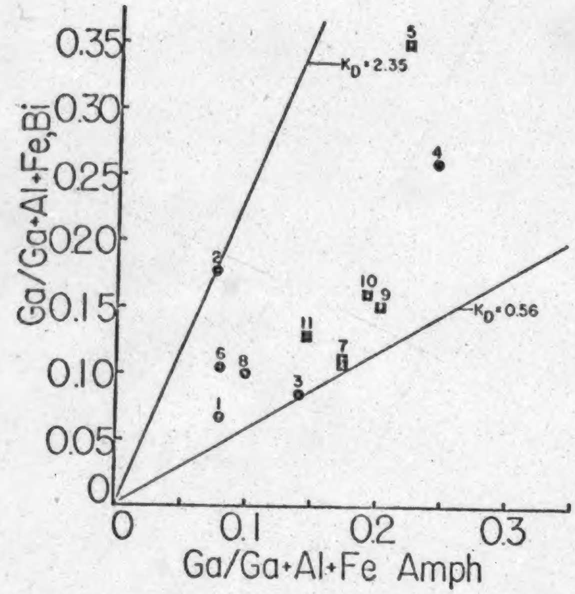

Fig. 53 a. Partition diagram for Ga.

Symbols and numbers as in Fig. 49.

K_D 2.35 calculated for number 2. K_D0.56 calculated for number 3.

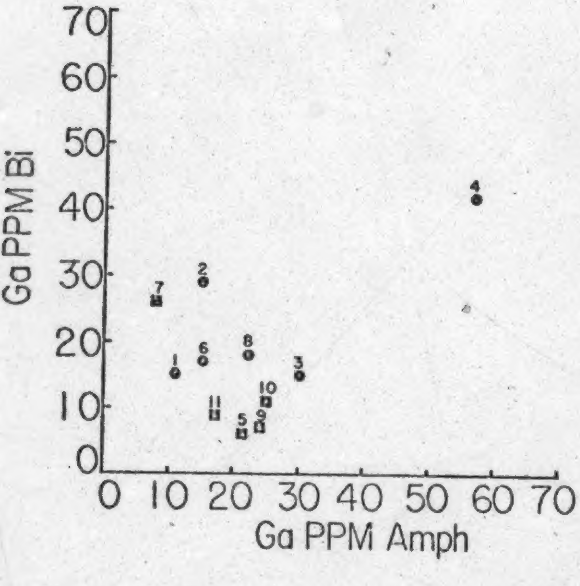

Fig. 53 b. PPM Ga biotite plotted against PPM Ga amphibole.

Symbols and numbers as in Fig. 49.

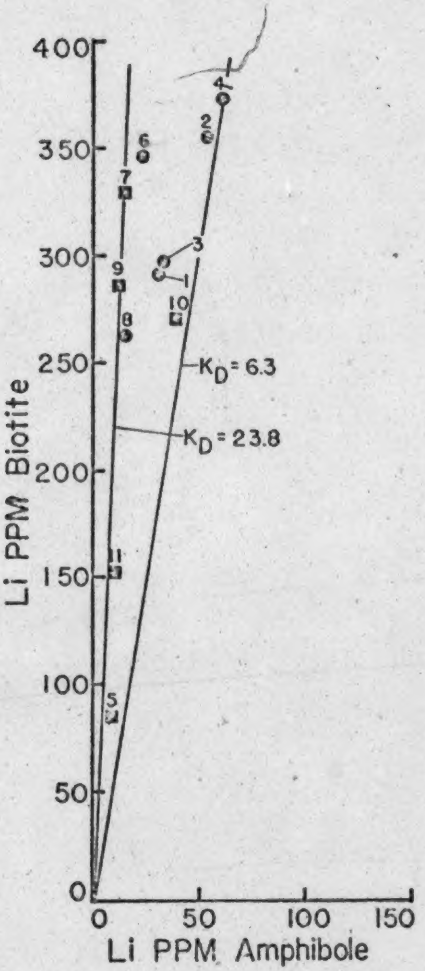

Fig. 54. PPM Li biotite plotted against PPM Li amphibole. K_D is calculated as Li/Σ oct Bi/ Li/ Σ oct amph, Σ oct = Fe + Mn + Mg. Symbols and numbers as in Fig. 49. K_D = 23.8 calculated for number 7; K_D = 6.3 calculated for number 4.

Nickel

Nickel should substitute for iron or magnesium in the silicate lattice. Plots of Fe and Mg against PPM Ni reveal some interesting relationships. First, only the faintest relationship exists between Ni and Fe in either actinolites or hornblendes and their coexisting biotites. Magnesium, on the other hand, shows an interesting relationship between Mg and Ni in the hornblende group (Fig. 55a). A nonlinear relationship exists up to about 80 x 10^3 PPM magnesium, whereupon the relationship changes to one in which Ni is independent of Mg. The actinolite group is uniformly low, and neither biotites nor actinolites show any relationship between Mg content and Ni content. Plots of Ti against Ni show no relationship.

Fig. 55b illustrates the partition of Ni between biotite and hornblende. The distribution coefficient is calculated as Ni/Σ oct, and ranges from 0.51 - 5.56. The distribution may be nonlinear, as indicated by 205-50W, T2-15, T4-2, T1-9 and 240-137. Unfortunately, T2-15, T1-9 and 240-137 are zoned, although T1-9 is only slightly zoned. Zoning appears to influence the pattern somewhat, although unzoned minerals do not show any systematic trends. Nickel would appear to be disequilibrated for both groups. The grouping of nickel suggests a different origin for the "amphibolites". High nickel values are to be expected in basaltic or ultrabasic rocks, thus the higher values for amphibolites suggest an igneous parent.

Chromium

Chromium has a more regular distribution than nickel. The general group relationships are the same as for Ni, except that the Mg dependence

Fig. 55 a.
PPM Ni (both amphiboles and biotites) plotted against PPM Mg x 10^3 for amphiboles and biotites.

Squares - amphibole.
Circles - biotite.
Filled squares - actinolite.

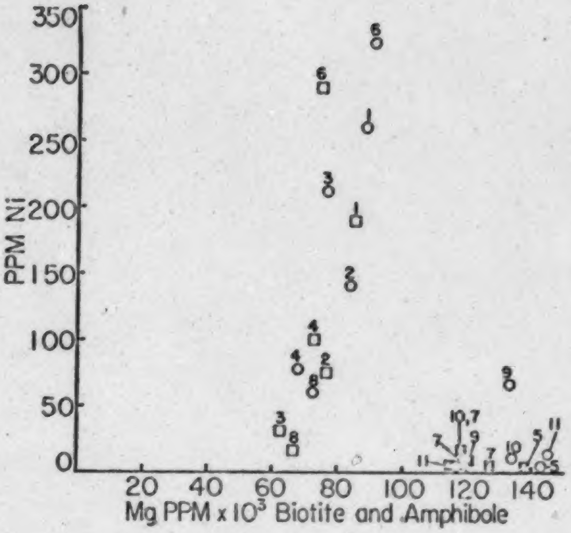

Fig. 55 b.
Partition diagram for Ni. Symbols and numbers are as in Fig. 49.

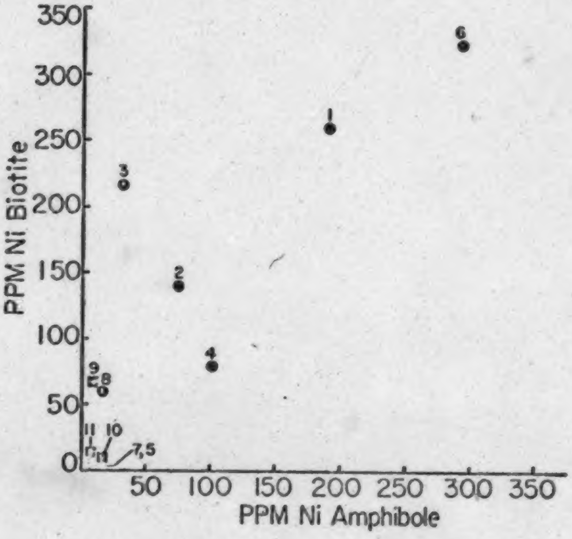

shown by Ni is not shown by Cr. Fig. 56a illustrates the range of concentration and degree of scatter. Some of the scatter may be due, as with nickel, to zoning in amphiboles. Fig. 56b plots Cr/Σ oct and gives the average distribution coefficient (0.93) for Cr. T1-1 lies conspicuously off the trend, which may be due to disequilibrium. Chromium would appear to be very nearly equilibrated within the rocks studied.

Cobalt

Cobalt shows a very interesting trend. Two populations exist, with separate distribution coefficients, as illustrated in Fig. 56. 30-13 is off either trend, which could be due to zoning, although T2-15, also zoned, falls right on the second trend. The distribution within each trend seems quite regular. Plots of Co against Fe, Mg and Ti show no correlation between these elements other than grouping in actinolite and hornblende groups. Ti plotted against Co shows a very general increase in Co in both biotite and amphibole as Ti increases. K_D shows no relationship to Ti, Fe or Mg. No explanation can be found for the two populations. Actinolites and hornblendes may be found in each group. Co shows an ambiguous trend, probably indicating diequilibrium within all rocks studied, but the two trends may be due to some other undetermined factor.

Zinc

Zinc may substitute for Mg or Fe in silicates which have OH bonds (Zemann and Wedepohl, 1972). Plots of Mg and Fe against Zn do not show any relationship between the two. Ti plotted against Zn shows a weak negative trend for hornblendes and their coexisting biotites. The trend for amphiboles is stronger than the "trend" for biotites, but is

Fig. 56 a.
PPM Cr biotite against PPM Cr amphibole.

Symbols and numbers as in Fig. 49.

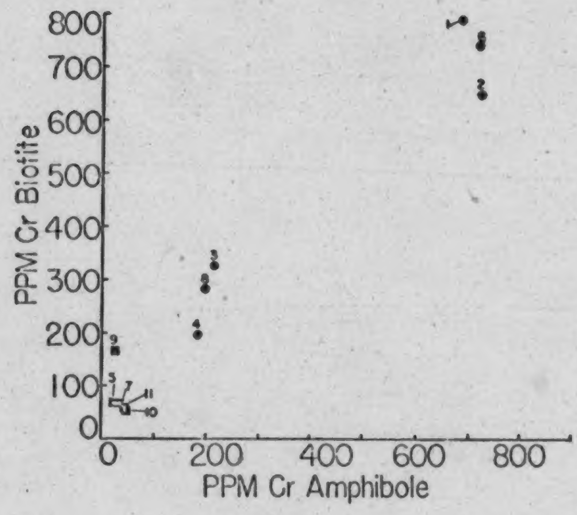

Fig. 56 b.
Partition diagram for Cr. Symbols and numbers as in Fig. 49.

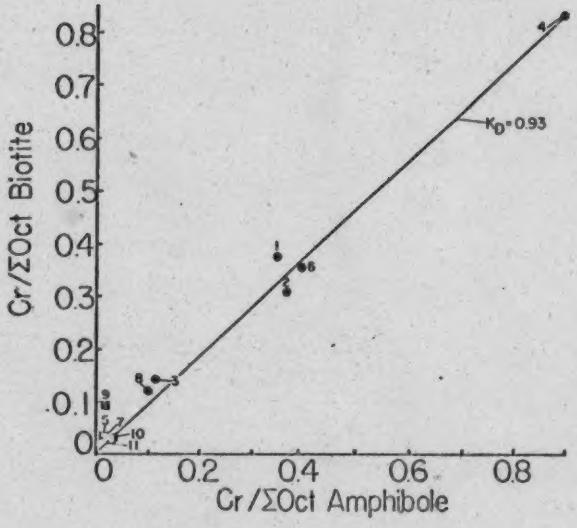

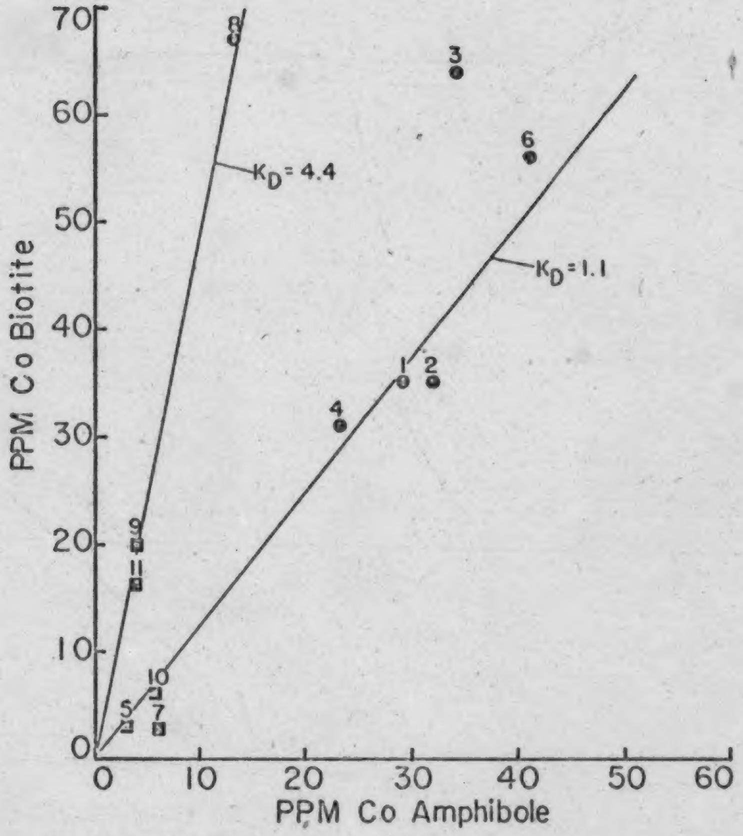

Fig. 57. PPM Co biotite against PPM Co amphibole. $K_D^{Bi\text{-}Amph}Co$ calculated as Co/Σ oct bi/ Co/Σ oct amph. Symbols and numbers as in Fig. 49. K_D = 4.4 calculated for number 9.

very weak. Fig. 58 gives the distribution pattern for Zn in biotite and amphibole. There is considerable scatter in this plot, and no readily apparent groupings appear. $K_DZn^{amph-bi}$ varies from 0.67 to 2.52, calculated as Zn/Zn + Fe + Mg. Calculating K_D as Zn/Σ oct does not substantially change the relationships. The distribution coefficient was calculated in terms of Fe and Mg, because these two elements are closest to Zn in behavior. Zn does not appear to be equilibrated in the rocks studied.

Copper

Copper values for biotite and amphibole are quite low. Cu shows no relationship to other octahedral cations. Fig. 59a illustrates the distribution of Cu between amphibole and biotite from Kootenay Point. Considerable scatter is evident. Fig. 59b plots Cu/Σ oct for the pairs. K_D varies between 0.42 and 2.38. Using only pairs with unzoned amphiboles produces no difference in the plots. Cu appears to represent disequilibrium in rocks from Kootenay Point.

Barium

Due to its large size, barium can only fit into the 12 fold sites of amphibole (the *A*-site) or biotite. For this reason, calculation of barium concentration in the calcic and subcalcic amphiboles may be made as Ba/Ba + Na + K, but should not be made as Ba/Ba + Ca + Na + K because the M_4 site is not available. The same conditions hold for rubidium because its size will not permit it to fit into the M_4 site of the amphibole. Ca or Na atoms occupy the 12 fold sites in biotite (Deer *et al*., 1966), and the calculation is made as Ba/Ba + Ca + Na + K. Both calcu-

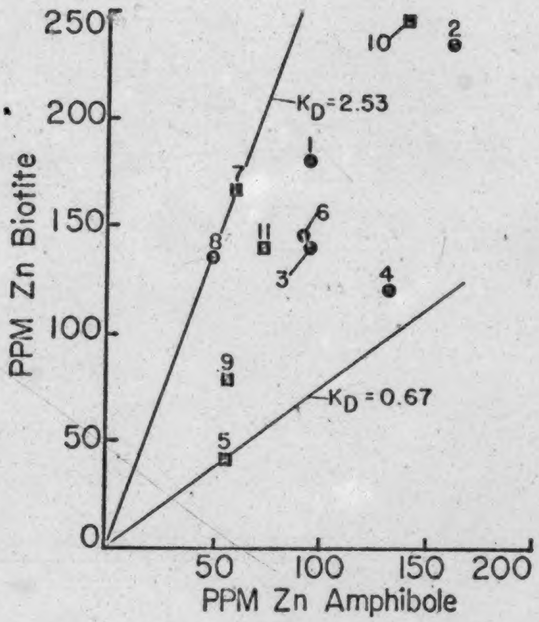

Fig. 58. PPM Zn biotite plotted against PPM Zn amphibole. K_D calculated as Zn/Zn + Mn + Mg biotite/Zn/Zn + Fe + Mg amphiboles. Symbols and numbers as in Fig. 49.

Fig. 59 a.
PPM Cu biotite plotted against PPM Cu amphibole.

Symbols and numbers as in Fig. 49.

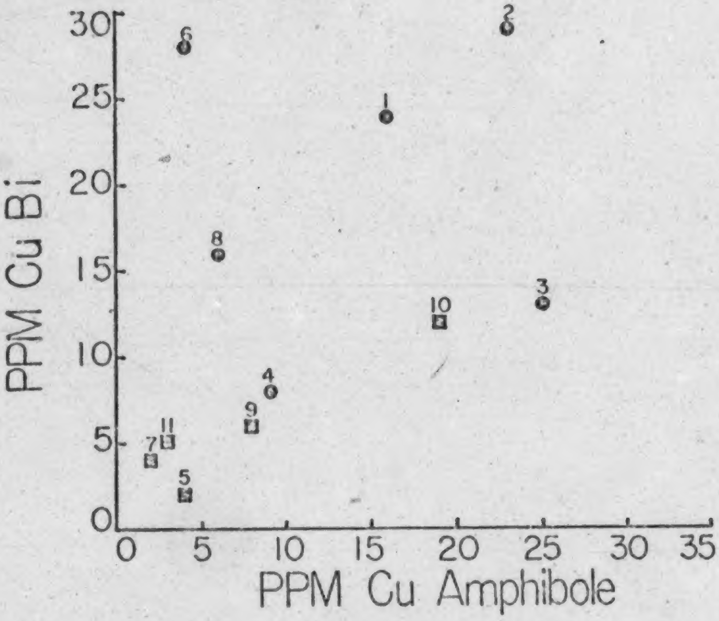

Fig. 59 b.
Partition diagram for Cu.

Symbols and numbers as in Fig. 49.

K_D = 5.38 calculated for number 6, K_D = 0.42 calculated for number 3.

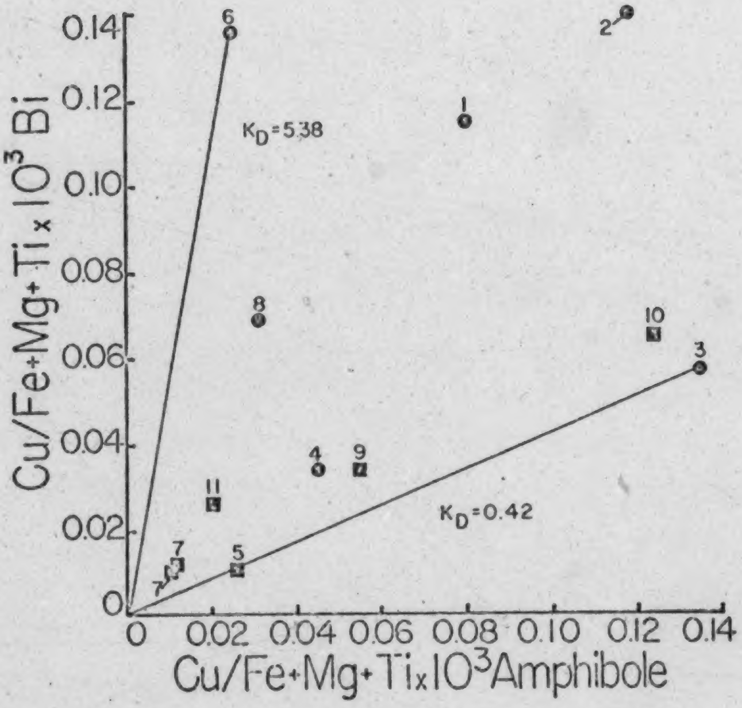

lation methods were used for amphiboles, with the result that Ba/Ba + Ca + Na + K gave large variations in K , whereas Ba/K or Ba/Ba + K gave more reasonable coefficients, as would be expected. Ba/Ba + K is used for diagrams presented and because the concentration of barium can be quite high, the non-ideal model developed by Ramberg and De Vore (1951) is used to calculate K_D.

Barium was plotted against K, but no relationship was found between the two. An enrichment in Ba by a factor of 5 over the other samples studied is found in Tl-1 and 240-137. There is no obvious reason for this anomaly; Tl-1, a high carbonate rock could have considerable barium, but 240-137, an amphibolite, should not.

Fig. 60 illustrates the partition relationships for Ba. At higher concentrations, Ba fractionates towards biotite, but no preference exists for Ba at lower concentrations. $K_D\mathrm{Ba}^{amph\text{-}bi}$ ranges from 0.27-9.5, an indication of the considerable scatter present. The scatter appears to bear no relationship to zoning in amphiboles. Subtracting the four strongly zoned amphiboles produces no substantial change in the distribution relationships.

Rubidium

Rubidium behaves in a manner similar to that of Ba because of its large size and single charge, and its geochemical behavior is closely similar to K (Cocco, Fanfani and Zanazzi, 1972). Rubidium is to be expected in either the A-site of the amphibole group or in the 12 fold site in the micas. Rubidium is fractionated into biotites, as expected (Fig. 61a,b). The distribution is nonlinear, with 205-50W falling well off the trend. Plots of K PPM against Rb PPM for amphiboles and bio-

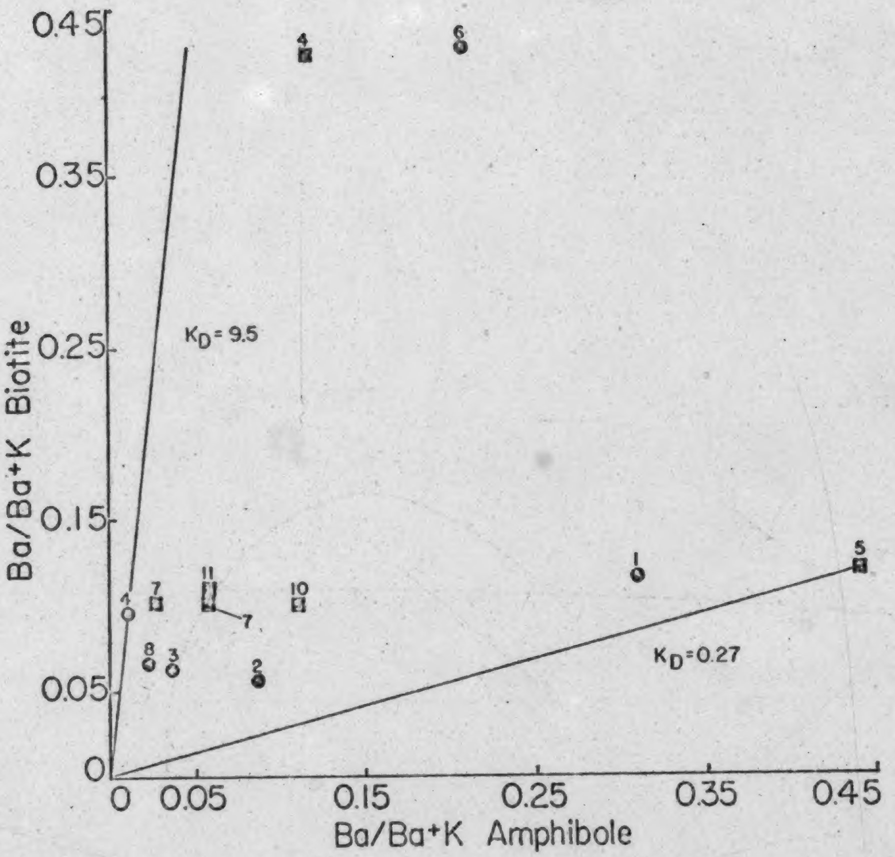

Fig. 60. Partition diagram for Ba. Symbols and numbers as in Fig. 49.

K_D = 9.5 calculated for number 4, K_D = 0.27 calculated for number 5.

tites show: 1) for amphiboles: no relationship exists between K content and Rb content; 2) for biotites: a very weak positive trend with increasing K. This trend is not considered significant in the light of the amount of scatter present. The partition relationships for Rb are shown in Fig. 61b.

The concentration of Rb is calculated as Rb/K for the same reasons given in the barium section. Considerable scatter is apparent, indicating lack of equilibration for Rb. 205-50W is farthest from the trend and is also the sample bearing the greatest concentration of Rb.

Strontium

Strontium can be expected to fit into the M_4-site of amphibole with some difficulty and fit into the A-site, but it will not fit into the other octahedral sites. In biotite, Sr would be found in the K sites. No relationship exists between K, Na or Ca and Sr in either biotite or amphibole, indicating that the distribution coefficient may be a function of chemical potential alone. The distribution of Sr is illustrated in Figs. 62a and 62b. Some scatter exists, but the preference of strontium for amphibole is well illustrated. The average distribution coefficient, calculated as Sr/Ca + Na + K(Bi)/Sr/Ca + Na + K (amph.) is 0.51 (Fig. 62b). Considerable deviation from the trend is exhibited by 240-137, T1-8 and 205-50W. Only 240-137 has a zoned amphibole. There is no ready explanation for T1-8 and 205-50W, but 205-50W contains the lowest amount of strontium of any of the samples.

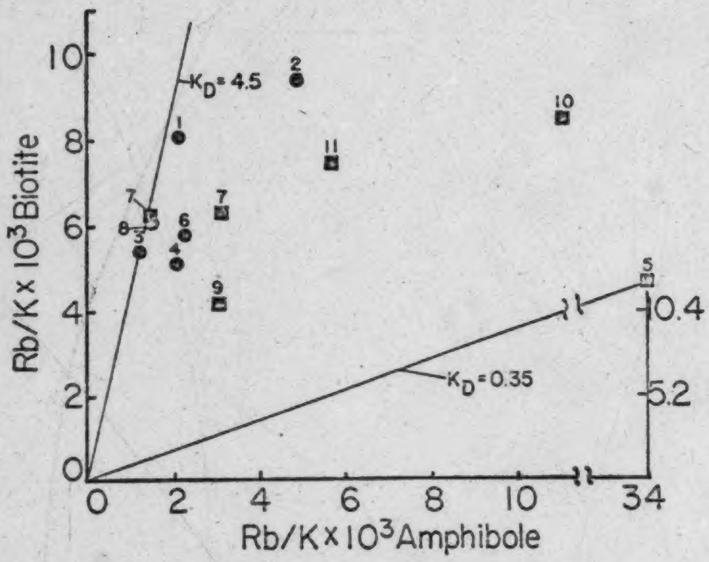

Fig. 61 a. Partition diagram for Rb. Symbols and numbers as in Fig. 49. K_D = 4.5 calculated for number 3; K_D = 0.35 calculated for number 5.

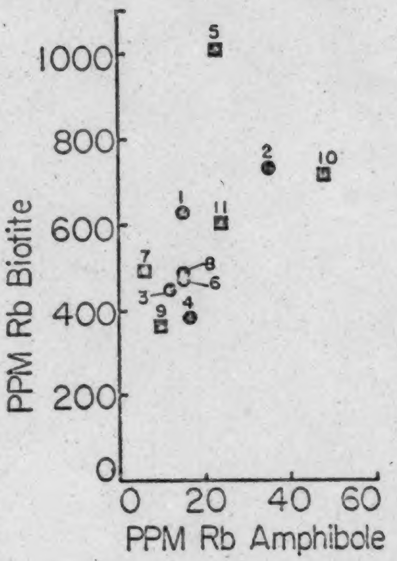

Fig. 61 b. PPM Rb biotite plotted against PPM Rb amphibole. Symbols and numbers as in Fig. 49.

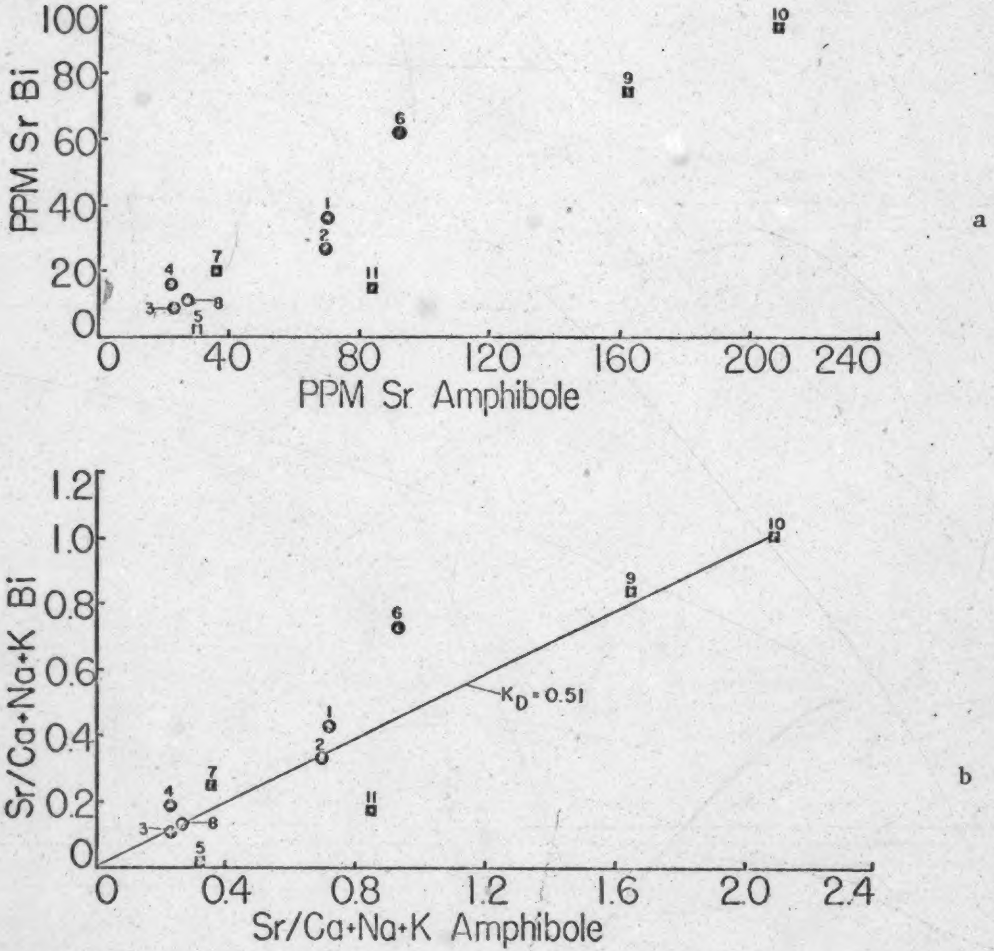

Fig. 62 a. PPM Sr biotite plotted against PPM Sr amphibole.

Fig. 62 b. Partition diagram for Sr.

Symbols and numbers for both a and b as in Fig. 49.

K_D - 0.51 calculated for number 10.

BEARING OF TRACE ELEMENT PARTITIONING ON CHEMICAL EQUILIBRIUM

The evidence from partitioning of major and trace elements between biotite and hornblende is not unequivocal, but the general impression is that a condition of disequilibrium exists between the mineral pairs for most elements. Among the octahedrally coordinated elements of the first transition series, only Mn and Cr appear to closely approach equilibrium. The scatter on the plots cannot be explained by control on the partition of the trace element by other elements competing for the same site, as has already been discussed. One or two other possibilities exist. The first is that the elements studied behave differently in actinolite than in hornblende, leading to different K_D in one or the other. Only Fe and Ni show a suggestion of differing behavior. Fe appears to distribute itself differently between actinolite and biotite than between hornblende and biotite, giving a lower K_D for act-bi pairs than for hb-bi pairs. Ni behaves in a systematic manner in biotite and coexisting hornblende when plotted against Mg, but no such systematic behavior is encountered in the actinolite group.

The second possibility is that the crystal field stabilization energy differs among the elements and the different minerals. That this is so has been discussed by Schwarcz (1967) and by Burns (1970), but the effect is to change the distribution coefficient for various elements. This change does not cause scatter of points, but results in systematic, predictable changes in K_D between elements. Schwarcz (1967) showed that, for hb-bi pairs, $K_{Mn}^{H/B} > K_{Fe}^{H/B} > K_{Co}^{H/B} > K_{Ni}^{H/B}$. This is generally true in the pairs studied, with $K_{Mn}^{B/H} = 0.53$, $K_{Fe}^{B/H} = \sim 1$, $K_{Co}^{B/H} = 1.1\text{-}4.4$ and $K_{Ni}^{B/H} = 0.9\text{-}5.5$, but the scatter and disequilibration of all four elements do not positively confirm the trend. The difference in CFSE between different mineral pairs suggests an explanation for the grouping of Fe and Ni. If the octahedral sites in actinolites are different than those in hornblendes, and some differences are indicated by Ross et al. (1969), the CFSE would be different for hornblendes, and for actinolites. Since differences in CFSE affect the distribution of transition metal cations, this could explain the differences in K_D for Fe and possibly provide some explanation for the behavior of Ni.

A possible explanation for the scatter in the Fe and Ti plots may be provided by the fact that both elements are known to exist in two oxidation states in natural materials. The lack of determination of Fe^{3+} does not allow a test of this hypothesis, but it is expected that Fe^{3+}, which has a CFSE, may distribute itself differently than Fe^{2+}, which does not. If the different pairs formed under different conditions of f_{O_2}, then the amounts of Fe^{3+} present may vary from sample to sample, causing variability in K_D which is not related to disequilibrium. The same thing is true of Ti^{3+}, but Ti^{4+} is probably overwhelmingly favored at these metamorphic grades.

Among the other octahedrally coordinated elements, Sr, Li and Ga (?), only Sr shows close approach to equilibrium. Part of the scatter in Li and Ga may be due to the fact that both may scatter between octahedral and tetrahedral sites, but the amount of either element present in the Al-Si tetrahedra should be small.

Among the large alkali cations, complete disequilibrium exists. Ba and Rb are strongly fractionated into biotite at higher concentrations, but no systematic trends can be found for either element. There is a possibility that the distribution of Rb is nonlinear, but this cannot be confirmed with the number of data points at hand.

The reasons for this lack of equilibrium lie in the behavior of the chemical system. The lack of equilibration of alkalis can be related to their behavior as mobile components. Examination of Tables 1 and 4 reveals anomalous K and Na ratios in rocks from Kootenay Point. Fig. 63 illustrates the Na_2O and K_2O trends with increasing SiO_2 for the 44 analyzed specimens from Kootenay Point. Despite the error range for these analyses, trends are clearly real and can be seen to correlate with modal mineralogy. The following observations may be made by examining the map (Fig. 3):

1) Potassium rich rocks are found in biotite amphibolite pods, such as those lying to the extreme west on the tip of the promontory. They are found in zones sandwiched by pegmatite and in the areas labeled "marble".

2) Exceptionally high soda rocks are found close to small pegmatite dikes which have observable thermal aureoles. These aureoles are characterized by a margin of green mica in sharp contact with the pegmatite. The mica zone dies off over a distance of about 1 cm to be replaced by reddish biotite, tremolite-actinolite and diopside with calcite and/or dolomite.

3) Rocks with low Na and K are found somewhat removed from aplites and pegmatites, but exceptions occur, such as T1-6.

It must be kept in mind that the map, even at the scale drawn, is generalized. All rocks are inhomogeneous on scales of more than one meter. The "marble" contains numerous monomineralic pods of tremolite or pale green actinolite, as well as a few zones of pure magnesian biotite and zones of pure carbonate. The amphibolites contain pods which

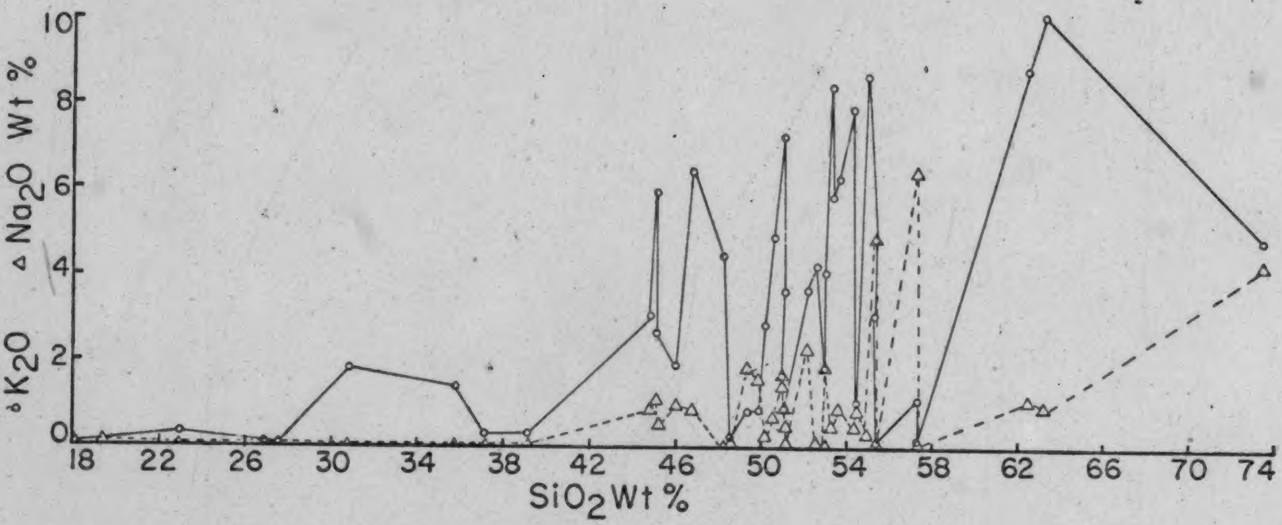

Fig. 63. K_2O (circles) and Na_2O (triangles) in weight percent plotted against SiO_2 for rocks from Kootenay Point.

are over 80% biotite, or 95% pargasitic hornblende.

From Tables 1 and 4, and Fig. 63, the remaining generalizations may be made:

4) High K_2O contents are correlated with high modal percentages of biotite where quartz is absent or high biotite and K-feldspar (microcline) where quartz is present.

5) Where Na_2O is low or zero, the only soda-bearing minerals in the rock are amphibole or diopside.

6) Where $Na_2O > K_2O$, quartz and plagioclase are present, except in the small aureoles.

7) As K_2O increases in a rock, Na_2O drops (generally). Where both drop together, K_2O and Na_2O are concentrated in one mineral (usually hornblende).

All observations can be best explained by differential mobility of alkali components. Any rock type, especially those plotting in the basalt-andesite or ultrabasic fields, should maintain a reasonable degree of homogeneity over the small distances involved here. It is obvious from the spatial distribution, chemistry and mineralogy of these rocks that inhomogeneity is the rule rather than the exception. If "amphibolites" alone are separated out, and if, as indicated at the beginning of this work, they are igneous in origin, such large variations are not to be expected. The lack of coherence between Na_2O and K_2O is also not to be expected in isochemical equilibrium systems. Thus we must conclude that metamorphism of rocks on Kootenay Point involved addition and subtraction of material, at least over distances of tens and perhaps hundreds of meters. The most likely mobile components are K and Na.

Other components, such as Si and Al may migrate. Solubility of Si is confirmed by fluid inclusion work from other areas, and the possibility of Al migration is suggested by the presence of biotite and feldspar in the carbonates.

The lack of Na_2O in many rocks can be explained in two ways. First, Na may not be as mobile an element as K. This has been found to be true for skarn rocks (Korzhinskii, 1957, 1965). Support for low mobility of Na on Kootenay Point can be found by examination of the spatial distribution of high soda rocks, as mentioned earlier. Second, Na may be as mobile as K, but it is not "stabilized" in the system unless there is enough excess SiO_2 and Al_2O_3 to form plagioclase. Support for this hypothesis lies in the fact that plagioclase and quartz occur together, and biotite may be subordinate to both.

Other reasons can be found, one obvious reason being that the original rocks were poor in soda. The only source for soda is plagioclase of low An content, and it is most prevalent in the pegmatitic and aplitic bodies from the Point. These bodies may also be a source for K. Another possibility is that P_{H_2O} controls the stability of biotite with respect to feldspar, and in high P_{H_2O} environments a hydrated phase such as biotite becomes stable, thus "fixing" K in the rock. P_{H_2O} would be related to P_{CO_2}, however, and evidence is present that P_{CO_2} was high in rocks containing biotite. It is felt that this latter possibility may be a control, along with differential mobility of K and favorable Si/Al ratio, on the formation of biotite over feldspar in high K rocks. This point cannot be proven, but fluid inclusion work on the silicate phases would provide information on the amount of CO_2 present and the composition of brine present at the time of crystallization.

Less mobile major cations like Mg, Fe and possibly Mn, more closely approach equilibrium during the prograde period of metamorphism, and then do not remobilize as readily during the time of cooling following the culmination of metamorphism. Titanium distribution is unexplainable by any of the above reasoning. Ti is one of the less mobile elements, and it may be that close approach to equilibrium for Ti is only possible where sustained high temperatures have existed for long periods of time.

Distribution of minor elements can be explained by change in chemical potential during the period of cooling. Some elements are quite soluble depending on brine composition and pH (Cu, Zn). The distribution of elements present in trace concentrations is very sensitive to changes in chemical potential. Thus, small changes will affect them to a larger extent than it will affect components present in larger amounts.

In summary, we may state with reasonable confidence that chemical equilibrium was not attained in rocks from the Point, but that some elements more closely approached equilibrium than others. The presence of aplites and pegmatites provide a source for K, and possibly for Na on a very small scale, but these elements were probably not introduced during intrusion. They may have been derived during the thermal event producing maximum metamorphism. Temperatures derived for metamorphism on the Point are consistent with partial melting of pegmatitic material at high total pressures. An alternative is to appeal to partial melting of material as yet unroofed existing still deeper and at higher temperatures.

ISOTOPE GEOLOGY

K-Ar

K-Ar age dating has been carried out throughout the region of the Kootenay Arc. Examination of the isotopic age map of Canada (Douglas, 1971) reveals the distribution of data points, with attendant ages. A compilation of all K-Ar age dates, including the ten ages from metamorphic rocks on Kootenay Point was made, and the results are plotted in Fig. 64. The bulk of all K-Ar ages for igneous rocks fall between 10 and 100 my, but a double peak is in evidence, with another concentration of ages between 120 and 180 my. The overwhelming majority of ages for metamorphic minerals fall between 10 and 90 my (including the 10 biotite dates from the Point). Only three ages from metamorphic hornblendes have been obtained. One of these is a 124 my date on an amphibolite pod about 1.5 km east of Kootenay Point (Baadsgaard, pers. comm., 1973). The other two are from the Shuswap Complex and give ages of 61± 6 and 79±8 my respectively (Wanless et al., 1967).

The meaning of these ages must be assessed with care, in view of the complex metamorphic history of the area. K-Ar ages are thought to represent the time at which the mineral dated becomes closed to Ar (Moorbath, 1967). This time, in view of activation energies derived for Ar in various minerals, may not be the actual time of crystallization of the mineral, but may be the time at which the temperature became low enough that diffusion of Ar was negligible. For micas, this temperature may be as low as 150-200°C (Moorbath, 1967). Amphibole activation energies for Ar are 3 to 4 times higher than those of biotite. Thus, amphiboles may retain argon at much higher temperatures, but the retentivity of amphi-

Fig. 64 a.

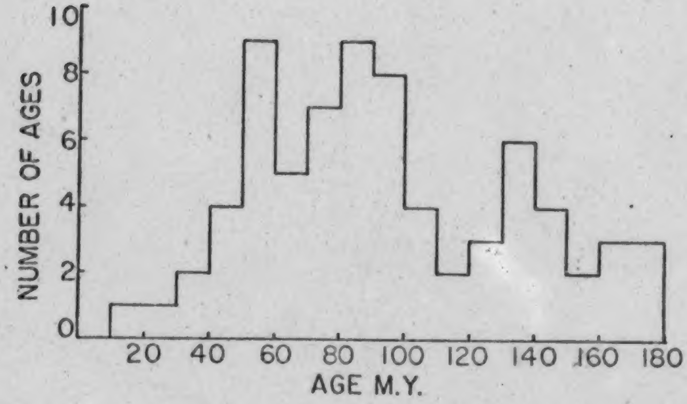

Fig. 64 b.

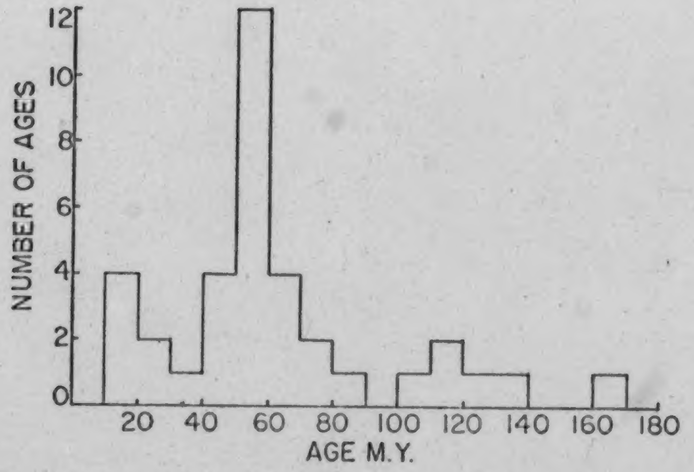

Fig. 64 a. Histogram plot of K-Ar ages from igneous rocks from the Kootenay Arc.

Fig. 64 b. Histogram plot of K-Ar ages for metamorphic minerals from the Kootenay Arc.

Data for Figs. 64 a and b are taken from the following: Lowdon (1960, 1961); Lowdon et al. (1962); Leech et al.,(1963); Wanless et al. (1964); Wanless et al. (1965); Wanless et al. (1966); Wanless et al. (1967).

bole has been shown to be dependent on composition by O'Nions et al. (1969). K-Ar ages from metamorphic minerals in the Kootenay Arc reflect the time that the mineral became closed to Ar, a time which may be considerably different from the actual time of crystallization (Moorbath, 1967; Dewey and Pankhurst, 1970). Igneous rocks which have not been deformed or subject to heating following crystallization should give the age of crystallization providing cooling was rapid.

With the above discussion in mind, an attempt can be made to interpret the data presented in Fig. 64. The igneous rocks show a wide spread of ages, with two groups evident, one centered around 70 my, the other 130-140 my. If the major metamorphism occurred at between 120-160 my, followed by continuous cooling, the spread of dates might be expected to tail from a concentration in this range. This is not the case, however, as the other concentration of ages occurs between 50 and 90 my. Available geological evidence suggests more than one period of metamorphism and further suggests that this later metamorphism has deformed and possibly recrystallized the margins of the older "batholithic" bodies like the Nelson and Kuskanax. Further support for this assumption is found in other parts of British Columbia and from the Cordillera in the United States. Ages from igneous bodies throughout both regions indicate an event somewhere between 50-70 my ago. Large outpourings of plateau type basalt lavas in central British Columbia are Miocene through Paleocene in age. Eocene and Paleocene lavas are quite extensive (Souther, 1972).

The assumption that K-Ar ages reflect the time the mineral has cooled has lead to the drawing of thermochrons by Dewey and Pankhurst (1970) for the Scottish Caledonides. The thermochrons mark the time the mineral was uplifted to a point below the thermal barrier leading to Ar diffusion. The pattern of thermochrons leads to the suggestion that less highly metamorphosed rocks will give ages closer to the true metamorphic age because they are uplifted through the barrier marking the closing temperature of the minerals sooner than more highly metamorphosed rocks.

Of the 36 ages from metamorphic minerals, most come from either greenschist or amphibolite facies. All but three are from micas. The youngest ages are found in the Shuswap metamorphic complex, which lies in the sillimanite zone or higher, but there is no systematic difference in age between minerals from amphibolite or greenschist facies. The entire spread shown in Fig. 64 may be found in either group. If the cooling theory is correct, then the amphibole ages should more nearly approximate the true age of metamorphism, but all three mentioned are intermediate between the postulated Jurassic event and the younger peak. The intermediate ages support the idea of overprinting, but obviously more data are needed.

The histogram for ages on metamorphic minerals, interpreted in the light of the above evidence, suggests a thermal event 50-70 my ago, and geological evidence cited earlier suggests that this thermal event may be associated with a younger metamorphism. The lack of any cluster of ages from metamorphic minerals around the interval of 130-180 my further substantiates this assumption, but K-Ar work on amphiboles and low-grade rocks is needed to confirm it. The cooling hypothesis, and that of a continuous metamorphic event as postulated by Dewey and Pankhurst (1970) for the Scottish Caledonides does not explain the situation found in the Kootenay Arc.

Rb-Sr

In Fig. 65, $^{87}Sr/^{86}Sr$ is plotted against $^{87}Rb/^{87}Sr$ for biotites and amphiboles from the Point. If the system in each rock became closed to ^{87}Sr at the same time, and if complete isotopic homogenization occurred, the lines joining amphibole and biotite should all be parallel, indicating that all minerals are the same age. This situation would be similar to that found for the Baltimore Gneiss by Wetherill et al. (1968).

Examination of Fig. 65 indicates that not all tielines joining pairs are parallel. Samples T4-2(2), 205-50W(5) and T4-6(7) are closely parallel, while the remainder are not. The biotite from 205-50W(5) is the best sample for isotopic dating because of the following: 1) It is the "cleanest" mica, having a difference of 0.04% between bulk K_2O and K_2O determined by microprobe analysis. 2) It has a very large $^{87}Rb/^{86}Sr$ ratio and a high proportion of radiogenic Sr. Thus, its position and the slope of the isochron associated with it are unlikely to be greatly affected by errors in assumption of the initial ratio, or determination of radiogenic strontium.

The age calculated for this biotite and for the hornblende coexisting with it is 48 ± 3 my. The age is in good agreement with the mean K-Ar ages of all the biotites. If we assume that this age reflects the time of the metamorphic event causing recrystallization of the minerals in rocks from the Point, the distribution of the other minerals can be explained in two ways:

First, if, as the K-Ar dates from igneous rocks and other geological data cited indicate, a period of metamorphism occurred in the Jurassic which affected these rocks, the position of the pairs and slope of the tielines result from overprinting and incomplete isotopic homogenization

Fig. 65. Rb-Sr mineral "isochrons" from amphibole-biotite pairs. Numbers refer to analyses in Table 21.

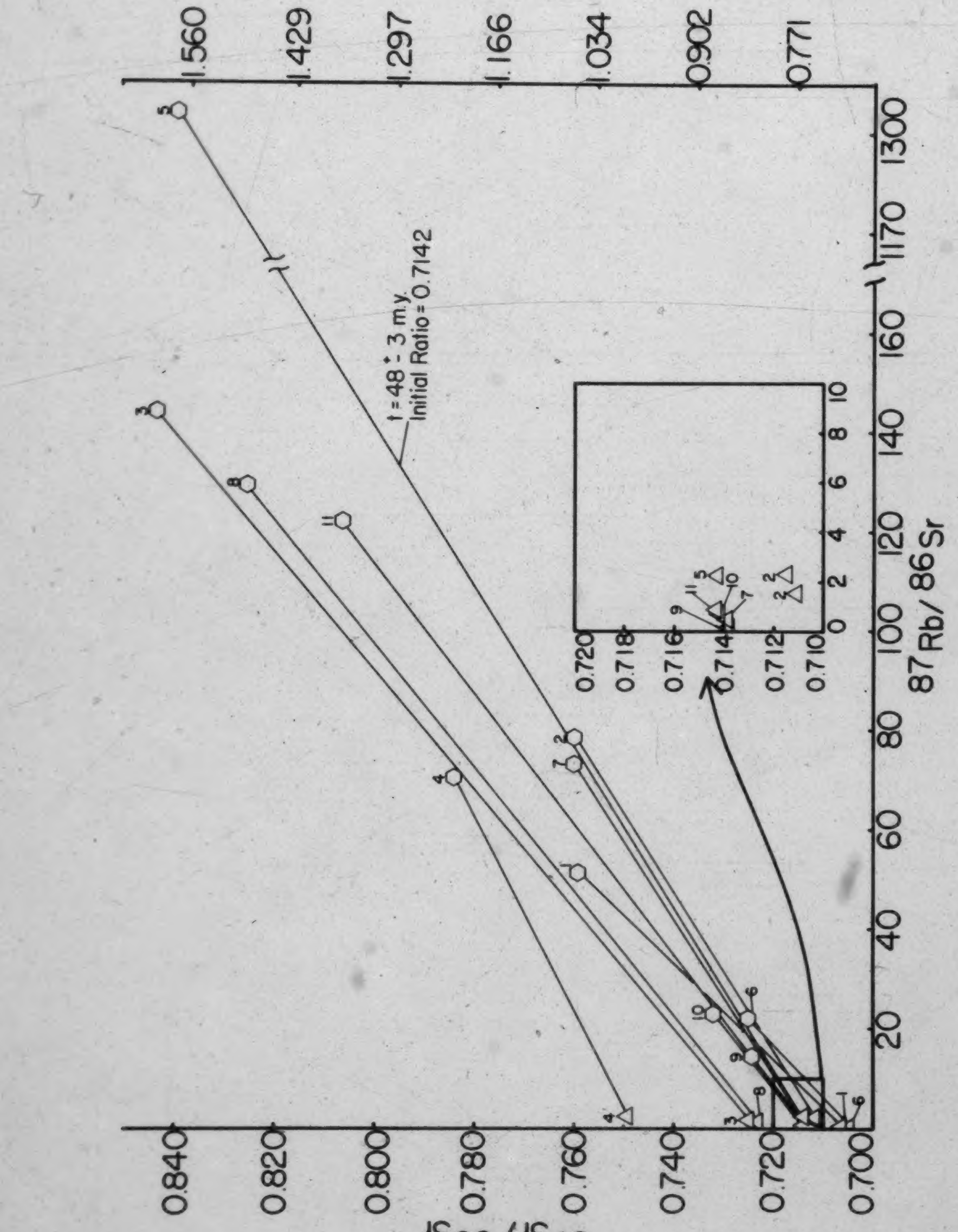
87Sr / 86Sr
0.700
0.720
0.740
0.760
0.780
0.800
0.820
0.840
87Rb / 86Sr
20
40
60
80
100
120
140
160
1170
1300
0.771
0.902
1.034
1.166
1.297
1.429
1.560
t = 48 ± 3 m.y.
Initial Ratio = 0.7142
0.710
0.712
0.714
0.716
0.718
0.720
0
2
4
6
8
10
1
2
3
4
5
6
7
8
9
10
11

of the previously formed minerals. In this case, Rb/Sr whole rock isochrons would give the earlier age, but the later event would cause loss of radiogenic Sr from biotite (relative to the whole rock) and gain of radiogenic Sr in amphibole (relative to the whole rock). The effect would be to rotate the tieline around the position of the whole rock, which would probably lie close to the present amphibole position, lowering the slope of the line. This rearrangement occurs because, if re-homogenization and equilibration are not complete, the minerals do not take up the new initial ratio of the whole rock at the time of metamorphism, but attain a value between it and the mineral ratio at the time of the event.

The overprint hypothesis is supported by the fact that all tielines are not parallel, but, with the exception of T3-12a (4), their pattern is systematically arranged with respect to 205-50W. All other pairs are "older" than 205-50W. T3-12a(4) is conspicuously against the trend and cannot be accounted for by experimental error. Further work is being done on this sample. The effect of zoning in the amphiboles also fits this hypothesis. Those amphiboles which are zoned lie outside the clustered group, except for T4-6a(7). Zoning is strongest in samples which are enriched in radiogenic Sr, but weakly zoned amphiboles do not necessarily have the lowest ratio. The strongly zoned amphiboles are enriched in Ca in the rim area, an indication of the possibility that Sr may have been incorporated during zoning. If the incorporated Sr is more radiogenic than the original, it would serve to raise the $^{87}Sr/^{86}Sr$ ratio of the amphiboles.

The second explanation is that, during cooling, or during a subsequent phase of metamorphism, Rb and Sr migrated in and out of the system with the K and Na rich fluids already known to exist. If a fluid with the average isotopic composition of the whole rock was introduced into the system, the effect would be the same as that of recrystallization and re-homogenization. If the fluid can react with either biotite or amphibole, it will change the $^{87}Sr/^{86}Sr$ ratio. The result would be to lower the $^{87}Sr/^{86}Sr$ ratio of the biotite (because the biotite would be likely to have more radiogenic Sr resulting from higher Rb content) and to raise the $^{87}Sr/^{86}Sr$ ratio of the amphibole. This would lower the slope of the line, and thus the "age". The situation is further complicated by the necessary assumption that Rb may be either gained or lost during the influx of fluids. If the fluid is high in Rb, it would increase the Rb content of both mica and amphibole, resulting in higher $^{87}Rb/^{86}Sr$ ratios and consequent lowering of "age". If the fluid was lower in Rb, the opposite would occur. Both elements would presumably be present in the fluids and would interact.

Evidence for the second hypothesis can be found in the distribution patterns for the alkalis, and the evidence for open systems with regard to alkalis discussed in the last section.

Neither hypothesis can be proved with the data presently available, but from the standpoint of simplicity, the first hypothesis is the more attractive. The author believes that the second cannot be ignored in the light of other evidence available and suggests that both processes may be coupled to produce the patterns seen here.

The bearing of Rb/Sr isotopic "ages" may be discussed with the above ideas in mind. It has been suggested by Moorbath (1967), and evidence has been presented by Hart (1964) that Sr may behave in a manner similar to that of Ar in minerals. If this is the case, then a mineral isochron age is the time of cooling to the temperature wherein Sr no longer diffuses from the mineral. Supporting evidence for the cooling hypothesis comes from the study of mineral ages in the Caledonides by Dewey and Pankhurst (1970). In view of the pattern of the ages of the pairs, and the pattern indicated by K-Ar ages, the present author believes that the Rb/Sr mineral ages reflect a metamorphic event and not a simple cooling. If cooling were the case, the scatter of slopes is surprising. Furthermore, the scatter of K-Ar ages (which is outside the error range indicated) is surprising because all of these must have reached the same temperature at the same time. The scatter could reflect different closure times with respect to reaction with the fluid, however, in which case the ages indicate the end of metasomatic processes in the Kootenay Arc.

Further work needs to be done to decide the answer to these questions. Most useful would be systematic Rb/Sr whole-rock isochron studies of igneous bodies in the area, as well as whole-rock isochron work on the amphibolites within the sedimentary sequences. Whole rock Rb/Sr data on sediments are likely to be equivocal, but may be useful if the rocks have behaved as closed systems. Comparisons of age patterns between igneous rocks, meta-igneous rocks and metasediments might help to decide this question. Low-grade slaty rocks which might be suitable for K-Ar whole-rock dating outcrop to the north, south and east of the study area. Ages from such rocks may, as suggested by Moorbath (1967), give the true metamorphic age.

In conclusion, it is worthwhile to discuss briefly the implications of both trace element and isotopic work with regards equilibration of phases present in rocks from Kootenay Point. If the spread of K-Ar ages from metamorphic rocks reflects an event around 50-70 my, then the rocks have had a maximum of 40 my to re-equilibrate to the new set of conditions. The actual time spent at higher temperatures is probably considerably less than this. If the age distributions result from continuous cooling of rocks which reached their thermal peak in the Jurassic, then they have had perhaps 100 my to re-equilibrate. In either case, viewed from the standpoint of classical concepts of chemical equilibrium in rocks and from comparison with experimental work, it is surprising that they have not done so. The available evidence suggests that neither isotopes, trace elements or major elements closely approached equilibrium except in two or three cases.

Viewed from the standpoint of irreversible reactions taking place in open systems, with mobile and inert components, under conditions which change with time and evolution of the complex, the lack of equilibrium is not surprising. Presumably, during the progression of a metamorphic event, fluid compositions change, fugacities of volatiles change and systems become closed (or open) at different times. These changes may occur in adjacent rocks (or small rock volumes), leading to different assemblages, partition coefficients and isotope values for the rocks and minerals in question. This is not to say that the laws of thermodynamics are disobeyed, or that the reactions do not proceed according to these laws, but that, in a natural system the variability of factors of equilibrium is such that actual equilibration is rare. In cases where equilibration does occur, the volumes over which it occurs may be small for major, minor and trace elements and for isotopes (Anderson, 1967).

CHAPTER V

GENERAL CONCLUSIONS REGARDING THE DEVELOPMENT OF THE KOOTENAY ARC

This chapter will deal with general conclusions regarding the origin of the Kootenay Arc and its place in the pattern of the Cordillera as a whole. This discussion, in its broader aspects, is of necessity somewhat speculative due to lack of detailed information of any kind for most of the regions to the north and south.

The Kootenay Arc is anomalous by structural standards. It deviates from the normal structural trend established over 2000 km of outcrop, from the Yukon south into the United States. Whether or not the Kootenay Arc is a metamorphic anomaly is less certain because detailed studies are restricted to small areas in the southern portion of the Cordillera. This author believes that the Kootenay Arc is not an anomalous metamorphic feature, and that it fits with the development of the Cordillera as a whole, both through timing and type of metamorphism. These conclusions will be discussed in more detail in the remainder of this section.

Metamorphism in the Kootenay Arc affected all rocks from Precambrian to Triassic age. All rocks younger than the Windermere (Horsethief Creek Group) are obviously polymetamorphic and have been affected by phase I and II folds. Zoned garnets in the Horsethief Creek, as well as identification of f_1 and f_2 foliations indicate that rocks are also polymetamorphic and polydeformational. The deformation and polymetamorphic character of the Milford Group rocks are readily recognizable, contradicting the conclusions of Read (1973).

Precambrian through Devonian and possibly Mississippian sedimentation is believed to represent shelf-slope-rise conditions with a source area to the east, represented by the craton (Gabrielse, 1972; Monger _et al._, 1972). The accumulation of sedimentary material is estimated at 11,500 meters by Monger _et al_. (1972). Sometime during the Proterozoic, rifting occurred parallel to the craton margin, a rift apparently the length of the entire North American cordillera (Burchfiel and Davis, 1972; Monger _et al._, 1972). This rift is postulated to place an unrecorded mass of continental crust to the west, and no evidence of such a body may be found in the sedimentary record. It is during this period that the main sedimentary units found in the central Kootenay Arc were deposited. The sediments indicate variations in character of the source area and type of sedimentation, generally going from eugeosynclinal (Windermere) to miogeosynclinal (Cambrian-Devonian-Carboniferous) and back to eugeosynclinal from Permian to middle Jurassic. This is a simplified sequence, but would generally hold for the entire Kootenay Arc (Yates, 1973). Yates (1973) considers that the Kootenay Arc derived its shape at this time, and that the sedimentary record does not indicate a plate junction during the entire history of deposition.

The Devono-Mississippian boundary marks the first appearance of west-derived sediments in the Canadian and United States cordillera (Monger _et al._, 1972; Burchfiel and Davis, 1972). Areas indicating westward souces are found in the northern Canadian cordillera and the southern cordillera of the United States. The presence of sediments with sources to the west indicates a land body to the west in Devonian or Mississippian times. This body may be continuous over the entire length of the North American Craton, but its existence is mainly speculative.

Most authors writing on the Cordillera agree that a major metamorphic-plutonic and deformational event occurred during late Triassic or early Jurassic time (Monger et al., 1972; Wheeler et al., 1972; Burchfiel and Davis, 1972; Coney, 1972). This event affects the entire North American Cordillera. It is during the Triassic-Jurassic period of disturbance that the Canadian Cordillera acquires its basic shape and tectonic elements, and the general form of the Cordillera of the United States is achieved by the end of this period. The Omineca crystalline belt, of which the Kootenay Arc is a part, is at least partly constructed during this time, based on K-Ar ages from various plutonic bodies. (See Monger et al., 1972 and Wheeler et al., 1972 for discussion.) The basic form of the Omineca crystalline belt is one of a paired metamorphic belt described by Miyashiro (1972). The Hinterland fold belt is bounded to the east by high-grade metamorphic rocks of the Shuswap and Wolverine complexes. This configuration has led Monger et al. (1972) to propose a subduction zone lying beneath the Hinterland belt during Triassic and Jurassic time. There are a number of problems with this interpretation when analyzed on a smaller scale. First, and perhaps most important, is that the timing of the Hinterland belt blueschists and the Shuswap terrain is different. The blueschists are interpreted as Triassic on stratgraphic grounds, but two dates of 165 and 129 my have been obtained for crossite bearing schists from the Dease Lake map area, placing it as Jurassic-Cretaceous (Monger and Hutchinson, 1971). Considerable discussion of a single small intrusive pluton in the Shuswap metamorphic complex yielding an age of 143 my has been generated, and this age is often cited as a closing date for Shuswap metamorphism (Monger and Hutchinson, 1971; Monger et al., 1972; Wheeler et al., 1972). Examination of the isotopic age map of Canada (Douglas, 1970) reveals several metamorphic and plutonic dates of about 50 MY for the complex, and cobbles of presumed Shuswap material are found in Eocene sediments to the south and west in the Bonaparte Lake map area (Campbell and Tipper, 1971). In the light of this evidence, it appears that Cretaceous-Jurassic ages for the Shuswap are not established. Burchfiel and Davis (1972) consider Shushwap type infrastructure to be related to independent thermal events in the backarc region, but, using this hypothesis, the implication is for interrupted subduction between Triassic-Jurassic and late Cretaceous-early Tertiary times.

There is considerable evidence, then, of a Triassic-Jurassic event, and this event moves material of island affinity eastward. I would suggest that this eastward movement of material marks the initial development of the structure of the Kootenay Arc, as the Paleozoic and Mesozoic sediments are trapped between the Purcell anticlinorium and the oncoming proto-Arc which represents the Omineca Crystalline belt. Some metamorphism may have occurred at this time, but its extent and grade is not known. There are indications within and to the north of the study areas of Jurassic-Cretaceous metamorphism. Read (1973) reports deformation of the Kuskanax Batholith, which dates at 178 my by K-Ar (from the "undeformed" core). The Nelson batholith is complex and obviously composite. Ages range from Jurassic to late Cretaceous, but it is deformed intensively at the margins. The "thermal aureole" reported by Fyles (1967) may not exist, thus deformation may be post-intrusion. The Crawford

Bay stock, White Creek Batholith and smaller batholiths from the Creston area give ages from 100 my to approximately 50 my.

Major reorganizations of the Cordillera in the United States are said to take place between 90-80 my and between 50-40 my (Coney, 1972). Major plutons comprising the Sierra Nevada plutonic complex range in age from 210 my to 80 my, with ages of the Peninsular batholith from 120-80 my (Coney, 1972). These ages fit well with ages from the Canadian Cordillera and from the region surrounding the Kootenay Arc. Another series of dates from about 50 my occurs throughout the United States and Canadian Cordillera, and I propose that these ages reveal a real metamorphic event which involves the entire North American Cordillera and correlates with the end of the Laramide orogenic period (Coney, 1972). The metamorphism responsible for the major mineral assemblages present in the higher grade portions of the central Kootenay Arc occurs during the Laramide pulse, but it may overprint earlier metamorphic events. The ages in the Kootenay Arc can not be interpreted as simple cooling ages, but a major remixing of isotopes caused by elevated temperatures during widespread regional metamorphism. The primary evidence for this interpretation is as scanty at present as that for Jurassic metamorphism. It lies in the interpretation of the Rb-Sr mineral isochrons from Kootenay Point, and several muscovite and biotite dates from surrounding regional metamorphic rocks and smaller plutonic bodies. It lies as well in the assumption that a major event affecting the Cordillera in the United States must also affect the Canadian Cordillera and leads to the assumption that the two are linked to a single cause.

Deformation must outlast metamorphism in the Kootenay Arc, as cataclasis without later recrystallization is evident in all smaller igneous bodies studied and in some of the metamorphic rocks. Furthermore, evidence for pervasive retrogression exists in all areas of the central arc studied. I would suggest that this retrogression occurs during falling temperatures and uplift of the rocks in the central Kootenay Arc.

The major metamorphism takes place under conditions of moderate to low thermal gradient and high pressure as the material is compressed and forced down during compression from the eastward migrating Omineca crystalline complex. There is no real evidence for a subduction zone in the region of the Kootenay Arc, although Coney (1972) postulates overriding of entrained subduction zones to be responsible for both the Savier-Columbian Orogeny and the later Laramide pulse. Monger et al. (1972) have proposed subduction zones, sometimes double, during Jurassic to Oligocene time, migrating progressively westward with time.

It is suspected that the Kootenay Arc behaves as a backarc downwarp of varying mobility from Triassic to at least Eocene times, whereupon it is uplifted as part of the Omineca crystalline complex. The Kootenay Arc is separated from the high-grade metamorphic rocks of the Shuswap metamorphic complex by mylonite zones which may extend the entire length of the Arc. The mylonites have been previously interpreted (Reesor and Moore, 1971) as due to gravity sliding, but they could be a major tectonic boundary between the Kootenay Arc and associated older complexes and the Shuswap metamorphic complex, marking a zone of differential uplift between the two tectonic and metamorphic regions. The pressures indicated for both Kootenay Arc metamorphism and Shuswap metamorphism necessitate more than 20 km of uplift between the end of metamorphism and the present.

It is hoped that this study has solved some of the complex problems which exist in the central Kootenay Arc, and perhaps more importantly, has indicated directions for further research. It is clear that the metamorphic and structural evolution of the Kootenay Arc is more complex than given here. A detailed geochronological study should be undertaken on metamorphic rocks from the Kootenay Arc to elucidate timing of metamorphism, while at the same time detailed petrological studies on the Nelson and Kuskanax "batholiths" should be undertaken. Further work on metamorphic rocks in the region of the isograds mapped during the course of this work should also be undertaken.

REFERENCES CITED

ALBEE, A. L. (1965) Phase equilibrium in three assemblages of kyanite-zone pelitic schists, Lincoln Mountain Quadrangle, Central Vermont. J. Petrology, 6, 246-301.

ANDERSON, A. T. (1967) The dimension of isotopic equilibrium attainment during prograde metamorphism. J. Geol., 75, 323-332.

ANNERSTEN, H. AND T. EKSTROM (1971) Distribution of major and minor elements in coexisting minerals from a metamorphosed iron formation. Lithos, 4, 185-204.

ATHERTON, M. P. (1968) The variation in garnet, biotite and chlorite composition in medium grade pelitic rocks from the Dalradian, Scotland, with particular reference to the zonation in garnet. Contrib. Mineral. and Petrology, 18, 347-371.

_____, AND W. M. EDMUNDS (1966) An electron microprobe study of some zoned garnets from metamorphic rocks. Earth and Planet. Sci. Letters, 1, 185-93.

BANNO, S. (1964) Petrologic studies on Sanbagawa crystalline schists in the Bessi-Ino district, central Sikoku, Japan. Tokyo Univ. Fac. Sci. J., Ser. 2, v. 15, 203-319.

BARTH, T. F. W. (1969) Feldspars. Wiley-Interscience, New York. 261 pp.

BENCE, A. E. AND A. L. ALBEE (1968) Empirical correction factors for the electron microanalysis of silicates and oxides. J. Geol., 76, 382-403.

BLACKBURN, W. H. (1968) The spatial extent of chemical equilibrium in some high grade metamorphic rocks from the Grenville of southeastern Ontario. Contrib. Mineral. Petrology, 19, 72-92.

BODART, D. E. (1969) Direct colorimetric determination of nickel with furildioxime. Z. Anal. Chem., 247, 32-36.

BOETTCHER, A. L. (1970) The system $CaO-Al_2O_3-SiO_2-H_2O$ at high pressures and temperatures. J. Petrology, 11, 337-379.

BONNICHSEN, B. (1969) Metamorphic pyroxenes and amphiboles in the Biwabik Iron Formation, Dunka River area, Minnesota. Mineral. Soc. Amer. Spec. Pap. 2, 217-241.

BROWN, E. H. (1967) The greenschist facies of Eastern Otago, New Zealand. Contrib. Mineral. Petrology, 14, 259-292.

BROWN, E. H. (1968) The Si^{4+} content of natural phengites: A discussion. Contrib. Mineral. Petrology, 17, 78-81.

BURCHFIEL, B. C. AND G. A. DAVIS (1972) Structural framework and evolution of the southern part of the cordilleran orogen, western United States. Amer. J. Sci., 272, 97-118.

BURNS, R. G. (1970) Mineralogical Applications of Crystal Field Theory. Cambridge University Press, Cambridge. 224 pp.

BUTLER, B. C. M. (1965) A chemical study of the Moine series. Quart. J. Geol. Soc. London, 121, 163-208.

_____ (1967) Chemical study of minerals from the Moine series of the Ardnamurchan area, Argyllshire, Scotland. J. Petrology, 8 233-267.

CAIRNES, C. E. (1928) Geological reconnaissance in Slocan and Upper Arrow Lakes area, Kootenay District, British Columbia. Geol. Surv. Can. Summary Rep. 1928, 94-108.

CAMPBELL, R. B. AND H. W. TIPPER (1971) Geology of Bonaparte Lake map area, British Columbia. Geol. Surv. Can. Mem. 363. 100 pp.

CHRISTIE, O. H. J. (1962) Feldspar structure and the equilibrium between plagioclase and epidote. Amer. J. Sci., 260, 149-153.

CIPRIANI, C., F. P. SASSI AND A. SCHOLARI (1971) Metamorphic white micas: definitions of paragenetic fields. Schweiz. Mineral. Petrology. Mitt., 51, 259-302.

COCCO, G., L. FANFANI AND P. F. ZANAZZI (1972) Rubidium. In K. H. Wedepohl, Ed., Handbook of Geochemistry. Springer-Verlag, Berlin. pp. 37-A-1 - 37-A-3.

COLEMAN, R. G. AND J. R. CLARK (1968) Pyroxenes in the blueschist facies of California. Amer. J. Sci., 266, 43-59.

CONEY, P. J. (1972) Cordilleran tectonics and North American plate motion. Amer. J. Sci., 272, 603-628.

COOPER, A. F. (1972) Progressive metamorphism of metabasic rocks from the Haast Schist Group of Southern New Zealand. J. Petrology, 13, 457-492.

_____ AND J. F. LOVERING (1970). Greenschist amphiboles from Haast River, New Zealand. Contrib. Mineral. Petrology, 27, 11-24.

CRAWFORD, M. L. (1966) Composition of plagioclase and associated minerals in some schists from Vermont, U. S. A. and South Westland, New Zealand, with inferences about the peristerite solvus. Contrib. Mineral. Petrology, 13, 269-294.

CRAWFORD, M. L. (1972) Plagioclase and other mineral equilibria in a contact metamorphic aureole. *Contrib. Mineral. Petrology*, 36, 293-314

CROSBY, P. (1960) *Structure and Petrology of the Central Kootenay Lake Area, British Columbia*. Ph.D. Thesis, Harvard University, Cambridge, Massachusetts. 298 pp.

_____ (1968) Tectonic, plutonic and metamorphic history of the central Kootenay Arc, British Columbia, Canada. *Geol. Soc. Amer. Spec. Pap*. 99. 94 pp

CROWLEY, M. S. AND R. ROY (1964) Crystalline solubility in the muscovite and phlogopite groups. *Amer. Mineral*., 49, 348-362

DEER, W. A., R. A. HOWIE AND J. ZUSSMAN (1966) *An Introduction to the Rock Forming Minerals*. Longmans, Green and Co., Ltd., London.

DE VORE, G. W. (1955) The role of absorption in the fractionation and distribution of elements. *J. Geol*., 63, 159-190

DEN TEX, E. (1971) The facies groups and facies series of metamorphism, and their relation to physical conditions in the earth's crust. *Lithos*, 4, 23-31.

DEWEY, J. F. AND R. J. PANKHURST (1970) The evolution of the Scottish Caledonides in relation to their isotopic age pattern. *Royal Soc. Edinburgh Trans*., 68, 361-388.

DOBRETSOV, N. L. (1968) Paragenetic types and compositions of metamorphic pyroxenes. *J. Petrology*, 9, 358-377.

DODDS, C. J. (1965) *A Study of Garnets and Host Rocks from the Central Kootenay Lake Area, Southeastern British Columbia*. M.Sc. Thesis, University of Alberta, Edmonton, Alberta. 154 pp.

DOUGLAS, R. J. W., ED. (1970) Geology and economic minerals of Canada. *Geol. Surv. Can. Econ. Geol. Rept.* 1. 838 pp.

EDMUNDS, W. M. AND M. P. ATHERTON (1971) Polymetamorphic evolution of garnet in the Fanad Aureole, Donegal, Eire. *Lithos*, 4, 147-161.

EKSTROM, T. (1972) Coexisting scapolite and plagioclase from two iron formations in northern Sweden. *Lithos*, 5, 175-185

ENGEL, J. C. (1972) Determination of purity of mineral separates used in K-Ar dating; an interpretative review. *Can. Mineral*., 11, 743-759.

ENGEL, A. E. J. AND C. G. ENGEL (1960) Progressive metamorphism and granitization of the major paragneiss northwest Adirondack Mountains, New York, Part II. *Geol. Soc. Amer. Bull*., 71, 1-58

ERNST, W. G. (1963) Significance of phengitic micas from low-grade schists. *Amer. Mineral*., 48, 1357-1373

ERNST, W. G., Y. SEKI, H. ONUKI AND M. C. GILBERT (1970) Comparative study of low-grade metamorphism in California coast ranges and outer metamorphic belt of Japan. Geol. Soc. Amer. Mem., 124. 276 pp.

EVANS, B. W.,(1964) Coexisting albite and oligoclase in some schists from New Zealand. Amer. Mineral., 49, 173-179.

_____, D. M. SHAW AND D. R. HAUGHTON (1969) Scapolite stoichiometry. Contrib. Mineral. Petrology, 24, 293-305.

FEDIUKOVA, E. AND Z. VEJNAR (1971) Optic and cryptic zoning of garnets in West Bohemian amphibolites. Lithos, 4, 205-212.

FLANAGAN, F. J. (1973) 1972 values for international geochemical reference samples. Geochim. Cosmochim. Acta, 37, 1189-1201.

FLEISCHER, M. (1969) U.S. Geological Survey standards - I. Additional data on rocks G-1 and W-1, 1965-1967. Geochim. Cosmochim. Acta, 33, 65-79.

FOSTER, M. D. (1956) Correlation of dioctahedral potassium micas on the basis of their charge relations. U. S. Geol. Surv. Bull. 1036-D, 57-67.

_____ (1960) Interpretation of the composition of trioctahedral micas. U. S. Geol. Surv. Prof. Pap. 354-B. 49pp.

FRANCIS, G. H. (1958) Petrological studies in Glen Urquart Inverness-shire. Brit. Mus. (Natural Hist.) Mineralogy Bull. vol. 1, no. 5, 123-169.

_____, (1964) Further petrological studies in Glen Urquart, Inverness-shire. Brit. Mus. (Natural History) Mineralogy Bull., vol. 1, no. 6, 165-198.

FRIEDMAN, G. (1960) Chemical analyses of rocks with the petrographic microscope. Amer. Mineral., 45, 69-78.

FYLES, J. T. (1964) Geology of the Duncan Lake Area, Lardeau District, British Columbia. B. C. Dept. of Mines and Petroleum Resources Bull. 49. 87 pp.

_____ (1967) Geology of the Ainsworth-Kaslo Area, British Columbia. B. C. Dept. of Mines and Petroleum Resources Bull. 53. 125 pp.

_____ AND G. E. P. EASTWOOD (1962) Geology of the Ferguson Area, Lardeau District, British Columbia. B. C. Dept. of Mines Bull. 45.

GABRIELSE, H. (1972) Younger Precambrian of the Canadian Cordillera. Amer. J. Sci., 272, 521-536.

GHOSE, N. C. (1968) Genesis of a calc-silicate skarn at Richughuta District Palaman, Bihar. Bull. Geochem. Soc. India, 3, 35-38.

GOLDSMITH, J. R. (1960) Exsolution of dolomite from calcite. J. Geol., 68, 103-109.

_____ AND D. L. GRAF (1960) Subsolidus relations in the system $CaCO_3$-$MgCO_3$-$MnCO_3$. J. Geol., 68, 324-335.

_____, _____ AND J. WITTERS (1962) Studies in the system $CaCO_3$-$MgCO_3$-$FeCO_3$: 1. Phase relations; 2. A method for major element spectrochemical analysis; 3. Compositions of some ferroan dolomites. J. Geol., 70, 659-688.

_____ AND H. C. HEARD (1961) Subsolidus phase relations in the system $CaCO_3$- $MgCO_3$. J. Geol., 69, 45-74.

_____ AND R. C. NEWTON (1969) P-T-X relations in the system $CaCO_3$-$MgCO_3$ at high temperatures and pressures. Amer. J. Sci. 267A, 160-190.

GOODMAN, R. (1972) The distribution of Ga and Rb in coexisting groundmass and phenocryst phases of some basic volcanic rocks. Geochim. Cosmochim. Acta, 36, 303-317.

GORBATSCHEV, R. (1969) Element distribution between biotite and Ca-amphibole in some igneous and pseudo igneous plutonic rocks. Neues Jahrb. fur Mineral. Abhandl., 111, 314-342.

GRANT, J. A. AND P. W. WEIBLEN (1971) Retrograde zoning in garnet near the second sillimanite isograd. Am. J. Sci., 270, 281-296.

GUIDOTTI, C. V. (1969) A comment on 'A chemical study of minerals from the Moine Schists of Ardnamurchan area, Argyllshire, Scotland' by B. C. M. Butler and its implications for the phengite problem. J. Petrology, 10, 164-170.

_____ (1970) The mineralogy and petrology of the transition from the lower to upper sillimanite zone in the Oquossoc Area, Maine. J. Petrology, 11, 277-336.

HART, S. R. (1964) The petrology and isotopic mineral age relations of a contact zone in the Front Range, Colorado. J. Geophys. Res., 72, 493-525.

HAUGHTON, D. R. (1971) Plagioclase-scapolite equilibrium. Can. Mineral., 10, 854-870.

HEITANEN, A. (1967) On the facies series in various types of metamorphism. J. Geol., 75, 187-214.

HOLDAWAY, M. J. (1965) Basic regional metamorphic rocks in part of the Klamath Mountains, Northern California. Amer. Mineral. 50, 953-977.

_____ (1966) Hydrothermal stability of clinozoisite plus quartz. Amer. J. Sci., 264, 643-667.

HOLDAWAY, M. J. (1972) Thermal stability of Al-Fe epidote as a function of f_{O_2} and Fe content. *Contrib. Mineral. Petrology*, 37, 307-340.

HOLLISTER, L. S. (1966) Garnet zoning: an interpretation based on the Rayleigh fractionation model. *Sci.*, 154, 1647-1651.

_____ (1969) Contact metamorphism in the Kwoiek area of British Columbia. An end member of the metamorphic process. *Geol. Soc. Amer. Bull.*, 80, 2465-2494.

HORMANN, P. K. AND G. MORTEANI (1972) Mineralogical and chemical composition of some carbonate minerals from the Zillerthal Alps, Tyrol, Austria. *Tschr. Mineral. Petrologisches Mitt.* 17, 46-59.

HUNAHASHI, M., C. W. KIM, Y. ONTA AND T. TSUCHIYA (1968) Co-existence of plagioclases of different compositions in some plutonic and metamorphic rocks. *Lithos*, 1, 356-373.

HUTCHEON, I. AND J. M. MOORE (1973) The tremolite isograd near Marble Lake, Ontario. *Can. J. Earth Sci.*, 10, 936-947.

IIYAMA, J. T. (1964) Etude des réactions d'échange d'ions Na-K dans la série muscovite-paragonite. *Bull. Soc. Franc. Mineral. Cristallogr.*, 87, 532-541.

INGAMELLS, C. O., J. C. ENGELS AND P. SWITZER (1972) Effect of laboratory sampling error in geochemistry and geochronology. *24th Int. Geol. Congr. Proc.*, Sec. 10, 405-415.

JONES, J. W. (1972) An almandine garnet isograd in the Rogers Pass Area, British Columbia: The nature of the reaction and an estimation of the physical conditions during its formation. *Contrib. Mineral. Petrology*, 37, 291-306.

KLEIN, C. (1969) Coexisting amphiboles. *J. Petrology*, 9, 281-330.

KORZHINSKII, D. S. (1957) *Physicochemical Basis of the Analysis of the Paragenesis of Minerals*. Consultants Bureau, New York. 142 pp.

_____ (1965) The theory of systems with perfectly mobile components and the process of mineral formation. *Amer. J. Sci.*, 263, 193-205.

_____ (1966) On the thermodynamics of open systems and the phase rule. (A reply to D. F. Weill and W. S. Fyfe). *Geochim. Cosmochim. Acta*, 30, 829-835.

_____ (1967) Factors determining the acidity and basicity of the environment of mineral formation. *Mineralium Deposita*, 2, 1-4.

_____ (1970) *Theory of Metasomatic Zoning*. Clarendon Press, Oxford. 159 pp.

KOSTYUK, E. A. AND V. S. SOBOLEV (1969) Paragenetic types of calciferous amphiboles of metamorphic rocks. *Lithos*, 2, 67-82.

KRETZ, R. (1959) Chemical study of garnet, biotite and hornblende from gneisses in south-eastern Quebec, with emphasis on distribution of elements in coexisting minerals. *J. Geol*., 67, 371-402.

______ (1960) The distribution of certain elements among coexisting Ca-pyroxenes, Ca-amphiboles and biotites in Skarns. *Geochim. Cosmochim*., 20, 161-191.

KURAT, G. AND H. G. SCHARBERT (1972) Compositional zoning in garnets from granulite facies rocks of the Moldanubicum zone, Bohemian Massif of lower Austria, Austria. *Earth and Planet. Sci. Letters*, 16, 379-387.

KWAK, T. A. P. (1970) An attempt to correlate non-predicted variations of distribution coefficients with mineral grain internal inhomogeneity using a field example studied near Sudbury, Ontario. *Contrib. Mineral. Petrology*, 26, 199-224.

LAMBERT, R. ST. J. (1959) The mineralogy and metamorphism of the Moine Schists of the Morar and Knoydart Districts of Inverness-shire. *Trans. Royal Soc. Edinburgh*, 63, part 3, no. 25, 553- 72.

LEAKE, B. E. (1965) The relationship between composition of calciferous amphiboles and grade of metamorphism. *In* W. S. Pitcher and G. W. Flynn, Eds., *Controls of Metamorphism*. Oliver and Boyd, Edinburgh, 299-318.

______ (1965) The relationship between tetrahedral Al and maximum possible octahedral Al in natural calciferous and subcalciferous amphiboles. *Amer. Mineral*. 50, 843-851.

______ (1968) Catalogue of analyzed calciferous and sub-calciferous amphiboles. *Geol. Soc. Amer. Spec. Pap*., 98.

______ (1970) The origin of the Connemara migmatites of the Cashal district, Connemara, Ireland. *Quart. J. Geol. Soc. London*, 125, 219-276.

LEECH, G. B., J. A. LOWDON, C. H. STOCKWELL AND R. K. WANLESS (1963) Age determinations and geological studies (including Isotopic ages - Rept. 4) *Geol. Surv. Can. Pap*. 63-17. 138 pp.

LITTLE, H. W. (1960) Nelson map area - west half, British Columbia. *Geol. Surv. Can. Mem*. 308. 205 pp.

LIVINGSTONE, K. W. (1968) *Geology of the Crawford Bay Map Area*. M. Sc. Thesis, University of British Columbia, Vancouver, British Columbia.

LOWDON, J. A. (1960) Age determinations by the Geological Survey of Canada. Report 1. Geol. Surv. Can. Pap. 60-17. 51 pp.

_____ (1961) Age determinations by the Geological Survey of Canada. Report 2. Geol. Surv. Can. Pap. 61-17. 127 pp.

_____, C. H. STOCKWELL, H. W. TIPPER AND R. K. WANLESS (1962) Age determinations and geological studies (including isotopic ages - Report 3.) Geol. Surv. Can. Pap. 62-17. 139 pp.

LYONS, J. B. AND S. A. MORSE (1970) Mg/Fe partitioning in garnet and biotite from some granitic, pelitic and calcic rocks. Amer. Mineral. 55, 231-245.

MAKANJUOLA, A. A. AND R. A. HOWIE. (1972) The mineralogy of the Glaucophane Schists and associated rocks from Ile de Groix, Brittany, France. Contrib. Mineral. Petrology, 35, 83-118.

MARAKUSHEV, A. A. (1964) Analysis of scapolite paragenesis. Geochem. Int., 114-126.

MATHER, J. D. (1970) The biotite isograd and the lower greenschist facies in the Dalradian rocks of Scotland. J. Petrology, 11, 253-275.

MIYASHIRO, A. (1953) Calcium-poor garnet in relation to metamorphism. Geochim. Cosmochim. Acta, 4, 179-208.

_____ (1958) Regional metamorphism of the Gosaisyo-Takanuki district in the central Abukuma Plateau. Tokyo Univ. Fac. Sci. J., Ser. 2, 2, 219-272.

_____ (1972) Metamorphism and related magmatism in plate tectonics. Amer. J. Sci. 272, 629-656.

MONGER, J. W. H. AND W. W. HUTCHISON (1971) Metamorphic map of the Canadian Cordillera. Geol. Surv. Can. Pap. 70-33. 61 pp.

_____, J. G. SOUTHER AND H. GABRIELSE (1972) Evolution of the Canadian Cordillera, a plate tectonic model. Amer. J. Sci., 272, 577-602.

MOORBATH, S. (1967) Recent advances in the application and interpretation of radiometric data. Earth-Sci. Rev., 3, 111-133.

MOXAM, R. L. (1965) Distribution of minor elements in coexisting hornblendes and biotites. Can. Mineral., 8, 204-240.

MUELLER, G. AND A. SCHNEIDER (1971) Chemistry and genesis of garnets in metamorphic rocks. Contrib. Mineral. Petrology, 31, 178-200.

MUNOZ, J. L. AND H. P. EUGSTER, (1969) Experimental control of fluorine reaction in hydrothermal systems. Amer. Mineral., 54, 943-959.

NIGGLI, P. (1954) *Rocks and Mineral Deposits*. W. H. Freeman and Co., San Francisco. 559 pp.

NOKLEBERG, W. J. (1973) CO_2 as a source of oxygen in the metasomatism of carbonates. *Amer. J. Sci.*, 273, 498-514.

O'NIONS, R. K. (1969) *Geochronology of the Bamble Sector of the Baltic Shield, South Norway*. Ph.D. Thesis, University of Alberta, Edmonton, Alberta.

_____, D. G. W. SMITH, H. BAADSGAARD AND R. D. MORTON (1969) Influence of chemical composition on argon retentivity in metamorphic calcic amphiboles from South Norway. *Earth and Planet. Sci. Letters*, 5, 339-345.

PARK, C. F. AND R. S. CANNON (1943) Geology and ore deposits of the Metaline Quadrangle, Washington. *U. S. Geol. Surv. Prof. Pap*. 202.

RAMBERG, H. AND G. DE VORE (1951) The distribution of Fe^{2+} and Mg^{2+} in coexisting olivines and pyroxenes. *J. Geol.*, 59, 193-210.

RAMSAY, C. R. (1973) *Metamorphism and Gold Mineralization of Archean Meta-sediments near Yellowknife, N.W.T., Canada*. Ph.D. Thesis, University of Alberta, Edmonton, Alberta.

_____ AND L. R. DAVIDSON (1970) The origin of scapolite in the regionally metamorphosed rocks of Mary Kathleen, Queensland, Australia. *Contrib. Mineral. Petrology*, 25, 41-51.

READ, P. B. (1973) Tectonic evolution of the central Kootenay Arc, British Columbia. *Geol. Soc. Amer. Abstr.*, 5, 95.

REESOR, J. E. AND J. M. MOORE (1971) Petrology and structure of Thor-Odin gneiss dome, Shuswap Metamorphic Comples, British Columbia. *Geol. Surv. Can. Bull.*, 195. 147 pp.

REITAN, P. H. (1972) Dependences of octahedral ion abundances in some metamorphic biotites (abstr.). *Amer. Geophys. Union. Trans.*, 53, 550.

RICE, H. M. A. (1941) Nelson map area - east half, British Columbia. *Geol. Surv. Can. Mem*. 228. 86 pp.

RIMSAITE, J. (1964) On micas from magmatic and metamorphic rocks. *Beitr. zur Mineral. Petrogr.*, 10, 152-183.

ROBINSON, P., M. ROSS AND H. W. JAFFE (1971) Composition of the anthophyllite-gedrite series, comparisons of gedrite-hornblende, the anthophyllite-gedrite solvus. *Amer. Mineral.*, 256, 1005-1041.

ROEDDER, E. (1972) The data of geochemistry: composition of fluid inclusions. U. S. Geol. Surv. Prof. Pap. 440JJ. 164 pp.

ROSENBERG, P. E. (1967) Subsolidus relations in the system $CaCO_3$- $MgCO_3$-$FeCO_3$. Amer. Mineral., 52, 787-796.

_____ (1968) Subsolidus relations on the dolomite join CaMg $(CO_3)_2$ - CaFe $(CO_3)_2$-CaMn $(CO_3)_2$. Amer. Mineral., 53, 880-889.

ROSS, M., J. J. PAPIKE AND K. W. SHAW (1969) Exsolution textures in amphiboles as indicators of subsolidus thermal histories. Mineral. Soc. Amer. Spec. Pap., 2, 275-299.

RUCKLIDGE, J. AND E. L. GASPARRINI (1969) EMPADR VII. University of Toronto, Dept. of Geology.

_____, _____, J. V. SMITH AND C. R. KNOWLES (1971) X-ray emission microanalysis of rock-forming minerals. VIII, Amphiboles. Can. J. Earth Sci., 8, 1171-1183.

SANDELL, E. B. (1959) Colorimetric Determination of Traces of Minerals. Interscience Pub., New York. 1032 pp.

SAXENA, S. K. (1966) Distribution of elements between coexisting biotite and hornblende in metamorphic Caledonides lying to the west and northwest of Trondheim, Norway. Neues Jahrb. fur Mineral. Mitt. 3, 67-80.

_____ (1968a) Crystal-chemical aspects of distribution of elements among certain rock-forming silicates. Neues Jahrb. fur Mineral. Abhandl. 108, 292-323.

_____ (1968b) Nature of mixing of ferromagnesian silicates and the significance of the distribution coefficient. Neues Jahrb. fur Mineral. Monatsch. 275-286.

_____ (1969a) Silicate solid-solutions and geothermometry. 3. Distribution of Fe and Mg between coexisting garnet and biotite. Contrib. Mineral. Petrology, 22, 259-267.

_____ (1969b) Distribution of elements in coexisting minerals and the problem of chemical disequilibrium in metamorphosed basic rocks. Contrib. Mineral. Petrology, 20, 177-197.

SCHOFIELD, S. J. (1920) Geology and ore deposits of the Ainsworth Mining Camp, British Columbia. Geol. Surv. Can. Mem., 117. 73 pp.

SCHWARCZ, H. (1967) The effect of crystal field stabilization on the distribution of transition metals between metamorphic minerals. Geochim. Cosmochim Acta, 31, 503-517.

SEIFERT, F. AND W. SCHREYER (1971) Synthesis and stability of micas in the system $K_2O-MgO-SiO_2-H_2O$ and their relations to phlogopite. Contrib. Mineral. Petrology, 30, 196-215.

SHAW, D. M. (1960a) The geochemistry of scapolite. Part 1. Previous work and general mineralogy. J. Petrology, 1, 218-260.

_____ (1960b) The geochemistry of scapolite. Part II. Trace elements, petrology and general chemistry. J. Petrology, 1, 261-285.

_____, R. L. BLOXAM, R. H. FILBY AND W. W. LAPKOWSKY (1963a) The petrology and geochemistry of some Grenville Skarns. Part I. Geology and petrography. Can. Mineral., 7, 420-440.

_____, _____, _____, _____ (1963b) The petrology and geochemistry of some Grenville Skarns. Part II. Geochemistry. Can. Mineral., 7, 578-616.

_____, H. P. SCHWARCZ AND S. SHEPPARD (1965) The petrology of two zoned scapolite skarns. Can. J. Earth Sci., 2, 577-595.

SKIPPEN, G. B. (1971) Experimental data for reactions in siliceous marbles. J. Geol. 79, 457-481.

SMITH, D. G. W. AND M. C. TOMLINSON (1970) An APL language computer program for use in electron microprobe analysis. State Geol. Surv. Univ. Kansas, Computer Contrib., 45. 28 pp.

SMITH, F. G. AND W. M. LITTLE (1959) Filling temperatures of H_2O-CO_2 fluid inclusions and their significance in geothermometry. Can. Mineral., 6, 380-388.

SMITH, J. V. (1965) X-ray emission microanalysis of rock-forming minerals. I: experimental techniques. J. Geol., 73, 830-864.

_____ (1972) Critical review of synthesis and occurrence of plagioclase feldspars and a possible phase diagram. J. Geol., 80, 505-525.

_____ AND P. H. RIBBE (1966) X-ray-emission micro-analysis of rock forming minerals. III: Alkali feldspars. J. Geol., 74, 197-216.

SNELLING, N. J. (1957) Notes on the petrology and mineralogy of the Barrovian Metamorphic zones. Geol. Mag., 94, 294-304.

SOUTHER, J. G. (1972) Mesozoic and Tertiary volcainism of the western Canadian Cordillera. Can. Dept. of Energy, Mines and Resources, Earth Phys. Branch, Publ., 42, 55-58.

SPRY, A. (1969) Metamorphic Textures. Pergamon Press, Ltd., Oxford. 350 pp.

STRENS, R. G. J. (1964) Epidotes of the Borrowdale Volcanic rocks of central Borrowdale. *Mineral. Mag.*, 33, 868-886.

SWEATMAN, T. R. AND J. V. P. LONG (1969) Quantitative electron-probe microanalysis of rock forming minerals. *J. Petrology*, 10, 332-379.

TAKENOUCHI, S. AND G. C. KENNEDY (1965) The solubility of carbon dioxide in Na Cl solutions at high temperatures and pressures. *Amer. J. Sci.*, 263, 445-454.

THOMPSON, J. B., JR. (1955) The thermodynamic basis for the mineral facies concept. *Amer. J. Sci.*, 253, 65-103.

_____ (1970) Geochemical reaction and open systems. *Geochim. Cosmochim. Acta*, 34, 529-551.

TURNER, F. J. (1970) *Metamorphic Petrology*. McGraw-Hill, New York. 403 pp.

VELDE, B. (1965) Phengite micas: synthesis, stability and natural occurrence. *Amer. J. Sci.*, 263, 886-913.

_____ (1967a) Quelques observations sur la teneur en aluminium des biotites, phengites et chlorites dans les Schistes cristallins. *Bull. Soc. Franc. Mineral. Cristallogr*. 90, 356-363.

_____ (1967b) Si^{4+} content of natural phengites. *Contrib. Mineral. Petrology*, 14, 250-258.

_____ (1968) The Si^{4+} content of natural phengites: A reply. *Contrib. Mineral. Petrology*, 17, 82-84.

WALKER, J. F. (1928) Kootenay Lake District, British Columbia. *Geol. Surv. Can. Summary Rep. Pt A*, 119-136.

_____ AND M. F. BANCROFT (1929) Lardeau map area, British Columbia, general geology. *Geol. Surv. Can. Mem*. 161. 142 pp.

WANLESS, R. K., R. D. STEPHENS, G. R. LACHANCE AND R. Y. H. RIMSAITE (1964) Age determinations and geological studies. Part 1: Isotopic ages, rep. 5. *Geol. Surv. Can. Pap*. 64-17. 126 pp.

_____, _____, _____, _____ (1965) Age determinations and geological studies. K-Ar isotopic ages, rep. 6. *Geol. Surv. Can. Pap*. 65-17. 101 pp.

_____, _____, _____ AND C. M. EDMONDS (1966) Age determinations and geological studies. K-Ar isotopic ages, rep. 7. *Geol. Surv. Can. Pap*. 66-17. 120 pp.

_____, _____, _____, _____ (1967) Age determinations and geological studies. K-Ar isotopic ages, rep. 8. *Geol. Surv. Can. Pap*. 67-2 part *A*. 141 pp.

WEILL, D. F. AND W. S. FYFE (1964) A discussion of the Korzhinskii and Thompson treatment of thermodynamic equilibrium in open systems. *Geochim. Cosmochim. Acta*, 28, 565-576.

_____, _____ (1967) On equilibrium thermodynamics of open systems and the phase rule (a reply to D. S. Korzhinskii) *Geochem. Cosmochim. Acta*, 31, 1167-1176.

WENK, E. (1970) Distribution of Al between coexisting micas in metamorphic rocks from the central alps. *Contrib. Mineral. Petrology*, 26, 50-61.

WETHERILL, G. W., G. L. DAVIS AND C. LEE-HU (1968) Rb-Sr measurements on whole rocks and separated minerals from the Baltimore Gneiss, Maryland. *Geol. Soc. Amer. Bull.* 79, 757-762.

WHEELE[illegible] O. (1963) Rogers Pass map area, British Columbia and Alberta. *Geol. Surv. Can. Pap.*, 62-32. 31 pp.

_____, J. D. AITKEN, M. J. BERRY, H. GABRIELSE, W. W. HUTCHISON, W. R. JACOBY, J. W. H. MONGER, E. R. NIBLETT, D. K. NORRIS, R. A. PRICE AND R. A. STACEY (1972) The Cordilleran structural province. *In* R. A. Price and R. J. W. Douglas, Eds., *Variations in Tectonic Styles in Canada*. *Geol. Ass. Can. Spec. Pap 11*. 688 pp.

WHITE, A. J. R. (1959) Scapolite bearing marbles and calc-silicate rocks from Tungkillo and Milendella, South Australia. *Geol. Mag.* 96, 285-306.

_____, B. W. CHAPPEL AND P. JAKES (1972) Coexisting clinopyroxene, garnet and amphibole from an 'eclogite', Kakanui, New Zealand. *Contrib. Mineral. Petrology*, 34, 185-191.

WINKLER, H. G. F. (1967) *Petrogenesis of Metamorphic Rocks*. Springer-Verlag, New York.

WINZER, S. R. (1973, in prep.) Zoned amphiboles from the Kootenay Arc, British Columbia. Submitted to *Contrib. Mineral. Petrology*.

WONES, D. R. (1967) *Layer Silicates*. Amer. Geol. Inst. Short Course Lecture Notes. pp. DRW 1-141.

YATES, R. G. (1973) Significance of the Kootenay Arc in Cordilleran tectonics. *Geol. Soc. Amer. Abstr.* 5, 125.

YODER, H. S. (1950a) The jadeite problem. Part I. *Amer. J. Sci.*, 248, 225-248.

_____ (1950b) The jadeite problem. Part II. *Amer. J. Sci.*, 248, 312-334.

_____ AND H. P. EUGSTER (1955a, b) Synthetic and natural muscovites. *Geochim. Cosmochim. Acta*, 8, 225.

ZEMANN, J. AND K. H. WEDEPOHL (1972) Zinc. In K. H. Wedepohl, Ed., Handbook of Geochemistry. Springer-Verlag, Berlin. pp. 30-D-1 - 30-D-12.

ZEN, E-AN (1961) Mineralogy and petrology of the system Al_2O_3-SiO_2-H_2O in some pyrophyllite deposits of North Carolina. Amer. Mineral., 46, 52-65.

ZIEBOLD, T. O. AND R. E. OGILVIE (1963) Quantitative analysis with the electron microanalyzer. Anal. Chem., 35 621-627.

_____, _____ (1964) An empirical method for electron microanalysis. Anal. Chem., 36, 822-827.

_____, _____(1966) Correlations of empirical calibration for electron microanalysis. In T. D. McKinley. Ed., The Electron Microprobe. John Wiley and Sons. pp. 378-389.

APPENDIX 1

ELECTRON PROBE MICROANALYSIS

All minerals were analyzed using an ARL-EMX microprobe equipped with light element facilities. The following general philosophy was adhered to throughout the two year period during which the analyses were made. First, standards were chosen for their structural and chemical similarity to the unknown in order to minimize the possibility of wavelength shift caused by valence change and differences in coordination. Thus, to the farthest extent possible, amphiboles were used as major element standards for amphiboles, micas for biotite and muscovite, feldspars for feldspar. Where standards were unreliable for certain elements, these elements were done using a standard dissimilar structurally, but with a concentration in the desired element which was close to the estimated concentration in the sample. An example would be Ti in the amphibole standard EPS 21-1. Because Ti in this standard is unreliable, Ti in EPS 12-1, a biotite, was used. Standards which had been analyzed by reputable analysts and used by a number of persons in the microprobe laboratory at the University of Alberta were used. Several of the standards were checked by Ramsay (1973) and Frisch (pers. comm.), as well as by the present author.

Secondly, when doing an analysis, sufficient counts were taken on standard and unknown to keep counting statistics reliable at the 99% confidence level. Runs were made using a 20 second count time at an accelerating potential of 15 kv and a beam current of 0.1 microamp (approximately 0.01 microamp specimen current). Those numbers that did not fit the criteria of homogeneity at the 99% confidence level were discarded, and further counts were taken.

Electron microprobe analyses may be corrected in a number of ways, but only two methods are used generally. One method (Smith, 1965) uses correction curves derived from a suite of standards of the same mineral as the unknown. This method demands a large number of standards, but is claimed to eliminate errors caused by poor standards and differences between standard and unknown. Another method, used by Sweatman and Long (1969) uses simple oxides as standards and corrects the raw results for atomic number, fluorescence and absorption. The method of Bence and Albee (1968), a development of the method of Ziebold and Ogilvie (1963, 1964, 1966), is widely used and is a compromise between the two, wherein a number of oxide and carefully selected mineral standards are used, empirical coefficients are derived and corrections applied for a specific takeoff angle and accelerating potential.

The method used by this laboratory uses a full library of standards and makes corrections for atomic number, fluorescence and absorption. These corrections are done by computer using the program PROBEDATA (Smith and Tomlinson, 1970) and the FORTRAN program EMPADR VII (Rucklidge and Gasparrini, 1969).

The mineral standard method is critically dependent on the reliability of the standard. Sweatman and Long (1969) believe that using a mineral standard, specially a complex mineral standard, can cause errors if only one analysis of the standard is done. Standards must be checked and applied carefully if this method is to succeed in producing reliable results. Utilizing oxide or simple mineral standards may lead to difficulties as well, because matrix corrections may be large and significant uncertainties remain in the correction formulae. Differences in bonding and coordination between elements in standard and sample may lead to wavelength shift, giving false intensity readings and introducing error. For this reason, standards were chosen which were of the same mineral type in as many cases as possible. With the proper choice of counting statistics and choice of standards, the maximum error will be that introduced by the errors in the standard analysis. (See Table A-1 for the standards used in this study.)

Of the standards used, EPS 12-1, 12-2, 21-1 and WS-1 have been evaluated by repeated analyses done in this laboratory. Results of comparisons on EPS 12-1, 12-2 and WS-1 may be found in Ramsay (1973). This author has done repetitive analyses on EPS 12-1, 12-2, and 21-1. Results for 12-1 and 12-2 agree with those of Ramsay; EPS 21-1 has been analyzed against EPS 21-2. These results indicate that the observed errors between two separate analyses are in most cases within the minimum statistical error to be expected at the 99% confidence level for the total counts recorded.

Tables A-3 and A-4 give the standards used for each element analyzed in each mineral from the regional metamorphic rocks and rocks from Kootenay Point respectively. It is immediately evident that a certain amount of deviation from the criteria listed earlier was necessary, especially for the regional rocks. Certain standards, like EPM-83 for feldspar, contain no Ti or Mg, or insufficient Ca for accurate determination. Therefore, another standard (WS-1) was substituted. For Al, which is not as reliable in the amphibole standards, EPM-83 or EPS 6-3 was substituted. This less than desirable substitution was made because of

TABLE A-1. STANDARDS USED IN MICROPROBE ANALYSES

Standard Number	Mineral	Standard Name	Source	Analyst	Reference
EPS 21-1	Amphibole	Gibbs 9	Rucklidge		Can. J. of Earth Sci. (1971)
WS-1	Amphibole	Kakanui Kaersutite	T. O. Frisch	White, Mason, Frisch	White *et al.*, 1972
EPS 12-1	Biotite	Evans Biotite 1	B. Evans	D. Carmichael	
EPS 12-2	Biotite	Evans Biotite 3		D. Carmichael	
EPS 6-3	Glass Mix	Ab 60	J. V. Smith (?)	J. V. Smith (?)	
EPM 83	Sanidine	Hohenfels	U. of Alta. Age Lab (HB)	A. Stelmach, D.G.W. Smith & class	
EPS 11-3	Orthoclase		B. Evans	Ingamells	
FSP-5	Anorthoclase	Anorthoclase	T. O. Frisch		Smith and Ribbe (1966)
FSP-4	Anorthite	An 100	T. O. Frisch		Smith and Ribbe (1966)
EPS 23-11	Wollastonite	Wollastonite	J. V. P. Long	Scoon	
EPS 12-6	Olivine	Olivine	B. Evans	D. Carmichael	
CPX-2	Clinopyroxene	Hess Pyroxene 35	Rucklidge	J. V. Smith	
CPX-4	Clinopyroxene	Evans Pyroxene 22	T. O. Frisch		
EPS 7-10		Manganese Metal	Fischer Chem. Co.		
EPS 22-7	Galena	Galena	U. of Alta. Collection	Not Analyzed Stoichiometry assumed	

TABLE A-2. REPEAT ANALYSES OF EPS 21-1, USING EPS 21-2 AS A STANDARD

EPS 21-1	Run 1, percent	Run 2, percent	Difference 1 - 2	Run 3, wet chem.*	Difference (½(1+2)-3)
Si	21.576	21.655	-.079	21.217	.398
Ti	0	.01	-.010	.012	.002
Al	8.776	8.695	+.081	9.886	1.150
Fe	2.845	2.842	+.003	2.728	.116
Mn	.028	.029	-.001	.047	.018
Mg	10.745	10.392	+.353	9.879	.690
Ca	7.874	7.933	-.059	8.734	.830
Na	.771	.777	-.006	.883	.109
K	.094	.097	-.003	.133	.037
Cl	.039	.039	0		0

Run 3 is the wet chemical analysis of amphibole No. 67 in Rucklidge _et al_. (1971); the microprobe analyses on this amphibole by Rucklidge _et al_. (1971) confirm many of the differences between the wet chemical and microprobe determinations shown here.

*Wet chemical analysis by Ingamells.

TABLE A-3

STANDARDS USED IN ELECTRON MICROPROBE ANALYSES OF REGIONAL METAMORPHIC MINERALS

Element	Muscovite	Biotite	Amphibole	Plagioclase	K-Feldspar
Si	WS-1	WS-1	WS-1	WS-1	WS-1
Ti	WS-1	WS-1	WS-1	WS-1	WS-1
Al	EPM 83	EPM 83	EPS 6-3	EPS 6-3	EPM 83
Fe	WS-1	WS-1	WS-1	WS-1	WS-1
Mn	EPS 7-10	EPS 7-10	EPS 7-10	EPS 7-10	EPS 7-10
Mg	WS-1	WS-1	WS-1	WS-1	WS-1
Ca	EPS 6-3	EPS 6-3	WS-1	EPS 6-3	EPS 6-3
Na	EPS 6-3	EPS 6-3	EPS 6-3	EPS 6-3	EPS 6-3
K	EPM 83	EPM 83	WS-1	WS-1	EPM 83
Cl	EPS 21-2	EPS 21-2	EPS 21-2	-	-
F	EPS 21-2	EPS 21-2	EPS 21-2	-	-
Ba	EPS 11-3	EPS 11-3	EPS 11-3	-	-

STANDARDS USED IN ELECTRON MICROPROBE ANALYSES OF REGIONAL METAMORPHIC MINERALS

Element	Carbonate	Garnet	Sphene	Epidote	Diopside	Chlorite
Si	WS-1	WS-1	WS-1	WS-1	WS-1	WS-1
Ti	WS-1	WS-1	WS-1	WS-1	WS-1	WS-1
Al	EPS 6-3	EPS 6-3	EPS 6-3	EPS 6-3	EPS 6-3	EP 117-83
Fe	WS-1	WS-1	WS-1	WS-1	WS-1	WS-1
Mn	EPS 7-10	EPS 7-10	EPS 7-10	EPS 7-10	EPS 7-10	EPS 7-10
Mg	WS-1	WS-1	WS-1	WS-1	WS-1	WS-1
Ca	WS-1	EPS 6-3	EPS 6-3	EPS 6-3	EPS 6-3	EPS 6-3
Na	EPS 6-3	EPS 6-3	EPS 6-3	EPS 6-3	EPS 6-3	EPS 6-3
K	WS-1	WS-1	WS-1	WS-1	WS-1	EPM 83
Cl	-	-	-	-	-	EPS 21-2
F	-	-	-	-	-	EPS 21-2
Ba	-	-	-	-	-	EPS 11-3

TABLE A-4

STANDARDS USED IN ELECTRON MICROPROBE ANALYSES OF MINERALS FROM KOOTENAY POINT

Element	Biotite	Hornblende	Plagioclase	K-Feldspar	Diopside
Si	EPS 12-2	EPS 21-1, WS-1	–	–	EPS 6-3, CPX-2
Ti	EPS 12-2	EPS 12-2, EPS 12-1, WS-1	–	–	CPX-4
Al	EPS 12-2	EPS 21-1, EPS 12-2, WS-1	–	–	CPX-4
Fe	EPS 12-2	EPS 21-1, EPS 12-2, WS-1	–	–	CPX-4
Mn	EPS 12-1, EPS 12-2 EPS 7-10	EPS 12-1 EPS 7-10	–	–	CPX-2
Mg	EPS 12-2	EPS 21-1 WS-1	–	–	CPX-2
Ca	EPS 21-1	EPS 21-1 WS-1	EPS 6-3	EPS 6-3	EPS 6-3 CPX-2
Na	EPS 12-2	EPS 21-1 EPS 12-2 WS-1	EPM 83	EPM 83	EPS 6-3 CPX-4
K	EPS 12-2	EPS 12-2	EPM 83	EPM 83	–
Cl	EPS 12-1	EPS 12-1	–	–	–
F	EPS 12-2	EPS 12-2	–	–	–
Cr	–	–	–	–	CPX-4
S	–	–	–	–	–

TABLE A-4 CONTINUED

Element	Epidote	Sphene	Scapolite	Carbonate, Calcite, Dolomite, Magnesite
Si	WS-1	EPS 21-1	FSP-5	-
Ti	WS-1	EPS 12-2	-	-
Al	WS-1	EPS 21-1	FSP-4	-
Fe	WS-1	EPS 21-1	-	EPS 12-6
Mn	EPS 12-1	EPS 12-1	-	-
Mg	EPS 12-1	EPS 21-1	-	EPS 12-6
Ca	EPS 12-1	EPS 21-1	FSP-4	EPS 23-11
Na	EPS 12-1	EPS 21-1	FSP-5	-
K	EPS 12-1	EPS 21-1	FSP-5	-
Cl	EPS 12-1	-	EPS 12-1	-
F	EPS 12-2	-	EPS 12-1	-
Cr	-	-	-	-
S	-	-	EPS 22-7	-

two biotite standards EPS 12-1 and 12-2 were destroyed by repolishing before the regional work was done. The effects of Al in two coordinations (in biotite and hornblende, and to some extent in pyroxene and epidote) are not completely known, but the differences between similar minerals from the region and the Point are small. Where different mineral standards were used, an attempt was made to use a standard with a higher concentration of the desired element to reduce multiplication of errors. This method worked in all cases except for Ti in sphene and Ca and Mg in the carbonates. The most serious complication involves the determination of Ca in the regional carbonates. For these, the Kakanui Kaersutite (WS-1) was used as a standard, resulting in a multiplication factor of 5 between standard and sample concentrations.

Table A-5 reports the general error ranges, in percent of the total present, for all elements analyzed in all minerals from the Point and the region. Where evaluation of the standard was not made (beyond that given in the laboratory), the error quoted is the statistical counting error at the 99% confidence level. This is done realizing that other errors are present, as discussed by Sweatman and Long (1969). Errors in the major elements usually are less than 3% of the total present and for minor and trace elements, generally less than 5%. Errors in a few early analyses in the course of this work may be uptto 10% of the total present for some elements.

WHOLE ROCK ANALYSES

Rock analyses were carried out by two different methods. XRF analyses were made on about 90 rocks from the Point through the courtesy of Dr. J. G. Holland of Durham University. Rocks from the Kootenay region were

TABLE A-5. GENERAL ANALYTICAL ERROR RANGES IN THE MICROPROBE MINERAL ANALYSES*

Percent Relative Error (Maximum Ranges)

Element	Minerals from Regional Metamorphic Rocks	Minerals from Kootenay Point
Si	<0.8	0.55-1.9
Ti	1.5	1.5-3.7
Al	<0.8-2.0	0.9-10
Fe	2.6	2.6-3.4
Mn	7	7
Mg	0.51	2.5-6.9
Ca	0.1	0.1-9
Na	N.D.	17-30
K	<0.8-1.1	0.9-1.1
Cl	2.5	2.5
F	2.5	2.5
Ba	2.5-7	2.5-7
Cr	2.5-7	2.5-7
S	2.5-7	2.5-7

*Note, lower limits in some cases below statistical counting error. Where errors in standards cannot be estimated (through cross-analysis) statistical counting errors are chosen. An accurate analysis of the precision of the microprobe results cannot be made using the data available. The statistical counting errors were evaluated from numbers of counts on samples, but such errors must also be evaluated for counts on standard, as well as for background on both sample and standard. Other analytical errors also contribute to the total error. The results shown on this table are only a rough guide.

analyzed using a modification of the method of Friedman (1960).

Samples from the Point were treated in the following manner: a 5 cm square block sample was cut from the hand specimen. Care was taken to cut away all weathered material. From this block, one or two thin sections were cut, usually at a diagonal or parallel and perpendicular to foliation. These sections were polished for microprobe work. The block was then crushed using a jaw crusher. A large porcelain mortar was then used for further reduction. Care was taken at this stage to avoid grinding, since contamination could result. Specimens were pounded to break them into sufficiently small size to go into the swingmill. The specimen was reduced to a fine powder in a rotary swingmill using tungsten carbide heads to minimize contamination. The mill was thoroughly cleaned between each specimen.

The powder was ground, homogenized by successive mixing and aliquots taken for mineral separation and for chemical analysis. Care was taken to assure thorough mixing before taking any aliquot. About 5 ounces of material were taken for XRF analysis. Four samples, chosen as representatives of the rock types on the Point, were taken as aliquots from the material separated for XRF analyses. These four samples were used as standards and were analyzed (wet chemically) by A. Stelmach of the Department of Geology. These analyses, with their corresponding XRF analyses are given in Table A-6.

Comparison of standards done by wet chemistry and the XRF analyses do not show good agreement. The average error encountered for major elements is about 15% of the total present. The worst major elements are Na, Mg and Al, others show error of about 10% of the total present. For the most part, the errors are not systematic; elements Si, Ti, Al, TABLE A-6. XRF ANALYSES AND WET CHEMICAL ANALYSES OF FOUR SELECTED ROCKS FROM KOOTENAY POINT

	1 Wet Chem. Analysis	2 XRF Anal.	3 % Diff. from Wet Chem. Anal.	1 Wet Chem. Analysis	2 XRF Anal.	3 % Diff. from Wet Chem. Anal.
Element	T1-5	T1-5	T1-5	T1-9	T1-9	T1-9
SiO_2	68.20	71.57	+ 4.94	43.16	43.35	+ 0.44
TiO_2	.25	.33	+32.00	2.21	2.17	- 1.81
Al_2O_3	16.16	10.46	-35.27	14.10	12.56	-10.92
FeO*	2.33	2.82	+21.03	11.35	11.82	+ 4.14
MnO	.06	.08	+33.33	.17	.18	+ 5.88
MgO	.71	.84	+18.31	11.27	14.19	+25.91
CaO	2.44	3.14	+28.69	10.43	10.30	- 1.25
Na_2O	3.90	5.42	+38.97	1.5	.72	-54.43
K_2O	4.13	4.90	+18.64	2.57	3.02	+17.51
P_2O_5	.11	.12	+ 9.09	.42	.37	-11.90
H_2O^+	.50	-	-	2.13	-	-
H_2O^-						
Total	99.61	99.68		99.62	98.68	
	1	2	3	1	2	3
Element	T1-1a	T1-1a	T1-1a	T4-8	T4-8	T4-8
SiO_2	51.98	51.73	- 0.48	48.20	49.60	2.90
TiO_2	.38	.45	+18.42	1.98	1.59	-19.70
Al_2O_3	6.94	7.27	+ 4.76	13.73	11.93	-13.11
FeO*	3.13	3.55	+13.42	12.13	12.63	+ 4.12
MnO	.06	.06	0	.17	.18	+ 5.88
MgO	18.50	21.37	+15.51	6.70	8.10	+20.90
CaO	12.50	11.39	- 8.88	12.03	11.88	- 1.25
Na_2O	.52	0	-100	1.65	1.59	- 3.64
K_2O	3.22	3.62	+12.42	.86	.86	0
P_2O_5	.44	.16	-63.64	.20	.23	+15.00
H_2O^+	2.11			1.84		
H_2O^-						
Total	99.87	99.60		100.00	98.59	

*+Fe_2O_3 converted to FeO

Ca, Na and P_2O_5 may be substantially above or below the wet chemical value. In general T1-1 and T1-9 give the best analyses, T4-8 is not as bad, and T1-5, a quartz syenite, gives the worst analysis. T1-1 is a calc-silicate, T1-9 and T4-8 are "amphibolites".

The analyses were carried out using a Phillips 12-12 X-ray fluorescence spectrometer equipped with automatic sample loader and tape printout. The analyses are compared to a set of curves generated by using a suite of about 20 standards and corrected to these curves by linear regression equation. Errors occur if the samples fall outside the range of calibration of the standards. However, all the standard samples chosen are within the ranges of the XRF standards used. Another source of error is inhomogeneity in the sample, resulting in a difference between the portion analyzed by wet chemistry and that by XRF. This seems unlikely in the light of care taken to assure homogeneity. If the entire sample was not used for the pellet, and care was not taken to homogenize the sample, an unrepresentative sample would result. Inhomogeneities also result if pressed pellets are used, since biotite or muscovite may align in layers giving bias in the results. The fact that K, Mg and Fe (the essential elements in biotite) are uniformly high suggests this possibility. Other errors may evolve from improper peak setting, wavelength shift, instrument instability and the type of correction used. The correction program itself is simplified in such a manner that samples falling near the extreme values of the standards might be biased. The author does not have data on operating conditions during the run, so no evaluation is possible.

Rocks from the region were analyzed using a modification of the method of Friedman (1960). Modes were obtained from thin sections using 1200 counts on each section. Where sections parallel and perpendicular to foliation were cut, the two were combined to obtain the mode used for calculation. Mineral densities were obtained from Deer, Howie and Zussman (1966) for minerals closest in composition to those in the sample. The modal percentage was corrected to weight percentage using the density figures. Electron probe analyses for minerals present in the rock were used in the calculation, as most of the silicate phases had been analyzed. Those minerals not analyzed (usually a carbonate or a plagioclase) but present were classified optically, and the analysis corresponding most closely to the optical determination used. In the case of biotite or hornblende, a mineral from a rock of similar composition and grade was used for the calculation. T4-8 was used as a standard and the calculation carried through. Table A-7 presents the results as well as the percentage difference from the amount present as determined by wet chemistry. The agreement is quite reasonable for all major elements except Na and K. Errors in K possibly result from the problem of the orientation of biotite, but may also result from the problem of detecting untwinned plagioclase or K-feldspar when quartz is present. The low total for SiO_2, heavily dependent on quartz, supports this suggestion. Misidentification of soda plagioclase would result in higher Na and lower Si. The average relative error for major elements is about 5%, with larger relative errors for TiO_2 and MnO. The errors involved are naturally dependent on errors in the microprobe analyses, as well as those due to errors in the mode. Another possible source of error is that of obtaining an unrepresentative thin section from an inhomogeneous rock. This source of error would affect percentages of

TABLE A-7. ROCK COMPOSITION BY MODAL ANALYSIS, AFTER THE METHOD OF FRIEDMAN (1960)

Element	Wet Chemical Analysis T4-8	Modal Analysis T4-8	% Difference of Amount Present
SiO_2	48.20	45.99	4.59
TiO_2	1.98	2.10	6.06
Al_2O_3	13.73	14.48	5.46
FeO	12.13	12.27	1.15
MnO	.17	.21	23.53
MgO	6.70	6.24	6.87
CaO	12.03	11.75	2.33
Na_2O	1.65	1.85	12.12
K_2O	.86	1.42	65.12
BaO	ND	tr	
Cl	ND	.02	
F	ND	.06	
H_2O	1.84	3.42	85.86
Total	99.29	99.81	

elements when comparing a bulk analysis against an analysis calculated from the mode. This type of error is not considered to be a problem here, since the size of the chemical system dealt with when discussing the results of the mineral analyses is smaller than that of the thin section used. The differences between wet chemical analysis and calculated composition do not exceed, in most cases, the statistical error that could be introduced in the point counting. This latter error will be simply related to the total number of points counted for each mineral.

APPENDIX 2

TRACE ELEMENT AND ISOTOPIC ANALYSIS

The determination of Co, Cu, Zn, Cr, Mn, Li, Ni, Ga, Ba, Rb and Sr, K and Ar is described in this appendix.

Separation procedures follow the crushing of the samples (refer to Appendix 1 for details). Mineral separations were done using the Franz Isodynamic Separator followed by gravity separation using heavy liquids (tetrabromoethane and methylene iodide). Repeated runs through the separator and heavy liquids were made until sample purity was 99.5% (based on grain counts under the binocular microscope). The main contaminants at the 0.5% level were either biotite or hornblende (visible), but sometimes small amounts of epidote appeared.

K-Rb procedure

The procedure for determining potassium and rubidium differs somewhat from the normal single-spike procedure. K was determined by isotope dilution along with Rb by K-Rb double spiking. A 40μg sample was weighed into a teflon beaker which had been soaked in 1:1 hot concentrated HNO_3 and thoroughly rinsed with demineralized water. Five ml of Aristar HF, 2 ml of distilled 50% HNO_3 and about 20μg Rb^{87} spike were added to the sample. This solution was allowed to evaporate to dryness and to bake gently for a short period of time, whereupon 1 ml 50% HNO_3 (distilled) was added and the process repeated. The residue was then taken up in 2 ml 50% distilled HNO_3 and 10 ml double-distilled H_2O. The solution was carefully stirred and allowed to cool to room temperature. An aliquot was taken from the ~ 12 ml of solution, and approximately 0.7 cc of K^{41} spike solution added. The aliquot weight was known, allowing the exact amount of K^{41} spike solution to be determined by difference. This solution, now spiked for both K and Rb, was run on the mass spectrometer.

Sr procedure

The isotope dilution procedure for extraction and determination of Sr is the same as that used by R. K. O'Nions (1969).

Ba procedure

Barium was determined by isotope dilution. Originally, the combined analysis of barium with strontium was attempted by double-spiking, as with K and Rb, but the method failed. Barium was determined alone using the following procedure:

A sample weighing about 0.01 g was spiked with Ba^{137} (81.9% enriched). The sample plus spike solution was allowed to evaporate to dryness, whereupon 3 ml HF (Aristar) and 3 ml 1:1 HNO_3 were added. The solution was again allowed to evaporate to dryness, and 0.5 cc HNO_3 (1:1) added. After the final evaporation, the residue was taken up in 1 ml 1:1 HNO_3 and transferred to a centrifuge tube. A few drops of H_2SO_4 (1:1) were added to precipitate barium sulfate. The precipitation often took several hours, especially in the case of amphibole samples where Ba is present in small amounts. Centrifuging aided in bringing down the precipitate. After concentrating the $BaSO_4$ precipitate, the supernate was decanted and the precipitate washed with double-distilled H_2O + HNO_3. The precipitate was then taken up in a very small amount of water and loaded directly on to a Ta filament for the mass spectrometer run.

Argon procedure

Argons were run by G. Bonnet of the University of Alberta on 0.5-1 gm samples of coarse biotite separated for this purpose. The method is described by O'Nions (1969).

Ba, Sr, Rb and K were run on a 6" solid source mass spectrometer utilizing rapid peak switching and digital output. The instrument was built by Dr. G. L. Cumming of the Physics Department of the University of Alberta.

Errors: Maximum errors for determinations in the University of Alberta isotope geology laboratories are: Ba ±1%, Rb ±2%, K ±2%, Ar ±2% (Baadsgaard, pers. comm.). Laboratory errors for normal Sr are ±1% for amounts greater than 30 ppm, and up to 10% for amounts of less than 3 ppm. Error in determination of Sr^{87} is ±1% at. Repeat Sr^{87*}/Sr^{87N} analyses done on clean biotite samples from the area do not show Sr accuracies that are as good as expected from repeats on laboratory standards, since Sr^{N} is very low. Errors of up to 10% in total Sr are encountered, but the error in the Sr^{87}/Sr^{86} ratio is considerably less because of the high proportion of Sr^{87*}.

Co, Cu, Zn, Cr, Mn, Li, Ga, Ni separation and determination

Ga and Ni were determined by colorimetry, following the extraction procedure to be described. All other elements were determined by atomic absorption. Initial amounts of trace elements were estimated from published analyses of biotite and hornblende. From the estimates, an optimum sample size was determined, taking into account the availability of sample and the amount of concentration required to bring the solution to be measured into the range of sensitivity of the instrument. A sample, usually 2-3 g, was chosen as optimum. The extraction procedure is that of Sandell (1959), while the furildioxeme procedure is that of Bodart (1969). Atomic absorption was used for measurement of the other elements. See Fig. A2-1 for detailed procedure.

International USGS reference samples G-1 and W-1 were run as a check on the accuracy of the determinations. The analytical data, along with ranges and accepted values are presented in Table A2-1. It is immediately obvious from examination of the values for the two standards that the G-1 analyses are anomalous. This standard has been circulated among several persons during the period of its residence in the laboratories of the University of Alberta (Baadsgaard, pers. comm.). It is also part of the early set of G-1 separates, which were not ground as finely as later batches (Fleischer, 1969). It appears, from comparison with the analyses for W-1, that G-1 has been contaminated or is no longer representative of the average because of successive fractionation due to poor aliquot technique. For these reasons, it is not used in the error estimation for the work presented here.

Examination of the values for W-1 indicates that some elements check more closely than others, so error must be estimated separately. Gallium would appear to have only the nominal error in the method, or about ±2% (relative). Lithium, using the average value, gives the relative difference of ±30%, Cr±7%, Cu±1%, Co±50%, Zn±15%, Mn±23% and Ni±43%. These must be considered maximum possible errors, the mean deviation being considerably less. Precision is about ±2% for all elements determined, and these are the error limits shown on the diagrams.

Fig. A2-1. Extraction procedure for trace elements from amphiboles and biotites.

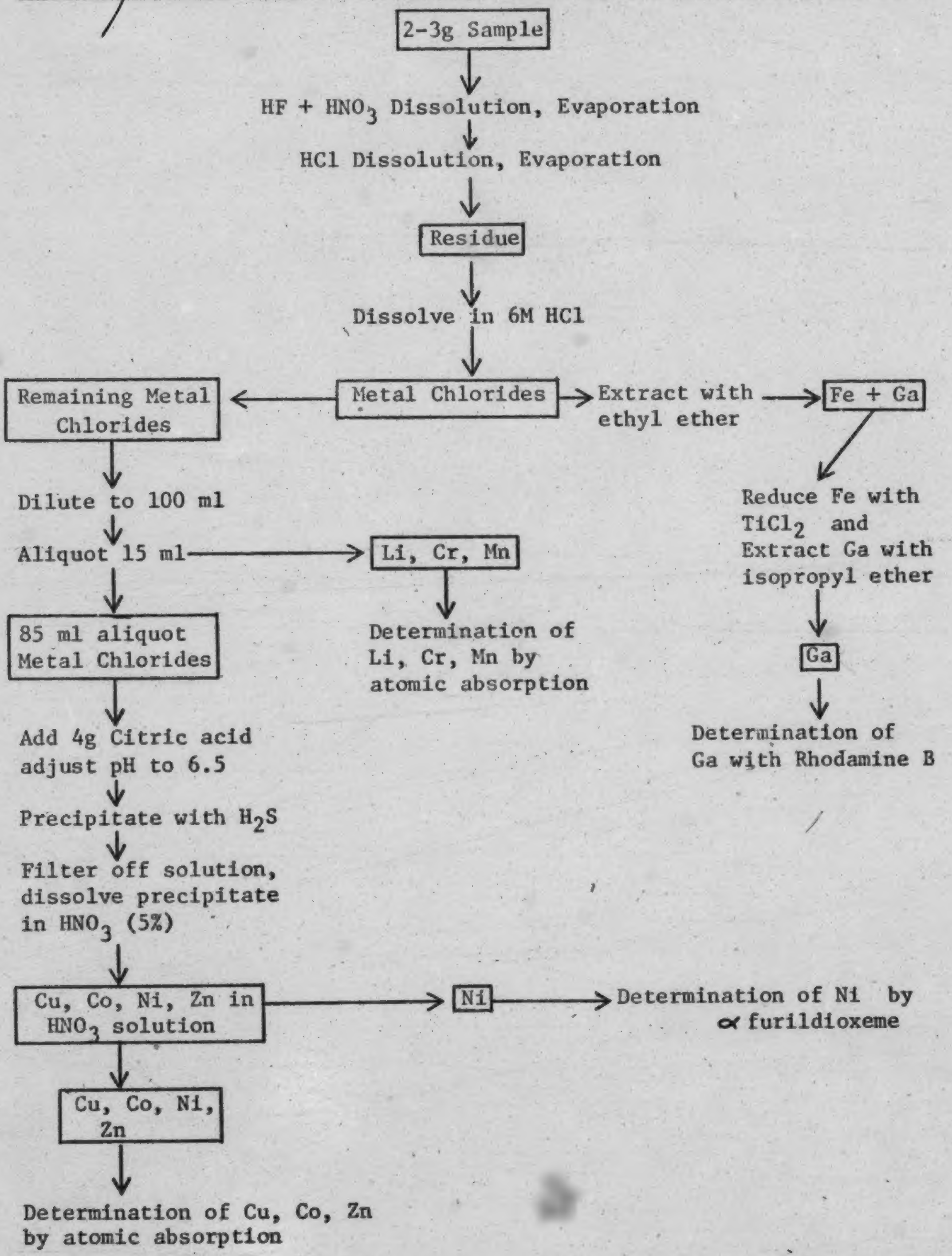
2-3g Sample
HF + HNO_3 Dissolution, Evaporation
HCl Dissolution, Evaporation
Residue
Dissolve in 6M HCl
Metal Chlorides
Remaining Metal Chlorides
Extract with ethyl ether
Fe + Ga
Reduce Fe with $TiCl_2$ and Extract Ga with isopropyl ether
Ga
Determination of Ga with Rhodamine B
Dilute to 100 ml
Aliquot 15 ml
Li, Cr, Mn
Determination of Li, Cr, Mn by atomic absorption
85 ml aliquot Metal Chlorides
Add 4g Citric acid adjust pH to 6.5
Precipitate with H_2S
Filter off solution, dissolve precipitate in HNO_3 (5%)
Cu, Co, Ni, Zn in HNO_3 solution
Ni
Determination of Ni by α furildioxeme
Cu, Co, Ni, Zn
Determination of Cu, Co, Zn by atomic absorption

Part of the problem with the use of W-1 or G-1 as reference standards is the wide range of values found by analysts from different laboratories. All elements except Co fall within the ranges found by other analysts; thus, only the Co analyses can be suspected as being actually incorrect. The others demonstrate the ability of this analyst to approximate average or accepted values. In two of the three cases where recommended values exist (Ga, Cu, Zn), these analyses are very close to the recommended value. The reader may use all values as an approximation of maximum relative error, keeping in mind that the largest deviations occur where average values are quoted.

K_2O in biotite, a note:

Engel (1972) and Ingamells et al. (1972) have done studies on the effect of sampling procedure and contaminants present on K_2O determinations on biotites used for K-Ar dating. Both authors, found differences involving sampling procedures, and Engel (1972) showed that quite large differences could be established between microprobe results and bulk determinations of K_2O. Table A2-2 gives K_2O determinations for microprobe results and for isotope dilution. The results show that up to 2% absolute difference between analytical results may be obtained. This difference is well outside the error of either analytical method. The cause lies in contamination of biotite by intercrystalline chlorite which is too fine to be removed by grinding even to the limits defined in this work. Chlorite can be seen in some grains in thin section, but on the whole they appear remarkably fresh. Using the differences found for this work, biotite analyses could be corrected for trace elements if values for chlorite were available.

TABLE A2-2. COMPARISON OF K_2O IN BIOTITE ANALYZED BY ISOTOPE DILUTION AND BY ELECTRON MICROPROBE

Sample	%K_2O (Microprobe)	%K_2O (Isotope Dilution)	Difference
205-50W	9.94	9.90	-0.04
T4-2	9.47	8.06	-1.41
T1-1	10.41	9.06	-1.35
T3-12a	9.24	7.92	-1.32
T1-9	9.49	8.78	-0.71
198-199-146E	10.15	8.20	-1.95
T2-15	9.73	9.05	-0.68
30-13E	9.91	8.52	-1.39
T4-6a	9.52	8.96	-0.56
T1-8	9.93	9.39	-0.54
240-137E	9.70	8.49	-1.21

TABLE A2-1. ANALYTICAL RESULTS FOR STANDARDS G-1 AND W-1.

		Ga	Li	Cr	Cu	Co	Zn	Mn	Ni
	Accepted Value	19.6*	22	20	13*	2.4	45	195	1
G-1	Range	15-18	17-25	9-43	8-20	1.3-10	25-55	147-245 210-350	1-21
	This Study	16	12	26	27	2	57	125	292
	Accepted Value	16*	14.5	114	110*	47	86*	1278	76
W-1	Range	13-37	8-15	76-148	100-140	33-54	42-95	903 1393	29-93
	This Study	16	10	123	111	24	73	981	43

*Recommended (Flanagan, 1973)

Ranges Fleischer (1969)

APPENDIX 3

ASSEMBLAGES FROM REGIONAL METAMORPHIC ROCKS NOT INCLUDED IN TABLE 3

Sample Number	Assemblages from Regional Metamorphic Rocks
5LBT-4	Dolomite - calcite - quartz - muscovite
5LBT-5	Quartz - K-feldspar - muscovite - carbonate
5LBT-6	Dolomite - calcite - quartz - muscovite
5LBT-7	Amphibole - chlorite-- quartz - feldspar - carbonate - magnetite - opaque
5LBT-8	Quartz - K-feldspar - chlorite - biotite - hematite - carbonate
5LBT-9	No thin section.
5LBT-10	K-feldspar - quartz - chlorite - muscovite - calcite
5LBT-11	K-feldspar - quartz - muscovite - chlorite - pyrite
5LBT-12	Quartz - K-feldspar - chlorite - muscovite - calcite
5LBT-13	Quartz - chlorite - calcite - hematite - dolomite - K-feldspar
5LBT-14	No thin section.
5LBT-18	Plagioclase - microcline - quartz - biotite - magnetite - sphene
5LBT-19	Microcline - quartz - plagioclase - biotite - sphene - muscovite
5LBT-21	Calcite - quartz - pyrite - feldspar - sphene - tremolite - phlogopite - chlorite
6LBT-23	No thin section.
6LBT-24	Biotite - plagioclase - K-feldspar - staurolite (?) - carbonate - rutile - ilmenite - pyrite
6LBT-25	Hornblende - quartz - plagioclase - magnetite - biotite - chlorite - K-feldspar (?)
6LBT-26	Hornblende - quartz - plagioclase - K-feldspar - magnetite
6LBT-27	Diopside - calcite - tremolite

6LBT-28	Tremolite - feldspar
6LBT-29	Tremolite - calcite
6LBT-30A	Muscovite - quartz - biotite - magnetite - rutile - pyrite - tourmaline - apatite
6LBT-30B	Calcite - tremolite - phlogopite - pyrite
6LBT-31	Quartz - albite - muscovite
6LBT-32	Actinolite - hornblende - plagioclase - quartz - K-feldspar - biotite - magnetite
6CBT-1	Quartz - muscovite - K-feldspar - chlorite - rutile
6CBT-2	Calcite - oligoclase - K-feldspar - quartz - biotite - chlorite - sphene
6CBT-3	Calcite
6CBT-4	Calcite - quartz - K-feldspar - phlogopite
6CBT-5	Quartz - K-feldspar (?) - muscovite - hematite - chlorite - ilmenite - magnetite - tourmaline
6CBT-6	Calcite - quartz - hematite
6CBT-7	Quartz - biotite - plagioclase - K-feldspar - muscovite - magnetite - sphene - tourmaline
9CBT-1	Calcite - diopside - actinolite - plagioclase - microcline - quartz - sphene
9CBT-2	Diopside - actinolite - An$_{40}$ plagioclase - microcline - scapolite - phlogopite - sphene - quartz
9CBT-3	Biotite - plagioclase An$_{38}$ - microcline - quartz - epidote - apatite - sphene
9CBT-4	Biotite - actinolite - diopside - plagioclase - K-feldspar - quartz
9CBT-5	Quartz - biotite - oligoclase - microcline - chlorite - pyrite - magnetite
9CBT-6a	Hornblende - plagioclase - K-feldspar - magnetite - sphene
9CBT-6	Calcite - diopside - actinolite - plagioclase - microcline - epidote - scapolite - phlogopite - quartz

11CBT-8	Diopside - actinolite - biotite - plagioclase - microcline - quartz
11CBT-9	Actinolite - diopside - plagioclase - microcline - quartz
11CBT-10	Hornblende - oligoclase - quartz - K-feldspar - biotite - magnetite
11CBT-11	Muscovite - biotite - albite - quartz - K-feldspar
11CBT-12	Muscovite - biotite - quartz - K-feldspar - plagioclase - magnetite - garnet - rutile
11CBT-13	Quartz - muscovite - K-feldspar - albite - garnet - chlorite - pyrite
11CBT-14	No thin section.
11CBT-17	Calcite - tremolite - phlogopite
11CBT-18	Tremolite - calcite
11CBT-19	Phlogopite - muscovite - quartz - plagioclase - K-feldspar - rutile - zircon
11RBT-1	Hornblende - plagioclase - quartz - biotite - chlorite - sphene - rutile - K-feldspar (?)
11RBT-2	Hornblende - plagioclase An_{30} - quartz - biotite - sphene - magnetite - K-feldspar
11RBT-3	Quartz - muscovite - rutile
12RBT-3a	Chlorite - biotite - muscovite - quartz - feldspar - galena - pyrite
12RBT-4	Biotite - muscovite - quartz - plagioclase - K-feldspar - hematite
6CCT-2	Quartz - plagioclase - K-feldspar
6CCT-4	Actinolite - quartz - K-feldspar - plagioclase - diopside - biotite - epidote - sphene
6CCT-5	Actinolite - epidote - biotite - diopside - microcline - quartz - plagioclase
6CCT-6	Hornblende - plagioclase - epidote (?) - sphene
6CCT-7	Quartz - K-feldspar - biotite

6CCT-9	Quartz - microcline - biotite - muscovite - albite - magnetite
6CCT-10	Quartz - K-feldspar - biotite - muscovite - albite - opaque
7CCT-11	Quartz - K-feldspar - biotite - muscovite - albite
7CCT-12	Hornblende - plagioclase - quartz - K-feldspar - biotite - sphene
7CCT-13	Missing
7CCT-14	K-feldspar - plagioclase - quartz - biotite - muscovite - rutile
7CCT-15	Quartz - K-feldspar - albite - biotite - muscovite
7CCT-16	Hornblende - plagioclase - K-feldspar - quartz - biotite - chlorite - sphene
7CCT-17	Quartz - biotite - muscovite - albite - K-feldspar
7CCT-18	Quartz - K-feldspar - plagioclase - actinolite - epidote - biotite - sphene
7CCT-19	Hornblende - quartz - plagioclase - biotite - garnet - sphene
7RT-1	Actinolite - diopside - quartz - K-feldspar - plagioclase - epidote
7RT-1 (upper band)	Hornblende - actinolite - diopside - epidote - quartz - plagioclase
7RT-2	Quartz - plagioclase An_{32} - microcline - actinolite - biotite
7RT-3	Diopside - plagioclase - actinolite - calcite - K-feldspar - epidote
7RT-4	Quartz - plagioclase - K-feldspar (?) - actinolite - epidote - biotite
7RT-5	Quartz - plagioclase - K-feldspar - actinolite - biotite
7RT-6	Diopside - actinolite - microcline - plagioclase - quartz
7RT-8	Biotite - quartz - K-feldspar - plagioclase - epidote
7RT-9	Hornblende - plagioclase - K-feldspar - quartz - sphene

7RT-10	Plagioclase - K-feldspar - quartz - biotite - chlorite - muscovite
7RT-11	Calcite - plagioclase - actinolite
7RT-12	Hornblende - plagioclase - quartz - chlorite - sphene - K-feldspar
7RT-13	Quartz - plagioclase - K-feldspar - actinolite - epidote
7RT-14	Quartz - microcline - plagioclase - biotite - chlorite
7RT-15	Feldspar - quartz
7RT-16	Hornblende - quartz - plagioclase - biotite - sphene - magnetite
7RT-18	Actinolite - biotite - quartz - plagioclase - sphene
8AT-1	Quartz - biotite - chlorite - K-feldspar - epidote (?)
8AT-2	Actinolite - diopside - calcite - muscovite
8AT-3	Quartz - microcline - actinolite - chlorite - plagioclase
8AT-4	Muscovite - quartz
8AT-5	K-feldspar - biotite - actinolite - albite - quartz - garnet
8AT-6	Biotite - chlorite - plagioclase - quartz - K-feldspar - garnet - magnetite
8AT-7	Quartz - K-feldspar - plagioclase - biotite - actinolite chlorite - sphene
8AT-9a	Hornblende - biotite - quartz - K-feldspar - plagioclase - epidote - sphene
8AT-9b	Quartz - K-feldspar - plagioclase - actinolite - hornblende - diopside - sphene
8AT-10	Quartz - microcline - albite - hornblende - pyrite
8AT-11	Quartz - microcline - albite - hornblende - sphene
8AT-12	Quartz - feldspar - biotite - muscovite - chlorite - magnetite
8AT-13	Calcite - dolomite - quartz

8AT-14	Hornblende - quartz - K-feldspar - plagioclase - magnetite
8AT-15	No thin section.
8AT-16	Quartz - garnet - actinolite (?)
8AT-17	Quartz - actinolite - diopside - epidote - biotite - plagioclase - microcline - pyrite - magnetite
8AT-19	Quartz - microcline - hornblende - biotite - actinolite - plagioclase - pyrite - sphene
8AT-20	Calcite - quartz - K-feldspar - phlogopite - diopside (?) - plagioclase - sphene
8AT-21	Quartz - microcline - hornblende - plagioclase - sphene - magnetite - pyrite
8AT-22	Quartz - biotite - actinolite - microcline - plagioclase - pyrite
8AT-23	Quartz - plagioclase - biotite - calcite - actinolite - pyrite
8AT-24	Quartz - plagioclase - microcline - biotite - muscovite - magnetite - pyrite
8AT-25	Quartz - hornblende - feldspar - biotite - calcite - hematite
8AT-26	Muscovite - quartz - chlorite - feldspar - rutile
10BT-1	Quartz - K-feldspar - albite - biotite
10BT-2	Biotite - muscovite - quartz - K-feldspar - plagioclase (An_{21})
10BT-5	Muscovite - biotite - quartz - feldspar (?) - magnetite
10BT-6	Muscovite - biotite - quartz - magnetite - K-feldspar - oligoclase
10BT-7	No thin section.
10BT-10	Tremolite - calcite - quartz - dolomite
10BT-11	Quartz - K-feldspar - plagioclase - actinolite - aegirine (?)
10BT-12	Hornblende - quartz - feldspar - sphene - biotite
10BT-14	Quartz - biotite - plagioclase - K-feldspar - garnet

10BT-15	Biotite - hornblende - quartz - K-feldspar - plagioclase - sphene - magnetite
10BT-16	Hornblende - quartz - sphene - plagioclase - epidote
12WP-1	Biotite - muscovite - K-feldspar - plagioclase - quartz - garnet
25-5	Actinolite - diopside - microcline - biotite - quartz - plagioclase - epidote - sphene
6Aug 4 a	Quartz - muscovite - garnet - plagioclase - K-feldspar - biotite - chlorite - opaque
34-22	Epidote - actinolite - calcite - sphene - apatite
29-36	Hornblende - quartz - plagioclase - K-feldspar - biotite - sphene - chlorite - epidote - scapolite - magnetite - hematite
27-7	Actinolite - epidote - biotite - microcline - plagioclase - quartz - opaque
24-13	Quartz - muscovite - biotite - feldspar - garnet - epidote - chlorite - opaque
25-11	Calcite - diopside - tremolite - phlogopite - microcline plagioclase
29-12	Quartz - biotite - muscovite
32-1 a	Muscovite - biotite - chlorite - quartz - feldspar - magnetite
29-36	Quartz - muscovite - biotite - plagioclase (An_{15}) - microcline - tourmaline - opaque
29-14	Garnet - plagioclase - biotite - quartz - K-feldspar - carbonate - chlorite - magnetite
35-6	Quartz - muscovite - feldspar - chlorite - biotite - opaque
6Aug-3a	K-feldspar - plagioclase - biotite - muscovite - quartz - sulfides - chlorite - zircon
42-16	Muscovite - quartz - feldspar
32-1 b	Quartz - feldspar - chlorite - biotite - muscovite - hematite - tourmaline - calcite

6Aug 4 b	Plagioclase - K-feldspar - biotite - quartz - muscovite - garnet - sulfides - magnetite
27-3	Quartz - muscovite - biotite - feldspar - magnetite - hematite
37-20	Quartz - chlorite - feldspar - muscovite - biotite - magnetite
3/8-1	Quartz - K-feldspar - biotite - plagioclase - muscovite
28-24	Chlorite - epidote - quartz - carbonate - biotite - magnetite
15-16	Quartz - K-feldspar - biotite - plagioclase (An$_{43}$) - muscovite - garnet
42-13	Hornblende - quartz - plagioclase - K-feldspar - pyrite - sphene - ilmenite - biotite - carbonate
32-6	Muscovite - chlorite - quartz - biotite (?) - feldspar - ilmenite - magnetite
35-2	Biotite - quartz - muscovite - plagioclase - K-feldspar - chlorite
29-29	Biotite - quartz - muscovite - albite - K-feldspar - hematite
27-6	Muscovite - quartz - feldspar - biotite - hematite - chlorite
31-12	Chlorite - plagioclase - muscovite - magnetite - K-feldspar - quartz
34-21	Chlorite - plagioclase - muscovite - magnetite - K-feldspar - quartz
23-3a	Hornblende - plagioclase (An$_{45}$) - quartz - K-feldspar - garnet - chlorite - actinolite - magnetite - sphene
37-13	Muscovite - quartz
25-2	Quartz - muscovite - hematite
6Aug 3 b	Quartz - biotite - plagioclase (An$_{45}$) - garnet - opaque
31-12	Quartz - actinolite - biotite - microcline - albite - oligoclase - epidote - calcite - sphene - opaque
3/8-2	Hornblende - quartz - plagioclase (An$_{42}$) - epidote - biotite - sphene

29-34	Hornblende - actinolite - epidote - calcite - plagioclase (An_{57}) - quartz - sphene
43-3	Muscovite - quartz - biotite - tourmaline - opaque
23-7	Hornblende - actinolite - epidote - microcline - plagioclase - quartz - carbonate - biotite - sphene
43-11	Hornblende - quartz - microcline - plagioclase (An_{15}) - carbonate - sphene
42-3	Muscovite - plagioclase - epidote - quartz - biotite - carbonate
28-17	Hornblende - quartz - plagioclase - microcline - sphene
29-36	Amphibole - chlorite - biotite - quartz - plagioclase - K-feldspar (?) - magnetite
35-5	Muscovite - quartz - feldspar - biotite - chlorite
3/8-3	Quartz - feldspar - scapolite - biotite - muscovite - epidote
31-11	Quartz - plagioclase - K-feldspar - muscovite - chlorite

ASSEMBLAGES FROM ROCKS FROM KOOTENAY POINT NOT INCLUDED IN TABLE 4

Sample	Assemblages from Kootenay Point rocks
340-143E	Plagioclase - K-feldspar - quartz - biotite - muscovite
30-19E	K-feldspar - An_{15} plagioclase - quartz - biotite - apatite - zoisite - amphibole
45-62E	K-feldspar - plagioclase - quartz - amphibole - biotite
50-35E	An_{36} plagioclase - K-feldspar - biotite - zircon - chlo-
40-20E	Calcite - dolomite - muscovite
100-110E	Tremolite - calcite
200-140E	Actinolite - biotite - scapolite - feldspar - quartz
110-40W	Plagioclase (An_{30}) - quartz - K-feldspar - biotite
112-45W	Tourmaline - muscovite - apatite
100-008	Muscovite - calcite
125-75E	Calcite

128-002E	Talc - muscovite (?)
135-05W	Muscovite - calcite - talc (?) - epidote
155-75W	Tremolite - phlogopite (?)
188-106E	Calcite - muscovite
250-110W	Microcline - albite - quartz - muscovite - biotite
260-310E	K-feldspar - plagioclase (An_{15}) - quartz - biotite
266-143E	K-feldspar - quartz - garnet - biotite

Note - Some of the above assemblages do not appear in Figure 3.

T1-2	K-feldspar - quartz - plagioclase - biotite - muscovite - chlorite
T1-3	No thin section.
T1-7	Tremolite - biotite - calcite
T2-1	No thin section.
T2-7	Tremolite - diopside - calcite - dolomite - biotite - scapolite
T2-11	No thin section.
T2-12	Calcite - phlogopite - dolomite - scapolite
T2-13	Plagioclase - microcline - quartz - biotite - muscovite
T2-14	K-feldspar - albite - quartz - biotite - muscovite - carbonate
T2-16	No thin section.
T2-17	Tremolite - diopside - calcite - dolomite - biotite
T3-1	Calcite - actinolite - diopside - biotite - talc (?)
T3-6	Diopside - tremolite - calcite - quartz
T3-7	Calcite - dolomite - biotite
T3-8	Calcite - tremolite - quartz
T3-10	Albite - oligoclase - microcline - quartz - biotite - chlorite - apatite

T4-1	Albite - orthoclase - quartz - biotite - muscovite
T4-3	K-feldspar - quartz - plagioclase (An_{17}) - biotite
T4-5	Albite - microcline - quartz - biotite
T4-7	Microcline - quartz - plagioclase

APPENDIX 4

ZONED AMPHIBOLES FROM THE
CENTRAL KOOTENAY ARC
BRITISH COLUMBIA

Submitted by:
Stephen R. Winzer
Department of Geology
University of Alberta
Edmonton, Alberta, Canada
April 12, 1973

ABSTRACT

Amphibolites from the central Kootenay Arc contain optically zoned amphiboles. Optical zoning is expressed by an actinolite rim surrounding a pargasitic hornblende core, and optical boundaries may be either sharp or gradual.

Six zoned amphiboles were analyzed for nine elements in traverses across each grain. Chemical zonation is congruent to optical zonation. The zoned amphiboles lie along the join pargasitic hornblende $(Na_{.37}K_{.22})_{.59}Ca_{1.92}(Fe_{1.99}Ti_{0.9}Al_{.59}Mn_{.05}Mg_{2.41})Si_{6.59}Al_{1.41}O_{22}(OH)_2$ - aluminous actinolite $(Na_{.15}K_{.06})_{.21}Ca_{1.92}(Fe_{1.56}Ti_{.02}Al_{.30}Mn_{.04}Mg_{3.15}$ $Si_{7.44}Al_{.56}O_{22}(OH)_2$. The zoned amphiboles can be explained by reactions taking place in small volumes of rock within single thin sections and result from a change in equilibrium within polymetamorphic rocks. The hornblende cores of the Kootenay amphiboles were formed during the peak of the last metamorphism in the Kootenay Arc, with the actinolite rims developing during cooling. The reaction: hornblende + high Mg/Fe biotite 1 + 0.852 quartz = aluminous actinolite + lower Mg/Fe biotite 2 + 0.213 plagioclase is proposed to explain the zoning observed. The appearance of a solvus in the actinolite-pargasitic hornblende series completes the reaction.

INTRODUCTION

Recent contributions to the study of the amphibole group include analyses of coexisting amphiboles (Ernst, 1968; Klein, 1968; Kisch and Warnaars, 1969; Robinson and Jaffe, 1969; Stout, 1972), exsolution phenomena in amphiboles (Ross, Papike and Shaw, 1969; Bonnichsen, 1969; Robinson, Ross and Jaffe, 1971), and general amphibole crystal structure and chemistry (Leake, 1965, 1968; Papike, Ross and Clark, 1969; Robinson, Ross and Jaffe, 1971). Despite such detailed study, little mention has been made of zoning in amphiboles, with the exception of Crawford (1971, Klein (1969), Robinson, Jaffe, Klein and Ross (1969) and Cooper and Lovering (1970). Kisch and Warnaars (1969) and Bonnichsen (1969) mention rimmed amphiboles and replacement in amphiboles, but no quantitative data are provided. Compton (1958) mentions rimmed actinolites which might be the reverse of the zoning shown in this study.

Several studies of zoned garnets from metamorphic rocks have been reported (Atherton and Edmunds, 1966; Atherton, 1968; Edmunds and Atherton, 1971; Fediukova and Vejnar, 1971; Hollister, 1966, 1969). The first three studies relate the zoning to the polymetamorphic history of the rocks.

Metamorphosed lower Paleozoic rocks from the Kootenay Arc, British Columbia contain zoned amphiboles. The purpose of this study is to present quantitative information regarding these amphiboles and to discuss their origin in the light of recent work on the amphiboles and zoned garnets from metamorphic rocks.

GEOLOGIC SETTING

The Kootenay Arc is a narrow structural belt of highly deformed rocks extending from Revelstoke, British Columbia, southeast, south and southwest until it crosses the International Boundary. Samples for this study were collected from the central part of the Kootenay Arc along the eastern shore of Kootenay Lake. The zoned amphiboles are found in amphibolite pods included in the Lower Paleozoic Lardeau Formation. These pods take the form of large boudins up to 10 meters thick and several hundred meters long that are sandwiched between granular calc-silicate rocks comprising the lithology of the lower Lardeau Formation (Fyles, 1964; Crosby, 1968). The amphibolites are probably metamorphosed basic volcanics that have been boudinaged by fairly intense deformation.

The samples were collected from a small promontory on Kootenay Lake. The sample area lies 4.5 km west of the hornblende and 3.5 km west of the garnet isograds. Regional metamorphic grade increases from east to west. The reactions forming tremolite (5Dolomite + 8quartz + H_2O = tremolite + 3calcite + $7CO_2$) and diopside (Tremolite + 3calcite + 2quartz = 5diopside + $3CO_2$ + H_2O) (Winkler, 1967) occur concurrently in rocks immediately adjacent to those containing zoned amphiboles. Temperatures of about 500°C have been obtained from these rocks through use of the calcite-dolomite thermometer (Winzer, 1973). The maximum temperatures obtained from stable isotopes (Ohmoto and Rye, 1970) from material 9 km north and at the same grade are in good agreement with those obtained from the sample area. Rocks from a small area 11.3 km NNW contain kyanite in unstable association with staurolite, but these rocks have been influenced by contact metamorphism, making their regional significance uncertain. Reactions forming staurolite from kyanite + chloritoid or forming staurolite + biotite + quartz from chlorite + muscovite take place at temperatures somewhat higher than those indicated for the sample locality (den Tex, 1971). The evidence cited above suggests that the rocks formed under conditions of the upper part of the garnet zone, at or just below the staurolite isograd, but no staurolite isograd can be mapped on the east side of Kootenay Lake.

All six samples are located in separate pods of amphibolite within 170 meters of each other. These pods are surrounded by actinolite and diopside gneisses, biotite, phlogopite and talc schists, micaceous marbles and pegmatites. They are cut by aplite and pegmatite dikes from a few centimeters to 10 meters thick (Map, Fig. 1). Although larger bodies show no chilled borders or aureoles, several smaller aplites and pegmatites have aureoles a few centimeters wide. No reaction zones are apparent at contacts between beds.

The central Kootenay Arc has a long metamorphic history, encompassing at least 100 m.y. K-Ar age dating indicates two metamorphic events, one occurring between 120 and 150 m.y., the other between 50 and 70 m.y. Rb/Sr mineral "isochrons" for eleven biotite-amphibole pairs from the sample area indicate recrystallization of older material about 50 m.y. ago and further indicate that complete isotopic homogenization was not achieved by the later event. Three phases of deformation have been differentiated by Fyles (1964, 1967) and by Crosby (1968), but the relationship between structure and metamorphism is not well understood.

Evidence of metasomatic introduction of at least K and Na exists for rocks lying above the hornblende and garnet isograds (Winzer, 1973).

Detailed chemical and petrographic work by Winzer (1973) indicates that in some rocks from the sample area biotite formed by metasomatic introduction of K and did not equilibrate with amphiboles with respect to Fe, Ti and trace elements.

ANALYTICAL METHODS

Six grains showing varying degrees of optical zonation were chosen from polished thin sections. These grains were photographed in plane-polarized transmitted and reflected light. Each was marked with a diamond scriber, and an area including the rim and central core of the grain was chosen for traversing. An ARL-EMX microprobe was used for all analytical work. A 15 kv acceleration potential and a 0.15 microamp beam current (approximately 0.015 microamp specimen current) were used for Ca, Na and K; 0.3 microamp (approximately 0.03 microamp specimen current) was used for the remaining six elements. ADP crystals were used for Ca and Si; RbAP for Na, Al and Mg; EDDT for K; LiF for Ti, Fe and Mn. The spot size was held to < 1 micron and checked frequently for drift. Using a one second count time and a Rikadenki three pen recorder, a continuous trace was initially made and was then used as a guide for locating ten or eleven stations on each grain. Ten ten-second counts were then taken within an area that was never more than three microns in diameter. If the number of counts varied outside of the range expected for a normal statistical distribution for a homogeneous material at the 99 percent confidence level, additional counts were taken. Each station was analyzed for nine elements with return to stations facilitated by reflected light photographs. Raw data were corrected for background, fluorescence, absorption and atomic number effects by means of the APL program PROBEDATA (Smith and Tomlinson, 1970). Standards used were the Kakanui kaersutite (Mason, 1968; White _et al._, 1972) and a well analyzed biotite. Both were previously analyzed by wet chemical methods and checked for homogeneity. The amphibole analyses for this study are believed to be accurate to within ± one percent of the total for all elements except Ti and Mn, which may have a slightly larger error.

PETROGRAPHY AND PETROLOGY

The specimens chosen are similar in hand specimen and occurrence. All amphibolite pods sampled are either partially enclosed in or cut by pegmatite and some are cut by later aplite dikes. No chill borders or reaction rims are detectable between the amphibolites and either intrusive. In hand specimen the amphibolites are dark green or greenish black foliated rocks containing optically zoned amphibole and varying amounts of biotite, feldspar, quartz, diopside, epidote, scapolite and sulfide minerals (for modal percentages, see Table 1). The pale colored minerals occur in discontinuous lenses. In several samples, diopside veins cut the foliations at high angles, and knots of diopside form. (For petrographic descriptions, see Appendix 1).

ZONED AMPHIBOLES

Continuous traverses and point traverses were made on zoned amphiboles from six specimens. One grain (T2-15) was chosen as representative of the maximum zoning found in all six grains. The data for T2-15 are presented in Table 2 and Figs. 2, 3 and 4. Fig. 4 illustrates the zoning trends for all six grains in terms of changes in tetrahedral Al and _A_-site occupancy.

General observations on amphibole zoning

1. Optically zoned amphiboles occur in rocks of suitable composition from the entire region lying at or above the hornblende isograd. In most cases, a dark green core hornblende is surrounded by a pale green or bluish-green rim of actinolite. In rocks from the region and from the sample area, two amphiboles are seen to coexist in apparent textural equilibrium, but some two amphibole assemblages consist of zoned hornblende and separate grains of bluish-green actinolite. Patchy "intergrowths" of actinolite within hornblende grains, as reported by Klein (1969), do occur in the region but are rare and occur at or very near the hornblende isograd.

A range of textures are found and are typified by the six amphiboles studied in detail. Where chemical zonation is not great, no sharp optical boundaries are observed, but where chemical zonation is large, the boundaries between rim and core are sharp, and in T2-15 and 375-140W even show a poorly defined Becke line between core and rim.

2. In every case the core is enriched in K, Na, Fe and Ti and the rim is enriched in Ca, Si and Mg.

3. Where changes of less than six weight percent occur in the major elements (Si, Mg and Al generally), the transition zone between core and rim is smaller than where large changes occur. There sharp changes in amounts of major elements and sharp optical boundaries indicate that aluminous actinolite and pargasitic hornblende exist as two separate phases.

4. Antipathetic variations occur between Fe and Mg, between Si and Al and between Ca and Na + K when large changes from rim to core occur. Where zoning is more subtle, variation is not always antipathetic, as in

240-137E, T2-15, T4-4b and T4-8b.

5. Core and rim zones on all grains differ by major differences in Ca, Mg and Si values. Both core and rim may show compositional variation, with the core portion showing compositional variation to the optical boundary with the rim, and a rim which is homogeneous, or shows subtle variation. Zoning trends are well illustrated by the plots of A-site occupancy against tetrahedral Al (Fig. 4).

DISCUSSION AND CONCLUSIONS

Crawford (1971) reports cryptically zoned amphiboles ranging in composition from $Ca_2Mg_3Fe_2Si_8O_{22}(OH)_2$ to $(Na,K)_{0.5}Ca_2Mg_{1.5}Fe_{2.8}Al_{0.7}Si_{6.6}Al_{1.4}(OH)_2$ along the actinolite-pargasite join. She attributes this variation to substitution of $(Na,K)_{1-X}Al_3Fe^{+2}_{1-X}Fe^{+3}_X$ for Mg_2Si_2 in the actinolite end member.

The present study concerns amphiboles along the join hornblende-actinolite, with some pargasite substitution, but indicates that while the above substitutions may be valid, the situation is likely to be more complex. The amphiboles studied by this author extend the possible range of solid solution further towards the pargasite end member as compared to Crawford (1971) and Cooper and Lovering (1970).

Examination of the plot for T2-15 (Fig. 3) indicates that as Na and K increase, Ti, Al^{IV}, Al^{VI} and Fe increase, while Si and Mg decrease. This relationship suggests that the same compensatory scheme operates for actinolite-hornblende as for gedrite (Robinson, Ross and Jaffe, 1971). The changes for calcium are subtle, but where tremolite is present, the change is quite sharp, as indicated by intensity traces for 375-140W where tremolite is present within the actinolite rim. Robinson, Ross and Jaffe (1971) suggest a control between A-site occupancy and tetrahedral Al. The amphiboles studied by this author show that the relation is sympathetic as demonstrated by the plots of tetrahedral Al against A-site occupancy (Fig. 4).

The geological implications of these zoned amphiboles are interesting. Atherton and Edmunds (1966), and Atherton (1971) in their work on zoned garnets suggest that the garnet core behaves as a closed system within the rock and that zoning patterns are indicative of changing equilibrium conditions during growth. Hollister (1966, 1969) provides a different model wherein the large difference between fractionation factors for Mn, Fe and Mg between garnet and rock exert primary influence on garnet zoning. The fractionation factor may vary with temperature and relative proportions of non-refractory minerals in the rock. Aspects of both models might apply to the amphibole zoning found in this study. To test for equilibrium, biotite coexisting with zoned amphiboles in the six specimens studied has been analyzed by electron microprobe. Representative analyses are presented in Table 3. Biotites from all six rocks are similar in that they show no zoning and appear to be approaching textural equilibrium with the surrounding minerals. Mg/Mg+Fe and Ti/Ti+Fe ratios have been plotted for both hornblende rim and core and the coexisting biotites (Fig. 5). Both plots show considerable scatter, indicative of a lack of close approach to equilibrium for both rim, core and coexisting biotite. This is in agreement with major and trace element data for these and other amphibole-biotite pairs from the same area. Examination of biotites coexisting with unzoned hornblende (from rocks of similar composition) indicates that they are generally more magnesian than those coexisting with zoned amphiboles. The difference in biotite composition for rocks very close (< 10m) together suggests that the change in biotite composition is related to the zoned amphibole. The textural relationships between biotite and amphibole suggests exchange with the rim (the biotite is usually not in contact with the core, but may be enclosed by the rim).

From the evidence cited above, it is concluded that the core zone of the amphiboles studied has been effectively isolated from the rock system with respect to major and most minor elements and represents conditions of the amphibolite facies metamorphism which last affected the area. Depending on internal conditions of the rock, some of the host hornblendes exsolved cummingtonite, quite possibly in equilibrium with the host, as suggested by Ross, Papike and Shaw (1969). The next step in the evolution of the zoned amphiboles was a retrogressive one. This retrogressive event could be due to slow cooling from the thermal peak reached during the main regional event, or it could be due to metasomatism under conditions of changing fluid composition in an open system. Reactions producing actinolite are usually associated with greenschist facies metamorphism, both regional and contact. Winkler (1967) suggests two prograde reactions: For contact metamorphism Chl+(Tr-Act)+Ep+Qtz = Hb+Anth+H_2O. For regional metamorphism Chl+(Tr-Act)+Ep+Qtz = Hb. Geological evidence, as well as textural evidence and lack of aureoles around the larger intrusions in the sample area, indicates that in the Kootenay amphiboles the effects result from regional metamorphism, but at lower temperatures and possibly different pressures and fluid compositions than the event producing the hornblende cores. The occurrence of similar textures from other locations within the region rule out local metasomatic effects.

The retrograde reaction involves significant exchange of Si, Al, Mg and Fe, and smaller amounts of Ca, Na and K. Biotites coexisting with unzoned hornblendes from the same area show generally higher Mg, Si and Al and lower Fe and Ti than biotites present in rocks containing zoned amphiboles. On the basis of the relationship between amphibole and biotite shown by the Mg/Mg+Fe and Ti/Ti+Fe plots, it is assumed that a biotite similar to that coexisting with unzoned hornblende existed prior to the retrograde reaction. This biotite (biotite 1) exchanges Mg, Fe, Si, Al and Ti with the hornblende (represented by the core composition) to form biotite 2 and the actinolite rim. A certain amount of Ca, Na, K and Al is left over to become incorporated into plagioclase, whose presence demands a small amount of quartz among the reactants. Using only the anhydrous formulae calculated from mineral analyses for T2-15 (hornblende, actinolite, biotite 2 and plagioclase), a balanced reaction can be obtained with suitable modification of biotite 1. The reaction is:

hornblende

$(Na_{.37}K_{.22})Ca_{1.92}(Fe_{1.99}Ti_{.09}Al_{.58}Mn_{.05}Mg_{2.41})Si_{6.59}Al_{1.41}O_{22}$ +

Biotite 1

$(K_{1.79}Na_{.07}Ca_{.06})(Fe_{2.11}Ti_{.25}Al_{.26}Mn_{.03}Mg_{3.10})Si_{5.76}Al_{2.24}O_{22}$ +

Aluminous Actinolite

$0.852SiO_2 = (Na_{.24}K_{.13})Ca_{1.908}(Fe_{1.79}Ti_{0.5}Al_{.47}Mn_{.04}Mg_{2.8})Si_{6.96}Al_{1.04}O_{22}$

Biotite 2

$+ (K_{1.88}Na_{.05}Ca_{.02})(Fe_{2.32}Ti_{.30}Al_{.36}Mn_{.03}Mg_{2.71})Si_{5.67}Al_{2.33}O_{22}$ +

Plagioclase

$0.213(Ca_{.26}Na_{.72}K_{.01})Al_{1.27}Si_{2.73}O_8$.

This reaction involves no hydration or dehydration. It can only be considered valid for T2-15, but the similarity of all zoned amphibole parageneses indicates that the general form of the reaction would hold, with modifications dependent on mineralogy. The same type of reaction can be written for 375-140W which has a plagioclase of An_{44} coexisting with the zoned amphibole and biotite. The composition of the original biotite turns out to be similar to the biotites coexisting with the less radically zoned amphiboles (T4-8a, T4-4b and 240-137E). The original biotites cannot be strictly compared to any biotite in the area coexisting with zoned or unzoned amphiboles because there is considerable range in rock composition, a factor of critical importance in determining biotite composition. The presence of epidote would produce some differences in the reaction, but these differences cannot be quantified without further data.

The reaction and the reasons for it are undoubtedly more complex than indicated here, especially with respect to the oxidation state of the iron and the water content of the hydrous phases. The data does not permit discussion of these problems, but they do indicate that the reaction can proceed without the necessity of introducing components from outside the thin section. The reaction, in general, demands some calcium from the reactants. This calcium can be provided by the biotite, but it could also be provided by a more anorthite-rich plagioclase among the reactants. The reaction would then have higher An plagioclase on the reactant side going to more Ab rich plagioclase on the product side. The reaction is balanced by changes in the Al content for biotite 1 and lessening the amount of quartz among the reactants.

If the system were open, exchange reactions involving K, Na and possibly Al and Si could explain the zoning found. The reaction would be considerably more complex than the one proposed because it involves exchange of at least two solid phases with a fluid. Because less mobile components like Mg and Fe are involved in the exchange, an earlier magnesium-iron silicate or carbonate is needed. Dolomite is usually present in adjacent rocks, but not in the amphibolites. Large amounts of chlorite are not present or indicated, thus the pre-existing phase must still be biotite. Feldspar components could be introduced during metasomatism. The exchange with the actinolite rim would be facilitated by the fluid and the instability of biotite 1 in the presence of changing fluid composition. Textural evidence does not favor formation of biotite by metasomatism in the six rocks studied, although carbonate and calc-silicate rocks surrounding the amphibolites are clearly metasomatic. This author has interpreted these textures as evidence of differential mobility of alkalis in different rocks (Winzer, 1973). It is considered that the reaction proceeds in small volumes of rock behaving as essentially closed systems, responding to changes of temperature and pressure following the thermal peak of metamorphism.

The reaction and the development of the actinolite rim on the zoned amphiboles are further complicated by the possible existence of solvi within the actinolite-pargasitic hornblende series. Coexisting hornblendes and actinolites have been discussed most recently by Klein (1969), Cooper and Lovering (1970), Cooper (1972) and Read (1973). Cooper and Lovering (1970) and Read (1973) both document the existence of forbidden compositional regions within the hornblende-actinolite series. Fig. 6, a plot of coexisting amphiboles from several areas, indicates forbidden compositional areas, and thus possible solvi in the series hornblende, or pargasitic hornblende-actinolite. Read (1973), on the basis of 70 analyses of amphiboles from the chlorite zone of central and western Otago, New Zealand, has found a compositional gap in the actinolite-hornblende series in the range of $Al^{IV} = 0.6-0.9$ ions to 23 oxygens at $M(4) = 2Ca$ narrowing to and disappearing at $Al^{IV} = 0.7$

at M(4) = 1.6Ca. There is some evidence for the presence of a solvus in the series actinolite-pargasitic hornblende in the central Kootenay Arc and in the zoned amphiboles. Fig. 7 is a plot of 40 amphibole analyses from regional metamorphic rocks and of rocks from the area discussed in this paper. All occur at or above the hornblende isograd. Tielines join coexisting pairs, one of which is plotted in Fig. 6 (5LBT-22). There is a lack of analyses falling between $Al^{IV}0.65$ and $Al^{IV}1.2$, with A-site occupancies of 0.35-0.4.

This plot must be used with care since compositional controls may produce some of the compositional range shown. Only 31-38 (5LBT-22) and 22-13 are pairs. 31-38 (5LBT-22) comes from just above the hornblende isograd; 22-13 comes from the area sampled for this study. These pairs, provided they coexist stably, are evidence for a solvus, but the stable coexistence of 31-38 (5LBT-22) is not certain.

Examination of Fig. 4 reveals a range in composition for the zoned amphiboles of from $Al^{IV} = 1.75$, A-site occupancy = 0.69 to $Al^{IV} = 0.55$, A-site occupancy = 0.17. Recalling the textural relations for rim and core for T2-15 and 375-140W, wherein a Becke line was found, and the evidence from Fig. 7 and the studies of Read (1973) and Cooper and Lovering (1970), the zoning for T2-15 suggests a discontinuous series, with the interference of a solvus.

The metamorphism in the central Kootenay Arc is quite similar to that of the Otago area (Winzer, 1973), thus a solvus might be expected at the temperatures and pressures found in the Kootenay Arc. If a solvus exists in the actinolite-hornblende series as present evidence suggests, then this solvus further complicates the reaction proposed. The present author considers that the zoned amphiboles developed as follows:

The original core pargasitic hornblende formed, along with the other minerals in the rock during the last metamorphic event in the Kootenay Arc. Following this event, during cooling of the rock, the core hornblende reacted with its coexisting minerals (or with a fluid), changing the composition of the rim in the direction of increasing actinolite. In some grains, the reaction ceased with only slight zoning produced, but in others, the reaction continued until the composition of the rim intersected the solvus, whereupon a new actinolite on the other side of the solvus would nucleate as a phase separate from the composition of the rim of the zoned grain. The reverse of this situation would occur during prograde reactions involving actinolite and hornblende across the hornblende isograd, in regions where the physical conditions are such that the solvus would be intersected.

The mechanism for producing the zoned amphiboles is thus more complex than that of Hollister (1966, 1969) for garnet and staurolite zoning. It is closer to the model of Atherton and Edmunds (1966), where the zoning is produced by a change in equilibrium conditions for the rock. The core hornblende is "refractory" in the sense of Hollister (1969) at the initiation of the reaction and perhaps for a portion of the period for which the reaction runs, for it gives up material used in the formation of the actinolite rim. The hornblende core would rapidly become isolated from the rest of the rock by growth of the actinolite rim. The reaction further differs from the type producing zoned garnets in that, for the hornblende-actinolite zoning, the interference of a solvus complicates the exchange. Further work is being done, both on reactions producing zoned amphiboles and on the definition of the solvus of the region.

ACKNOWLEDGMENTS

I am indebted to Professor Richard St. J. Lambert and Dr. D. G. W. Smith for valuable comments concerning the manuscript and also to Dr. Richard C. Fox for editorial comments. I am grateful to Dr. D. G. W. Smith for making available the microprobe facilities which are supported by N.R.C. Grant #554648. This work was done while under the support of an N.R.C. pre-Doctoral Scholarship.

REFERENCES CITED

Atherton, M.P. (1968) The variations in garnet, biotite and chlorite compositions in medium grade pelitic rocks from the Dalradian, Scotland. Contrib. Mineral. Petrology, 18, 347-371.

____ and W.M. Edmunds (1966) An electron microprobe study of some zoned garnets from metamorphic rocks. Earth and Planet. Sci. Lett. 1, 185-193.

Bonnichsen, B.(1969) Metamorphic pyroxenes and amphiboles in the Biwabik Iron Formation, Dunka River area, Minnesota. Mineral. Soc. Amer. Spec. Pap. 2, 217-241.

Compton, R.R. (1958) Significance of amphibole paragenesis in the Bidwell Bar region, California. Amer. Mineral. 43, 890-907.

Cooper, A.F. (1972) Progressive metamorphism of metabasic rocks from the Haast Schist Group of Southern New Zealand. J. Petrology, 13, 457-492.

_____ and J. F. Lovering (1970) Greenschist amphiboles from Haast River, New Zealand. Contrib. Mineral. Petrology, 27, 11-24.

Crawford, M.L. (1971) Zoned amphiboles on the actinolite-pargasite join. Geol. Soc. Amer. Abstr. 3, #7, 533.

Crosby, P. (1968) Tectonic, plutonic and metamorphic history of the Central Kootenay Arc, British Columbia, Canada. Geol. Soc. Amer. Spec. Pap. 99. 94 pp.

Den Tex, E. (1971) The facies groups and facies series of metamorphism, and their relation to physical conditions in the earth's crust. Lithos, 4, 23-31.

Edmunds, W.M. and M.P. Atherton (1971) Polymetamorphic evolution of garnet in the Fanad aureole, Donegal, Eire. Lithos, 4, 147-161.

Ernst, W.G. (1968) Amphiboles. Springer-Verlag, New York. 125 pp.

Fediukova, E. and Z. Vejnar (1971) Optic and cryptic zoning of garnets in west Bohemian amphibolites. Lithos, 4, 205-212.

Fyles, J.T. (1964) Geology of the Duncan Lake Area, Lardeau District, British Columbia. Bull. B.C. Dept. Mines and Petrol. Res. 49. 87 pp.

_____ (1967) Geology of the Ainsworth-Kaslo area, British Columbia. Bull. B.C. Dept. Mines and Petrol. Res. 53. 125 pp.

Hollister, L. S. (1966) Garnet zoning: an interpretation based on the Rayleign fractionation model. Science, 154, 1647-1651.

_____ (1969) Contact metamorphism in the Kwoiek area of British Columbia: an end member of the metamorphic process. Geol. Soc. Amer. Bull. 80, 2465-2494.

Kisch, H.J. and F.W. Warnaars (1969) Distribution of Mg and Fe in cummintonite-hornblende and cummingtonite-actinolite pairs from metamorphic assemblages. Contrib. Mineral. Petrology, 24, 245-267.

Klein, C. (1968) Coexisting amphiboles. J. Petrology, 9, 281-330.

_____ (1969) Two amphibole assemblages in the system actinolite-hornblende-glaucophane. Amer. Mineral. 54, 212-237.

Leake, B.E. (1965) The relationship between composition of calciferous amphiboles and grade of metamorphism. In W. S. Pitcher and G. W. Flynn, Eds. Controls of metamorphism. Oliver and Boyd, Edinburgh, 299-318.

_____ (1968) Catalogue of analyzed calciferous and sub-calciferous amphiboles together with their nomenclature and associated minerals. Geol. Soc. Amer. Spec. Pap. 98. 210 pp.

Mason, B. (1968) Eclogitic xenoliths from volcanic breccia at Kakanui, New Zealand. Contrib. Mineral. Petrology, 19, 316-327.

Ohmoto, H. and R.O. Rye (1970) The Bluebell Mine, British Columbia. 1. Mineralogy, paragenesis, fluid inclusions and isotopes of hydrogen, oxygen and carbon. Econ. Geol. 65, 417-437.

Papike, J.J., M. Ross and J.R. Clark (1969) Crystal-chemical characterization of clinoamphiboles based on five new structural refinements. Mineral. Soc. Amer. Spec. Pap. 2, 117-136.

Read, P.B. (1973) Metamorphic amphiboles from the chlorite zone of central and western Otago, New Zealand. Abstr. Mineral. Assoc. Can. 90.

Robinson, P. and H.W. Jaffe (1969) Chemographic exploration of amphibole assemblages from central Massachusetts and southwestern New Hampshire. Mineral. Soc. Amer. Spec. Pap. 2, 251-274.

______, ______, C. Klein and M. Ross (1969) Equilibrium coexistence of three amphiboles. Contrib. Mineral. Petrology, 22, 248-258.

______, M. Ross and H. W. Jaffe (1971) Composition of the anthophyllite-gedrite series, comparisons of gedrite and hornblende, and the anthophyllite-gedrite solvus. Amer. Mineral. 256, 1005-1041.

Ross, M, J.J. Papike and K.W. Shaw (1969) Exsolution textures in amphiboles as indicators of subsolidus thermal histories. Mineral. Soc. Amer. Spec. Pap. 2, 275-299.

Shido, F. and A. Miyashiro (1959) Hornblendes of basic metamorphic rocks. J. Fac. Sci. Univ. Tokyo, Sec. II, 12, 85-102.

Smith, D.G.W. and M.C. Tomlinson (1970) An APL language computer program for use in electron microprobe analyses. Computer Contrib. #45, State Geol. Surv., Univ. Kansas, Lawrence, 28 pp.

Stout, J.H. (1972) Phase petrology and mineral chemistry of coexisting amphiboles from Telemark, Norway. J. Petrology, 13, 99-145.

White, A.J.R., B.W. Chappell and P. Jakes (1972) Coexisting clinopyroxene, garnet and amphibole from an 'eclogite', Kakanui, New Zealand. Contrib. Mineral. Petrology, 34, 185-191.

Winkler, H. G. F. (1967) Petrogenesis of Metamorphic Rocks. Springer-Verlag, New York, 237 pp.

Winzer, S.R. (1973) Metamorphism and Chemical Equilibrium in Some Rocks from the Central Kootenay Arc, British Columbia. Ph.D. thesis, University of Alberta, Edmonton, Alberta.

Appendix 1

PETROGRAPHIC DESCRIPTION

This description applies to all rocks examined in this study. See Table 1 for mineral percentages and other details.

All rocks are holocrystalline-lepidoblastic to nematoblastic foliated biotite amphibolites.

Amphibole (hornblende) is anhedral to subhedral, usually with embayed boundaries. Grains are commonly poikilitic, enclosing quartz, biotite and plagioclase. All grains are zoned with cores pleochroic α yellowish-green to greenish brown, $\beta = \gamma$ (usually) green or yellow green but in 375-140W β = yellow green and γ = dark green or olive green. Rims are pleochroic α paler green, sometimes with a bluish tinge, $\beta = \gamma$ yellow green or green. Some rims disappear on rotation of the stage because the γ absorption colors for the rim are the same as for the core. Rims poikilitically enclose quartz and biotite (some grains) while in others the actinolite rim separates the core from another hornblende. Very fine, colorless cummingtonite is exsolved in the cores of T1-9a, T2-15 and 375-140W.

Biotite is euhedral to subhedral and about 1-2 mm long. It is pleochroic red or brownish red to yellow brown or colorless. Biotite is commonly enclosed in the rim, sometimes in the core of the amphiboles. Chlorite (penninite) occurs as an alteration product of biotite, and is found in cleavage traces of biotite. In some cases it replaces over half the grain. Plagioclase is anhedral and may be either twinned or untwinned. It occurs both in "veins" and scattered throughout the rock. Some grains are normally zoned. Microcline has the same habit as plagioclase. Microcline twinning occurs in patches in an otherwise untwinned grain. Epidote occurs in only two sections. It is poikilitic, irregular and anhedral and appears to be being absorbed by growing hornblende. Chemically this mineral lies between epidote and clinozoisite, but optically it is identifiable as epidote. Sphene occurs in all amphibolites as subhedral to euhedral grains up to 2 mm long.

TABLE 1. MODAL ANALYSES*

	T2-15	T4-4b	230-137E	375-140W	T4-8b	T1-9a
Biotite	42.1	9.6	tr	5.2	1.5	24.3
Hornblende	26.2	54.2	91.7	72.1	66.4	67.1
Plagioclase	22.4 (An26)	5.3 (An41)	3.2 (An44-38)	21.0 (An44)	14.0 (An37)	1.5 (An37)
Microcline		6.0	0.3	0.3	2.9	0.6
Quartz	8.9	11.0	1.3	0.1	5.1	
Epidote		11.3			6.7	
Sphene	tr	2.2	3.3	1.3	3.4	3.2
Scapolite		tr			tr	
Calcite						2.1
Dolomite		0.3	0.1			
Chlorite		0.1				1.2
Opaque				tr (Pyr.)	tr (Pyr-Mt)	

*Based on 1200 counts per section

TABLE 2. ELECTRON MICROPROBE ANALYSES OF ZONED AMPHIBOLES
FROM KOOTENAY LAKE

	Rim			Core			Rim			
T2-15	1	2	3	4	5	6	7	8	9	10
SiO_2	47.58	51.05	50.83	43.59	43.17	44.04	47.99	47.55	47.25	48.04
TiO_2	.41	.21	.21	.76	.76	.77	.73	.38	.39	.38
Al_2O_3	8.8	5.05	5.00	11.24	11.02	11.11	11.04	7.65	8.18	7.77
FeO	14.64	12.82	12.76	15.67	15.6	15.60	15.55	14.02	14.14	14.02
MnO	.34	.34	.34	.36	.37	.36	.36	.35	.35	.35
MgO	12.85	14.51	14.58	10.59	10.6	10.70	12.97	12.71	12.55	12.95
CaO	12.18	12.32	12.44	11.89	11.75	11.90	12.02	12.08	12.21	12.18
Na_2O	.83	.52	.47	1.23	1.23	1.14	1.14	.84	.77	.80
K_2O	.67	.33	.34	1.09	1.12	1.12	1.10	.62	.59	.59
Total	98.3	97.15	96.96	96.44	95.62	96.75	102.91	96.2	96.42	97.09
Structural formula on the basis of 23 oxygens										
Si	6.958	7.437	7.422	6.594	6.592	6.631	6.733	7.087	7.031	7.087
Al	1.042	.563	.578	1.046	1.408	1.369	1.267	.913	.969	.913
Total	8	8	8	8	8	8	8	8	8	8
Al	.474	.304	.283	.598	.575	.603	.599	.430	.465	.439
Ti	.045	.023	.023	.087	.088	.087	.078	.043	.043	.042
Fe	1.790	1.561	1.558	1.983	1.993	1.964	1.825	1.748	1.759	1.730
Mn	.042	.042	.042	.047	.048	.045	.043	.044	.044	.044
Mg	2.800	3.151	3.174	2.388	2.412	2.402	2.713	2.824	2.783	2.847
Total	5.150	5.081	5.080	5.103	5.116	5.101	5.218	5.089	5.094	5.102
Ca	1.908	1.924	1.947	1.928	1.923	1.920	1.807	1.929	1.947	1.926
Na	.235	.146	.133	.361	.365	.334	.310	.243	.222	.228
K	.125	.061	.062	.211	.218	.216	.197	.117	.112	.111
Total	2.268	2.131	2.142	2.500	2.506	2.470	2.314	2.289	2.281	2.265

TABLE 3. BIOTITE ANALYSES

	T2-15	240-137E	375-140W
SiO_2	37.47	37.67	37.25
TiO_2	2.59	1.74	1.87
Al_2O_3	15.11	16.12	16.07
FeO	18.30	13.07	15.97
MnO	.24	.11	.14
MgO	12.04	15.96	13.36
CaO	.09	.06	tr
Na_2O	.16	.35	.10
K_2O	9.73	9.80	9.70
F	.17	.26	1.95
Cl	.07	.03	0
Total	95.97	95.17	96.41
Ions per 22 oxygens			
Si	5.667	5.602	5.636
Al^{IV}	2.333	2.398	2.364
Total	8.000	8.000	8.000
Al^{VI}	.360	.428	.502
Ti	.295	.195	.213
Fe	2.315	1.626	2.021
Mn	.031	.014	.018
Mg	2.714	3.538	3.013
Total	5.714	5.800	5.767
Ca	.015	.010	0
Na	.047	.101	.029
K	1.877	1.859	1.872
Total	1.939	1.970	1.902

TABLE 2. ELECTRON MICROPROBE ANALYSES OF ZONED AMPHIBOLES FROM KOOTENAY LAKE

	Rim			Core			Rim				Adj.grain		Rim	Core			
	T2-15-1	2	3	4	5	6	7	8	9	10	T4-4b-1	2	3	4	5	6	7
SiO_2	47.58	51.05	50.83	43.59	43.17	44.04	47.99	47.55	47.25	48.04	40.73	40.76	43.16	41.11	41.29	41.14	41.08
TiO_2	.41	.21	.21	.76	.76	.77	.73	.38	.39	.38	1.02	.98	.46	.71	1.05	1.16	1.09
Al_2O_3	8.80	5.05	5.00	11.24	11.02	11.11	11.04	7.65	8.18	7.77	13.55	13.56	11.49	13.07	13.37	13.26	13.25
FeO	14.64	12.82	12.76	15.67	15.60	15.60	15.55	14.02	14.14	14.02	17.99	18.07	17.36	17.99	17.94	17.68	17.78
MnO	.34	.34	.34	.36	.37	.36	.36	.35	.35	.35	.27	[illegible]	.26	.27	.27	.27	.29
MgO	12.85	14.51	14.58	10.59	10.6	10.7	12.97	12.71	12.55	12.95	8.75	8.70	10.09	8.87	8.70	8.57	8.86
CaO	12.18	12.32	12.44	11.89	11.75	11.90	12.02	12.08	12.21	12.18	11.69	11.55	12.03	12.07	11.62	11.63	11.74
Na_2O	.83	.52	.47	1.23	1.23	1.14	1.14	.84	.77	.80	1.36	1.38	1.11	1.23	1.41	1.41	1.34
K_2O	.67	.33	.34	1.09	1.12	1.12	1.10	.62	.59	.59	1.35	1.38	1.06	1.39	1.37	1.33	1.28
Total	98.30	97.15	96.96	96.44	95.62	96.75	102.91	96.20	96.42	97.09	96.71	96.66	97.03	96.75	97.02	96.45	96.72
Structural Formula on the basis of 23 oxygens																	
Si	6.958	7.437	7.422	6.594	6.592	6.631	6.733	7.087	7.031	7.087	6.247	6.256	6.252	6.306	6.303	6.311	6.289
Al	1.042	.563	.578	1.406	1.408	1.369	1.267	.913	.969	.913	1.753	1.744	1.458	1.694	1.697	1.689	1.711
Total	8	8	8	8	8	8	8	8	8	8	8	8	8	8	8	8	8
Al	.474	.304	.283	.598	.575	.603	.599	.43	.465	.439	.696	.708	.595	.669	.708	.708	.679
Ti	.045	.023	.023	.087	.088	.087	.078	.043	.043	.042	.118	.113	.052	.082	.121	.134	.126
Fe	1.79	1.561	1.558	1.983	1.993	1.964	1.825	1.748	1.759	1.730	2.308	2.320	2.200	2.308	2.289	2.269	2.276
Mn	.042	.042	.042	.047	.048	.045	.043	.044	.044	.044	.036	.035	.034	.035	.035	.036	.038
Mg	2.800	3.151	3.174	2.388	2.412	2.402	2.713	2.874	2.783	2.847	1.999	1.991	2.280	2.028	1.978	1.960	2.021
Total	5.150	5.081	5.080	5.103	5.116	5.101	5.218	5.089	5.094	5.102	5.157	5.167	5.161	5.122	5.131	5.107	5.140
Ca	1.908	1.924	1.947	1.928	1.923	1.920	1.807	1.929	1.947	1.926	1.921	1.899	1.953	1.984	1.900	1.911	1.926
Na	.235	.146	.133	.361	.365	.334	.310	.243	.222	.228	.403	.411	.327	.381	.417	.420	.399
K	.125	.061	.062	.211	.218	.216	.197	.117	.112	.111	.264	.271	.205	.272	.267	.259	.249
Total	2.268	2.131	2.142	2.500	2.506	2.470	2.314	2.289	2.281	2.265	2.588	2.581	2.485	2.637	2.584	2.590	2.574

TABLE 2. ELECTRON MICROPROBE ANALYSES OF ZONED AMPHIBOLES FROM KOOTENAY LAKE

	Rim		Core									Rim	Rim		Core		
	T4-4b8	9	240-137	2	3	4	5	6	7	8	9	10	325-170W	2	3	4	5
SiO_2	40.98	42.87	44.40	43.84	43.83	43.40	43.62	43.8	44.0	44.36	44.54	47.92	47.73	48.2	43.95	42.93	42.81
TiO_2	.81	.45	.82	.85	.91	1.07	1.13	1.13	1.02	.97	.85	.35	.37	.33	.77	1.17	1.29
Al_2O_3	13.26	11.43	12.71	12.84	12.9	13.1	13.06	12.96	12.78	12.6	12.45	9.36	9.76	8.27	12.16	12.89	12.84
FeO	17.99	17.39	11.82	11.82	11.68	11.74	11.83	11.65	11.65	11.69	11.78	10.76	13.13	12.17	13.88	13.9	14.15
MnO	.27	.26	.21	.22	.21	.24	.21	.22	.21	.21	.21	.19	.21	.22	.24	.27	.26
MgO	8.88	9.87	12.57	12.45	12.52	12.33	12.39	12.53	12.6	12.69	12.64	14.55	13.47	13.72	11.37	11.02	10.9
CaO	11.89	11.96	12.42	12.36	12.28	12.36	12.38	12.43	12.38	12.45	12.39	12.63	12.51	12.39	12.33	11.94	12.05
Na_2O	1.34	1.14	1.3	1.38	1.41	1.47	1.42	1.31	1.39	1.38	1.32	.89	.8	.73	1.17	1.35	1.38
K_2O	1.36	1.08	.81	.81	.83	.94	.95	1.01	.95	.86	.83	.67	.69	.54	.8	.95	.95
Total	96.77	96.46	97.06	96.57	96.59	96.64	96.99	97.03	96.97	97.22	97.01	97.32	98.69	96.56	96.67	96.42	96.63
STRUCTURAL FORMULA ON THE BASIS OF 23 OXYGENS																	
Si	6.282	6.543	6.531	6.489	6.482	6.431	6.439	6.456	6.486	6.517	6.554	6.951	6.889	7.077	6.557	6.438	6.418
Al	1.718	1.457	1.469	1.511	1.518	1.569	1.561	1.544	1.514	1.483	1.446	1.049	1.111	.923	1.443	1.562	1.582
Total	8	8	8	8	8	8	8	8	8	8	8	8	8	8	8	8	8
Al	.678	.598	.734	.728	.731	.719	.711	.707	.706	.699	.713	.551	.552	.508	.695	.716	.687
Ti	.094	.052	.091	.095	.102	.119	.125	.125	.113	.107	.094	.038	.040	.037	.087	.132	.145
Fe	2.307	2.22	1.454	1.464	1.445	1.455	1.46	1.436	1.436	1.436	1.449	1.305	1.586	1.494	1.732	1.743	1.774
Mn	.035	.033	.026	.027	.027	.030	.026	.027	.026	.027	.026	.023	.026	.028	.030	.034	.033
Mg	2.028	2.246	2.755	2.747	2.761	2.722	2.726	2.753	2.768	2.779	2.773	3.146	2.902	3.002	2.529	2.462	2.436
Total	5.142	5.149	5.060	5.061	5.066	5.045	5.048	5.048	5.049	5.048	5.055	5.063	5.106	5.069	5.073	5.087	5.075
Ca	1.953	1.955	1.956	1.961	1.946	1.963	1.959	1.963	1.955	1.959	1.954	1.963	1.937	1.949	1.971	1.918	1.935
Na	.397	.337	.371	.396	.405	.421	.407	.375	.397	.393	.376	.250	.225	.208	.337	.393	.400
K	.266	.209	.151	.153	.157	.178	.179	.190	.179	.162	.156	.125	.127	.101	.152	.181	.183
Total	2.616	2.501	2.478	2.510	2.508	2.562	2.545	2.528	2.531	2.514	2.486	2.338	2.289	2.258	2.460	2.492	2.518

TABLE 2. ELECTRON MICROPROBE ANALYSES FROM KOOTENAY LAKE

	Rim		Adjacent grain			Core										Rim
	6	7	8	9	10	T4-8b1	2	3	4	5	6	7	8	9	10	11
SiO_2	43.53	45.22	43.41	43.38	43.42	42.42	41.81	41.77	41.39	40.85	41.38	41.23	41.17	41.31	42.7	46.97
TiO_2	1.13	.68	.93	1.17	1.05	.66	.88	1.14	1.1	1.12	1.27	1.28	1.22	1.24	.64	.3
Al_2O_3	11.74	11.37	12.4	12.42	12.4	12.82	12.76	12.98	13.12	13.33	12.85	12.88	12.93	12.81	11.97	7.93
FeO	14.37	14.18	14.29	14.17	14.15	16.95	16.89	17.27	17.21	17.3	17.15	17.04	17.08	17.12	16.72	14.4
MnO	.24	.22	.23	.23	.22	.23	.25	.25	.27	.25	.27	.27	.27	.28	.26	.25
MgO	10.95	11.62	10.98	10.93	11.02	9.69	9.38	9.38	9.09	9.04	9.1	9.15	9.1	9.23	9.95	12.6
CaO	11.74	12.23	12.26	12.22	12.21	12.02	11.94	11.9	12.07	11.87	11.92	11.97	12.05	12.02	11.91	12.19
Na_2O	1.21	1.02	1.05	1.15	1.15	1.14	1.14	1.26	1.22	1.24	1.25	1.25	1.28	1.22	1.13	.85
K_2O	.92	.86	1.15	1.05	1.01	1.33	1.4	1.41	1.37	1.38	1.38	1.44	1.34	1.39	1.12	.69
Total	95.82	97.39	96.69	96.73	96.62	97.27	96.45	97.37	96.84	96.39	96.59	96.52	96.43	96.63	96.4	96.18
STRUCTURAL FORMULA ON THE BASIS OF 23 OXYGENS																
Si	6.57	6.686	6.503	6.492	6.501	6.413	6.385	6.333	6.313	6.267	6.328	6.312	6.308	6.317	6.499	7.026
Al	1.43	1.314	1.497	1.508	1.499	1.587	1.615	1.667	1.687	1.733	1.672	1.688	1.692	1.683	1.501	.974
Total	8	8	8	8	8	8	8	8	8	8	8	8	8	8	8	8
Al	.658	.667	.693	.683	.689	.698	.682	.653	.672	.678	.645	.636	.644	.626	.646	.423
Ti	.128	.076	.105	.132	.118	.075	.102	.130	.126	.129	.146	.148	.141	.143	.074	.034
Fe	1.814	1.754	1.790	1.773	1.772	2.143	2.157	2.190	2.196	2.220	2.194	2.181	2.188	2.190	2.129	1.802
Mn	.030	.027	.029	.030	.028	.030	.032	.032	.035	.033	.035	.035	.035	.036	.033	.032
Mg	2.463	2.560	2.452	2.437	2.459	2.184	2.134	2.120	2.067	2.067	2.074	2.087	2.079	2.105	2.257	2.809
Total	5.093	5.084	5.069	5.055	5.066	5.130	5.107	5.125	5.096	5.127	5.094	5.087	5.087	5.100	5.139	5.100
Ca	1.898	1.937	1.968	1.96	1.958	1.946	1.953	1.933	1.972	1.952	1.954	1.963	1.978	1.970	1.942	1.953
Na	.355	.292	.305	.334	.334	.334	.338	.371	.361	.370	.372	.372	.379	.361	.332	.247
K	.177	.161	.220	.201	.192	.256	.273	.272	.267	.270	.270	.280	.261	.272	.217	.132
Total	2.430	2.390	2.493	2.495	2.484	2.536	2.564	2.576	2.600	2.592	2.596	2.615	2.618	2.603	2.491	2.332

TABLE 2. ELECTRON MICROPROBE ANALYSES FROM KOOTENAY LAKE

	Rim	Core						Rim			Adj. grain
	T1-9a1	2	3	4	5	6	7	8	9	10	11
SiO_2	48.92	43.2	43.54	43.34	43.53	43.63	43.8	46.57	50.07	49.68	42.31
TiO_2	.15	.92	1.02	1.09	1.06	1.08	1.02	.81	.37	.66	1.00
Al_2O_3	5.97	12.76	12.85	12.78	12.63	12.9	12.88	12.25	8.7	11.98	12.29
FeO	11.17	13.15	13.09	12.86	12.74	12.88	12.87	12.75	11.27	12.82	13.16
MnO	.19	.21	.22	.22	.21	.21	.21	.21	.2	.19	.2
MgO	15.34	11.69	11.79	11.88	11.94	11.92	12.04	13.37	15.26	14.69	11.44
CaO	12.52	12.32	12.2	12.02	12.59	12.29	12.29	12.24	12.42	12.25	12.3
Na_2O	.63	1.26	1.41	1.57	1.45	1.4	1.4	1.31	1.36	.81	1.3
K_2O	.39	.92	.9	.87	.87	.85	.82	.81	.65	.59	1.01
Total	95.28	96.43	97.03	96.64	97.02	97.17	97.34	100.32	100.29	103.67	95.0
STRUCTURAL FORMULA ON THE BASIS OF 23 OXYGENS											
Si	7.247	6.454	6.549	6.451	6.457	6.455	6.464	6.625	7.046	6.777	6.438
Al	.753	1.546	1.451	1.549	1.543	1.545	1.536	1.375	.954	1.223	1.562
Total	8	8	8	8	8	8	8	8	8	8	8
Al	.290	.701	.795	.693	.665	.704	.704	.679	.490	.704	.642
Ti	.016	.103	.114	.123	.119	.12	.113	.086	.039	.068	.115
Fe	1.385	1.643	1.624	1.601	1.58	1.594	1.589	1.517	1.327	1.462	1.674
Mn	.024	.027	.028	.028	.027	.026	.026	.026	.024	.022	.026
Mg	3.387	2.604	2.607	2.636	2.64	2.629	2.649	2.834	3.2	2.986	2.594
Total	5.102	5.078	5.168	5.081	5.031	5.073	5.081	5.142	5.08	5.242	5.051
Ca	1.988	1.972	1.939	1.916	2.001	1.947	1.943	1.866	1.872	1.791	2.005
Na	.181	.364	.406	.453	.417	.401	.401	.361	.37	.215	.383
K	.073	.176	.17	.165	.164	.161	.155	.146	.116	.102	.195
Total	2.242	2.515	2.515	2.534	2.582	2.509	2.499	2.373	2.358	2.108	2.583

TABLE 3. BIOTITE ANALYSES

	T4-4b	T4-8b	T1-9a
SiO_2	36.16	36.30	37.10
TiO_2	2.04	1.66	1.73
Al_2O_3	15.13	15.29	15.81
FeO	17.57	17.99	14.01
MnO	.18	.20	.14
MgO	11.64	12.00	14.73
CaO	.06	.08	.20
Na_2O	.12	.10	.32
K_2O	9.46	8.97	9.49
F	.08	.29	.15
Cl	.04	.04	.03
Total	92.48	92.92	93.71
Ions per 22 oxygens			
Si	5.639	5.665	5.625
Al^{IV}	2.361	2.335	2.375
Total	8.000	8.000	8.000
Al^{VI}	.420	.455	.045
Ti	.223	.18	.196
Fe	2.291	2.329	1.776
Mn	.024	.026	.018
Mg	2.706	2.768	3.329
Total	5.664	5.758	5.769
Ca	.01	.013	.032
Na	.033	.03	.094
K	1.882	1.771	1.835
Total	1.925	1.814	1.962

FIGURE CAPTIONS

Fig. 1 Metamorphic map, Kootenay Bay, British Columbia

Fig. 2 Camera lucida tracing for T2-15. Numbered dots correspond to station points in Fig. 3. Heavy line is the optical boundary of the grain; the lighter line enclosed by it is the approximate optical boundary of the core hornblende. The tracing shows the textural relationships of the other minerals in the slide.

Fig. 3 Station plot for T2-15. Stations as located in Fig. 2. Dotted lines are interpolated from intensity traces. Transitions between stations 3 and 4 take place over a distance of about 20 microns.

Fig. 4 Tetrahedral Al against A-site occupancy plots for all grains studied. A-site occupancy calculated as Na + K.

T2-15. See camera lucida tracing for station locations (Fig. 2). Points 1, 2, 3, 7, 8, 9 and 10 are optically identifiable as actinolite. The change occurs over a distance of about 20 microns between stations 3 and 4 and about 50 microns between stations 6 and 7. The optical boundary is sharper than for less radically zoned amphiboles. A poorly defined Becke line is present between points 3 and 4.

375-140W. This is a composite grain, with the optical boundary with the adjacent grain lying between points 7 and 8. The separation is marked by tremolite, and another tremolite is present in the rim between points 2 and 3. These tremolites are not shown in this plot; they appear on the intensity traces for the mineral. Stations 1, 2 and 7 are optically identifiable as actinolite. Stations 8, 9 and 10 are located on the adjacent grain. Transitions between rim and core take place over a distance of about 20 microns. Transitions between actinolite and tremolite occur over a distance of less than 10 microns.

240-137E. All stations except 10 are optically identifiable as hornblende. The transition between station 9 and station 10 is gradual, occurring over a distance of 60 microns. The optical transition is marked by gradual paling of the dark green hornblende.

T1-9a. This is a composite grain with the optical boundary at point 10. Totals for points 8, 9 and 10 are somewhat high, which may explain the deviation of points 9 and 10 from the general zoning trend. Points 1, 8, 9 and 10 are optically identifiable as actinolite. Transition takes place over 50-75 microns. The optical boundary is fuzzy, but sharper than those of the less radically zoned amphiboles.

T4-4b. This is a composite grain, with points 1 and 2 located on an adjacent zoned amphibole of nearly the same composition. Points 3 and 9 are optically identifiable as actinolite.

T4-8b. Only station 10 is identifiable as actinolite optically. The transition occurs in about 30 microns. The optical boundary is not sharp.

Fig. 5. Plots of Mg/Mg+Fe and Ti/Ti+Fe for the core and the rim of each amphibole grain and coexisting biotite. The biotite is generally located within 1 mm of the hornblende except for 240-137E and T4-8b where only a few flakes of biotite appear in the entire slide.

Fig. 6 Tetrahedral Al against A-site occupancy plot for coexisting paris of actinolite-hornblende taken from the literature and another location in the Kootenay Arc. A-site occupancy is calculated as Na + K.

X from Klein, 1969

▲ from Cooper and Lovering, 1970; Cooper, 1972

● this study (5LBT-22). 5LBT-22 is composed of hornblende-actinolite albite-biotite and sphene. Actinolite is present as a separate phase and also as rims surrounding pargasitic hornblende cores. Contact between actinolite grains and pargasitic hornblende grains (unzoned) is sharp.

It should be noted that the amphiboles present represent different parageneses, especially those of Klein. Haast River amphiboles and paragenesis are quite similar to those of the Kootenay Arc. This plot indicates a solvus in the hornblende-actinolite series. The position of the solvus may be a function of temperature and pressure as well as crystal chemistry (see Shido and Miyashiro, 1959; Compton, 1958; Klein, 1969; and Cooper and Lovering, 1970). The position and width of the solvus may be a function of temperature, pressure, composition and paragenetic history.

Fig. 7 Plot of A-site occupancy against tetrahedral Al for 40 amphiboles from the central Kootenay Arc. A-site occupancy calculated as Na + K. 31-38 and 13-22 are pairs. 31-38 is plotted on Fig. 6 as 5LBT-22.

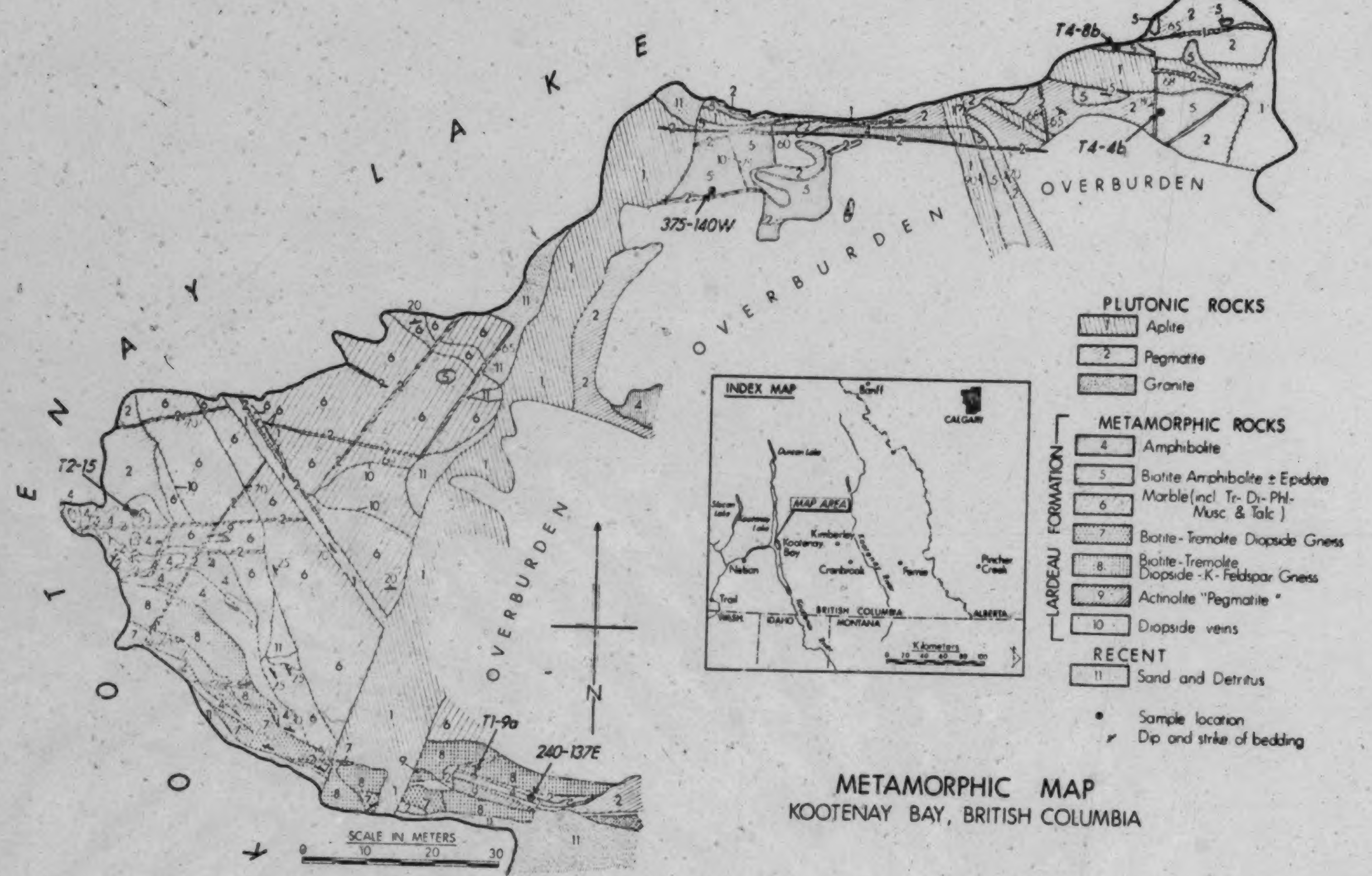
KOOTENAY LAKE
OVERBURDEN
OVERBURDEN
OVERBURDEN
T4-8b
T4-4b
375-140W
T2-15
T1-9a
240-137E
N
SCALE IN METERS
0 10 20 30
INDEX MAP
Banff
CALGARY
Duncan Lake
Slocan Lake
Kootenay Lake
MAP AREA
Kimberley
Kootenay Bay
Nelson
Cranbrook
Fernie
Pincher Creek
Trail
WASH
IDAHO
BRITISH COLUMBIA
MONTANA
ALBERTA
Kilometers
PLUTONIC ROCKS
1 Aplite
2 Pegmatite
3 Granite
METAMORPHIC ROCKS
LARDEAU FORMATION
4 Amphibolite
5 Biotite Amphibolite ± Epidote
6 Marble (incl. Tr-Di-Phl-Musc & Talc)
7 Biotite-Tremolite Diopside Gneiss
8 Biotite-Tremolite Diopside-K-Feldspar Gneiss
9 Actinolite "Pegmatite"
10 Diopside veins
RECENT
11 Sand and Detritus
● Sample location
Dip and strike of bedding

METAMORPHIC MAP
KOOTENAY BAY, BRITISH COLUMBIA

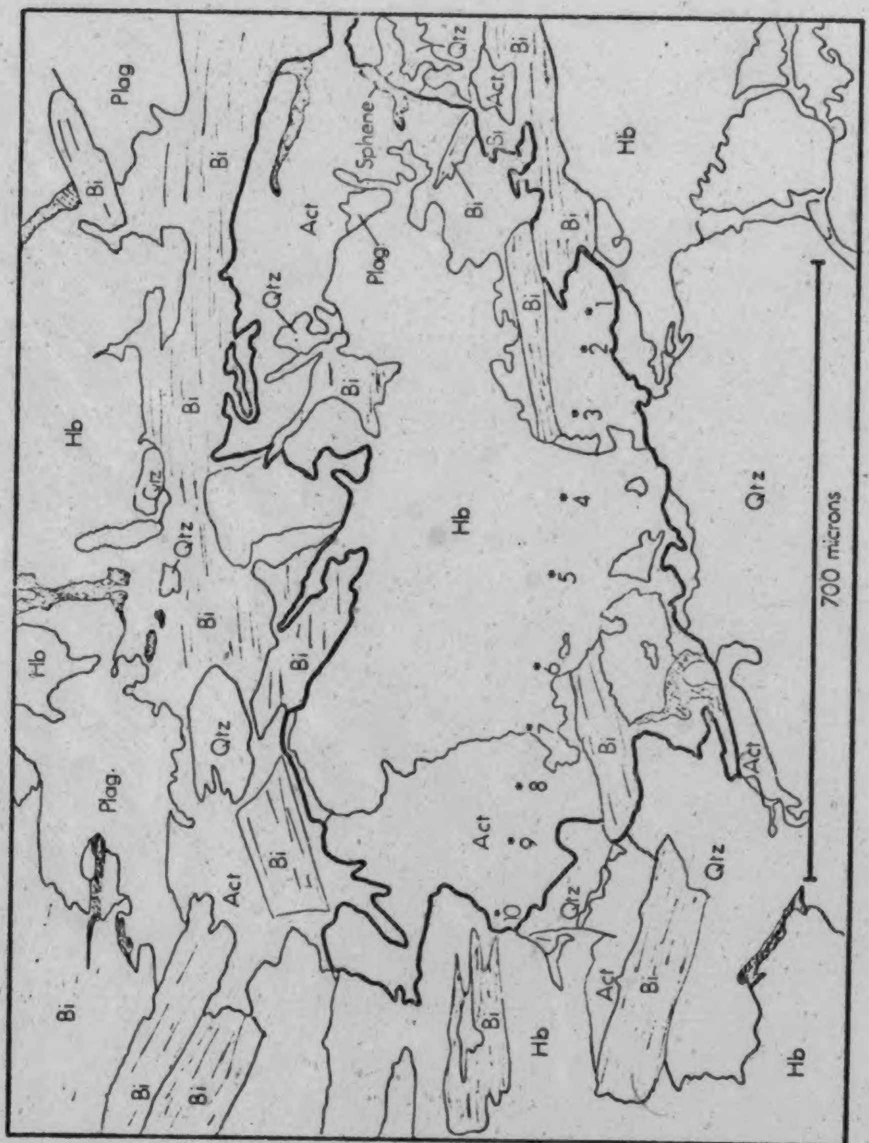
Plag
Bi
Bi
Hb
Qtz
Qtz
Qtz
Bi
Hb
Plag.
Qtz
Act
Bi
Bi
Bi
Bi
Act
Qtz
Bi
Bi
Sphene
Plag
Qtz
Act
Bi
Bi
Bi
Bi
Hb
1
2
3
4
5
6
7
8
9
10
Hb
Act
Qtz
Qtz
Bi
Act
Bi
Qtz
Act
Bi
Hb
Hb
700 microns

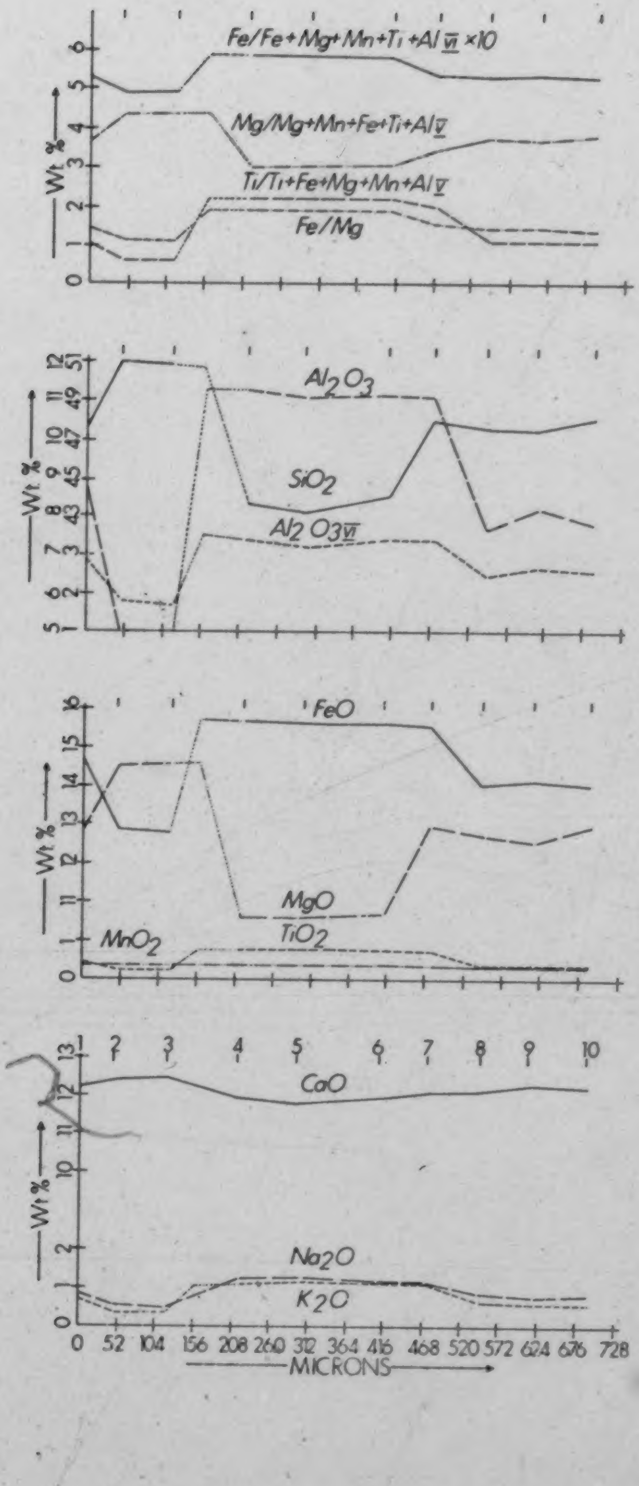
Fe/Fe+Mg+Mn+Ti+Al vi ×10
Mg/Mg+Mn+Fe+Ti+Al v
Ti/Ti+Fe+Mg+Mn+Al v
Fe/Mg
Wt %
0
1
2
3
4
5
6
Al2O3
SiO2
Al2 O3 vi
5 1
6 2
7 3
8 43
9 45
10 47
11 49
12 51
FeO
MgO
TiO2
MnO2
0
1
11
12
13
14
15
16
CaO
Na2O
K2O
1
2
3
4
5
6
7
8
9
10
0
2
10
11
12
13
0
52
104
156
208
260
312
364
416
468
520
572
624
676
728
MICRONS

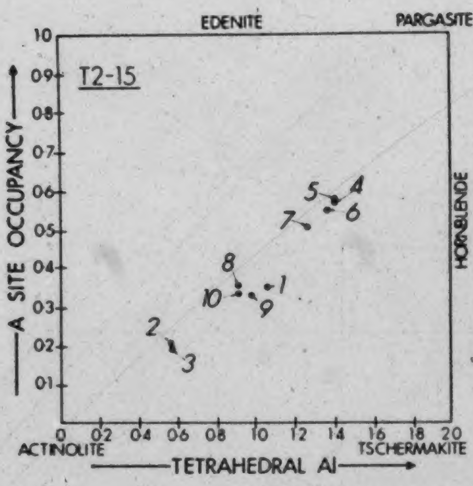
T2-15
EDENITE
PARGASITE
HORNBLENDE
ACTINOLITE
TSCHERMAKITE
A SITE OCCUPANCY
TETRAHEDRAL Al
0.1 0.2 0.3 0.4 0.5 0.6 0.7 0.8 0.9 1.0
0 0.2 0.4 0.6 0.8 1.0 1.2 1.4 1.6 1.8 2.0
1 2 3 4 5 6 7 8 9 10

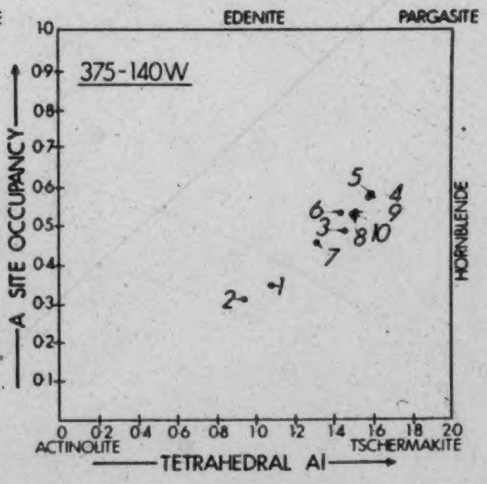
375-140W
EDENITE
PARGASITE
HORNBLENDE
ACTINOLITE
TSCHERMAKITE
A SITE OCCUPANCY
TETRAHEDRAL Al
0.1 0.2 0.3 0.4 0.5 0.6 0.7 0.8 0.9 1.0
0 0.2 0.4 0.6 0.8 1.0 1.2 1.4 1.6 1.8 2.0
1 2 3 4 5 6 7 8 9 10

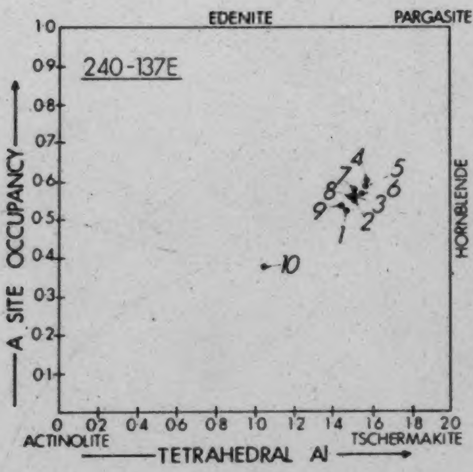
240-137E
EDENITE
PARGASITE
HORNBLENDE
ACTINOLITE
TSCHERMAKITE
A SITE OCCUPANCY
TETRAHEDRAL Al
0.1 0.2 0.3 0.4 0.5 0.6 0.7 0.8 0.9 1.0
0 0.2 0.4 0.6 0.8 1.0 1.2 1.4 1.6 1.8 2.0
1 2 3 4 5 6 7 8 9 10

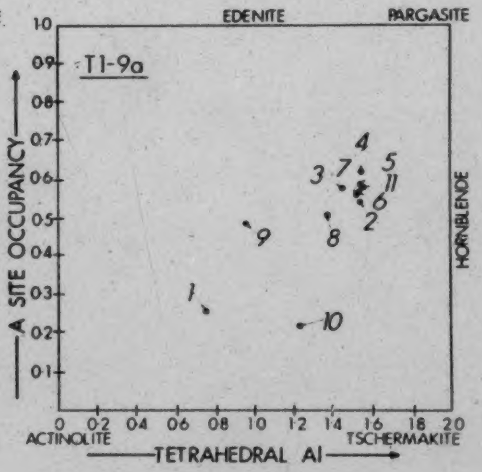
T1-9a
EDENITE
PARGASITE
HORNBLENDE
ACTINOLITE
TSCHERMAKITE
A SITE OCCUPANCY
TETRAHEDRAL Al
0.1 0.2 0.3 0.4 0.5 0.6 0.7 0.8 0.9 1.0
0 0.2 0.4 0.6 0.8 1.0 1.2 1.4 1.6 1.8 2.0
1 2 3 4 5 6 7 8 9 10 11

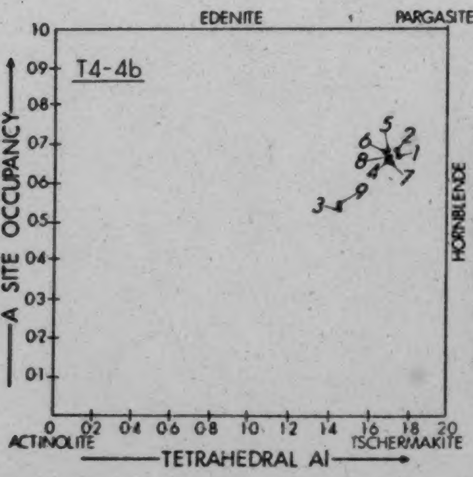
T4-4b
EDENITE
PARGASITE
HORNBLENDE
ACTINOLITE
TSCHERMAKITE
A SITE OCCUPANCY
TETRAHEDRAL Al
0.1 0.2 0.3 0.4 0.5 0.6 0.7 0.8 0.9 1.0
0 0.2 0.4 0.6 0.8 1.0 1.2 1.4 1.6 1.8 2.0
1 2 3 4 5 6 7 8 9

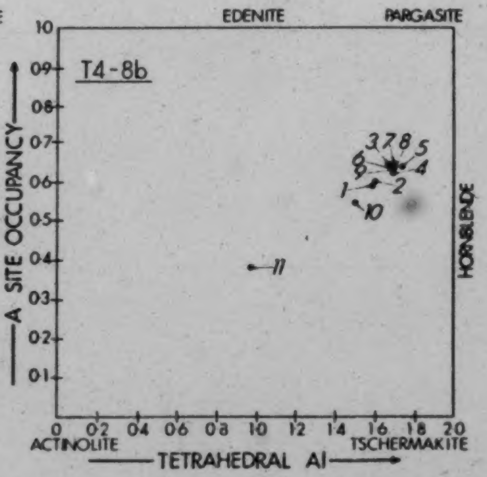
T4-8b
EDENITE
PARGASITE
HORNBLENDE
ACTINOLITE
TSCHERMAKITE
A SITE OCCUPANCY
TETRAHEDRAL Al
0.1 0.2 0.3 0.4 0.5 0.6 0.7 0.8 0.9 1.0
0 0.2 0.4 0.6 0.8 1.0 1.2 1.4 1.6 1.8 2.0
1 2 3 4 5 6 7 8 9 10 11

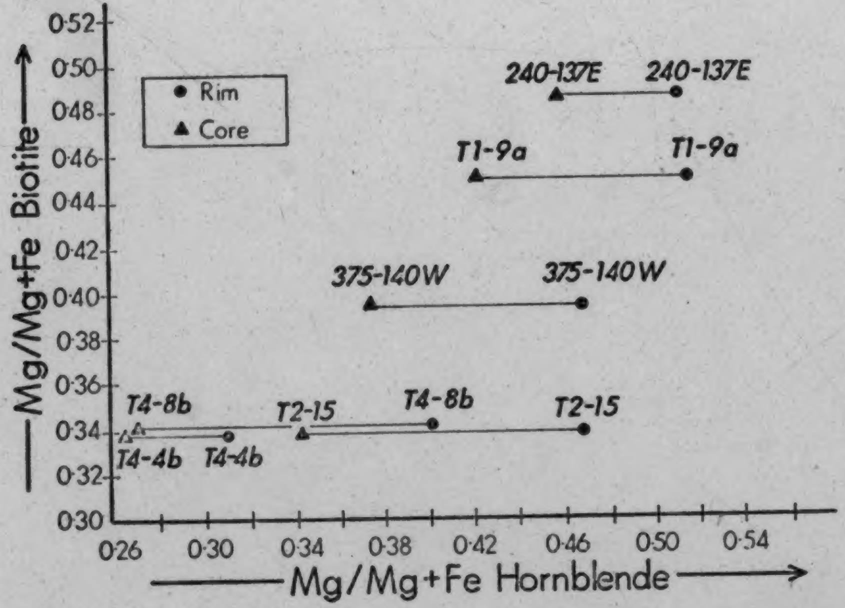

● Rim
▲ Core
240-137E
240-137E
T1-9a
T1-9a
375-140W
375-140W
T4-8b
T2-15
T4-8b
T2-15
T4-4b
T4-4b
0·52
0·50
0·48
0·46
0·44
0·42
0·40
0·38
0·36
0·34
0·32
0·30
0·26
0·30
0·34
0·38
0·42
0·46
0·50
0·54
Mg/Mg+Fe Biotite
Mg/Mg+Fe Hornblende

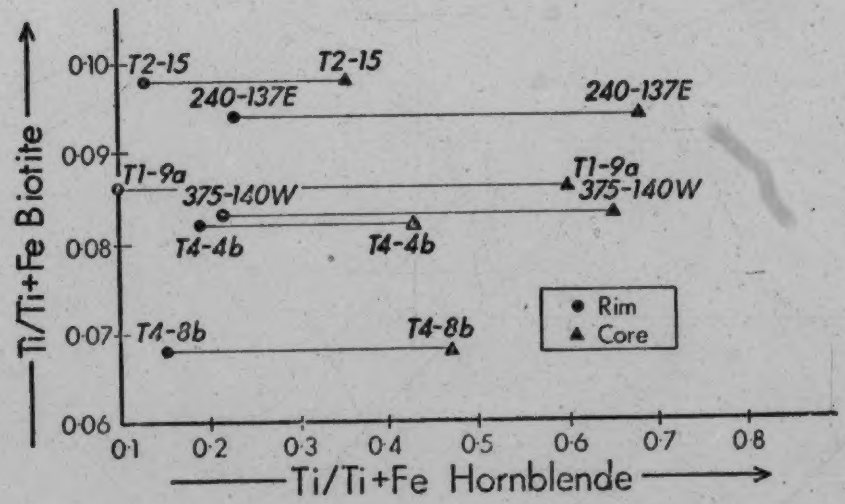

T2-15
T2-15
240-137E
240-137E
T1-9a
T1-9a
375-140W
375-140W
T4-4b
T4-4b
● Rim
▲ Core
T4-8b
T4-8b
0·10
0·09
0·08
0·07
0·06
0·1
0·2
0·3
0·4
0·5
0·6
0·7
0·8
Ti/Ti+Fe Biotite
Ti/Ti+Fe Hornblende

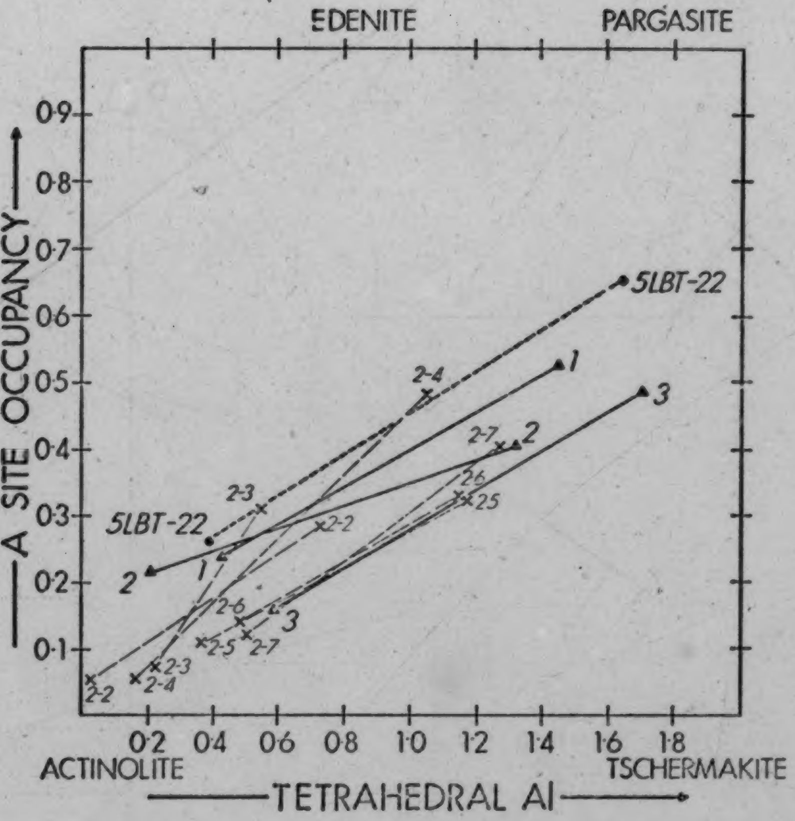
EDENITE
PARGASITE
A SITE OCCUPANCY
0·1
0·2
0·3
0·4
0·5
0·6
0·7
0·8
0·9
5LBT-22
5LBT-22
1
1
2
2
3
3
2-4
2-3
2-2
2-7
2-6
25
2-6
2-5
2-7
2-3
2-4
2-2
0·2
0·4
0·6
0·8
1·0
1·2
1·4
1·6
1·8
ACTINOLITE
TSCHERMAKITE
TETRAHEDRAL Al

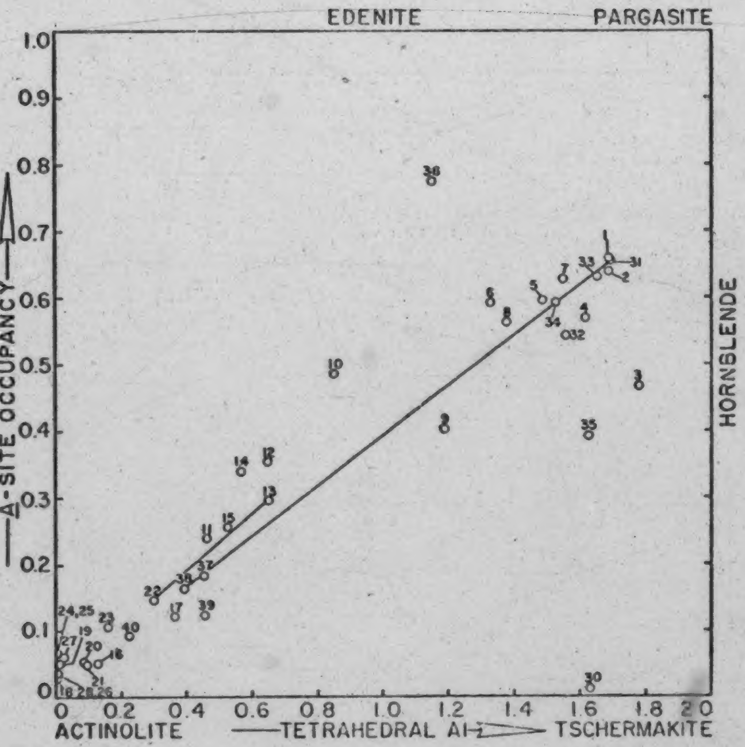
EDENITE
PARGASITE
HORNBLENDE
ACTINOLITE
TSCHERMAKITE
—TETRAHEDRAL Al→
—A-SITE OCCUPANCY→
1.0
0.9
0.8
0.7
0.6
0.5
0.4
0.3
0.2
0.1
0
0.2
0.4
0.6
0.8
1.0
1.2
1.4
1.6
1.8
2.0
38
1
33
31
7
2
5
6
34
4
8
32
10
3
9
35
14
12
13
15
11
37
22
36
17
39
24,25
23
40
19
27
20
16
21
18
28
26
30